# Cooperative Diversity for Distributed Multicarrier Relaying Systems

Guerrero, Laura Yadira

*Awarding institution:*
King's College London

# Cooperative Diversity for Distributed Multicarrier Relaying Systems

By

**Laura Yadira Guerrero Olivares**

A thesis Accepted by the King's College London, University of London for the degree of Doctor of Philosophy

Centre for Telecommunication Research
King's College London
Strand, London WC2R 2LS
United Kingdom

October 2012

“Deserve your dream”

-Octavio Paz

# Abstract

We introduce a Cooperative Distributed Multistage Spatial Diversity (CDMSD) scheme. By means of prior derived relaying topologies our algorithm relies on a robust and low complexity transceiver entity. CDMSD is implemented such as to improve throughput enhancement, coverage extension and spectral efficiency improvement.

The benefits are provided by achieving full diversity and frequency selectivity. Simulation results are presented and compare to traditional non-distributed networks to support the analytical framework. Additionally fractional frame duration and transmitted power control are implemented to achieve higher data transmission rates.

Providing a performance near optimum, our protocol has gained significantly in research momentum, mainly due to its ability to boost capacity and its inherent attribute of scalability to ad hoc and wireless sensor networks.

CDMSD makes full use of MC-CDMA frequency domain spreading properties by introducing immerse collaboration and distributed frequency diversity in a multi-hop network architecture which has drawn much attention in industry and academia in terms of reliable performance.

# Acknowledgements

I dedicate this research work to my children Sofia, Leonardo and Paola Isabella.
I owe my deepest gratitude to my parents Laura and Guillermo.
Many people have contributed to the completion of this thesis. I am especially grateful and would like to express my sincere appreciation to Dr. Fatin Said, my supervisor, for her professionalism and competence during my research project and support and preparation of this thesis. Gratitude is also expressed to Professor Hamid Aghvami for his expertise and suggestions in this study.

It is a pleasure to thank those who made this thesis possible with their continue support Yazmin, Paulino and Lucas, my grandparents Isabel and Rafael, Marisela and relatives for their unfailing support, patience, and encouragement, during the period of my research in the United Kingdom. My heartfelt gratitude is extended to my friends Antonia Noemi and Silvia. My appreciation to my colleagues at the Centre for Telecommunications Research for their helpful discussions and useful advice during the course of the study.

There are many things I have learned during the past years being involved with CTR. I want to thank all academic members for the support during the development of the concept presented in this thesis. I am particularly grateful to Dr Mischa Dohler.
My office hours I have spent with incredible guys from around the word with the same goal at CTR is unforgettable. I cannot name you all, but I want to thank a couple of very special people: Wahida, Leila, Mona, Lodhi, Imra, Thanos and Kostas. Thanks to Prof Mohammad, Dr Reza and Dr Vasilis and their continuo support in the EE division. My thanks also extended to those who have directly or indirectly given their support in terms of advice, encouragement, moral or technical though minor.

Finally the financial support from “Consejo Nacional de Ciencia y Tecnologia” (CONACyT) sponsorship is gratefully acknowledged.

# Table of Contents

# List of Figures

# List of table

# List of Acronyms

**AF** Amount of Fading

**AWGN** Additive White Gaussian Noise

**BER** Bit Error Rate

**CBDD** Circular Block Delay Diversity

**CDD** Cyclic Delay Diversity

**CDMA** Code Division Multiple Access

**C-OFDM** Coded-Orthogonal Frequency-Division Multiplexing

**CP** Cyclic Prefix

**CSI** Channel State Information

**dB** Decibel

**DD** Delay Diversity

**DFT** Discrete Fourier Transform

**DPS** Digital Phase Sweeping

**DS** Direct Sequence

**EGC** Equal Gain Combining

**FDM** Frequency-Division Multiplexing

**FFT** Fast Fourier Transform

**GHz** Giga Hertz

**HDT** Hybrid Diversity Transmitter

**Hz** Hertz

**ICI** Inter-Channel Interference

**IFFT** Inverse Fast Fourier Transform

**ISI** Inter-Symbol Interference

**LCP** Linear Constellation Precoders

**LoS** Line of Sight

**MAI** Multiple Access Interference

**MC-CDMA** Multi Carrier-Code Division Multiple Access

**MGF** Moment Generating Function

**MIMO** Multiple Input Multiple Output

**MISO** Multiple Input Single Output

**ML** Maximum Likelihood

**MMSE** Minimum Mean Square Error

***M*-PSK** *M*-ary phase shift keying

***M*-QAM** *M*-ary quadrature amplitude modulation

**MRC** Maximum Ratio Combining

**MT** Multi Tone

**NLoS** Non-Line of Sight

**OFDM** Orthogonal Frequency-Division Multiplexing

**ORC** Orthogonality Restoring Combining

**PEP** Pairwise Error Probability

**PD** Phase Diversity

**PAPR** Peak-to-Average-Power Ratio

**PDP** Power Delay Profile

**QoS** Quality of Service

**RMS** Root Mean Square

**RVs** Random Variables

**SER** Symbol Error Rate

**SIMO** Single Input Multiple Output

**SISO** Single Input Single Output

**SNR** Signal to Noise Ratio

**SF** Space Frequency

**SFBC** Space Frequency Block Code

**ST** Space Time

**STBC** Space Time Block Code

**STC** Space Time Coding

**STF** Space Time Frequency

**STM** Space Time Multipath

**STTC** Space Time Trellis Code

**TDMA** Time Division Multiple Access

**TUB** True Upper Union Bound

**VDSL** Very High Bit-Rate Digital Subscriber Line

**WLANs** Wireless Local Area Networks

**WMANs** Wireless Metropolitan Area Networks

**WSSUS** Wide-Sense Stationary Uncorrelated Scattering

e.g. For Instance

i.i.d. Independent and Identically Distributed

i.e. That is

*pdf* Probability Density Function

*cdf* Cumulative Distribution Functions

var Variance

# List of Symbols

$B$ Signal Bandwidth

$F$ Frame Length

$G$ Processing Gain

$K$ Rician $K$-Factor

$L$ Number of Multipaths

$M$ Modulation Order

$N$ Number of Subcarriers

$P$ Symbols per User in an MC-CDMA System

$\hat{P}$ Number of Primary Antennas in Hybrid Scheme

$R$ Rate of Block Codes

$\hat{S}$ Number of Secondary Antennas in Hybrid Scheme

$T$ Symbol Duration

$U$ Number of Active Users

$B_c$ Coherence Bandwidth

$E_b$ Bit Energy

$E_c$ Chip Energy

$E_s$ Symbol Energy

$f_s$ Subcarrier Spacing

$f_D$ Doppler Frequency

$f_{Dmax}$ Maximum Doppler Frequency

$G_c$ Spatial Coding Gain

$G_d$ Spatial Diversity Gain

$G_{fq}$ Frequency Diversity Gain

$G_{sm}$ Spatial Multiplexing Gain

$G_t$ Time Diversity Gain

$N_0$ One Sided Noise Power Spectrum Density

$N_{rx}$ Number of Receive Antennas

$N_{tx}$ Number of Transmit Antennas

$T_c$ Coherence Time

$T_s$ OFDM Symbol Duration

$\alpha$ Amplitude of Multipath

$\Omega$ Mean Square Value of ®

$\sigma^2$ Variance

$\tau_m$ Mean Delay

$\tau_{max}$ Maximum Selay Spread

$\tau_{rms}$ RMS Delay Spread

$\gamma$ Instantaneous SNR

$\bar{\gamma}$ Average SNR

$\Gamma(x)$ Complete Gamma Function

$\Phi\gamma$ Moment Generating Function of Instantaneous SNR

$P_\alpha(\alpha)$ *pdf* of $\alpha$

$E\{x\}$ Expectation of $x$

$F_N$ $N \times N$ FFT Matrix

$F_N^H$ $N \times N$ IFFT Matrix

$I_N$ $N \times N$ Identity Matrix

$\theta^t$ CDD Matrix

$\theta^f$ PD Matrix

$\mathcal{G}$ Orthogonal Block Codes' Generator Matrix

$|\mathbf{H}|$ Frobenius Norm of $\mathbf{H}$

$|.|$ Absolute Value

$X^H$ Hermitian Transpose of $A$

${}_2F_1$ Gauss Hypergeometric Function

$F_1$ Appell Hypergeometric Function

$(a)_n$Pochhammer Symbol

diag Diagonal of Matrix

max Maximum of Argument

min Minimum of Argument

max arg Maximum among Arguments

# Chapter 1

# Overview

## 1.1 Introduction

This chapter shows the background and motivation for the research results presented in this work and draws an outline for the remainder of the thesis. Also, the contributions to new knowledge are listed at the end of this chapter.

Wireless networks consist of a number of nodes which communicate with each other over a wireless channel. Recently, in an effort to improve the performance of wireless networks, there has been increased interest to answer: how should the signals be distributed to and collected from wireless terminals in the most efficient manner. The developments in this direction will yield enhanced coverage, throughput, and Quality of Service (QoS), as well as cost-efficient and compact wireless terminals. Simple calculations indicate that the provision of the very high data rates envisioned in future wireless systems in reasonably large areas does not seem to be feasible unless significant new spectrum release or the density of the access points is increased dramatically. Currently, there is no indication that significant new spectrum will be available in the near future; and, a drastic increase in the number of access points is not economically justifiable.

In recent years, there has been significant advances in signal processing techniques (such as interference cancellation algorithms) and collocated antenna architectures which are generally referred to as smart antennas (such as MIMO and adaptive antennas) [1] [2]. Although incorporation of these techniques in future wireless systems is crucial, for practical reasons, these techniques alone do not seem to be sufficient in enabling almost-ubiquitous very high data rate coverage. For instance, it may be inefficient to deploy complex antenna systems at wireless terminals; besides, in the presence of heavy shadowing, even the smartest antennas will not be of much help. Therefore, more

fundamental enhancements are necessary for the very ambitious capacity, throughput, and coverage requirements of future.

The vision for this new generation includes provision of a broadband component for which various implementation technologies are being considered Multi Carrier Code Division Multiple Access (MC-CDMA) system, one scheme being widely researched [3] [4] [5], is a multiple access scheme used in OFDM- based telecommunication systems, which is a promising candidate to support higher data rates in a mobile environment.

Orthogonal frequency-division multiplexing (OFDM) technique has gained a lot of attention in recent years due to its ability to prevent ISI in broadband wireless channels. It is based upon the principle of frequency-division multiplexing (FDM) but utilized as a digital modulation scheme. The bit stream that is to be transmitted is split into several parallel bit streams, typically dozens to hundreds. Thus, the available frequency spectrum is divided into several sub-channels and each low-rate bit stream is transmitted over one sub-channel by modulating a subcarrier using standard modulation schemes. The subcarrier frequencies are chosen so that the modulated data streams are orthogonal to each other and with this the inter-channel interference (ICI) which is normally defined as crosstalk between the sub-channels, is eliminated. Above all, channel equalization is simplified by using many slowly modulated narrowband signals instead of one rapidly modulated wideband signal.

OFDM has already developed into a popular scheme for wideband digital communication systems. Among numerous applications, IEEE 802.11 a-*g* which are the standards for wireless local area networks (WLANs) plus the digital audio broadcasting (DAB) systems. In recent years, the certification of IEEE 802.16 standards i.e., fixed and mobile worldwide interoperability for microwave access (WiMAX) systems will introduce OFDM into the cellular wireless networks [3] [4].

Despite all the benefits of OFDM, the quest for designing very high-speed wireless links that offer acceptable quality-of-service (QoS) in both line of sight (LoS) and nonline of sight (NLoS) environments still constitutes a significant research and engineering challenge.

There is a long path to pace until we are entitled to call the development of transmission technologies to be mature It will then be the time when research can move on to more

important things than designing transceivers which operate as close as possible to the predicted capacity limits.
Until this will happen, however, the existence of researchers like me is justified and the work which I expose within this thesis will be read. Indeed, this thesis is about increasing the capacity of wireless systems under the constraints of limited bandwidth and limited transmission power.

In its original formulation, the capacity of a communications channel characterises the maximum amount of error-free information (in bits) which can be transmitted over that channel in a given time (in seconds) over a given bandwidth (in Hertz). Shannon was the first to present the fundamental limits of digital communication systems, which allowed him to analytically derive the capacity for an additive Gaussian noise channel [5] This capacity bound evolved over the consecutive years to encompass wireless single-input-single-output (SISO) and later wireless multiple-input-multiple-output (MIMO) channels.

The latter can be accomplished by systems where several antenna elements are available at the transmitter and receiver side. The landmark contributions by Telatar [5] and Foschini & Gans [6] have demonstrated that the capacity of a MIMO system exceeds the capacity of a SISO system. However, recently explored MIMO channels promise to meet the required spectral efficiency of up to several tens of bits/s/Hz in dependency of the communication scenario [4] [5] . The immediate price to pay is an increased transceiver complexity. However, these costs fall short in comparison to the potential capacity gained.

The capacity for MIMO channels derived in [4] and [5] are known to depend on the correlation between the transmitting and receiving antenna elements [1]. The reason is that the extra capacity is provided through spatially uncorrelated sub-channels. A high correlation among the antenna elements reduces the MIMO wireless channel towards that of a single link channel. Therefore, failing to provide uncorrelated antenna elements prevents the deployment of high capacity MIMO systems. The main challenge a MIMO communications engineer thus faces in practice is to design an antenna array with mutually uncorrelated antenna elements. Correlation among the antenna elements is

firstly influenced by the surrounding environment and secondly by the transceiver hardware design.

Even though MIMO OFDM architecture has reached a stage, both from a theoretical and a hardware implementation perspective, where they can be considered ready for use in practical systems, there is still a large number of open research problems. Towards that end, in addition to advanced signal processing techniques, some major modifications in the wireless network arquitecture itself, which will enable effective distribution and collection of signals to and from wireless users, are sought.
A solution to overcome this problem by means of spatially distributed antenna elements, termed Cooperative Antenna Arrays, is introduced and analysed in this thesis. The integration of multihop capability in conventional wireless networks is one such promising architecture to upgrade the simplicity of OFDM. Focusing mainly on this area, an overview of MIMO OFDM techniques is given in the next section.

## 1.2 Background

Towards that end, in the last few years there has been quite an interest in the generic multihop networks in both industry and academia. The intermediate relayers/routers in such multihop-augmented networks may be some fixed low-op

### 1.2.1 Performance Gains of MIMO Systems

The performance improvements due to MIMO systems can be classified as Array gain, Diversity gain and Spatial multiplexing gain Next a brief of these techniques is given.

**Array Gain & Interference Reduction**
The use of antenna arrays with specific processing at the transmitter and the receiver side yields a gain which results in an increase in average receive SNR due to a coherent combining effect. Interference reduction techniques are employed to mitigate effects of co-channel interference, which arise due to the frequency reuse in wireless channels. Beamforming is a popular method to achieve both Array gain and Interference reduction. It uses arrays of multiple transmitters or receivers that controls the directionality of, or sensitivity to, a radiation pattern.

**Spatial Multiplexing & Spatial Diversity Gains**

### 1.2.2 Fundamental Tradeoffs in MIMO Systems

The simultaneous incorporation of the above mentioned MIMO transmission techniques can be realized in a communication system.

Originally, the signalling strategy for MIMO systems (considering flat fading channels) was primarily focused on either achieving the full spatial diversity gain ($N_{tx}N_{rx}$) available from the channel or enhancing the data rates ($\min\{N_{tx,}N_{rx}\}$) through spatial multiplexing [7] [8] [9], where $N_{tx}$ and $N_{rx}$ represent the number of transmit and receive antennas, respectively. Also, some schemes were presented that can switch between the two modes depending on the instantaneous channel conditions. It was realized by Zheng and Tse in [10] that it was possible for a given scheme to simultaneously achieve both the full diversity and multiplexing gains. However, any MIMO scheme that targets to achieve diversity/multiplexing gains or a combination of both is governed by some fundamental tradeoffs which are as follows:

**Diversity-Code Rate Tradeoff**

Space-time coding (STC) has remained the reliable choice for spatial (transmit) diversity since its formulation. Diversity, which makes the asymptotic error rate decrease as a function of SNR, whereas coding gain determines the vertical shift of the error performance curve. STBC were shown to achieve full spatial diversity but no coding gain. In simple terms, any ST code is said to be an optimal code if it achieves the full spatial diversity without losing the spectral efficiency.

**Diversity-Multiplexing Tradeoff**

By using the incremental SNR, a MIMO system with *Ntx* transmit and *Nrx* receive antennas can either decrease the probability of error (diversity) or increase the spectral efficiency (spatial multiplexing), thereby making it possible for a given scheme to simultaneously achieve both types of gains [10]. However, the diversity-multiplexing tradeoff determines the amount of each type of gain that may be extracted by any coding method and is represented by an optimal tradeoff curve formulated in [11].

**Diversity-Code Rate-Multiplexing Tradeoff**

The diversity-multiplexing criterion is independent of spectral efficiency of any given code, while diversity-code rate tradeoff does not consider the achievable multiplexing gain. In fact, these two tradeoffs are related and determine the maximum diversity and multiplexing gain of given ST code for a certain spectral efficiency.

### 1.2.3 OFDM Systems – a Spatial Diversity Perspective

With the minimal of complexity, OFDM based systems provide the excellent opportunity to use the spatial and in particular, transmit diversity schemes such as STC in broadband frequency selective channels. These transmit diversity methods in conjunction with simple OFDM and MC-CDMA systems are the main topic of this thesis and next, a brief of the known state of art in the subject field is presented.

OFDM based systems employ parallel subcarriers for data transmission, thereby providing an additional frequency domain, besides time and space, for the STC techniques. Hence, the maximum theoretically achievable diversity level ($N_{tx}N_{rx}L$) cannot be achieved, where $L$ represents the number of resolvable multipaths. The ST, coded diversity scheme have been proposed, establishing that the theoretical diversity limits can be achieved by trading complexity, additional processing and incorporating precoding arrangements. The most noticeable works in this regard are given in the contributions [12]-[13].

It was shown that by using an OFDM block size, $N_{tx}L$, maximum spatial and frequency diversity can be achieved; Finally, the least complex transmit diversity method to extract multipath diversity is cyclic delay diversity (CDD). It has gained enormous interest and currently being considered for several OFDM based system standards. CDD is based on delay diversity (DD) of [14], in which the same information bearing symbols are transmitted from separate antennas with different time delays, thereby causing multipath replicas that help in achieving diversity at reception. This comes at the cost of implementation issues like specific guard period, ISI and time delays. CDD caters the adverse effects of DD by introducing cyclic delays instead of time delays. It introduces echos/replicas of the originally transmitted signals and thus increases the frequency selectivity of the channel. CDD can be used for any number of transmit antennas and can

be applied to existing systems without changing the receiver. It exists in literature in many forms, where it slightly differs in terms of its placement in the system. Also, it is a time domain equivalent of phase diversity (PD) and can very nicely be cast into the framework of DPS, CBDD of [15]. It is the simplest approach to introduce transmit diversity for OFDM based systems that itself has no building diversity and can compete with STC techniques with no additional complexity at the receiver [16] [17].

Here, it is important to mention that due to the enormity of the literature on the subject field, it is impossible to cover each approach/scheme, therefore an effort has been made to cover the majority of frameworks that are related to the scope of this thesis.

### 1.3 State of the Art

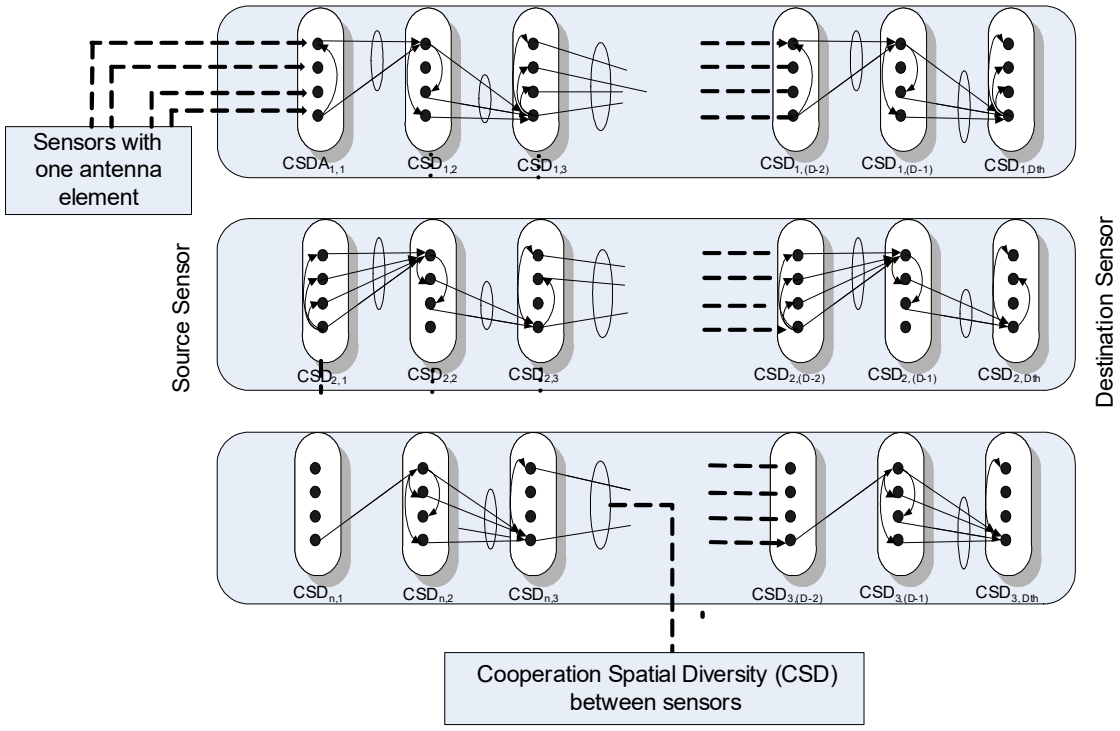


Figure 1.1 Cooperative Distributed Multistage Spatial Diversity (CSD) scheme.

The concept of Cooperative Antenna Arrays with application to cellular networks has been introduced in February 2000 [6]. The generalization of the concept to distributed–MIMO multi-stage communication networks with application of distributed space-time codes has been introduced shortly after [10]. The description here relates to the

generalised CSD multi-stage communication system as depicted in Figure 1.1. Consider, a source sensor terminal (s-ST) communicating with a target sensor terminal (t-ST) via a given number of relaying sensor terminals (r-STs). Spatially adjacent r-STs are grouped into CSDs, thereby forming a relaying CSD (r-CSD) tier. The s-ST and t-ST themselves might be a member of a CSD, henceforth referred to as source CSD (s- CSD) and target CSD (t-CSD), respectively. The system of a s-CSD communicating with a t-CSD communicating with a t-CSD via several tiers of r-CSDs is referred to as a CSD multi-stage communication system. The optimum choice of r-STs, as well as their optimum grouping into CSDs, is beyond the scope of this thesis. It is therefore assumed here that the fractional resource allocation algorithms developed here are applied to the given topology.

The s-ST, t-ST and r-STs may possess any number of antenna elements, depicted as large dots in Figure 1.1. Furthermore, the STs may or may not cooperate among each other within the same CSD tier. The cooperative link is shown as a dash-dotted line. Each r-ST of the same r-CSD transmits the prior agreed spatial branch of a space-time code word, where the encoding bases on the received and detected symbol from the previous r-CSD tier. The resulting MIMO sub-channels are shown as grey lines.

Clearly, a cooperative deployment yields a higher capacity; however, at the expenses of additional complexity, relaying power and bandwidth. The latter two are assumed to be negligible in the current analysis, as being justified in Chapter 3. The increase of capacity vs performance# is thus due to more complex transivers only, which have to accomplish intra (cooperation) and inter (multi-stage) CSD relaying. It is assumed here that not all available antenna elements need to be active for the intra and/or inter CSD relaying process.

In its infancy, the concept of Cooperative Antenna Arrays evolved from the contributions by [18] and [19] on relaying and by [4] and [20] on MIMO communications aspects.

The methodologies suggested in [18] have been studied in [19]. In this study, SISO relaying has enable an extension of the serving area of a BS by utilizing r-MTs at the coverage edge to provide data services to MTs  in the network gain on average in performance. Simple relaying protocols have also been suggested which are based on shortest distance relaying. The gains of the relaying process have been attributed to the non-linear pathloss equation, which reduces the aggregate pathloss when breaking a long distance into several shorter communication distances.

Relaying Communication Systems. The method of relaying has been introduced in 1971 by van der Meulen in [21] and has also been studied by Sato [22]. A first rigorous information theoretical analysis of the relay channel has been exposed by Covern in [23], a more detailed description to which can be found in his book [15]

In these contributions, a source MT communicates with a target MT directly and via a relaying MT. In [23] the maximum achievable communication rate has been derived in dependency of various communication scenarios, which include the cases with and without feedback to either source MT or relaying MT, or both. The capacity of such a relaying configuration was shown to exceed the capacity of a simple direct link. Interesting milestones into the above-mentioned theoretical studies have been the contributions by Sendonaris, Erkip and Aazhang, which date back to 1998 [24].

The simples' cooperative protocol has been extended by the same authors to more sophisticated schemes, which can be found in the excellent contributions [26] and [27]. Note that in its original formulation [24], no distributed space-time coding has been considered.

The contributions by Laneman in 2000 [13] are a conceptual and mathematical extension to [24], here energy-efficient multiple access protocols are suggested base on decode-and forward and amplify-and-forward relaying technologies.

The case of distributed space-time coding has been analyzed by Laneman in his PhD dissertation [28]. He has demonstrated that cooperation yield full spatial diversity, which allows drastic transmit power saving at the same level of outage probability for a given communication rate. However, [28] does not incorporate an analysis of distributed-MIMO multi-stage communication systems as proposed within this thesis. On the other hand a landmark contribution on relaying systems deploying multiple antennas at transmitting and receiving side has been made by Guptar and Kumar [28]. The network topology exposed therein is the most generic one can think of, i.e. any MT may communicate with any other MT in the network such as to achieve a maximum system capacity. Gupta and Kumar were the first to statistically analyze the information theoretically offered throughput for a large scale relaying networks [34].

Nonetheless, the analysis exposed in this thesis is inspired by other protocols and algorithms [29][30] [31] [32] [33] and the scheme presented and depicted in Figure 1.1, considers only stage-by-stage relaying. In [36], an information theoretic scheme for

obtaining an achievable communication rate region in a network of arbitrary size and topology has been derived.
Specific distributed space-time coding schemes have also been suggested recently, e.g [37]. Contributions on MIMO systems have flourished ever since the publication of the landmark papers by Telatar [4] and Foschini & Gans [5] on capacity and Foschini [9], Alamouti [8] and Tarokh [12][34] on the construction of suitable space-time transceivers.

### 1.4 Aim & Organization of the Thesis

The work during recent years on Cooperative Antenna Arrays, was understood, that a deployment, capacity and performance analysis of generic communication topologies as depicted in Figure 1.1 would be more beneficial in understanding relaying systems.
To simplify analysis and understanding, investigations first concentrated on an end-to-end scenario where a given source MT separated by various relaying hops. Analysis was then extended to the case where each relaying hop contained more than one relaying MT, henceforth referred to as the relaying stage. In due course it became apparent that enough problems were unsolved for such a communication scenario, some of which are exposed and solved in this thesis.

It is the aim of this thesis to design communication protocols which yield optimum or near-optimum end-to-end data throughput for an information source communicating with an information sink via a given number of topologically imposed relaying stages. As will be demonstrated, such protocols have to guarantee an optimum assignment of resources to each relaying stage as a function of the channel conditions. These protocols are henceforth referred to as fractional resource allocation strategies.
For a potential deployment, these strategies have to be a simple and robust as possible. Their role is to allocate resource in terms of power, bandwidth and frame duration to each relaying stage dependent upon of the prevailing channel conditions.
Only after that, allocation strategies can be developed which achieve maximum end-to-end throughput. Since the notion of capacity assumes transceivers of infinite (or very high) complexity, their deployment is only justified in systems which deploy such transceivers.

Once the throughput maximizing protocols are derived for a single end-to-end communication link, they can then be enhanced to allow optimum throughput in multiple end-to-end communication links. This can be seen as a further step towards the realization of generic system as introduced in [35]; however, with reference to the amount of material pressed in this thesis, this has been left open for future research.
To accomplish a logical thread in deriving the fractional allocation strategies, the thesis has been organized as follows.

The thesis consists of seven chapters and covers the frameworks presented by the author in [38]-[43]. In Chapter 2, the fundamentals of mobile radio channel are briefly reviewed. Then, Rayleigh, Rician and Nakagami-*m* multipath fading models are characterized for frequency flat case and further extended for selective environments. In the second half of Chapter 2, the basic principles and data detection techniques of OFDM and MC-CDMA systems are reviewed.
Chapter 3 starts by revisiting the design and performance criterion of STC and CDD OFDM presented in [44] [45]. Then, the orthogonal block codes are reviewed with their implementation as ST block codes and CDD, followed by a time domain encoding strategy.

By showing that a MIMO OFDM system employing STBC can be represented by an equivalent SISO model, the closed form symbol error probabilities of orthogonal block coded OFDM system are presented for Nakagami-*m* fading channels.
Besides, CDD is presented for OFDM system. First, the transformation of spatial diversity into frequency is shown by using PD which is a frequency domain equivalent of CDD. The relationship between the channel delay spread and cyclic delays values for different antenna branches is established. Finally, the performance and comparison between CDD and orthogonal block coded OFDM is presented that helps in highlighting the excellent performance of CDD. In more details, the major contributions of Chapter 3 can be summarized as follows, presents CDD and STBC for orthogonal block codes system. Both schemes are generalized for arbitrary number of transmit antennas.

Then in chapter 4, the transformation of an CDD MC-CDMA system to a single transmit antenna system with relatively enhanced delay spread is discussed followed by the representation of MIMO MC-CDMA system employing STBC with an equivalent SISO

model. Then, the Nakagami-*m* channel model with frequency correlated MC-CDMA subcarriers and MRC detection technique is used for the performance analysis of these two systems. The exact and closed-form expressions for the average SER of *M*-ary signals are derived by transforming the single integrals (containing the MGF of the instantaneous SNR of CDD and STBC MC-CDMA systems) into higher transcendental functions[9][10] . Finally, considering a complete MC-CDMA system with different loading conditions and respective optimum detection techniques, a comparison in terms of complexity and performance between these two schemes is conducted. Also, the error rates of these schemes were compared with and without frequency domain interleaving.

Chapter 5. The performance of multi-hop multiple-input, multiple-output (MIMO) communication scenarios is evaluated for space time block coded (STBC) and the proposed distributed cyclic delay diversity (CDD) technique. By increasing the frequency selectivity, multi-stage CDD with low complexity implementation yields significant performance improvement as relaying network. Both diversity techniques based on frequency-correlated MC-CDMA subcarriers networks are investigated by using the moment generating function (MGF) over correlated Nakagami-m fading channels. The system performance evaluation is provided for the exact average symbol error rate (SER) and the end-to-end bit error rate (BER). In order to maximize the end-to-end throughput [bits/s/Hz], explicit allocations strategies are derived and analysed. Simulation results are also presented which show excellent agreement with the analytical framework.

Chapter 5 derives throughput-maximizing resource allocation strategies assuming space-time block encoded and ST systems. The deployed finite complexity transceivers lead to different optimization criteria, and hence to different allocation strategies than in the previous chapter. The derivation of the allocation strategies is partially facilitated by the closed form expressions of the symbol error rate of space-time block codes with different channel statistics and gain.

Finally, the environment effects are fundamental in performance evaluation of the throughput. As part of the research difference scenarios has been considered. A comparison between Direct and 2 hops links are presented that helps in highlighting the excellent performance of the relaying networks.

Chapter 6 presents the Performance Analysis of Distributed Cooperative Serial Spatial Diversity Relaying Sensor Network for Multicarrier Based Systems. A sensor network based on Cooperative spatial diversity cyclic delay diversity (CDD) and space-time (ST) block coded for distributed Multicarrier (MC) system is investigated. The distributed multi-hop network architecture makes full use of MC-CDMA frequency domain spreading properties and provides excellent spatial and frequency diversity. This scheme benefits from full diversity of orthogonal ST-block and employs CDD to increase the channel selectivity. Multi-stage CDD as proposed with low complexity implementation yields significant performance improvement as relaying network.

Our relaying scheme has the best rate when used with optimum transmit antennas configurations. Equipped with CDD, fraction of the total number of transmit antennas is used to extract the frequency (multipath) diversity, while the source and target sensor employing ST block codes provide maximum spatial diversity. The benefits provided by achieving full diversity (spatial and multipath) and increasing frequency selectivity are evaluated in terms of symbol error rate (SER) and end-to-end bit error rate (BER). Additionally fractional frame duration and transmitted power are implemented to achieve higher data transmission rates. Furthermore, Monte-Carlo simulation results are presented when compared to traditional non-distributed networks to support the analytical framework.

Chapter 7, the thesis is concluded by summarizing its contributions and also highlighting important open research directions and still-to-be-explored impact areas. We also describe how to include real-world impairments into the analysis, such as interference, etc.

### 1.4.1 Contribution to New Knowledge

The performance analysis of STBC and CDD orthogonal block coded OFDM and MC-CDMA were investigated in this thesis. In chapter 3 the closed form expressions for exact SERs of orthogonal block coded OFDM system was derived by using the frequency domain modelling of Nakagami-*m* selective channels for indoor networks ideals for relaying systems. This is an extension of [73], where the derivation was limited to frequency flat Rayleigh fading model. The analysis developed avoids the need for

complex numerical integration or lengthy Monte-Carlo simulations. By showing that a MIMO OFDM system employing STBC can be represented by an equivalent SISO model and following the unified approach for evaluating the error performance over fading channels of [76], the average error rates were derived in the form of single finite-range integral.

As the integrand contains the MGF of the instantaneous SNR of blocks codes, the exact and closed-form expressions for the average SER of *M*-ary signals were derived by transforming the single integral into higher transcendental Gauss and Appel hypergeometric) functions. In chapter 3 it was verified that a CDD OFDM system transforms the spatial diversity into frequency diversity and the receiver effectively sees the signal coming from a single antenna, hence converting an $N_{tx}$ antenna system to a single antenna with enhanced frequency selectivity of $N_{tx}L$. The channel coded error rate comparison between CDD and orthogonal block codes for simple OFDM revealed that CDD performs extremely well and becomes competitive with block codes.

Few of the major contributions of this thesis were presented in Chapter 5 and Chapter 6. These include the performances of CDD and orthogonal block coded MC-CDMA systems operating in Nakagami-*m* fading channel with correlated subcarriers for Cooperative Distributed Relaying networks. On the other hand, by using the MGF of the correlated Nakagami-*m* random variable, explicit closed-form formulas for the exact average SER of *M*-ary signals for MC-CDMA system employing diversity techniques were derived with MRC detection technique. It was shown that the frequency correlated subcarriers restricts the diversity order to $N_{tx}N_{rx}L$. Further, considering a complete MC-CDMA system with different loading conditions and respective optimum detection techniques, a comparison in terms of complexity and performance between CDD and STBC scheme was conducted.

The comparison was done for variable number of antennas relaying. It was concluded that the enhanced frequency selectivity induced by the CDD relaying provides additional coding gain when used with channel codes, which provides an alternative approach to extract frequency diversity. It may be the simplest solution to realize an excellent performance, low complexity and highly spectrally efficient MIMO architecture. The basic idea is to extract the spatial diversity with ST, whereby the presence of CDD helps

in achieving the maximum frequency diversity from the broadband channel. The Cooperative scheme achieves this goal by using an arbitrary number of transmit relaying antennas and by trading the number of cyclically delayed relaying, converts a low-delay-spread broadband channel into a highly selective one. Similarly, for high-delay-spread channels, fewer such relaying can be employed to achieve the same performance. Hence, it is interplay between the spatial and frequency diversity.

### 1.4.2 Link Level Performance and Deployment Guidelines

In order to increase data rate and reliability of wireless communication systems the implementation of Link Adaptation has been considered as a promising solution.
So far conventional link adaptation algorithms switch between different combinations of modulation/coding rates, by tracking the changing channel conditions, as a means to increase spectral efficiency. Transmitter and receiver performance were analysed by generating Bit Error Rate (BER) and Packet Error Rate (PER) curves to validate the link performance.

# Chapter 2

# Fundamentals

## 2.1 Introduction

Prior to describing the research analyses, the proposed system evaluations, and research findings, this chapter introduces the relevant theoretical background and fundamentals. Brief presentations of background on mobile wireless channel models, Rayleigh, Rician, Nakagami-m fading models that will be employed consistently in later chapters. Some transmit diversity schemes that considered most applicable to the area of research are briefly introduced below in conjunction with OFDM and MCCDMA. After having discussed the wireless channel they experience and the gains one can expect from such deployments are also reviewed in this chapter.

## 2.2 Mobile Wireless Channel

In wireless communication, the communication medium between terminals is called a mobile radio channel. Radio wave propagation through this wireless channels is a complicated phenomenon characterized by various effects, such as noise, interference, and fading. Noise is the most common form of distortion in a communication system, which results from operating temperatures of the ohmic elements in the receivers, thereby limiting its sensitivity. The degradation in cellular networks can also result from intra, inter, adjacent, and co-channel interferences which vary with frequency reuse patterns and duplexing modes. Multiple access interference (MAI) exists in multiple access networks, where multiple access networks, where multiple users share the network resources of time, frequency, code or the combination of them, to increase the number of users supported by the network. Multipath propagation of the signal caused fading in mobile radio channel. Multipath fading can be divided into two broader categories, i.e.Large-scale fading and small-scale fading [46] [47].

Large-Scale Fading is represented by the average signal power attenuation due to motion over large areas and is affected by prominent terrain contours such as hills, forests and man-made structures, clumps of buildings, etc.). The statistics of large-scale fading provide a way of computing an estimate of the average signal strength loss as a function of distance. This is described in terms of path loss and shadowing.
Path Loss: The decay of the mean signal power with distance from the transmitter it is defined as path loss. It includes all of the possible elements of loss associated with its interactions between the propagating wave and any object between the transmitter and the receive antennas. In free space, the mean signal power decreases with the square of the distance from the transmitter. In wireless channels, where often no direct LoS path exists between the transmitter and receiver, the signal power decreases with a power higher than two and is typically in the order of three to five [46] [47].

**Shadowing:** It is also caused by the obstruction of the transmitted waves by hills, building, walls, trees, etc., resulting in some paths with increased loss, while others less obstructed reaching the receiver with increased signal strength. This varying signal strength exhibit a log-normal behaviour and generally modelled by log-normal distribution [46]. Provided that the other fading (small-scale fading) components are removed by correct averaging, the effects of mean pathloss and shadowing can be noted by plotting the average signal level for different points in a propagation medium against distance, which fits into a line [47]. The slope of the line depends on the frequency used for transmission, antenna height and propagation environment.

The associated standard deviation of the large scale fading depends on the medium and has been observed to vary between 5 to 12 dB [46]. When designing communication system, a power margin is set aside to compensate for these type of fading. Small-Scale fading commonly known as multipath fading, this refers to the drastic changes in signal amplitude and phase that can be experienced as a result of small changes in spatial separation between the receiver and the transmitter. It occurs as a result of reflection, scattering and diffraction of the transmitted electromagnetic wave at natural and man-made objects. A multitude of waves arrive from many different directions with varying delays, amplitudes and phases, caused by the mobility of either the receiver, the moving objects or both, in the wireless channel. At the receiver, the superposition of these waves

result in amplitude and phase variations of the composite received wave resulting in time-variant multipath propagation.

The varying signal strength due to small-scale fading is highly sensitive even to small displacement in the order of the wavelength and may result in a totally different wave superposition. The attenuation of received signal strength caused by large-scale fading (shadowing and path loss) can be counteracted completely by power control/margins and are not considered further in this thesis. Also, the thesis considers only a single cell scenario with MAI. Next, an overview of the wireless channel is discussed with respect to multipath fading characteristics.

### 2.2.1 Time-Variant Multipath Propagation

The small-scale fading manifests itself in two mechanisms of time-variance of the channel due to motion and signal time-spreading. A statistical description of multipath channel based on Bello's model [48] has been used here to explain these mechanisms, since a deterministic description appears impossible in practice. Bello proposed the concept of wide sense stationary uncorrelated scattering (WSSUS) which treats signal variation arriving with different delays as uncorrelated and assumes that such a channel is effectively WSS in both time and frequency domains. In this case the model contains four functions; two describe the signal time-spreading (one in the time and the other in the frequency domain) and two describe the time variance of the channel due to motion (also covering both time and frequency domains). Next, these functions and the way they are connected with each other are briefly reviewed.

The mobile wireless channel is described by the time-variant channel impulse response $h(\tau,t)$, which represents the response of the channel at time $t$ due to an impulse applied at $t$-$\tau$. The Fourier transform of $h(\tau,t)$ is the time-variant channel transfer function $H(f)$. The assumption of WSS represents a channel whose fading statistics remain constant over short periods of time or small spatial distances. This makes the mean value of the channel random process independent of time and its auto correlation depending only on the time differences. In multipath propagation environments, the channel impulse response is

composed of a large number of scattered impulses received over $L$ different paths and can be expressed as [47]

$$h(\tau, t) = \sum_{l=0}^{L-1} \alpha_l e^{j(2\pi f_{D,l} t + \theta_l)} \delta(\tau - \tau_l) \tag{2.1}$$

where $\delta(\cdot)$ is the Kronecker delta function with $\alpha_l$ , $f_{D,l}$, $\theta_l$ and $\tau_l$ are the amplitude, Doppler frequency, phase and the propagation delay of the $l$th path, respectively. The Doppler frequency $f_{D,l} = \frac{v_c f_c}{c} \cos \Theta_l$ depends on the velocity $v_c$ of the receiver, the speed of light $c$, the carrier frequency $f_c$ and the angle of incidence $\theta_l$ of the $l$th path.

The correlation function of the channel impulse response is sufficient to characterize the time-variant behaviour or the fading rapidity of wireless channels. Defining the autocorrelation function as [46]

$$R(\tau_i, \tau_j, \Delta t) = \frac{1}{2} E\{h(\tau_i, t) h^*(\tau_j, t + \Delta t)\} \tag{2.2}$$

where $\Delta t$ denotes the observation time difference. Under the presumption of WSSUS, random processes $h(\tau_i, t)$ and $h(\tau_j, t)$are uncorrelated for $\tau_i \neq \tau_j$(scattering at two different paths is uncorrelated in most radio transmissions), the autocorrelation function of (2.2) simplifies to

$$R(\tau_i, \tau_j, \Delta t) = \phi(\tau_i, \Delta t) \delta(\tau_i - \tau_j) \tag{2.3}$$

where $\phi(\tau, \Delta t)$ represents the delay cross-power spectral density [2] [48], and the wireless channel characterized by (2.3) is referred to as WSSUS channel. The Fourier transform of $\phi(\tau, \Delta t)$ in $\Delta t$ yields the scattering function which provides a measure of average power output of the channel as a function of delay $\tau$ and the Doppler frequency $f_D$. The scattering function can be expressed as

$$\bar{S}(\tau, f_D) = \int_{-\infty}^{\infty} \phi(\tau, \Delta t) e^{-j2\pi f_D \Delta t} d(\Delta t) \tag{2.4}$$

By integrating (2.4) over the Doppler frequency $f_D$, the power delay density spectrum is obtained which is identical to the delay cross-power spectral density $R(\tau_i)$ at $\Delta t = 0$. This power delay density spectrum gives the average power of the channel output as a

function of the delay $\tau$ and can be viewed as a scattering function averaged over all Doppler shifts. By further assuming that $L$ paths have the normalized autocorrelation function, but different average powers and denoting the average power of $l$th paths as $P_l$, then (2.2) can be written as

$$P_l = \frac{1}{2} E\{h(\tau_l, t) h^*(\tau_\iota t)\}$$

(2.5)

where $P_l, l = 0,1,2, \ldots, L-1$ represents the power delay profile (PDP) of the channel which is characterized by excess delay, mean delay and most importantly root mean square (RMS) delay spread. The delay of any path relative to first arriving path is called excess delay, while total excess delay is also called the maximum delay spread $\tau_{max}$, represents the difference between the delay of the first and the last path. If the duration of the transmitted symbol is significantly larger than $\tau_{max}$, the channel produces the minimum of ISI. This effect is efficiently exploited in OFDM where the duration per transmitted symbol increases with the number of subcarriers and hence, the amount of ISI is reduced.

The most common and simplest approach to quantify the time-spreading of multipath channel is by using the PDP characteristic parameters in the time domain, in particular the mean delay and RMS delay spread. The PDP is described in the delay dimension to yield $L$ individual paths or taps of power $P_0, \ldots, P_{L-1}$. Mean delay which is the delay corresponding to the centre of gravity of the profile is given by

$$\tau_m = \frac{1}{P_T} \sum_{l=0}^{L-1} P_l \, \tau_l$$

(2.6)

where the total power in the channel is $P_T = \sum_{l=0}^{L-1} P_l \, P_T$.

RMS delay spread is the second moment or spread of the paths. It takes into account the relative powers of the paths as well as their delays, thereby making it a better indicator of system performance and is defined by [46]

$$\tau_{rms} = \sqrt{\frac{1}{P_T} \sum_{l=0}^{L-1} P_l \tau_l^2 - \tau_m^2}$$

(2.7)

The coherence bandwidth $B_c$ of a wireless channel measures the frequency range over which the fading process is correlated; i.e. the bandwidth over which the correlation function of two samples of the channel response taken at the same time but at different frequencies falls below a suitable value. It is inversely proportion to the delay spread $\tau_{rms}$ and defined as the bandwidth over which the frequency correlation function is above ½ and can be approximated by $B_c \approx 1/5_{\tau_{rms}}$. More specifically for a correlation level $\rho_c$, it can be expressed as [46]

$$B_c \geq \frac{1}{2\pi\tau_{rms}} \cos^{-1} \rho_c \tag{2.8}$$

Frequency selectivity, which is an important characteristic of wireless channel is determined by the coherence bandwidth. If all the spectral components of the transmitted signal are affected in a similar manner, the fading is said to be frequency non-selective or, equivalently, frequency flat. This is the case for narrowband systems in which the transmitted signal bandwidth $B$ is much smaller than the channel's coherence bandwidth $B_c$. On the other hand, if the spectral components of the transmitted signal are affected by different amplitude gains and phase shifts, the fading is said to be frequency selective. This applies to broadband systems in which the transmitted signal bandwidth $B$ is larger than the coherence bandwidth $B_c$. The coherence bandwidth also helps in evaluating the performance of spreading and frequency interleaving techniques that are used to exploit the inherent frequency diversity $G_{fq}$ of the wireless channel. In the case of OFDM based system, frequency diversity is exploited if the separation of the subcarriers transmitting the same information exceeds the coherence bandwidth. The maximum achievable frequency diversity is exploited if the separation of the subcarriers transmitting the same information exceeds the coherence bandwidth as $G_{fq} \approx B/B_c$ and consequently, depends on the delay spread $\tau_{rms}$ of the channel [24] [49].

The maximum Doppler frequency $f_{D_{max}}$ quantifies the frequency-dispersive properties of multipath channel. For OFDM, if the sub-channel spacing is significantly larger than the maximum Doppler frequency $f_{D_{max}}$, the channel produces a negligible amount of ICI. An equally important wireless channels' parameter is the channel coherence time $T_c$. This is the duration over which the channel characteristics can be considered as time invariant. $T_c$

is inversely proportional to the $f_{D_{max}}$ and can be defined as the time over which the time correlation function is above ½ and can be approximated as [50] [46]

$$T_c \approx \frac{9}{16\pi f_{D_{max}}} \tag{2.9}$$

The channel is said to be time selective, if the duration of the transmitted symbol is larger than the coherence time $T_c$. Conversely, if it is smaller than $T_c$, the channel is said to time non-selective or time flat. Time selective and non-selective channels are also referred as fast and slow (quasi-static) fading channels, respectively. The coherence time of the channel is important for evaluating the performance of FEC, channel coding and interleaving techniques that try to exploit the inherent time diversity $G_t$ of the mobile radio channel. Normally, block fading models are used for such analysis. Unlike quasi-static fading, block fading channels assume that a frame may span multiple independent fading blocks where in each block the fading remains invariant. Time diversity is exploited when the separation between successive time slots carrying the same information exceeds the coherence time $T_c$, and is approximated by the ratio between the frame duration which consists of a number of time slots and the coherence time $T_c$, given by

$$G_t \approx \frac{T_{frame}}{T_c} \tag{2.10}$$

which consequently depends on the maximum Doppler frequency $f_{Dmax}$ of the channel.

## 2.3 Modelling of Multipath Channels

Statistical characterization of wireless fading channels has remind a very important research area and considerable efforts have been devoted for the accurate modelling of such propagation environments. The results of these intense efforts provide a range of relatively simple and accurate statistical models for wireless channels which depends on the particular propagation environment and the underlying communication scenario. In this section, a review of Rayleigh, Rician and Nakagami-*m* fading models is presented. First, these models are explained for frequency flat fading channels and then extended for broadband frequency selective scenario. Finally, considering the OFDM based system, the frequency domain modelling of subject channels is also presented.

### 2.3.1 Frequency Flat Fading Channels

The signal transmitted through the wireless channel is subjected to envelop and phase distortions. Among these two distortions, the later results in severe performance degradation of coherent modulated systems unless measures are taken to compensate for them at the receiver. Conversely, non-coherent modulation does not require phase information at the receiver and the performance remains independent of phase variations for such systems.

Most often, system analysis are conducted with ideal coherent modulation which assumes perfectly corrected phase variations and only the fading envelope statistics are taken into account at the receiver. The same assumption has been invoked in this thesis. In frequency narrowband environments, the received signal is subjected to two random processes. First, it is modulated by fading path amplitude and then further corrupted by additive white Gaussian noise (AWGN). The path amplitude $\alpha$, defined in (2.1), is a random variable (RV) with the mean square value and probability density function (PDF) denoted by $\Omega = E[\alpha^2]$ and $p_\alpha(\alpha)$, respectively. AWGN is typically assumed to be statistically independent of $\alpha$ and characterized by a one-sided power spectral density of $N_0$ (Watts/Hz).

The instantaneous and average SNR can then be defined as $\gamma = \alpha^2 \frac{E_s}{N_0}$ and $\bar{\gamma} = \Omega \frac{E_s}{N_0}$, respectively, where $E_s$ is the energy per symbol. Following [51] [12], the PDF of γ can be calculated by introducing a change of variables in the fading PDF $p_\alpha(\alpha)$of $\alpha$, expressed as

$$P_\gamma(\gamma) = \frac{P_\alpha\left(\sqrt{\Omega\gamma/\bar{\gamma}}\right)}{2\sqrt{\gamma\bar{\gamma}/\Omega}} \tag{2.11}$$

with the associated moment generating function (MGF) given by

$$\Phi_\gamma(\mu) = \int_0^\infty p_\gamma(\gamma) e^{\mu\gamma} d(\gamma) \tag{2.12}$$

Next, the PDFs and MGFs of Rayleigh, Rician and Nakagami-*m* channel model are revisited.

**Rayleigh Model**

Rayleigh distribution is frequently used to model multipath fading in NLoS environments with the channel fading amplitude $\alpha$ distributed according to [57]

$$P_\alpha(\alpha) = \frac{2\alpha}{\Omega}\exp\left(-\frac{\alpha^2}{\Omega}\right) \qquad \alpha \geq 0$$

(2.13)

Using (2.11), the instantaneous SNR $\gamma$ of a Rayleigh channel is exponentially distributed and can be expressed as

$$P_\gamma(\gamma) = \frac{1}{\bar{\gamma}}\exp\left(-\frac{\gamma}{\bar{\gamma}}\right) \qquad \gamma \geq 0$$

(2.14)

and the respective MGF given by (72)

$$\Phi_\gamma(\mu) = (1 - \mu\bar{\gamma})^{-1}$$

(2.15)

**Rician Model**

Rician model is also known as Nakagami-*n*, it is usually employed to characterize propagation environments where there exists a strong LoS path with many random indirect weaker components. In this case, the channel fading amplitude $\alpha$ is distributed according to [57]

$$P_\alpha(\alpha) = \frac{2(1+n^2)e^{-n^2}\alpha}{\Omega}\exp\left(-\frac{(1+n^2)\alpha^2}{\Omega}\right)I_0\left(2n\alpha\sqrt{\frac{1+n^2}{\Omega}}\right), \quad \alpha \geq 0$$

(2.16)

where $I_0$ is the zeroth-order modified Bessel function of first kind and $n$ is the Nakagami-$n$ fading parameter ranging from 0 to ∞, which is also related to the Rician $K$ factor by $K = n^2$. The parameter $K$ represents the ratio of the power received in the LoS path to the total power received via indirect scattered paths. Using (2.11), the instantaneous SNR $\gamma$ of a Rician channel is non-central chi-square distributed and given by

$$P_\gamma(\gamma) = \frac{(1+n^2)e^{-n^2}}{\bar{\gamma}}\exp\left(-\frac{(1+n^2)\gamma}{\bar{\gamma}}\right)I_0\left(2n\sqrt{\frac{1+n^2\gamma}{\bar{\gamma}}}\right), \quad \gamma \geq 0$$

(2.17)

with the corresponding MGF and fading figure expressed as

$$\Phi_\gamma(\mu) = \frac{(1+n^2)}{(1+n^2)-\mu\bar{\gamma}} \exp\left[\frac{n^2\mu\bar{\gamma}}{(1+n^2)-\mu\bar{\gamma}}\right]$$

(2.18)

$$AF_n = \frac{1+2n^2}{(1+n^2)^2}, \qquad n \geq 2$$

(2.19)

**Nakagami-*m* Model**

This fading model, introduced by Nakagami in [53], has received considerable attention due to its great versatility in terms of flexibility and accuracy in providing a better match to various empirically obtained measurement data than Rayleigh or Rician distributions. It is often gives the best fit to land, indoor-mobile multipath propagation as well as scintillating ionospheric radio links [54] [51]. The Nakagami-*m* PDF is in essence a central chi-square distribution given by [53]

$$P_\alpha(\alpha) = \frac{2}{\Gamma(m)}\left(\frac{m}{\Omega}\right)^m \alpha^{2m-1}\exp\left(-\frac{m}{\Omega}\alpha^2\right), \quad \alpha \geq 0$$

(2.20)

where $\Gamma(\cdot)$ is the Euler Gamma function and $m$ is the Nakagami-*m* fading parameter ranging from 0 to ∞. Using (2.11), the instantaneous SNR $\gamma$ of a Nakagami-*m* channel is gamma distributed and given by

$$P_\gamma(\gamma) = \frac{1}{\Gamma(m)}\left(\frac{m}{\bar{\gamma}}\right)^m \gamma^{m-1}\exp\left(-\frac{m\gamma}{\bar{\gamma}}\right), \qquad \gamma \geq 0$$

(2.21)

with the corresponding MGF is expressed as

$$\Phi_\gamma(\mu) = \left(1-\frac{\mu\bar{\gamma}}{m}\right)^{-m}$$

(2.22)

The fading figure and $m$ parameter are related by

$$m = \frac{1}{AF_m} = \frac{\Omega^2}{E[\alpha^2-\Omega^2]}, \qquad m \geq \frac{1}{2}$$

(2.23)

The Nakagami-*m* PDF is plotted for various values of $m$ parameter with $\Omega = 1$.This distribution, with the flexibility of $m$ parameter, spans the widest range of fading figure from 0 to 2. As special cases, it includes the one-sided Gaussian and Rayleigh distribution for $m = 1/2$ and $m$=1 respectively. For the limit as $m \longrightarrow +\infty$, $m$=1, the Nakagami-*m* fading channel converges to a non-fading AWGN channel. Furthermore, when $m$ >1,

equating (2.19) and (2.22), the Nakagami-*m* distribution gives a one-to-one mapping between the *m* parameter and the *n* parameter (equivalently, the Rician *K* factor), making it possible to closely approximate the Rician distribution.

This mapping can be expressed as

$$m \approx \frac{(1+n^2)^2}{1+2n^2}, \quad n \geq 0, \qquad n \approx \sqrt{\frac{\sqrt{m^2-m}}{m-\sqrt{m^2-m}}}, \quad m \geq 1 \tag{2.24}$$

### 2.3.2 Frequency Selective Fading Channels

In broadband environment, the spectrum of the signals is affected by the channel transfer function as they propagate through the frequency selective channel.

Selective fading can be modelled by the equivalent impulse responses of (2.1). Assuming the slow fading channels, in which the *L* multipaths remain constant over a period of time, thus making the path amplitudes $\{\alpha_l\}_{l=0}^{L-1}$, phases, $\{\theta_l\}_{l=0}^{L-1}$ and delays $\{\tau_l\}_{l=0}^{L-1}$ constant over a symbol interval. Thanks again to WSSUS and considering the fact that in realistic environments, often the different paths of a given impulse response are originated by different scatters, exhibiting negligible correlations and making it reasonable to model all $\{\alpha_l\}_{l=0}^{L-1}$ paths as statistically independent RVs.

This modelling makes it straightforward to extend the flat fading notations of section 2.3.1 by assuming the *l*th resolvable path amplitude $\alpha_l$ an RV with mean-square value $\Omega_l = E\lfloor \alpha_l^2 \rfloor$, PDF $p_{\alpha_l}(\alpha_l)$ and can be from any one of the Rayleigh, Rician or Nakagami PDFs. Extending the flat fading analysis, the instantaneous and average SNR per symbol of the *l*th multipath in the frequency selective scenario can be expressed by $\gamma_l = \alpha_l^2 \frac{E_s}{N_o}$, respectively.

The channels PDP is typically a decreasing function of delay and directly related to $\{\Omega_l\}_{l=0}^{L-1}$. It can assume various forms depending on propagation conditions and whether the model is for indoor or outdoor environments. Generally, it can be represented by $\Omega_l = \Omega_0 e^{-l\delta}$ where $\delta \geq 0$ is the rate of average power decay and $\Omega_0$ is the average power of the first multipath (tap).

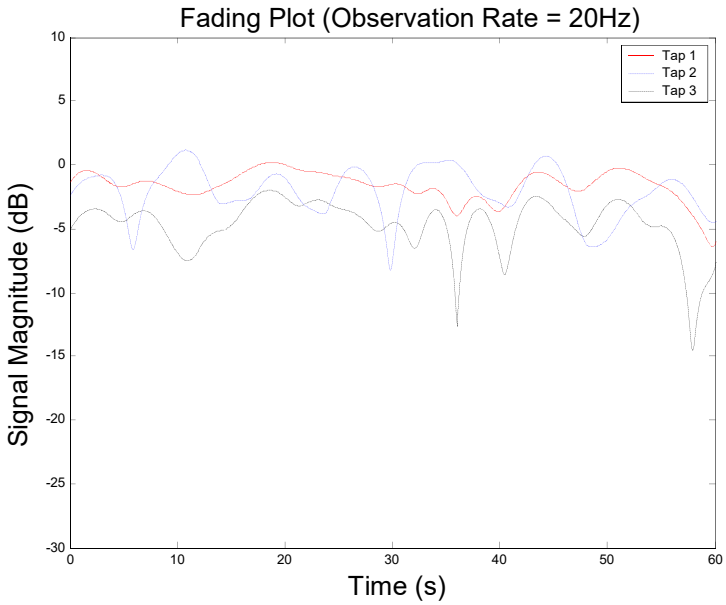


a) Example of a frequency selective fading channel.

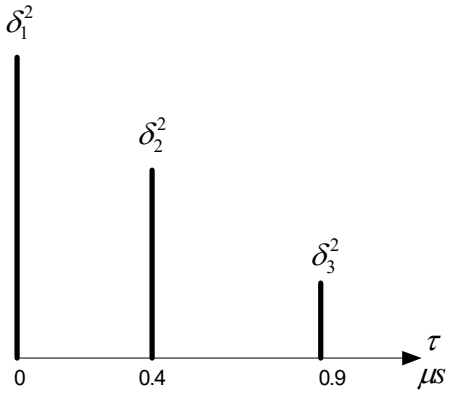


. (b) Corresponding delay domain channel impulse response.

Figure 2.1 Example of a frequency selective fading channel and channel impulse responde.

### 2.3.3 Frequency Domain Nakagami-m Channel Modelling

For the performance analysis of OFDM based systems, it is necessary to derive the statistics of the multipath channel in the frequency domain. The frequency domain modelling of Nakagami-*m* has been presented in [52] [55] [56]. In [52], it is shown that

the channel frequency response can be well approximated by Nakagami-*m* random variables (RVs) with frequency domain fading parameter $m_f$ and mean power $\Omega_f$, which, in general, are different from their time domain counterparts $m$ and $\Omega$, respectively. Although, for the special case of Rayleigh ($m$=1), both time and frequency domain fading remains the same.

Considering the time-domain channel impulse response of (2.1), each path amplitude $\alpha_l$ can be represented by a Nakagami-*m* RV and the pdf can be expressed by including the path index $l$ to the expression of (2.20). The modified PDF becomes

$$P_{\alpha_l}(\alpha_l) = \frac{2}{\Gamma(m_l)}\left(\frac{m_l}{\Omega_l}\right)^{m_l} \alpha_l^{2m_l-1}\exp\left(-\frac{m_l}{\Omega_l}\alpha_l^2\right), \quad \alpha \geq 0 \tag{2.25}$$

In an OFDM-based system, the $N$-point discrete Fourier transforms (DFT) of the channel frequency response at the $k$th subcarrier can be expressed as

$$H(k) = \frac{1}{\sqrt{N}}\sum_{l=0}^{L-1} \alpha_l e^{-j2\pi kl/N} \tag{2.26}$$

which confirms that the channel frequency responses at each subcarrier are the DFT of the same impulse responses and hence, correlated in frequency. Now, based on the original derivations of [53] [57], it can be shown that $\beta(k) = |H(k)|$also approximately follows the Nakagami-*m* distribution with the pdf

$$P_\beta(\beta) = \frac{2}{\Gamma(m_f)}\left(\frac{m_f}{\Omega_f}\right)^{m_f} \beta^{2m_f-1}\exp\left(-\frac{m_f}{\Omega_f}\beta^2\right), \quad \beta \geq 0 \tag{2.27}$$

and the frequency domain fading parameter $m_f$ and mean power $\Omega_f$ given by

$$m_f = \frac{(\sum_{k=0}^{L-1}\Omega_k)^2}{\sum_{k=0}^{L-1}\left(\frac{\Omega_k^2}{m_k}\right) + \sum_{k=0}^{L-1}\sum_{l=0,l\neq k}^{L-1}\Omega_k\Omega_l} \tag{2.28}$$

$$\Omega_f = \frac{1}{N}\sum_{k=0}^{L-1}\Omega_k \tag{2.29}$$

Assuming equal fading parameters for all paths $(m_l = m)$and exponential PDP, (2.28) and (2.29) simplify to

$$m_f = \frac{1}{\left(\frac{1}{m} - 1\right)\left(\frac{1 - e^{-2L\delta}}{1 - e^{-2\delta}}\right)\left(\frac{1 - e^{-\delta}}{1 - e^{-L\delta}}\right)^2 + 1} \tag{2.30}$$

$$\Omega_f = \frac{1 - e^{-L}}{1 - e^{-\delta}}\left(\frac{\Omega_0}{N}\right) \tag{2.31}$$

From the above, it can be summarized:

- for constant PDP with $\delta = 0$ the frequency domain fading parameters become $m_f = \left(\frac{Lm}{Lm - m +}\right)$ and $\Omega_f = \left(\frac{L}{N}\right)\Omega$
- for flat fading with $\delta = \infty$ and $m_f = m$ and $\Omega_f = (1/N)\Omega$ when $m$<1, then $m \leq m_f < 1$ and when $m > 1$, then $1 \leq m_f < m$.
- finally, for Rayleigh fading case $m = m_f = 1$, i.e., Rayleigh fading in the time domain always yields Rayleigh fading in the frequency domain.

## 2.4 OFDM Data Structure & Detection

Parallel data transmission, commonly known as multi-carrier (MC) communication provides an effective approach to prevent ISI. The principle of MC modulation, as shown in Fig.2.2, is to convert a high rate data stream into *N* low rate substreams, where *N* is the number of subcarriers used for data transmission. Each substream is modulated on its assigned subcarrier $f_k, k = 0, \ldots, N - 1$ which divide makes the available channel bandwidth subdivided into *N* successive narrow sub-channels that appear frequency flat.

The data symbol rate per subcarrier is reduced to a factor proportional to the number of assigned subcarrier and with that the effect of delay spreads and consequently ISI, Significantly decreases, thereby reducing the complexity of equalizers. FDM is the most common realization of MC communication as [58] where the subchannels are completely separated in frequency domain and ICI is controlled by ensuring the subchannels spacing greater than the Nyquist bandwidth [24]. However, this complete frequency separation leads to inefficient use of available spectrum. OFDM provides an effective and profitable

bandwidth utilization solution by allowing the spectrum to overlap between adjacent subchannels.

It employs rectangular pulse shaping with the subcarrier, thereby maintaining the orthogonality between them. In wireless environments, one of the main design goals for an OFDM system is that the channel can be considered as time-invariant during one OFDM symbol and the fading per subcarrier can be considered as flat. This condition can only be fulfilled if the OFDM symbol duration is smaller than the coherence time of the channel and the subcarrier spacing smaller than the coherence bandwidth. If these conditions are fulfilled, the realization of low complexity receivers become possible.

An OFDM modulator takes $N$ serial source symbols to produce a sequence $S(k) = k = 0, \dots, N-1$. The source symbols may, for instance, be obtained after source and channel coding, time-interleaving and appropriate symbol mapping. These source symbols of rate $1/T$ and then placed on $N$ parallel substreams, where $T$ is the individual symbol duration.

By doing so, the rate per substream reduces to $1/T_s = 1/NT$, where $T_s = NT$ is the OFDM symbol duration with the respective OFDM symbol rate given by $1/T_s$. Throughout the thesis, frequency domain variables like the source symbols $S(k), k = 0, \dots, N-1,$ are written with capital letters. Also, for brevity but without loss of generality, the transmission of a single but arbitrary sequence $S(k)$ is considered in this section, so that no additional time index is required. The reason being the isolated assumption of $S(k)$ becomes valid, since ISI and ICI can be avoided with OFDM. These parallel substreams are then modulated on $N$ subcarriers with a spacing of $f_s = 1/T_s$ which provides spectral overlap as well as orthogonality between the signals. The complex envelope of an OFDM symbol with rectangular pulse shaping can be expressed as [59] [49]

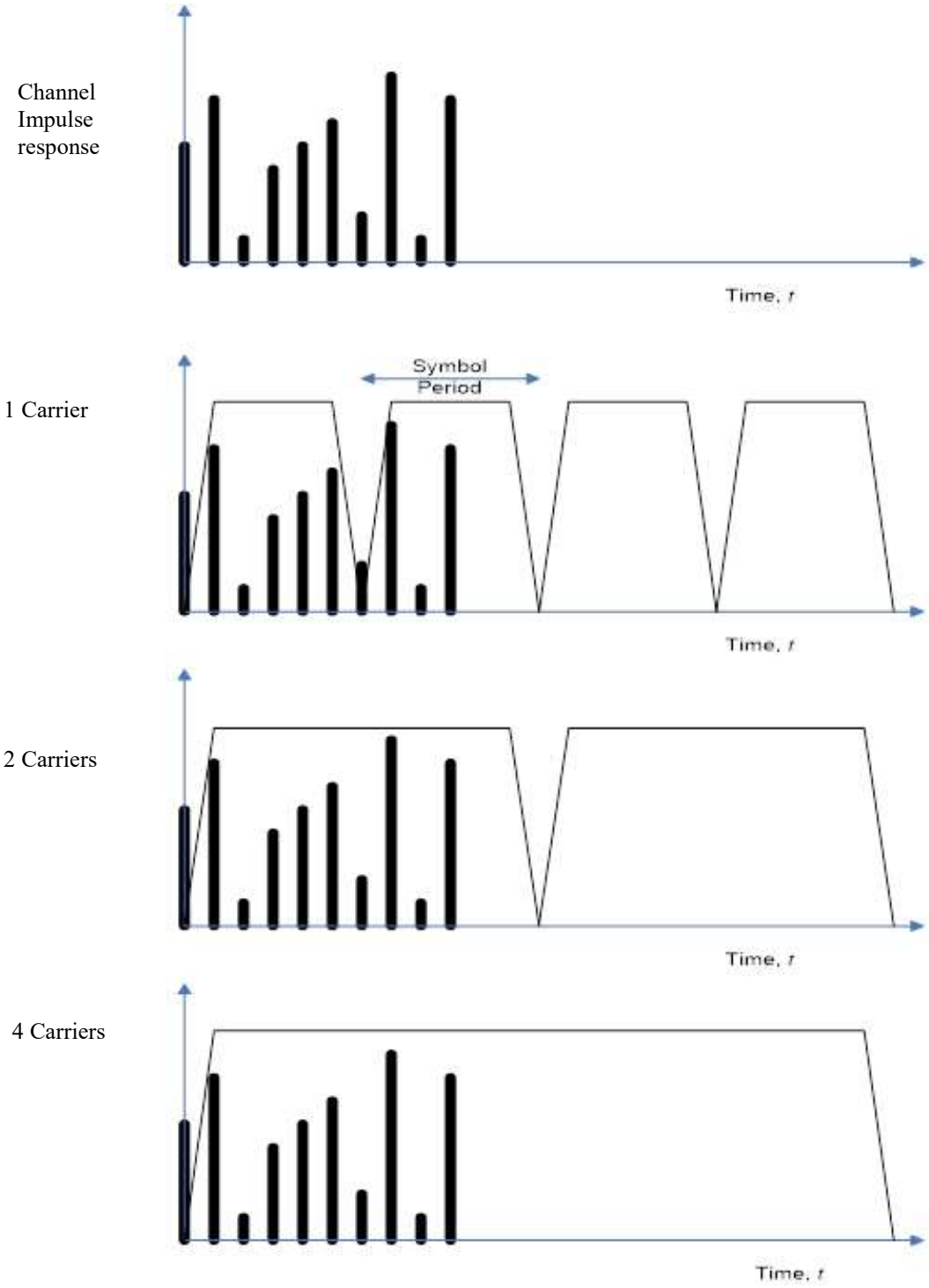


Figure 2.2. Principle of multicarrier modulation

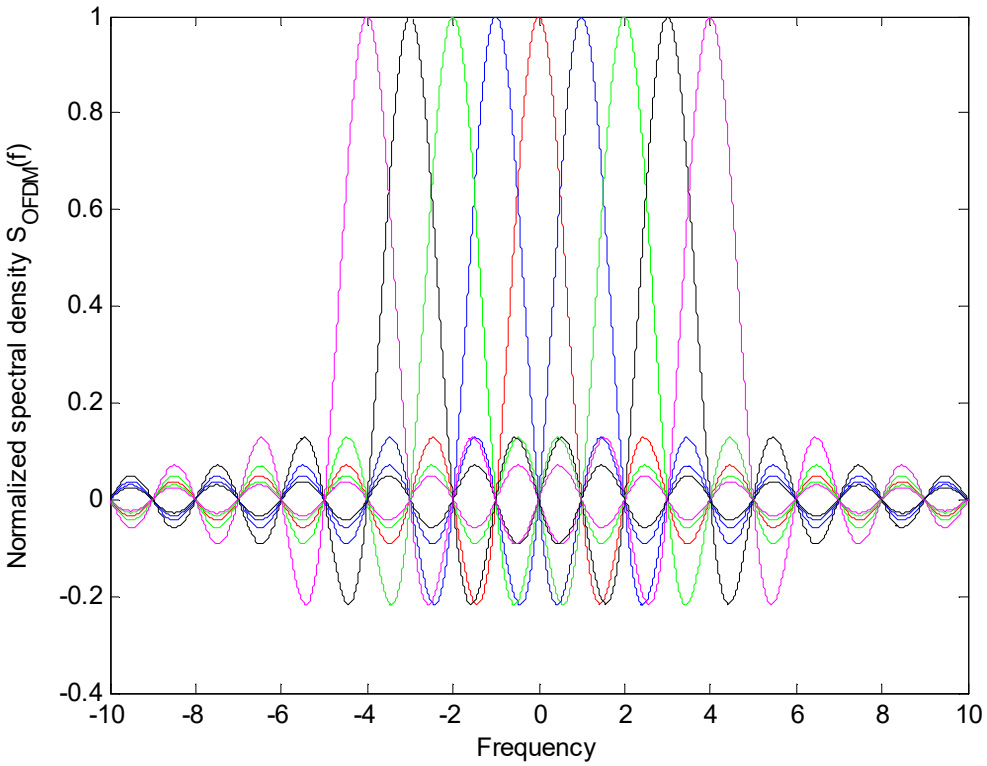


Figure 2.3 Normalized energy density spectrum of an OFDM symbol versus the normalized frequency $f_T$

$$s(t) = \frac{1}{\sqrt{N}} \sum_{k=0}^{N-1} S(k) \text{rect}\left(\frac{t}{T_s} - \frac{k}{2}\right) e^{j2\pi f_k t} \tag{2.32}$$

where $1/\sqrt{N}$ is the energy normalization factor and the subcarrier frequencies at positions

$$f_k = \frac{k}{T_s}, \qquad k = 0, \ldots, N-1 \tag{2.33}$$

with the centre of the frequency spectrum being located at $(N-1)/2T_s$. The energy density spectrum $|X(f)|^2$ of an OFDM symbol is the sum of the energy density spectra of $N$ independently modulated subcarriers, given by

$$|X(f)|^2 = \frac{1}{N} \sum_{k=0}^{N-1} \left| S(k) T_s \frac{sin(\pi(f - f_k)T_s)}{\pi(f - f_k)T_s} \right|^2 \tag{2.34}$$

and shown in Figure 2.3, versus the normalized frequency $f_T$ with $N$=9 subcarriers.

This spectrum is generated with the symbols $S(k), k = 0, \ldots, 7$ being transmitted.

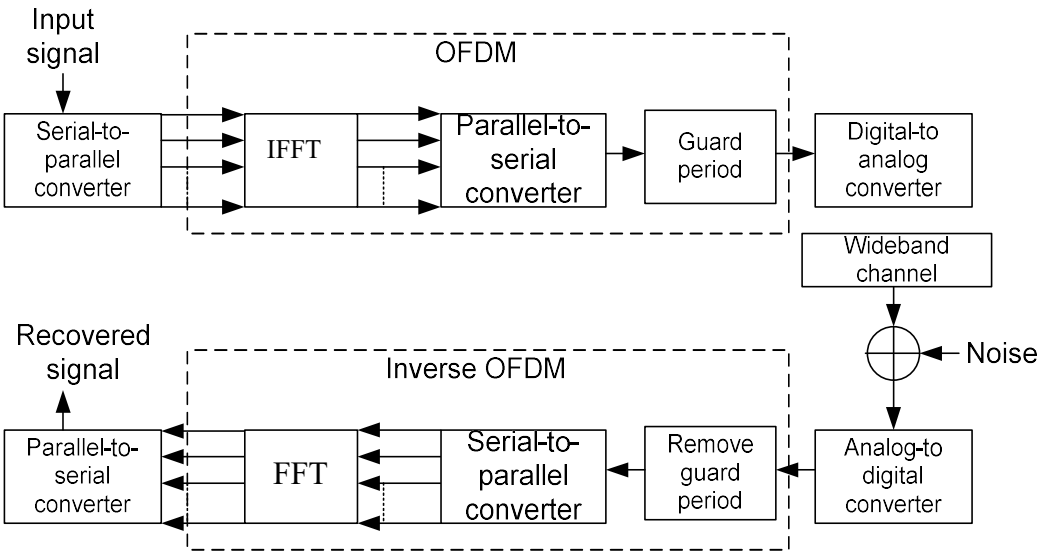


Figure 2.4 OFDM system model.

One of the major breakthroughs that made OFDM highly attractive in the present era is its implementation in the discrete domain by using the inverse discrete Fourier transform which is more computationally efficient, inverse fast Fourier transform (IFFT) [25]. The block diagram of an OFDM modulator employing IFFT and the respective demodulator equipped with FFT is shown in Figure 2.3 Figure. 2.4. If the complex envelop $s(t)$ of (2.32) is sampled at time $t = nT_s/N$ for $n$=0,…, $N$-1 $n = 0, \ldots, N-1$ with the sampling rate $N/T_s$, then the resulting samples can be expressed as

$$s(n) = \frac{1}{\sqrt{N}} \sum_{k=0}^{N-1} S(k) e^{j2\pi kn/N}, \qquad n = 0, \ldots, N-1 \tag{2.35}$$

which shows that the sampled sequence $s(n)$, $n$ =0,…,$N$-1 is the IFFT of the source symbol sequence $S(k)$; $k$ = 0,..,$N$-1. As the number of subcarrier increases, the OFDM symbol duration $T_s$ becomes large compared to the maximum delay spread $\tau_{max}$ of the channel and with that, the amount of ISI reduces. The complete elimination of ISI and perfect orthogonality (zero ICI) between all signals on the $N$ subcarriers is achieved by introducing a guard interval of duration $T_g \geq \tau_{max}$ between the adjacent OFDM symbols [47]. The guard interval is actually a cyclic prefix (CP) added to each OFDM symbol and obtained by extending the duration of an OFDM symbol to $T_s' = T_g + T_s$. The discrete length of the CP has to be $L_g \geq \lceil \tau_{max} N/T_s \rceil$ samples to prevent ISI.

The sampled sequence $s(n)$ with the addition of CP can be represented by

$$s(n) = \frac{1}{\sqrt{N}} \sum_{k=0}^{N-1} S(k) e^{j2\pi kn/} \quad , \qquad n = -L_g, -L_g + 1, \dots, N-1$$

(2.36)

and passed through a digital to analogue (DA) converter whose output ideally should be the signal waveform $s(n)$ given in (2.35) with the extended OFDM symbol duration $T_s'$. The waveform passes through the wideband channel and then further perturbed by the noise at the receiver. Invoking central limit theorem, this noise which contains the inherent disturbances of transmission system is modelled as AWGN [47]

The received signal is then down-converted with an analogue to digital (AD) converter and after the removal of first $L_{cp}$ samples that is corrupted by ISI of each OFDM symbol, the rest of received signal is fed to the OFDM demodulator for DFT/IFFT operation. With complete elimination of ICI and ISI, the received FFT operated signal, $Y(k); k = 0, \dots, N-1$ can be considered separately for each subcarrier and can be represented as [49].

$$Y(k) = H(k)S(k) + Z(k), \qquad k = 0, \dots, N-1$$

(2.37)

where $H(k)$ is the frequency response on the $k$th subcarrier given in (2.26) and $Z(k)$ represents AWGN with the real and imaginary components assumed to be statistically independent Gaussian distributed RVs having zero mean and equal variance of $\sigma_{Z(k)}^2 = E[|Z(k)|^2]$ for $k = 0, \dots, N-1$.

In Figure. 2.4, using the expression of (2.37) the OFDM system is shown by an equivalent simplified model as a discrete time-frequency transmission system with a set of $N$ parallel channels with different complex-valued attenuation factors. Based on this simplified model (2.37) can be represented in the matrix-vector notation as

$$\mathrm{y} = \mathrm{Hs} + \mathrm{z}$$

(2.38)

when the transmitted signal **s**, received signal **y** and AWGN column vectors **z** are given by $\mathbf{s} = [S(0), S(1), \dots, S(N-1)]^T$, $\mathbf{y} = [Y(0), Y(1), \dots, Y(N-1)]^T$, $\mathbf{z} = [Z(0), Z(1), \dots, Z(N-1)]^T$, respectively. Also, the interference free $N \times N$ diagonal channel matrix **H** is given by

$$H = \begin{bmatrix} H(0) & 0 & \cdots & 0 \\ 0 & H(1) & \cdots & 0 \\ \vdots & \vdots & \ddots & \vdots \\ 0 & 0 & \cdots & H(N-1) \end{bmatrix} \tag{2.39}$$

From (2.38), it can be seen that the equalization required in frequency selective channels can simply be achieved by one complex-valued multiplication per subcarrier, which becomes the major motivation for using OFDM in broadband environments where the realization of bandwidth efficient systems supporting simple receiver structures become possible. However, like any other transmission method, the advantages obtained from employing OFDM are also associated with some drawbacks. Although not in the scope of this thesis, some of these major implementation issues are briefly highlighted below

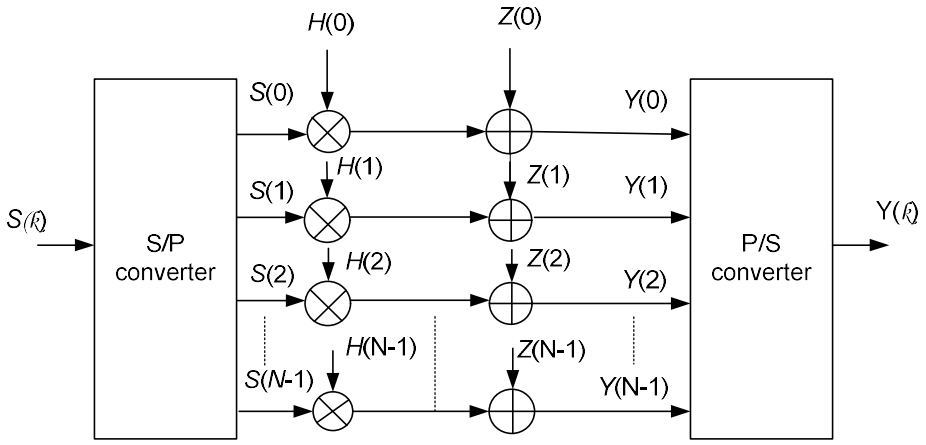


Figure 2.5 Simplified OFDM system model

**Peak-to-Average-Power Ratio (PAPR):**

For wireless applications, efficient power amplification is essential for adequate area coverage and enhanced battery life. Since the OFDM symbols are composed of independently modulated sine waves giving the envelope a Gaussian distribution. This results in high PAPR and puts high demands on linear amplifiers. For an OFDM signal with $N$ subcarriers, PAPR of the transmitted signal has been shown to be $N$ [49]. Hence for $N = 256$ only, PAPR becomes as high as 24 dB and when passed through a non-linear power amplifier, the signal may suffer significant spectral spreading and in-band distortion. To tackle PAPR conventional approaches such as using linear amplifiers or to back off the operating point of a certain type of nonlinear amplifiers result in significant

power efficiency penalties. PAPR reduction techniques has remained an active and important area of research.

Schemes ranging from pre-distortion of the transmitted signal with complementary nonlinearity to simple and some very systematic data encoding strategies on OFDM subcarriers were presented. Also, in context to combined spread spectrum and OFDM systems, new set of spreading codes have been proposed to reduce PAPR. An extensive review and possible measures for reducing PAPR can be found in [49] [60].

**Time & Frequency Synchronization:** Sensitivity to synchronization errors is one of the main OFDM problems. It is of vital importance in all OFDM systems that orthogonality between subcarriers is maintained. When this orthogonality is compromised, energy from one subcarrier leaks onto an adjacent subcarrier which ultimately results in erroneous symbol retrieval. The investigation of synchronization errors is not part of this thesis and the related work can be found in the references within [61].

**Reduced Spectral Efficiency:** The addition of CP or the guard period to OFDM symbols results in the loss of data rate. Typical values are around 20%. However, single carrier systems face a similar reduced spectral efficiency due to pulse shaping with filter roll-offs of finite steepness [13] [49]. Therefore, with respect to the interference free data detection, mostly a 20% reduced data rate is considered to be a good compromise. Yet again, to reduce the loss in data rates, techniques such as impulse response shortening have been proposed [62].

When one OFDM block is sent, the last $L_g$ OFDM symbols at the end of the first block depicted by the red shaded areas in [49], will overlap the subsequent block thus distorting the first $L_g$ symbols of the subsequent block as denoted in [62].

### 2.5 MC-CDMA Signal Structure & Data Detection

The success of OFDM in broadcast applications motivated many researchers around the world to investigate the suitability of MC and in particular, OFDM for broadband mobile communications networks and several novel MC based spread spectrum techniques were proposed [63][66]. In general, spread spectrum signals are characterized by the multiple

repetition of each data symbol which is achieved by multiplication with a high rate spreading code in either time, frequency or both domains. The time domain spreading typically employs adjacent time slots to transmit the data modulated chips of a spreading code. In contrast, frequency domain spread spectrum systems provide greater design flexibility by transmitting the data modulated chips of the spreading sequence on not necessarily neighbouring subcarriers.

Apart from the single carrier direct sequence CDMA (SC DS-CDMA) system which employs time domain DS spreading, the two main MC based techniques are MC-CDMA [63][65] and MC DS-CDMA [67]. The former spread the data only in the frequency domain, while the latter incorporates both time and frequency domain spreading. Multi-tone CDMA (MT-CDMA), which is a variant of MC DS-CDMA, was also presented in [66]. A detailed overview and comparison of these techniques can be found in the excellent contributions by Hara and Prasad [68] and Yang and Hanzo [69]. Both MC-CDMA and MC DS-CDMA mitigates the degradation due to severe multipaths with the help of OFDM. Typically in a MC-CDMA system, flat fading is maintained on each subcarrier which ensures no ISI as well as any impairment of the subcarrier auto-correlation. Hence, the number of users supported by the system remains independent of the correlation characteristics of the spreading codes. Conversely, in MC DS-CDMA, the DS spread subcarriers are subjected to frequency selective fading which makes the total number of users supported by the system not only dependent on the time and frequency domain spreading but also on the auto and cross correlation characteristics of the codes [69].

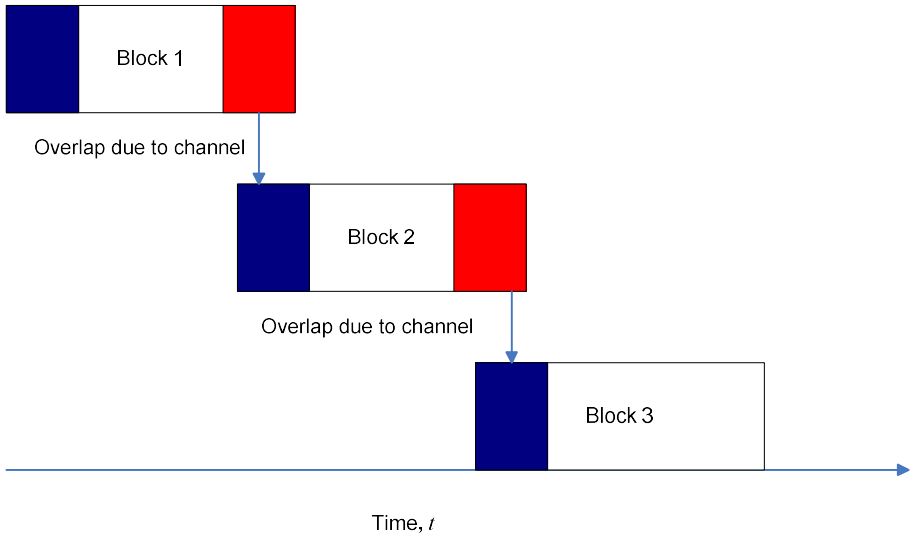


(a)

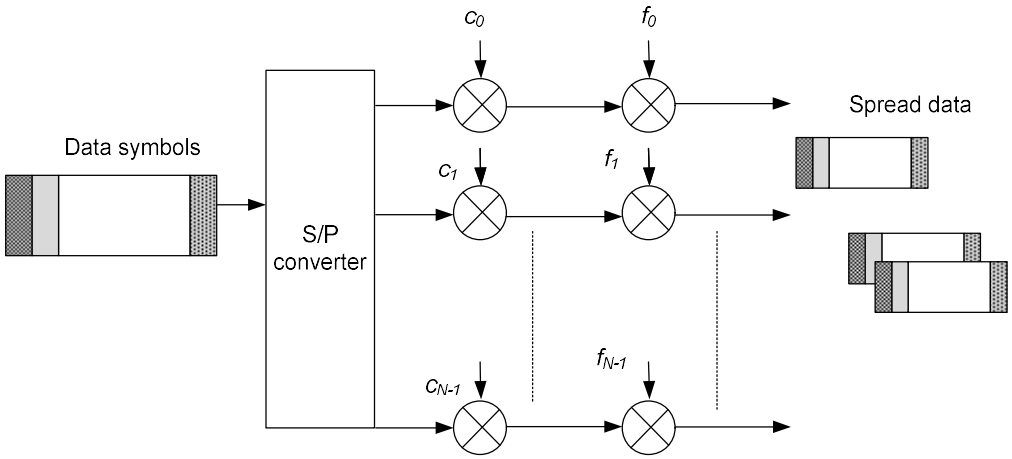


(b)

Figure 2.6 MC-CDMA systems.(a) Graphical example of interblock interference. (b) Principle of spreading of single user data by MC-CDMA

Moreover, the frequency selective fading per subcarrier requires multi-finger Rake receivers for MC DS-CDMA system, thereby increasing the complexity and making it less attractive then MC-CDMA. In short, the simple but flexible structure of MC-CDMA system uses spread and coded signals over parallel subcarriers, thereby guaranteeing symbol detection and making full advantage of frequency diversity. All these characteristics makes it one of the most promising multi-access schemes for future cellular networks.

The principle of MC-CDMA for a single user is shown in Figure. 2.6, representing the serial concatenation of DS spreading and MC modulation. The high speed data stream is first spread and then OFDM modulated in such a way that the chips of the spread data symbols are transmitted in parallel on different subcarriers. If the number of subcarriers is equal to the spreading code length which is the case in Figure. 2.6, MC-CDMA requires the total bandwidth for the transmission of a single data symbol. Each data symbol is copied on $N$ substreams before multiplication with one chip of the spreading code per substream. This frequency domain spreading offers additional flexibility by making signal reconstruction simple and less complex at the receiver.

The block diagram of a synchronous downlink MC-CDMA system model is shown in Figure. 2.6 b. The same model holds for the $u$th user in the uplink scenario due to the

absence of other users' signals. The number of users supported by the system is and restricted by$U \leq G$, where $G$ is the spreading factor (SF). The equiprobable source data stream of the $u$th user is modulated and mapped as symbols selected from the $M$-ary phase shift keying ($M$-PSK) or $M$-ary quadrature amplitude modulation ($M$-QAM) signal constellation. The source stream may, for instance, be obtained after source and channel coding, time-interleaving, etc. The processing gain of a MC-CDMA system is defined as $G = N/P$ where $P$ represents the number of symbols that a user may transmit during a signalling interval. The modulated symbols are converted into $P = N/G$ parallel streams, or in order words each symbol is copied SF times and multiplied with the spreading code (Walsh-Hadamard) of the $u$th user which makes the chip rate $G$ times higher than the data symbol rate. In the downlink case, the other users are spread by their specific sequences and the resulting spread chips of all $U$ users are added synchronously and modulated by an $N$ point IFFT. Finally, to mitigate the hostile effects of multipath fading, a CP is added between each MC-CDMA symbol and thereafter the signal is transmitted after up-conversion.

Ignoring the CP, the IFFT modulated data can be expressed as

$$s(t) = \sqrt{E_c} \sum_{u=0}^{U-1} \sum_{p=0}^{P-1} \sum_{g=0}^{G-1} b_p^u c_g^u e^{j\frac{2\pi}{T}(gP+p)t} \tag{2.40}$$

where $E_c$ is the energy per OFDM symbol, and $E_c = E_s = N$, where $E_s$ is the energy per symbol before spreading. $T$ is the signalling interval during which $P$ symbols per user are generated $b_p^u$ and $c_g^u$ are the $p$th symbol and $g$th chip of the $u$th user, respectively.

For analytical convenience and simplicity, if $P = 1$ is considered, i.e. only a single data symbol $b^u$ for each user $u$, then this assumption makes $G = N$. Based on this assumption, the simplified MC-CDMA system block diagram is shown in Figure. 2.7, where $F_N^H$ and $F_N$ are the IFFT and FFT matrices, respectively.

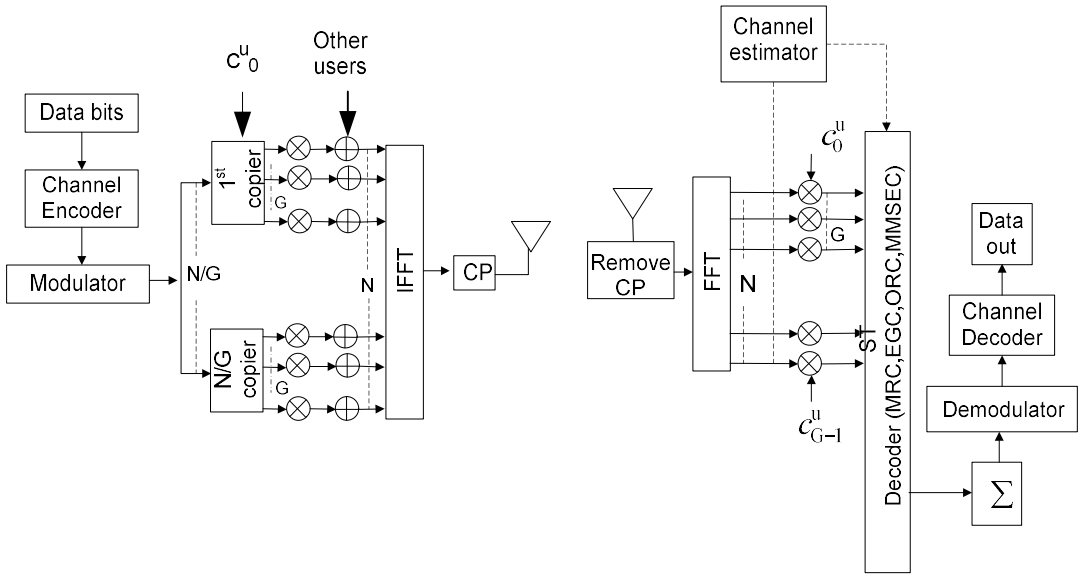


Figure 2.7 Simplified MC-CDMA system model (downlink).

At the receiver, after the removal of CP and subsequent FFT processing the received signal is subjected to despreading and detection. Ignoring the assumption of $P = 1$ for the time being, the fact that the $p$th symbol of user $u$ is detected independently from the $p'$ symbols, where $p \neq p'$ for all users. Thus, without loss of generality, the subscript $p$ can be omitted altogether for (2.40) and the $G = N$ subcarriers conveying the same symbol can be considered for detection. This validates the assumption of (2.39) and the received signal at the $k$th subcarrier can be expressed as

$$Y(k) = \sqrt{E_c} \sum_{u=0}^{U-1} b^u c^u(k)\, H^u(k) + Z(k) \tag{2.41}$$

where $Z(k)$ is the discrete AWGN term and the user index $u$ in the channel transfer function $H^u(k)$ in (2.26) differentiates between the uplink and downlink scenarios; as in the uplink case, the received signal is the sum of the signals of different users passing through different channels, depending on the location of the users. By assuming $G = N$, $E_c$ is the energy per subcarrier or chip. The decision variable $d^{u'}$ of the $u'$th user's symbol can be expressed as [68]

$$d^{u'} = \sum_{k=0}^{N-1} q(k)\, c^{u'}(k) Y(k) \tag{2.42}$$

where $q(k)$ is a frequency domain equalization gain factor which varies with the employed single and multiuser diversity combining/detection schemes. Using (2.41) in (2.42), the decision variable $d^{u'}$ can be divided into desired signal ($DS$), MAI and noise term ($\eta$), expressed as $d^{u'} = DS + MAI + \eta$, where the individual terms are given by

$$DS = \sqrt{E_c} b^{u'} \sum_{k=0}^{N-1} H^{u'}(k) q(k) \tag{2.43}$$

$$I_{MAI} = \sqrt{E_c} \sum_{u \neq 0, u \neq u'}^{U-1} b^u \, b^u \sum_{k=0}^{N-1} c^u(k) c^{u'}(k) H^u(k) q(k) \tag{2.44}$$

$$\eta = \sum_{k=0}^{N-1} c^{u'}(k) \, Z(k) q(k) \tag{2.45}$$

If $N$ is assumed to be large and spreading codes and users' bits to be random, the MAI can be modelled as additive zero mean Gaussian by invoking the central limit theorem. Since both the MAI and $\eta$ are independent and Gaussian, the sum of these is also a zero mean Gaussian process with the variances $\sigma_{MAI}^2$ plus $\sigma_\eta^2$ [60]. The instantaneous SNR for MC-CDMA is thus obtained as

$$\gamma = \frac{(DS)^2}{\left(\sigma_{MAI}^2 + \sigma_\eta^2\right)} \tag{2.46}$$

The gain factor $q(k)$ determines the performance of the MC-CDMA system. These equalization/combining methods are extensively covered in [49] [60] [68]. Next, a brief review of some of the single user detection schemes is presented which fall within the scope of this thesis.

**Maximum Ratio Combining (MRC):** This scheme is, in general, the optimum diversity combining technique with respect to BER [87]. In MRC, a stronger signal which is always more reliable than its weaker counterparts, is assigned a higher weight and the diversity

branches are weighted by their respective complex conjugate channel coefficients. For MRC, the equalization gain factor of (2.42) can be expressed as

$$q(k) = H^*(k) \tag{2.47}$$

MRC provides the best performance for a single user case, since the absence of MAI builds the optimal combining scenario. Thus, for $U = 1$, the BER with MRC is identical to the matched filter (MF) bound which is the lower bound of the bit error probability of any data detector[87]. For this reason, MRC is often used to determine
the lower bound on the performance of multi-access systems.

**Equal Gain Combining (EGC):** In contrast to MRC, this combining scheme attempts to correct the channel induced phase rotations leaving the faded amplitudes uncorrected [60]. It weights all diversity branches i.e., the number of subcarriers for a MC-CDMA system. The equalization gain factor of (2.42) can be expressed as

$$q(k) = \frac{H^*(k)}{|H(k)|} \tag{2.48}$$

and with that, the enhanced MAI caused by (2.43) can be avoided.

**Orthogonality Restoring Combining (ORC):** Also known as zero forcing (ZF) for channel inversion equalization. It targets to completely eliminate the MAI by restoring the orthogonality between the spreading codes. For ORC, the equalization gain factor of (2.42) becomes

$$q(k) = \frac{1}{H(k)} \tag{2.49}$$

which corresponds to the inverse of the assigned channel coefficients [47] .The associated drawback of ORC is that for small amplitudes of channel coefficients the noise is pronounced and may ultimately force SNR to go to zero on some subcarriers [49]

**Minimum Mean Square Error (MMSE) Combining:** MMSE is the optimal equalization method for a fully loaded MC-CDMA system [68] Equalization according to MMSE criterion minimizes the mean square value of error between the transmitted signal and the output of the equalizer. The mean square error is minimized by using the orthogonality rule which states that the mean square error can be minimized, if the

combiner/equalizer coefficients are selected in such a way that the error is orthogonal to the received signal [49]. The equalization coefficients of (2.42) based on MMSE criterion can be expressed as

$$q(k) = \frac{H^*(k)}{|H(k)|^* + \gamma^{-1}} \tag{2.50}$$

where $\gamma$ is the SNR per subcarrier which shows that for the computation of MMSE equalization coefficients, an estimate of the actual SNR per subcarrier is required. For $\gamma \to \infty$, the MMSE equalizer is equal to the ORC equalizer.

## 2.6 Summary

This chapter discussed the fundamentals of mobile radio channel and basic signal structures of OFDM and MC-CDMA systems. First, the different propagation phenomenon such as path loss, shadowing and multipath fading were discussed and their effects on system's performance were reviewed. Then, Rayleigh, Rician and Nakagami-*m* fading models were formulated for the use in later chapters. This chapter also covered the basic principles and data detection techniques of OFDM and MC-CDMA systems. By using the equivalent simplified models of these systems, their signal structures were revisited. For MC-CDMA system, different single users detection techniques were reviewed that are extensively used for analytical and simulation results.

# Chapter 3

# MIMO-OFDM

### 3.1 Introduction

MIMO-OFDM systems have been widely researched and are by far the most common technique used to realise such a system. In this chapter, the workings of STC and CDD for OFDM systems are discussed extensively.

In particular, several MIMO-OFDM systems are considered in Section 3.2 and 3.3 Where the calculation of the weighted metrics for STBC-OFDM system is extended from SISO case and from several papers in the body of literature, the closed-form symbol error probabilities of orthogonal block coded OFDM system are presented for Nakagami-*m* fading channels. The analysis developed here avoids the need for complex numerical integration or lengthy Monte-Carlo simulations.

CDD is presented for OFDM, which its transformation of spatial diversity into frequency is shown by using the equivalent frequency domain system model, i.e. PD. The relationship between the channel delay spread and cyclic delays values for different antenna branches is established. Then, the performance of CDD OFDM is analysed to see how robust a STBC-OFDM and CDD-OFDM systems are in highly frequency selective channels and how these can possibly overcome the effects by changing the number of subcarriers used. MIMO-OFDM systems are compared as ST-OFDM vs CDD-OFDM in order to analyse the viability of using OFDM systems. More important STBC and CDD are highly suboptimal codes which fall short of optimal DMT trade off let alone capacity of MIMO channel.

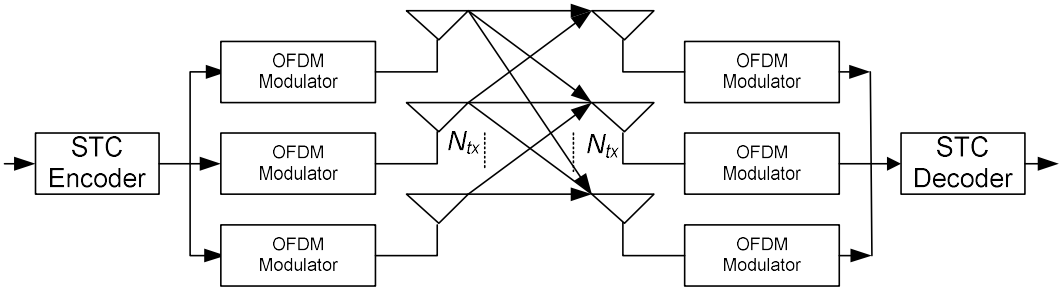


Figure 3.1 Graphical representation of the STC OFDM system model.

### 3.2 STC OFDM System Model

A MIMO OFDM system with $N$ overlapping subcarriers employing arrays of $N_{tx}$ transmit and $N_{rx}$ receive antennas is shown in Figure. 3.1. The number of OFDM subcarriers, i.e. $N$, which makes the generated ST codeword consisting of $N_{tx}N$ modulated symbols and can be expressed as

$$S = \begin{bmatrix} S_1(0) & S_1(1) & \cdots & S_1(N-1) \\ S_2(0) & S_2(1) & \cdots & S_2(N-1) \\ \vdots & \vdots & \ddots & \vdots \\ S_{N_{tx}}(0) & S_{N_{tx}}(1) & \cdots & S_{N_{tx}}(N-1) \end{bmatrix} \tag{3.1}$$

The $n$th row $\mathbf{s}_n = S_n(0), S_n(1), \ldots, S_n(N-1),\ n = 1,2,\ldots,N_{tx}$, represents the encoded data sequence for the $n$th transmit antenna. then placed on $N$ different OFDM subcarriers and after subsequent IFFT processing, A CP of length $L_g$, $L$ is appended to each OFDM frame during the guard interval, which makes the overall OFDM frame length, $N + L_g$ where $L$ is the maximum number of multipaths in fading channel. The transmitted signals pass through the $N_{rx} \times N_{tx}$ MIMO wireless channel which can be expressed as

$$H(k) = \begin{bmatrix} H_{1,1}(k) & \cdots & H_{1,N_{tx}}(k) \\ \vdots & \ddots & \vdots \\ H_{N_{rx,1}}(k) & \cdots & H_{N_{rx},N_{tx}}(k) \end{bmatrix} \tag{3.2}$$

where $H_{r,n}(k)$ is the frequency responses of the channel for the $k$th subcarrier and the antenna pairs $(r,n)$, which are exactly the same as expressed in (2.26) with the exception of antenna indices.

At the receiver, the ISI free signal is extracted from the total signal by removing the CP and subjected the signal to FFT processing is implemented. The resultant frequency domain signal of (2.37) can now be expressed at the *r*th receive antenna as

$$Y_r(k) = \sum_{n=1}^{N_{tx}} H_{r,n}(k) S_n(k) + Z_r(k), \quad k = 0, \dots, N-1 \tag{3.3}$$

where $Z_r(k)$ is the noise term explained in chapter 2

The channel frequency responses can be split into channel impulse responses and FFT coefficients given by

$$H_{r,n}(k) = \mathrm{h}_{r,n}^H \mathrm{w}_f(k) \tag{3.4}$$

where $h_{r,n}(l) = \alpha_{r,n}(l)$ of (2.1), with $\mathbf{h}_{r,n} = \left[\alpha_{r,n}(0), \alpha_{r,n}(l), \dots, \alpha_{r,n}(L-1)\right]^H$ is the $L$ sized vector containing the impulse responses of all non-zero paths and $\mathrm{w}_f(k) = \left[1, e^{-j2\pi k/}\ , e^{-j2\pi k2/}\ , \dots, e^{-j2\pi k(L-1)/N}\right]^T$ represents the respective FFT coefficients.

### 3.2.1 Performance Analysis

The pairwise error probability (PEP) based performance and design criterion of [70] was extended for broadband STC OFDM system in [44] [45]. Assuming the perfect availability of CSI at the receiver, the ML decision rule for the received signal of (3.2.3) (3.3) is given by

$$\hat{s} = \underset{s}{\operatorname{argmin}} \sum_{r=1}^{N_{rx}} \sum_{k=0}^{N-1} \left| Y_r(k) - \sum_{n=1}^{N_{tx}} H_{r,n}(k) S_n(k) \right|^2 \tag{3.5}$$

where the minimization is over all possible codewords $\mathbf{s} = \{S_n(k)_{n.k}\}$. Considering equal transmitted power at all transmit antennas and using the Chernoff bound [18] where, the average PEP of an STC OFDM system over a frequency selective fading channel can be obtained by averaging the conditional PEP of (3.6) with respect to the channel coefficients $h_{r,n}(l)$ and can be upper bounded for a slow Rayleigh fading channel as [71][44][45][79]

$$P(s \to \hat{s}) \leq \left( \prod_{\upsilon=1}^{r_h} \left( 1 + \lambda_r \frac{E_s}{4N_0} \right) \right)^{-N_{rx}}$$

$$\leq \left( \prod_{\upsilon=1}^{r_h} \lambda_r \right)^{-N_{rx}} \left( \frac{E_s}{4N_0} \right)^{-r_h N_{rx}} \tag{3.6}$$

The STC OFDM can achieve a diversity gain of $G_d = r_h N_{rx}$and a coding gain of $G_c = \left( \prod_{\upsilon=1}^{r_h} \lambda_r \right)^{1/r_h}$ in selective environments and to minimize the code error probability, a code with the maximum diversity and coding gain has to be chosen [79].

### 3.2.2 Orthogonal Block Coded OFDM System

The data stream is first modulated and mapped as symbols selected from the signal constellations, such as *M*-PSK or *M*-QAM. Then, these modulated symbols are encoded by a $T_b \times N_{tx}$ column orthogonal matrix $\mathcal{G}$ [73] .The entries of the matrix $\mathcal{G}$ are the linear combinations of modulated symbols and their conjugates. The code rate *R* of STBC is defined as $R = F/T_b$, i.e. the number of $T_b$ time slots required to generate one complete codeword from *F* symbols to be transmitted from $N_{tx}$ antennas, whereas the spectral efficiency is given by

$$\eta_{stbc} = \frac{r_b}{B} = \frac{r_s MR}{r_s} = \frac{FM}{T_b} \; bits/s/Hz \tag{3.7}$$

where *B, $r_b$, $r_s$* are the bit, symbol rate and bandwidth, respectively.

In order to achieve full transmit diversity, the transmission matrix $\mathcal{G}$ is constructed based on the orthogonal design, such that

$$G \cdot G^H = \text{constant}(|S_1|^2 + |S_2|^2 + \cdots + |S_F|^2)\mathbf{I}N_{tx} \tag{3.8}$$

where $S_f$ represents the modulated symbols encoded by the ST block encoder and $\mathbf{I}_{N_{tx}}$ is an $N_{tx} \times N_{tx}$ identity matrix and $G^H$ is the Hermitian of *G*.

In [73], it was shown that the rate of STBC with full transmit diversity is less than or equal to one, $R \leq 1$. The code with full rate ($R = 1$, such as, Alamouti scheme) requires no bandwidth expansion, while the code with $R < 1$ require a bandwidth expansion of $1/R$. For STBC with $N_{tx}$ transmit antennas, the transmission matrix are normally referred to as $G_{N_{tx}}$ and achieves full diversity by maintaining orthogonality between its rows. This means that in each block the signal sequences from any two transmit antennas are

orthogonal. For example, if $\boldsymbol{s}_n = S_{1,n}, S_{2,n}, \ldots, S_{T_b,n}$ is the transmitted sequence from the $n$th antenna, then

$$\mathbf{s}_n \cdot \mathbf{s}_{\hat{n}} = \sum_{t_b=1}^{T_b} S^*_{t_b,n} \cdot S_{t_b,\hat{n}} = 0, \qquad n \neq \hat{n}, \qquad n, \hat{n} = 1,2, \ldots, N_{tx} \tag{3.9}$$

where $\mathbf{s}_n \cdot \mathbf{s}_{\hat{n}}$ denotes the inner product of the sequences $\mathbf{s}_n$ and $\mathbf{s}_{\hat{n}}$.

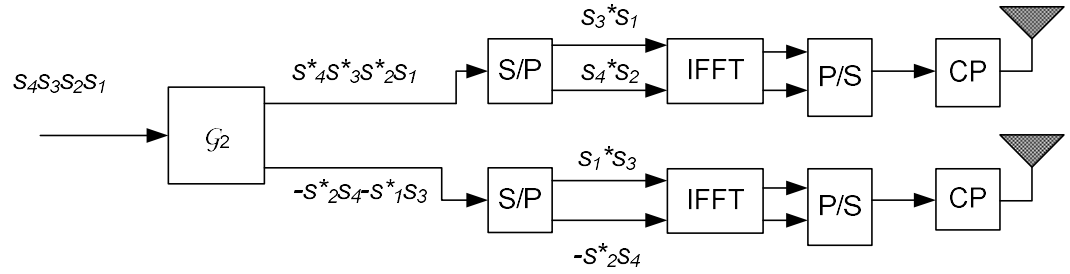


Figure 3.2 ST block coded OFDM system models.

### 3.2.3 Time Domain Orthogonal Block Coded OFDM Systems

Among many important design parameters of an OFDM system, the FFT/IFFT size plays a crucial role in determining the equipment cost and complexity. The frequency domain encoding leads to multiple IFFT operations, for a single OFDM symbol at the transmitter. The complexity of ST OFDM systems can be significantly decreased by realizing the block encoder in the time domain. This can be interpreted as *time-domain implementation* of STBC OFDM.

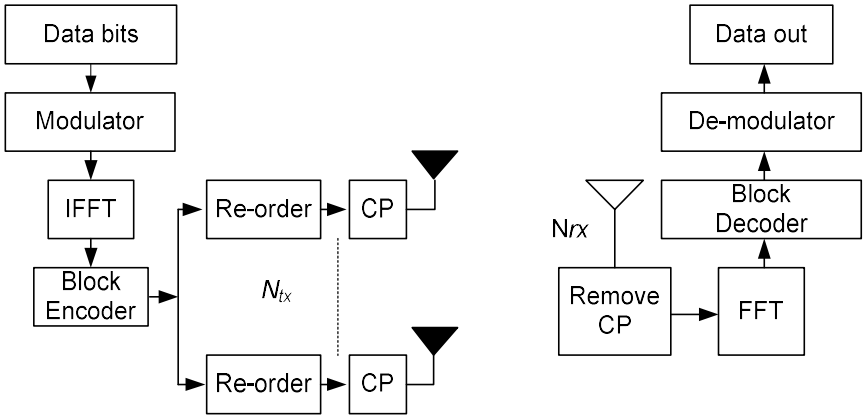


Figure 3.3 Time domain implementation of STBC OFDM system.

A time domain implementation of STBC OFDM with $N_{tx}$ transmit antennas is shown in Figure. 3.3. Assuming transmission in baseband, the data stream is first modulated by a PSK/QAM modulator. The modulated symbols are then fed to a serial to parallel converter, which takes *N* serial symbols and converts them into parallel data vectors given by

$$s_i^f(k) = [S_i(0), S_i(1), \dots, S_i(N-1)]^T \tag{3.10}$$

where $i = 1,2, \dots, N-1$ and $k = 1,2, \dots, N-1$ are the OFDM symbol and subcarrier indices, respectively. To differentiate between the frequency and time domain OFDM symbol vectors, the former is represented by $s_i^f(k)$, while the later by $\mathbf{s}_i(t)$.

Each parallel vector $s_i^f(k)$ is then processed by the IFFT block. This block converts the OFDM symbols from frequency to time domain represented by

$$s_i(t) = \frac{1}{\sqrt{N}} \sum_{k=0}^{N-1} S_i(k) e^{j\frac{2\pi}{N}kt}, \qquad t = 0,1, \dots, N-1 \tag{3.11}$$

Then, the symbols $s_i(t)$ are sent to a ST block encoder which processes the signals according to the frequency domain transmission matrix $GN_{tx}$ [73]. In the STBC OFDM system of [74], the same matrix was considered, replacing the individual modulated symbol by OFDM symbols and then taking the separate IFFT of each of the encoder's output. This implementation is associated with additional computational load as multiple IFFT operations are performed for a single OFDM symbol.

### 3.4 Symbol Error Probabilities of STBC OFDM

This section presents the error rate performance evaluation of orthogonal block coded OFDM system. For simplicity, the standard frequency domain system model of Figure. 3.1 is considered. The equiprobable data stream containing *Fa* information bits is modulated and mapped as symbols $b_1, b_2, \dots, b_F$ selected from the *M*-PSK or *M*-QAM signal constellation $\mathcal{A}$, where $a = \log_2 M$. These symbols are parsed into length *N* vectors $\mathbf{s}_i$ as given in (3.10), where $i = 1,2, \dots, \hat{F}$ is the OFDM symbol index with $\hat{F} = F/N$. For notational convenience, the index *f* used to represent frequency domain has been dropped from (3.10) and will not be used further in this thesis. The vectors $\mathbf{s}_i$ are encoded by STBC

transmission matrix $GN_{tx}$ as explained in section 3.3. Each output branch of $GN_{tx}$ is IFFT processed, then CP is added and transmitted simultaneously from $N_{tx}$antennas.

The signals pass through the wideband channel and after the CP removal and subsequent FFT processing, the received signal at the *r*th receive antenna can be expressed as

$$\begin{bmatrix} y_r^1 \\ \vdots \\ y_r^{\hat{T}_b} \end{bmatrix} = GN_{tx} \begin{bmatrix} H_{r,1} \\ \vdots \\ H_{r,N_{tx}} \end{bmatrix} + \begin{bmatrix} z_{r,1} \\ \vdots \\ z_{r,N_{tx}} \end{bmatrix} \tag{3.12}$$

where $GN_{tx}$ is the $\hat{T}_b \times N_{tx}$ transmission matrix containing the OFDM symbols $\mathbf{s}_i$ and their conjugates, with $\hat{T}_b \hat{t}_b = 1,2, \ldots \hat{T}_b$and $\hat{T}_b = \hat{t}_b T_s$ ($T_s$ is the OFDM symbol duration). The terms $\mathbf{z}_{r,N_{tx}}$, each of length *N*, denote uncorrelated AWGN vectors at the (*r,n*)th antenna pair. The frequency domain received vectors, each of Length *L* are represented by $y_r^{\hat{t}_b}$. The channel matrices $\mathbf{H}_{r,n} = \text{diag}\left[H_{r,n}(0), H_{r,n}(1), \ldots, H_{r,n}(N-1)\right]$with each of the frequency responses $H_{r,n}(k)$ given by (2.25) and $\left|H_{r,n}(k)\right| = \beta_{r,n}(k)$ considered as Nakagami-*m* RVs.

Assuming the channel responses remain constant for $\hat{T}_b$ time-slots and perfect CSI is available at the receiver, then using the decoding method of [73], the recovered OFDM symbols can be written as

$$\begin{bmatrix} \hat{\mathrm{s}}_1 \\ \vdots \\ \hat{\mathrm{s}}_{\hat{F}} \end{bmatrix} = \begin{bmatrix} \kappa \sum_{n=1}^{Ntx} \left|\mathrm{H}_{r,n}\right|^2 & \cdots & 0 \\ \vdots & \ddots & \\ 0 & & \kappa \sum_{n=1}^{Ntx} \left|\mathrm{H}_{r,n}\right|^2 \end{bmatrix} \begin{bmatrix} \mathrm{s}_1 \\ \vdots \\ \mathrm{s}_{\hat{F}} \end{bmatrix} + \begin{bmatrix} \hat{\mathrm{z}}_1 \\ \vdots \\ \hat{\mathrm{z}}_{\hat{F}} \end{bmatrix} \tag{3.13}$$

where $\kappa$ is a constant, which for $G_2 H_3$ and $\mathcal{H}_4$, $\kappa$= 1, while for $G_3$ and $G_4$, $\kappa$=2 [73]. The exact expressions of modified noise terms $[\hat{z}_1, \ldots, \hat{z}_{\hat{F}}]^T$vary from symbol to symbol and depends as well on the number of transmit and receive antennas and can be taken from [75] . Finally, the diagonal channel matrix can be expressed as $\left|\mathbf{H}_{r,n}\right|^2 = \text{diag}\left[\left|H_{r,n}(0)\right|, \left|H_{r,n}(1)\right|^2, \ldots, \left|H_{r,n}(N-1)\right|^2\right]$.

From (3.13), it can be noticed that orthogonal block codes together with a linear combiner at the receiver transform the fading MIMO channel into a SISO channel with a lower probability of deep fades. Now, considering the total transmit power constraint and equal

power per transmit antenna, the instantaneous SNR at the *k*th subcarrier and *r*th receive antenna of STBC OFDM system can be expressed as

$$\gamma_{r,stof}(k) = \frac{1}{RN_{tx}}\frac{E_s}{N_0}\left(\sum_{n=1}^{N_{tx}}\left|H_{r,n}(k)\right|^2, \quad k = 0,1,\ldots,N-1\right) \tag{3.14}$$

where $\left|H_{r,n}(k)\right|^2 = \beta_{r,n}^2(k)$ as explained in chapter 2

By invoking the assumption of independent channel taps for all (*r,n*) antenna pairs, the average SNR per modulated symbol can simply be expressed as

$$\bar{\gamma}_{r,stof} = \frac{1}{RN_{tx}}\frac{E_s}{N_0} \tag{3.15}$$

The square of a Nakagami RV, i.e. $\gamma_r = \gamma_{r,stof} = \beta_{r,n}^2(k)$, follows the Gamma distribution with *pdf* and MGF of (2.21) and (2.22) for the STBC OFDM system can now be expressed as

$$P_{\gamma_r}(\gamma_r) = \frac{\left(\frac{\hat{m}}{\bar{\gamma}_r}\right)^{\hat{m}}}{\Gamma(\hat{m})}\gamma_r^{\hat{m}-1}\exp\left(-\frac{\hat{m}}{\bar{\gamma}_r}\gamma_r\right), \quad \gamma_r \geq 0 \tag{3.16}$$

And

$$\Phi_{\gamma_r}(\mu) = \int_0^{\infty} e^{-\mu\gamma_r} p_{\gamma_r}(\gamma_r)d\gamma_r = \left(1 + \frac{\mu\bar{\gamma}_r}{\hat{m}}\right)^{-\hat{m}} \tag{3.17}$$

The parameter $\hat{m} = \hat{m}_{(stof)}$ becomes

$$\hat{m}_{(stof)} = \frac{E^2\left[\sum_{n=1}^{N_{tx}}\beta_{r,n}^2(k)\right]}{\mathrm{var}\left[\sum_{n=1}^{N_{tx}}\beta_{r,n}^2(k)\right]} = mN_{tx} \tag{3.18}$$

For $N_{rx}$ receive antennas $\hat{m} = \hat{m}_{stof} = mN_{rx}N_{tx}$. From (3.18), it can be noticed that diversity gain for the STBC OFDM is only $N_{tx}$ and it does not take advantage of any of the selectivity available in the broadband channel.

Next, the closed-form error rate expressions of STBC OFDM system with coherent *M*PSK and *M*-QAM modulation are derived by using the well known approach for evaluating the error performance of a digital communication system over fading channels

[51]. That is, the SER of orthogonal STBC OFDM is evaluated by averaging the conditional SER $P_s(E|\gamma_r)$ over the *pdf* of the instantaneous SNR $\gamma_r = \gamma_{r,stof}$ and expressed as

$$P_s(E) = \int_0^{\infty} P_s\,(E|\gamma_r) p_{\gamma_r}(\gamma_r) d\gamma_r \tag{3.19}$$

### 3.4.1 *M*-PSK

The conditional SER for coherent *M*-PSK signals is given by [11] [46]

$$P_s(E|\gamma_r) = \frac{1}{\pi}\int_0^{(M-1)\pi/M} \exp\left\{-\frac{\gamma_r g_{MPSK}}{\sin^2\theta}\right\} d\theta \tag{3.20}$$

where $g_{MPSK} = sin^2(\pi/M)$. Using (3.17), (3.29) and (3.20), the average SER with *M*-PSK modulation becomes

$$P_s(E) = \frac{1}{\pi}\int_0^{(M-1)\pi/M} \Phi_{\gamma_r}\left(\frac{g_{MPSK}}{\sin^2\theta}\right) d\theta$$

$$= \underbrace{\frac{1}{\pi}\int_0^{\frac{\pi}{2}} \Phi_{\gamma_r}\left(\frac{g_{MPSK}}{\sin^2\theta}\right) d\theta}_{I_{1,MPSK}} + \underbrace{\frac{1}{\pi}\int_{\frac{\pi}{2}}^{\frac{(M-1)\pi}{M}} \Phi_{\gamma_r}\left(\frac{g_{MPSK}}{\sin^2\theta}\right) d\theta}_{I_{2,MPSK}} \tag{3.21}$$

For binary PSK, i.e. $M$ = 2, only the first integration part of (3.21) is required. The derivation of terms, $I_{1,MPSK}$ and $I_{2,MPSK}$ is given in Appendix C. By employing (C.0.7) and (C.0.12) in (3.21), and using the average SNR $\bar{\gamma}_{r,stof}$ value of (3.15), the closed form expression for the average SER of the STBC OFDM with *M*-PSK modulation can be given as

$$P_s(E) = \Phi_{\gamma_r}(g_{MPSK})\left\{\frac{1}{2\sqrt{\pi}}\frac{\Gamma(\widehat{m}+1/2)}{\Gamma(\widehat{m}+1)}\;\; {}_2F_1\left(\widehat{m}, \frac{1}{2}; \widehat{m}+1; \frac{1}{\frac{1+g_{MPSK}\bar{\gamma}_r}{\widehat{m}}}\right)\right.$$

$$\left. -\frac{\sqrt{1-g_{MPSK}}}{\pi} F_1\left(\frac{1}{2}, \widehat{m}, \frac{1}{2}-\widehat{m}, \frac{3}{2}; \frac{1-g_{MPSK}}{1+\frac{g_{MPSK}\bar{\gamma}_r}{\widehat{m}}} - g_{MPSK}\right)\right\} \tag{3.22}$$

Where $\widehat{m} = \widehat{m}_{stof} = mN_{rx}N_{tx}$. The terms ${}_2F_1$ and $F_1$ are the Gauss and Appell hypergeometric functions, respectively and given in Appendix C.

### 3.4.2 *M*-QAM

The conditional SER for coherent *M*-QAM signals is given by [11] [51]

$$P_s(E|\gamma_r) = \frac{4q}{\pi}\int_0^{\pi/2} \exp\left\{-\frac{\gamma_r g_{MQAM}}{\sin^2\theta}\right\} d\theta - \frac{4q^2}{\pi}\int_0^{\pi/4} \exp\left\{-\frac{\gamma_r g_{MQAM}}{\sin^2\theta}\right\} d\theta \tag{3.23}$$

where $q = \left(1 - 1/\sqrt{M}\right)$ and $g_{MQAM} = 3/2\,(M-1)$. Using (3.17), (3.19) and (3.23), the average SER with *M*-QAM modulation becomes

$$P_s(E) = \underbrace{\frac{4q}{\pi}\int_0^{\pi/2} \Phi_{\gamma_r}\left(\frac{g_{MQAM}}{\sin^2\theta}\right) d\theta}_{I_{1,MQAM}} - \underbrace{\frac{4q^2}{\pi}\int_0^{\pi/4} \Phi_{\gamma_r}\left(\frac{g_{MQAM}}{\sin^2\theta}\right) d\theta}_{I_{2,MQAM}} \tag{3.24}$$

Considering the similarity of $I_{1,MQAM}$ to $I_{1,MPSK}$, only $I_{2,MQAM}$ needs to be solved and derived in Appendix C. Finally, by employing (C.0.7) and (C.0.15) in (3.24), and using the average SNR $\bar{\gamma}_{r,stof}$ values of (3.15), the closed-form expression for the average SER of the STBC OFDM with *M*-QAM modulation can be expressed as

$$P_s(E) = \frac{2q}{\sqrt{\pi}}\frac{\Gamma\left(\widehat{m}+\frac{1}{2}\right)}{(\widehat{m}+1)}\Phi_{\gamma_r}(g_{MQAM})\quad {}_2F_1\left(\widehat{m}, \frac{1}{2}; \widehat{m}+1; \frac{1}{1+\frac{g_{MQAM}\bar{\gamma}_r}{\widehat{m}}}\right)$$
$$-\frac{2q^2\Phi_{\gamma_r}\left(2_{g_{MQAM}}\right)}{\pi(2\widehat{m}+1)}F_1\left(1, \widehat{m}, 1; \widehat{m}+\frac{3}{2}; \frac{1+\frac{g_{MQAM}\bar{\gamma}_r}{\widehat{m}}}{1+\frac{2_{g_{MQAM}}\bar{\gamma}_r}{\widehat{m}}}, \frac{1}{2}\right) \tag{3.25}$$

### 3.4.3 Performance Results

In this section, numerical error rates based on the derivations are presented and verified with the simulation results. All results are produced for SER versus SNR, defined as the transmitted symbol energy over the noise power spectral density ($E_s = N_0$) . The number of OFDM subcarriers has been fixed to $N$ = 64. Perfect channel estimation has been employed for all error rate curves. The practically worst case fading profile, i.e. $m$ = 1 (Rayleigh fading) is being used for numerical results, while for simulations, a selective Rayleigh channel with varying channel orders (taps) is employed. The taps are generated

by using Jakes model**Error! Reference source not found.**. The number of impinging rays constituting a single tap is fixed to 12 and a Doppler frequency of 20 Hz is used. To obtain the numerical SER curves, the sums involving the series representation of Gauss and Appell hypergeometric functions are truncated after 35 terms.

Analytical results are generated by using (3.25).of $L$ = 1 and 3, respectively. The performance of a simple OFDM system ($N_{tx} = 1$) is also plotted for reference. In all simulation results, full rate transmission matrix $G_2$ is used for $N_{tx} = 2$, while for $N_{tx} = 3,4$ transmit antennas, half rate matrices $G_3$ and $G_4$ of [71] have been chosen. To compensate for the rate loss for $N_{tx} = 3,4$ antennas, STBC curves are generated with QPSK, while $N_{tx} = 1,2$ employ BPSK modulation. This gives a net rate of 1 bits/sec/Hz for all transmit antenna configurations. The close matching of simulation and analytical results can also be observed.

The M-QAM SERs are plotted for communication scenarios with different spectral throughout Figures 3.4-3.7. The Monte-Carlo simulations have been accomplished with the previously described C++ simulation platform[1], where the simple case of a single sub-carrier has been simulated.

Figure 3.4 depicts the SER versus the SNR in [dB] labeled on the number of receive antennas for transmission schemes exhibiting a spectral efficiency of 2 bits/s/Hz. Here, the solid lines represent the analytically derived SER, whereas the markers correspond to specific points obtained by means of Monte-Carlo simulations. For all configurations, the simulations clearly corroborate the analytical results. Furthermore, increasing the number of receive antennas obviously enhances the performance of the transceiver.

The reader is reminded that STBCs do not provide any coding gain, but only diversity gain. From the analysis on O-MIMO channels (c.f. Chapter 2), the diversity gain is known to saturate with an increasing number of total antenna elements. This is once again corroborated by means of Figure 3.5. Having only one receive antenna, i.e. r =1. the diversity gain provided by the half-rate STBC outweighs the loss in transmission rate. For example, to achieve a SER of $10^{-5}$, the full-rate QPSK scheme requires 30 dB, whereas

[1] The C++ simulation platform was provided by Dr Fatin Said

the half-rate 16-QAM scheme with 4 transmits antennas needs only 25dB, thereby saving 5dB transmission power. With four receive antennas, however, diversity is already saturated (fairly) independent of the number of transmit antennas. That explains why the full-rate scheme now outperforms the half-rate schemes. For example, to achieve a SER of $10^{-5}$ , the full-rate QPSK scheme requires 10 dB, whereas the half-rate 16-QAM scheme with 4 transmit antennas needs 2.5 dB more transmission power.

Figure 3.5 depicts the SER versus the SNR [dB] labeled on the number of receive antennas for transmission schemes exhibiting a spectral efficiency of 3 bits/s/Hz. Although not shown here, the Monte-Carlo simulations coincide again with the analytical results. The same explanations as above hold to explain the tendencies of the performance curves. Clearly, the ¾ rate STBC outperforms any other code for a low number of receive antennas, whereas the full rate code performs almost as good as the ¾ rate code. Similar conclusions can be drawn for Figure 3.6 and Figure 3.7, which depict transmission schemes with a spectral efficiency of 4 bits/s/Hz and 6 bits/s/Hz, respectively.

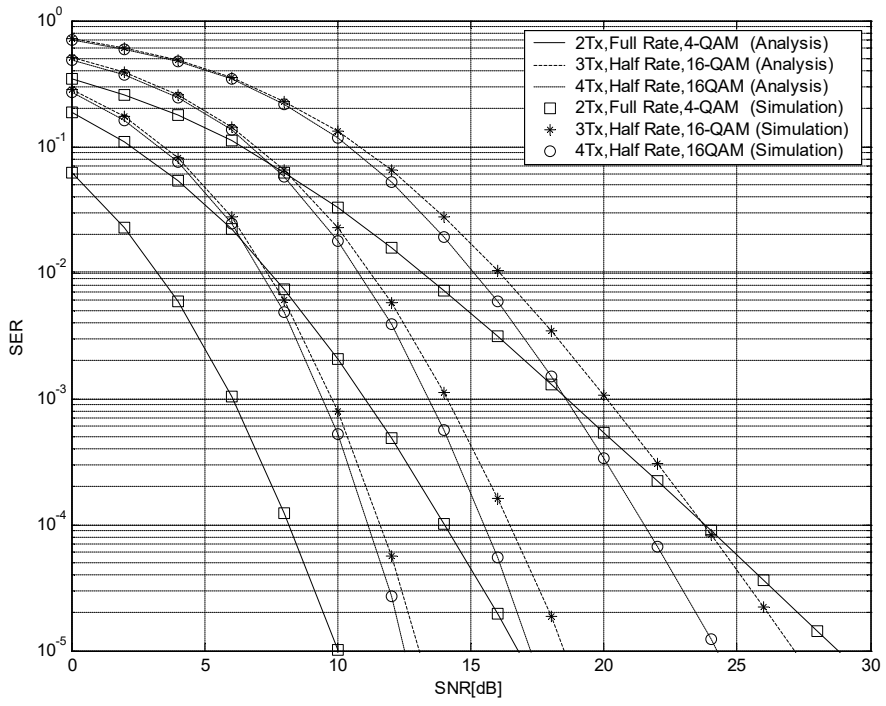


Figure 3.4 SER versus SNR labeled on the number of receive antennas for systems operating at 2 bits/s/Hz

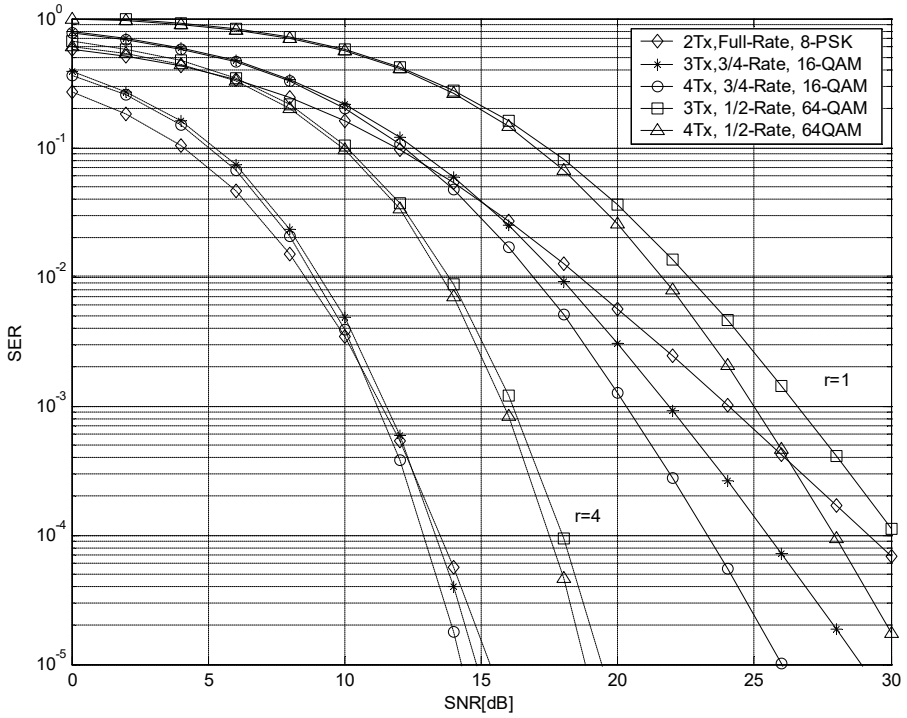


Figure 3.5 SER versus SNR labeled on the number of receive antennas for systems operating at 3 bits/s/Hz

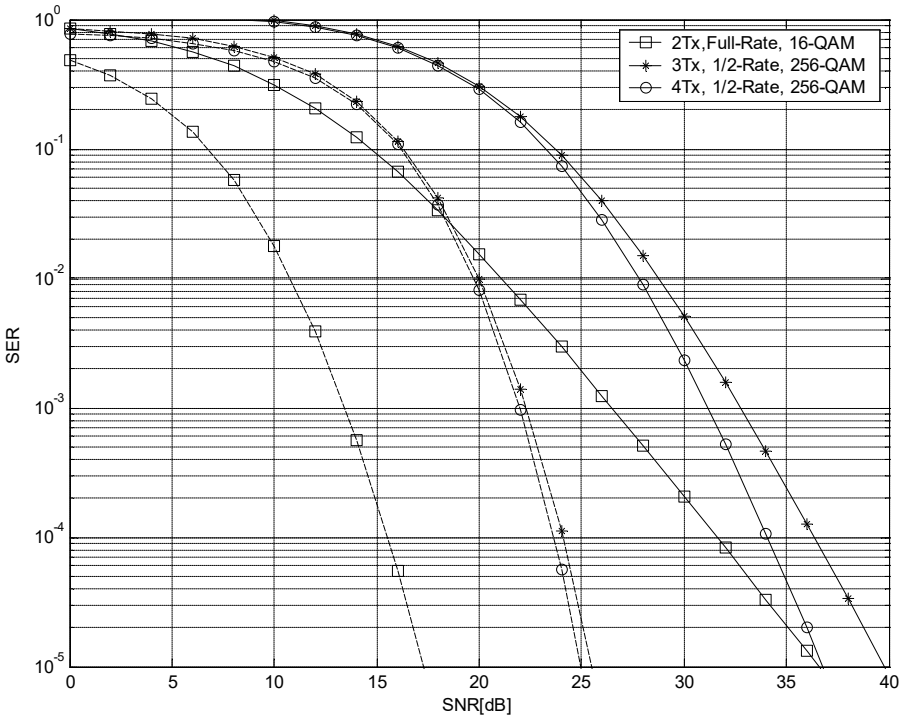


Figure 3.6 SER versus SNR labeled on the number of receive antennas for systems operating at 4 bits/s/Hz

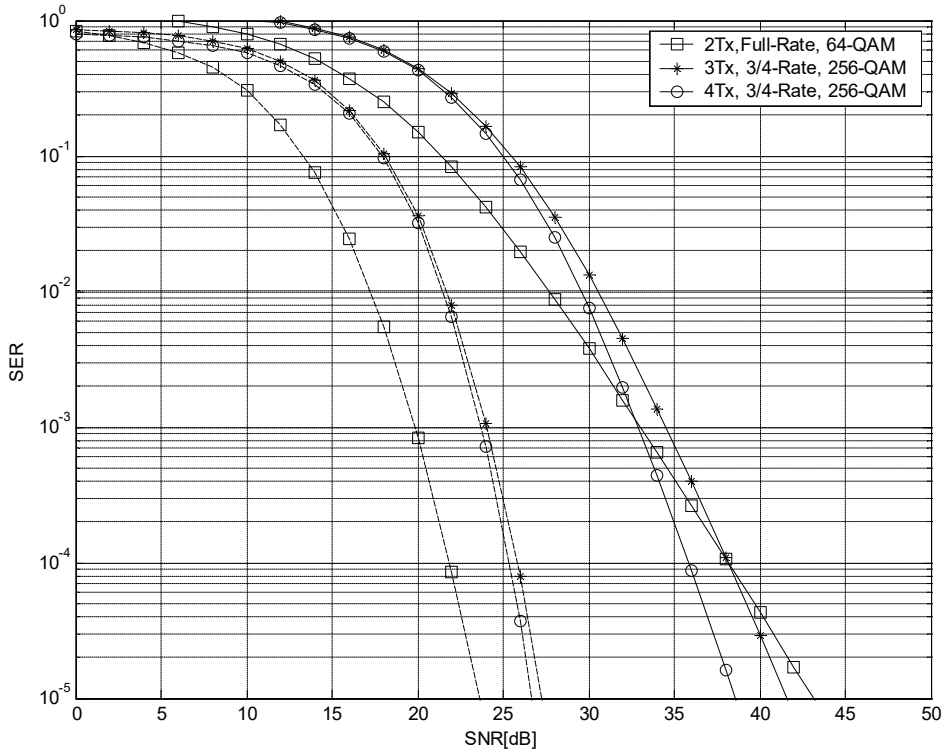


Figure 3.7 SER versus SNR labeled on the number of receive antennas for systems operating at 6 bits/s/Hz

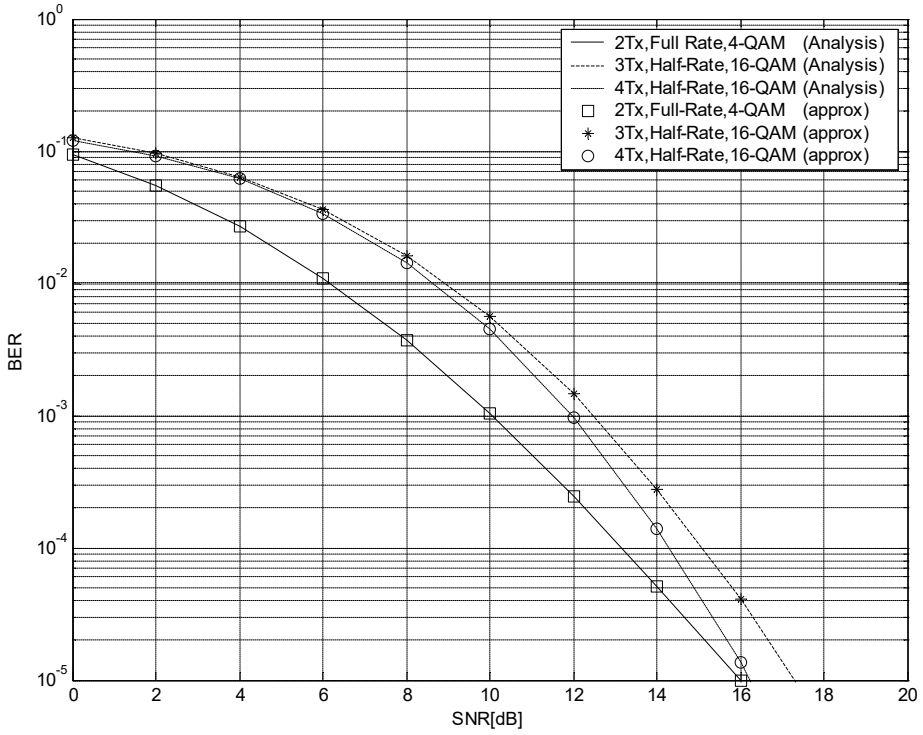


Figure 3.8 Exact and approximate BER versus SNR for systems with two receive antennas operating at 2 bits/s/Hz.

The performance of the numerically obtained exact BERs are compared with the approximate BERs given by (3.30) in Figure 3.8. Simulated is a system equivalent to Figure 3.4, i.e. with a spectral efficiency of 2 bits/s/Hz. The exact and approximate BERs clearly coverage for an increasing SNR.

## 3.5 Cyclic Delay Diversity for OFDM

### 3.5.1 CDD OFDM System Model

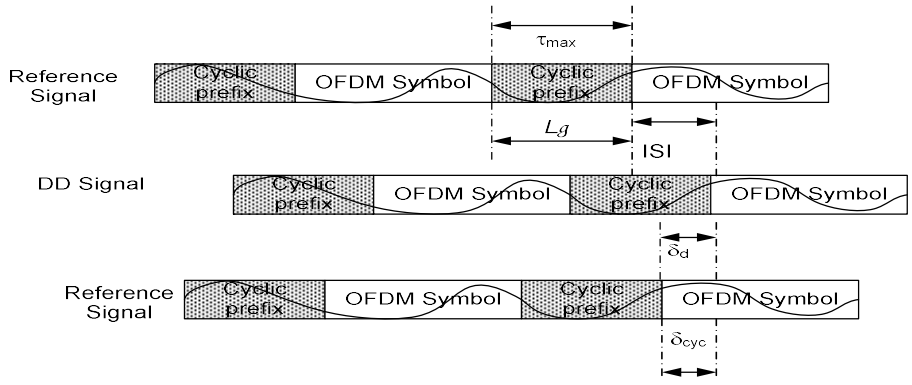


Figure 3.9 Principles of DD and CDD

The block diagram of a multiple antenna OFDM system equipped with CDD is shown in Figure 3.10. The equiprobable data stream is first channel encoded, then modulated and mapped as symbols selected from the *M*-PSK or *M*-QAM signal constellations. The modulated symbols are fed to a serial to parallel converter, which takes *N* serial symbols and converts them into parallel data streams for OFDM processing. After the IFFT, the signal can be represented as

$$s(\tau) = \frac{1}{\sqrt{N}} \sum_{k=0}^{N-1} S(k)\, e^{j\frac{2\pi}{N}k\tau} \tag{3.26}$$

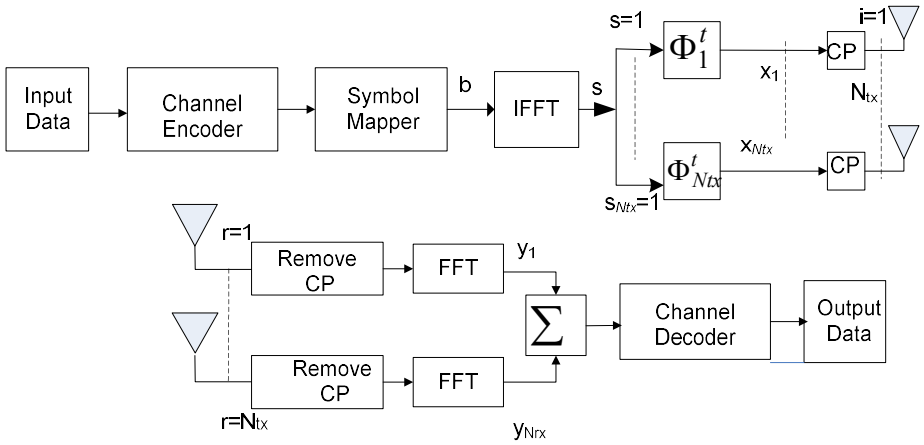


Figure 3.10 CDD OFDM system model.

Then, signal $s(\tau)$is replicated on $N_{tx}$ CDD branches and each branch is cyclically shifted or delayed by a branch specific delay, $\theta_n^t,\ n = 1,2,\ldots,N_{tx}$. Due to the insertion of these cyclic delays, (3.26) becomes

$$\underbrace{s\big((\tau - \theta_n^t) \bmod_N\big)}_{Cyclically\ delayed\ signal} = \frac{1}{N} \sum_{k=0}^{N-1} \underbrace{e^{-j\frac{2\pi}{N}\theta_n^t} S(k)}_{Phase\ delayed\ signal} e^{j\frac{2\pi}{N}k\tau} \tag{3.27}$$

From the above expression, it can be observed that a cyclic delay of $\Theta_n^t$ in the time domain is equivalent to a multiplication of phase factor $e^{-j2\pi/N\theta_n^t}$ in the frequency domain, where the phase is linearly increasing with the subcarrier index. This equivalence is the property of DFT which confirms that CDD can also be implemented in the frequency domain (i.e., before the IFFT operation), and termed as PD. The actual realization of PD becomes unattractive as it requires multiple IFFT operations that result in increasing the

system computational load; however, it provides a convenient approach to theoretically analyze such techniques.

In a CDD OFDM system, the spatial diversity of the cyclically delayed antennas is converted into frequency diversity. This is achieved by appropriately selecting the cyclic delays values $\Theta_n^t$ for $N_{tx}$ antenna branches. The chosen delay values are such that the $L$ multipaths of all $N_{tx}$ channels become consecutive in their delay lags. By doing so, the overall system can be represented by a SISO frequency selective channel with an enhanced delay spread of $N_{tx}L$ taps [15] To show this, the above defined CDD OFDM system model is expressed in the vector matrix form by replacing (3.26) with

$$s = \boldsymbol{F}_N^H b \tag{3.28}$$

where the column vectors **b** and **s** represent the length $N$ OFDM symbols before and after the IFFT processing, respectively. The $N \times N$ IFFT matrix is given b $\boldsymbol{F}_N^H$.

The vector **s** is then replicated on $N_{tx}$antennas, where each antenna branch is cyclically shifted by CDD matrice $\Theta_n^t,\ n = 1, \dots, N_{tx}$s. Finally, after the insertion of CP, (which is at least the length of the last $L$ samples of each vector $\Theta_n^t s$) the signals are simultaneously transmitted from the $N_{tx}$antennas. Ignoring CP, the signal transmitted from the $n$th antenna is given by

$$x_n = \frac{1}{\sqrt{N_{tx}}} \Phi_n^t s = \frac{1}{N_{tx}} \Theta_n^t \boldsymbol{F}_N^H \mathrm{b} \tag{3.29}$$

where $1/\sqrt{N_{tx}}$ is the power normalization factor and

$$\Theta_n^t \begin{bmatrix} 0 & I_{(n-1)L} \\ I_{N-(n-1)L} & 0 \end{bmatrix} \qquad \forall n \in [1, N_{tx}] \tag{3.30}$$

where $\boldsymbol{I}_N$ is $N \times N$ Identity matrix. For $n$=1, $\boldsymbol{I}_0$ represents 0.

Next, the construction of cyclic delayed matrices $\Theta_n^t$ as given in (3.30) is discussed by modelling the CDD OFDM system in the frequency domain.

### 3.5.2 Conversion-Spatial to Frequency Diversity

CDD converts the spatial diversity into frequency and the receiver sees the signals coming from only a single antenna [15] [17] To verify it analytically, an equivalent frequency

domain transmitter model is shown in Fig 3.11, where the CDD matrices $\Theta_n^t$ are replaced by their frequency domain equivalent PD matrices $\Theta_n^f$ and placed before the IFFT blocks. At the receiver, after the removal of CP, the received signals are processed by the $N \times N$ FFT matrices $F_N$. The input-output relationship from $\mathbf{x}_n$to $\mathbf{y}_r$ (see Fig 3.11), can be written as

$$y_r = \sum_{n=1}^{N_{tx}} H_{r,n} x_n + z_r \qquad \forall r \in [1, N_{rx}]$$

(3.31)

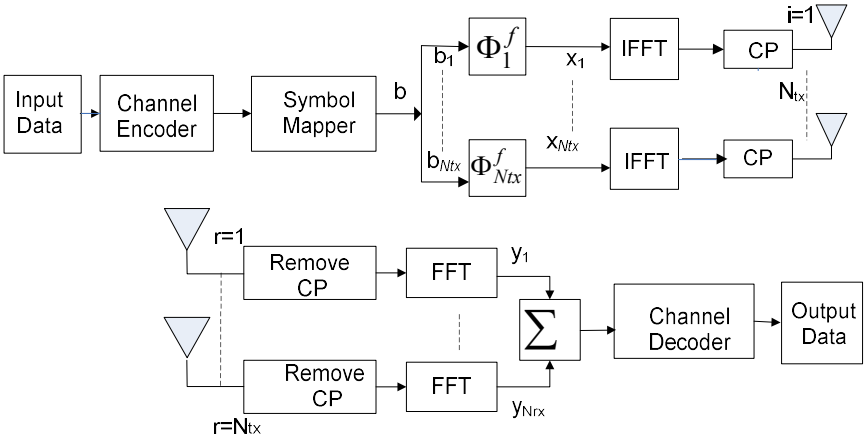


Figure 3.11 Frequency domain equivalent CDD OFDM system model.

which are length $N$ column vectors corresponding to one OFDM symbol. Here, $\boldsymbol{z}_r$ is the i.i.d. AWGN vector for the $r$th receive antenna and $\mathbf{H}_{r,n} = \text{diag}\big[H_{r,n}(0), \ldots, H_{r,n}(N-1)\big]$ with $H_{r,n}(k)$ given in (2.26)

The matrix $\mathbf{H}_{r,n}$can be split into impulse responses and DFT part as

$$\mathrm{H}_{r,n} = \sum_{l=0}^{L-1} h_{r,n}(l) W_l \qquad \forall r \in [1, N_{rx}]$$

(3.32)

where a

$$W_l = \text{diag}\big[1, e^{-j2\pi l/N}, \ldots, e^{-j2\pi l(N-1)/N}\big]$$

(3.33)

From (3.23), it can be noted that different channels may have different channel multipaths $\sum_{l=0}^{L-1} h_{r,n}(l)$, but they possess the same delay lags $l$ in the FFT domain, as evident by $\mathbf{W}_l$. In order to shift the $L$ multipaths of each channel corresponding to $N_{tx}$ antennas in such a

way that all channel multipaths become consecutive in their delay lags, the matrices $\Theta_n^f$ have to be selected as

$$\Theta_n^f = \text{diag}\left[1, e^{j\Theta_n^f}, \dots, e^{j\Theta_n^f(N-1)}\right] \qquad \forall n \in [1, N_{tx}] \tag{3.34}$$

with entries [82]

$$\Theta_n^f = -2\pi(n-1)L/N \tag{3.35}$$

which makes

$$W_l\Theta_n^f = W_{l+(n-1)L} \qquad \forall l \in [0, L-1], \quad n \in [1, N_{tx}] \tag{3.36}$$

Hence, for each receive antenna the equivalent channel vector becomes

$$\mathrm{h}_r = \left[\left(h_{r,1}\right)^T, \left(h_{r,2}\right)^T, \dots, \left(h_{r,N_{tx}}\right)^T\right] \tag{3.37}$$

with the *l*th entry of $\mathbf{h}_r$ being $h_r(l) = h_{r,\lfloor 1/L \rfloor+1}(l \bmod L)$

Now, since $\mathbf{h}_r$ has length $N_{tx}L$, it can be viewed as coming from a single frequency selective channel. Based on (3.36), the diagonal matrix $\mathbf{H}_{r,n}$ can fully be expressed in terms of longer equivalent channels as

$$H_r = \sum_{n=1}^{N_{tx}} \mathrm{H}_{r,n}\Theta_n^f = \sum_{l=0}^{N_{tx}L-1} h_r(l)W_l \qquad \forall r \in [1, N_{rx}] \tag{3.38}$$

Thus, the PD matrices $\Theta_n^f$ shift the delay lags of the *n*th channel from $[0, L-1]$ to $[(n-1)L, n(L-1)]$.

The actual implementation of CDD is achieved in the time domain (i.e. via matrices $\Theta_n^t$, shown in Figure 3.10 As discussed earlier, the CDD and PD matrices are linked via the DFT transformation. The IFFT of the PD matrices $\Theta_n^f$ can be expressed as [15]

$$F_N^H\Theta_n^f = \begin{bmatrix} f_0^T \\ \vdots \\ f_{N-1}^T \end{bmatrix}\Theta_N^f = \begin{bmatrix} f_{(n-1)L}^T \\ \vdots \\ f_{(n-1)L-1}^T \end{bmatrix} \tag{3.39}$$

where $f_k^T$ is the $k$th row of $\boldsymbol{F}_N^H$. It shows that left multiplying $\Theta_n^f$ by $\boldsymbol{F}_N^H$ is equivalent to permuting the rows of $\boldsymbol{F}_N^H$ circularly. Hence, $\Theta_n^t$ are the $N \times N$ permutation matrices such that

$$\Theta_n^t \boldsymbol{F}_N^H = \boldsymbol{F}_N^H \Theta_n^f \tag{3.40}$$

The structure of permutation matrices $\Theta_n^t$ become as given in (3.30)

### 3.5.3 Performance Analysis

In this section, the error rate analysis of CDD OFDM system is presented. As shown in section, a multiple antenna OFDM system employing CDD, collapses to a single transmit antenna system with a selective channel of order $N_{tx}L$, provided that the delay values for each transmit antenna is chosen according to the CDD matrices $\Theta_n^t$ (3.30). By doing so, the received signal of (3.31) can be expressed as

$$y_r = \mathbf{H}_r s + z_r \qquad \forall r \in [1, N_{rx}] \tag{3.41}$$

where $\mathbf{H}_r$ is the modified channel matrix of (3.38)

The channel transfer function $H_{r,n}(k)$ of (2.26) can now simply be expressed in terms of modified channel matrix as

$$H_r(k) = \frac{1}{\sqrt{N}} \sum_{l=0}^{N_{tx}} h_r(l) e^{-j2\pi k} /$$

(3.42)

Also, the frequency domain Nakagami-*m* fading parameters of (2.30) and (2.31) becomes

$$m_f^{cdd} = \frac{1}{\left(\frac{1}{m} - 1\right)\left(\frac{1 - e^{-2N_{tx}L\delta}}{1 - e^{-2\delta}}\right)\left(\frac{1 - e^{-\delta}}{1 - e^{-N_{tx}L\delta}}\right)^2 + 1} \tag{3.43}$$

And

$$\Omega_f^{cdd} = \frac{1 - e^{-N_{tx}L\delta}}{1 - e^{-\delta}}\left(\frac{\Omega_0}{N}\right) \tag{3.44}$$

Considering the total transmit power constraint and equal power per transmit antenna, the instantaneous SNR at the *k*th subcarrier and *r*th receive antenna of CDD OFDM system can be expressed as

$$\gamma_{r,cddof}(k) = \frac{1}{N_{tx}}\frac{E_s}{N_0}(|H_r(k)|^2), \qquad k = 0,1,\dots,N-1$$

(3.45)

where $|H_r(k)|^2 = \beta_r^2(k)$. By invoking the assumption of independent channel taps for all (*r*,*n*) antenna pairs, the average SNR per modulated symbol can be written as

$$\bar{\gamma}_{r,cddof} = \frac{1}{N_{tx}}\frac{E_s}{N_0}$$

(3.46)

Next, closely following the MGF based approach which was used for the performance evaluation of STBC OFDM system in the previous section, it is straightforward to show that the square of Nakagami RV, i.e. $\gamma_r = \gamma_{r,cddof} = \beta_r^2(k)$ , follows the Gamma distribution with *pdf* and MGF given in (3.16) and (3.17), respectively and for CDD OFDM, the parameter $\hat{m} = \hat{m}_{(cddof)}$ becomes

$$\hat{m}_{(cddof)} = \frac{E^2|\beta_r^2(k)|}{var|\beta_r^2(k)|} = m$$

(3.47)

From (3.47) it is evident that the diversity gain is only *m* which confirms that for an uncoded CDD OFDM system, the performance remains the same as for the case of simple uncoded OFDM. Hence, the closed-form expression for the average SER of the uncoded CDD OFDM with *M*-ary modulation can thus be obtained by replacing $\bar{\gamma} = \bar{\gamma}_{r,cddof}$ and $\hat{m} = \hat{m}_{(cddof)}$ in (3.22) and (3.25), respectively. However, when employed with channel coding methods the selectivity introduced by CDD branches significantly minimize the error rates.

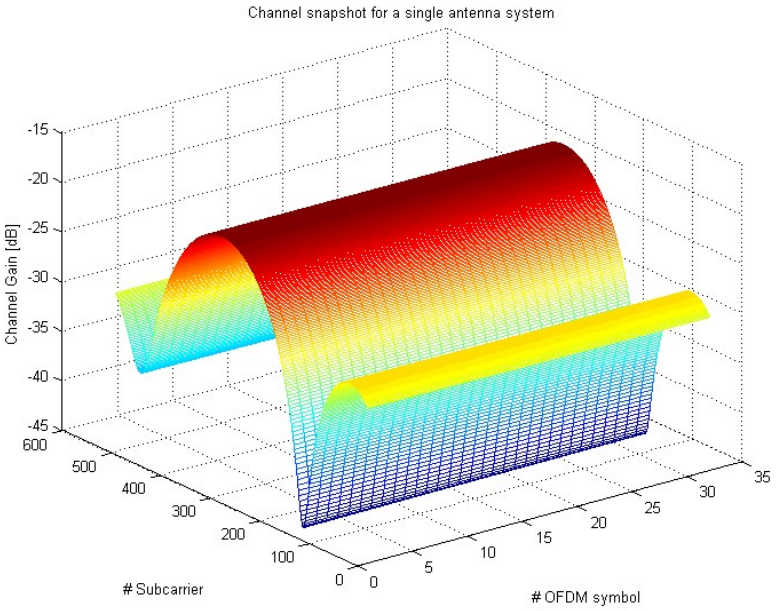


(a) Channel snapshop for 1Tx-1RX

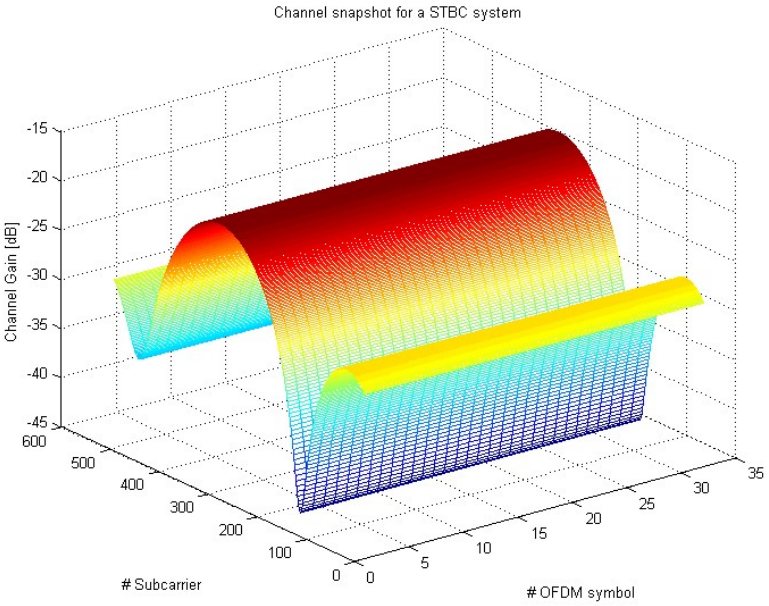


(b) 2Tx-1Rx STBC systems

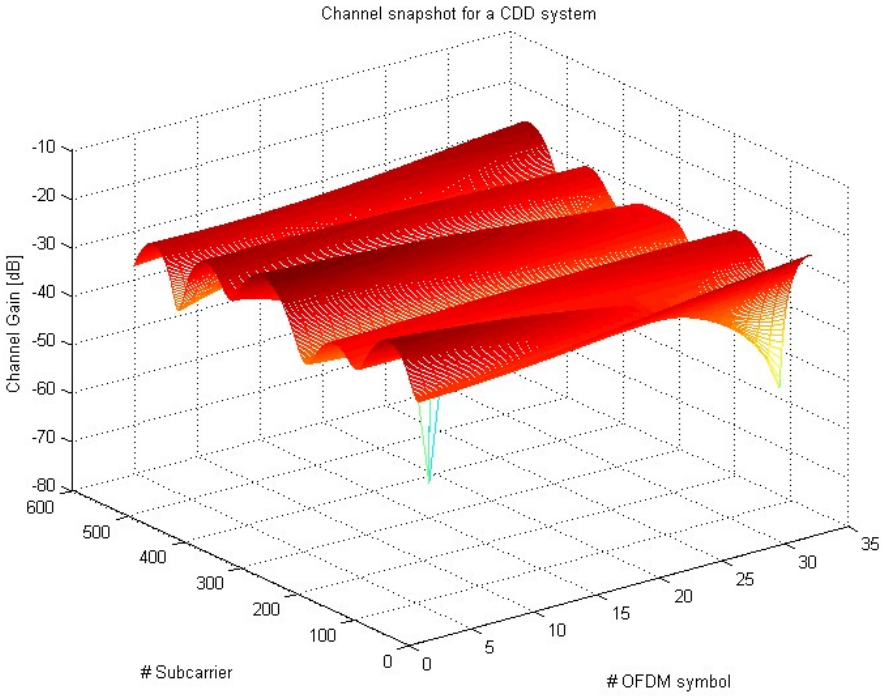
Channel snapshot for a CDD system
Channel Gain [dB]
-10
-20
-30
-40
-50
-60
-70
-80
600
500
400
300
200
100
0
# Subcarrier
0
5
10
15
20
25
30
35
# OFDM symbol

(c)

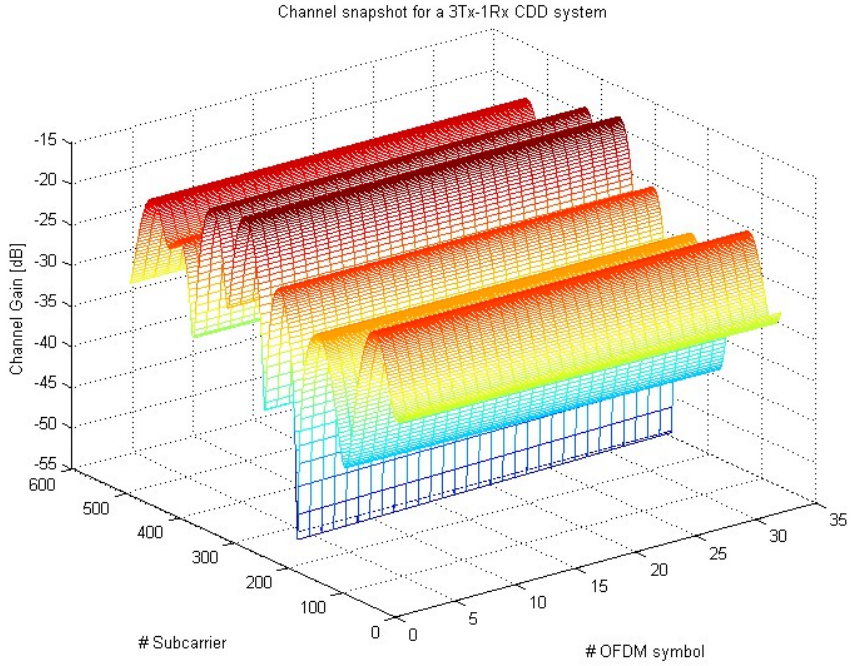
Channel snapshot for a 3Tx-1Rx CDD system
Channel Gain [dB]
-15
-20
-25
-30
-35
-40
-45
-50
-55
600
500
400
300
200
100
0
# Subcarrier
0
5
10
15
20
25
30
35
# OFDM symbol

(d)

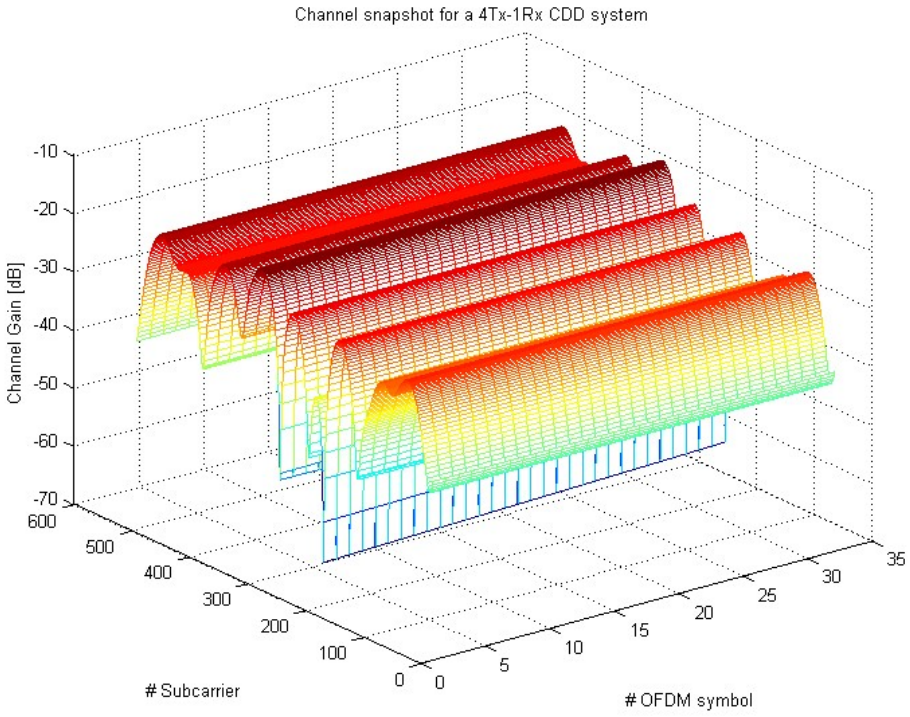


(e)

Figure 3.12 Snapshots showing the performance of normalized channel using CDD-OFDM providing Frequency Selectivity.

(a) For 1Tx-1Rx STBC-OFDM system (b) Normalization of 2Tx-1Rx STBC-OFDM Gc2 (c) No normalization of the channel (d) For 2Tx-1Rx CDD system (e) For 3Tx-1Rx CDD system( f) For 4Tx-1Rx CDD system (g) For 2Tx-1Rx CDD system2

### 3.6 Summary

In this chapter, STC and CDD for OFDM were presented with a complete system description and performance analysis. The comparison is done for both, channel coded and uncoded OFDM systems and helps in understanding the excellent performance of CDD with the minimal of complexity.

By showing that an MIMO OFDM system employing STBC can be represented by an equivalent SISO model and following the unified approach for evaluating the error performance over fading channels of [76], the exact and closed-form expressions for the

[2] The program used has been implemented by the author.

average SER of *M*-ary signals were derived by transforming the single integral into higher transcendental functions.

The transformation of spatial diversity into frequency was explained with the help of PD. The optimum relationship between the channel delay spread and cyclic delays values for different antenna branches was established.

It was shown that the uncoded error rates of a CDD OFDM remain unchanged to a simple OFDM system because of the fact that CDD converts the spatial diversity into frequency. However, the channel coded results showed that the enhanced selectivity introduced by CDD greatly helps in improving the system performance. The simulation results elaborated he excellent performance of CDD with no additional complexity at the receiver. The transformation of spatial diversity into frequency was explained with the help of PD. In the next chapter, while considering the frequency correlated system's subcarriers, closed-form symbol error probabilities of orthogonal block codes and CDD are derived for MC-CDMA system.

## Annex

### A.2 OFDM Obstacles

Having understood the basics of OFDM and highlighting its advantages, it should be noted that this method does have several drawbacks. Most notably, OFDM systems have high peak to average power ratios (PAPR) at the *Tx* output and more sensitive to phase noise. In this section, these issues are described before showing that although this system may not be perfect, it is in fact widely deployed in many systems today.

The ratio between the OFDM symbol with the most power and the average power of one OFDM block is called the instantaneous PAPR

$$\text{PAPR} = \frac{\max|x|^2}{\text{E}\{|x|^2\}} \qquad \text{A.2.1}$$

### OFDM Peak-to-Average Power Ratio

According to the definition a multicarrier signal is the sum of many independent signals modulated onto subchannels of equal bandwidth. This can of signals can be denoted by a multicarrier signal consisting of N subcarrxiers is given by

$$x(t) = \frac{1}{\sqrt{N}} \sum_{n=0}^{N-1} X_n \cdot e^{j2\pi n \Delta f t}, \quad 0 \le t < NT$$

A.2.2

where , $j = \sqrt{-1}$ is $\Delta f$ the subcarrier spacing, and NT denotes the useful data block period. In OFDM the subcarriers are chosen to be orthogonal (i.e. $\Delta f = 1/NT$). The PAPR of the transmit signal is defined as

$$PAPR = \frac{\max\limits_{0 \le t < N} |x(t)|^2}{1/NT \cdot \int_0^{NT} |x(t)|^2 dt}$$

A.2.3

For analytical propose, an approximation will be made in that only NL equidistant samples of *x(t)* will be considered where only L is an integer that is larger than or equal to1. The PAPR computed from L-times oversampled time domain signal samples is given by its definition as Peak-to-Average Power Ratio by

$$\text{PAPR} = \frac{\text{Peak Amplitud of the Signal}}{\text{Average Value of the Signal}}$$

A.2.4

or mathematically,

$$\text{PAPR} = \frac{\max\limits_{0 \le k \le N-1} |x_k|^2}{\text{E}[|x_k|^2]}$$

A.2.5

where E[·]denotes expectation.

CCDF of PAPR

The CCDF Complementary Cumulative Distribution Function (CCDF) is the most commonly used performance measure for PAPR reduction techniques. The CDF of the amplitude of a signal sample is given by,

$$\text{F}(\text{PAPR}_0) = 1 - e^{-\text{PAPR}_0}$$

A.2.6

The CCDF of a data block with Nyquist rate sampling is given by,

$$\begin{aligned} \text{Prob}[\text{PAPR} > \text{PAPR}_0] &= 1 - \text{Prob}[\text{PAPR} \le \text{PAPR}_0] \\ &= 1 - \text{F}(\text{PAPR}_0)^{\text{N}} \\ &= 1 - (1 - e^{-\text{PAPR}_0})^{\text{N}} \end{aligned}$$

A.2.7

To derive this expression it is assumes that the N time domain signal samples are mutually independent and uncorrelated.

Coding can also be used to reduce the PAPR of OFDM. A simple idea introduced in is to select those symbol blocks (codewords) that minimize or reduce the PAPR for transmission. This reduction scheme is implemented in the following example.

Table 1 PAPR values of all possible data blocks for an OFDM signal with four sub-carriers and BPSK Modulation

| ata Block X | PAPR (dB) | Data Block X | PAPR (dB) |
|---|---|---|---|
| [1,1,1,1]T | 6.0 | [-1,1,1,1]T | 2.3 |
| [1,1,1,-1]T | 2.3 | [-1,1,1,-1]T | 3.7 |
| [1,1,-1,1]T | 2.3 | [-1,1,-1,1]T | 6.0 |
| [1,1,-1,-1]T | 3.7 | [-1,1,-1,-1]T | 2.3 |
| [1,-1,1,1]T | 2.3 | [-1,-1,1,1]T | 3.7 |
| [1,-1,1,-1]T | 6.0 | [-1,-1,1,-1]T | 2.3 |
| [1,-1,-1,1]T | 3.7 | [-1,-1,-1,1]T | 2.3 |
| [1,-1,-1,-1]T | 2.3 | [-1,-1,-1,-1]T | 6.0 |

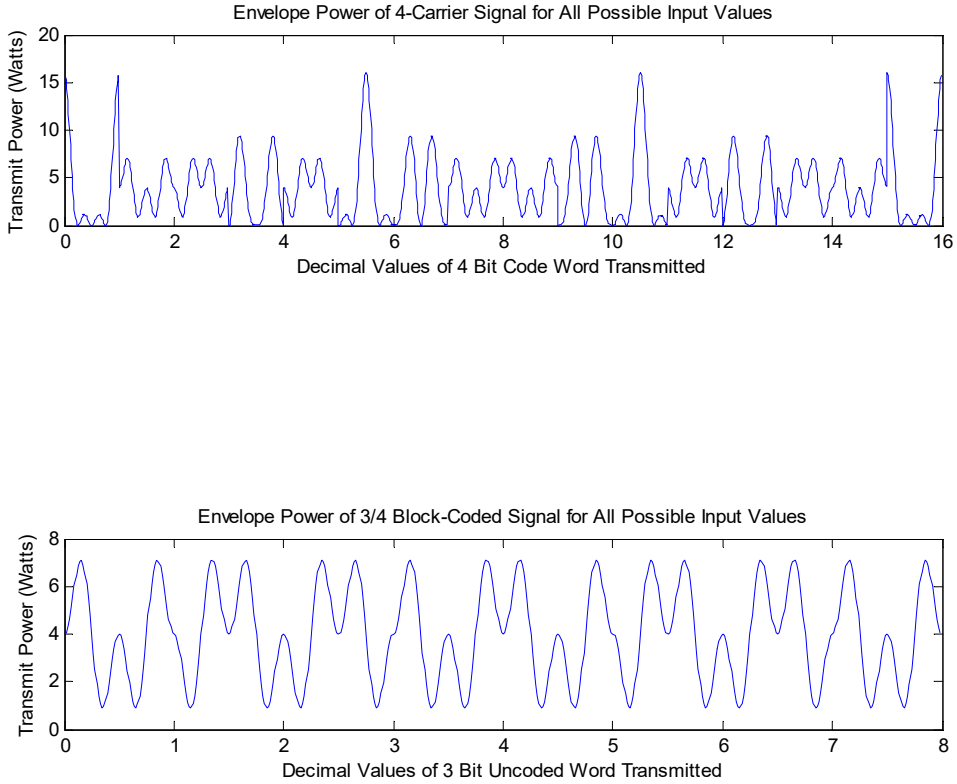


Figure 3.13 Uncoded word Transmitted

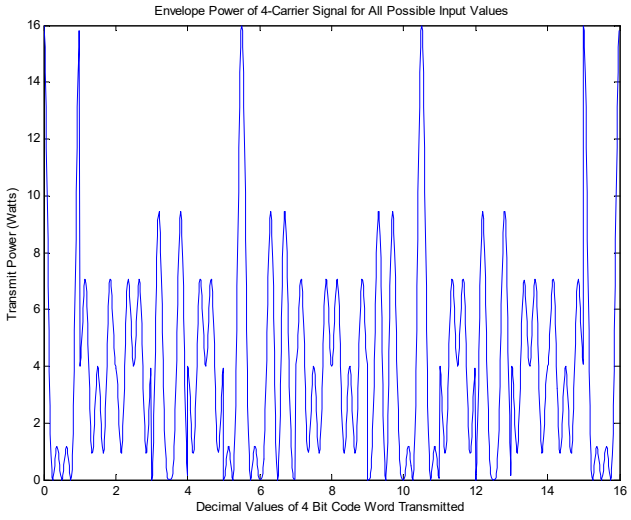


Figure 3.14 PAPR

# Chapter 4

# Multi-user MIMO Performance

## 4.1 Introduction

This chapter presents explicit closed-form formulas for the exact average SER of *M*-ary signals are derived with MRC detection technique. The Nakagami-*m* channel model with frequency correlated MC-CDMA subcarriers is used for this error rate analysis.

In radio, multi-user MIMO (MU-MIMO) is a set of advanced MIMO, multiple-input and multiple-output, technologies that exploit the availability of multiple independent radio terminals in order to enhance the communication capabilities of each individual terminal. To contrast, single-user MIMO only considers access to the multiple antennas that are physically connected to each individual terminal. MU-MIMO can be seen as the extended concept of space-division multiple access (SDMA) which allows a terminal to transmit (or receive) signal to (or from) multiple users in the same band simultaneously. Like the relationship between OFDM and OFDMA, MU-MIMO (and, similarly, SDMA) can be thought of as an extension of MIMO applied in various ways as a multiple access strategy. A significant difference is that the performance of MU-MIMO relies on precoding capability than OFDMA so that if the transmitter does not use precoding, the performance advantage of MU-MIMO is not achievable.

Multiple access MIMO, MIMO-SDMA, many transmit antenna MIMO-SDMA, Cooperative MIMO, Network MIMO and Ad-hoc MIMO are all family terminologies within MU-MIMO, as each of those technologies leverages multiple users as a degree of freedom in achieving successful radio transmission.

Multi-user MIMO can leverage multiple users as spatially distributed transmission resources, at the cost of somewhat more expensive signal processing. In comparison, conventional, or single-user MIMO considers only local device multiple antenna dimensions. Multi-user MIMO algorithms are developed to enhance MIMO systems when the number of users, or connections, numbers greater than one (admittedly, a useful concept). Multi-user MIMO can be generalized into two categories: MIMO broadcast channels (MIMO BC) and MIMO multiple access channels (MIMO MAC) for downlink and uplink situations, respectively. Single-user MIMO can be represented as point-to-point, pairwise MIMO.

In this chapter, closed-form expressions for the exact SER of the CDD and STBC MCCDMA systems with correlated subcarriers over the Nakagami-*m* fading model of [23] are presented By extending the analysis of Chapter 3, it is shown that a CDD MC-CDMA system collapses to a single transmit antenna system with relatively enhanced delay spread (i.e. spatial diversity is transformed into frequency). Similarly, MIMO MC-CDMA system employing STBC can be represented by an equivalent SISO model [99][100][101][102]. Then, following the unified approach for evaluating the error performance over fading channels of [51] and using the alternative representation of the Gaussian Q-functions, the average error rates for the CDD and STBC MC-CDMA systems are presented in the form of single finite-range integrals.

These integrands contain the MGF of the instantaneous SNR of CDD and STBC schemes, respectively. Then, following the framework of section 3.4, the exact and closed-form expressions for the average SER of *M*-ary signals in Nakagami-*m* fading channel are derived by transforming the single integrals into higher transcendental functions such as the Gauss and Appel hypergeometric functions. The development of the proposed equations are based on previous works presented [78] [79]

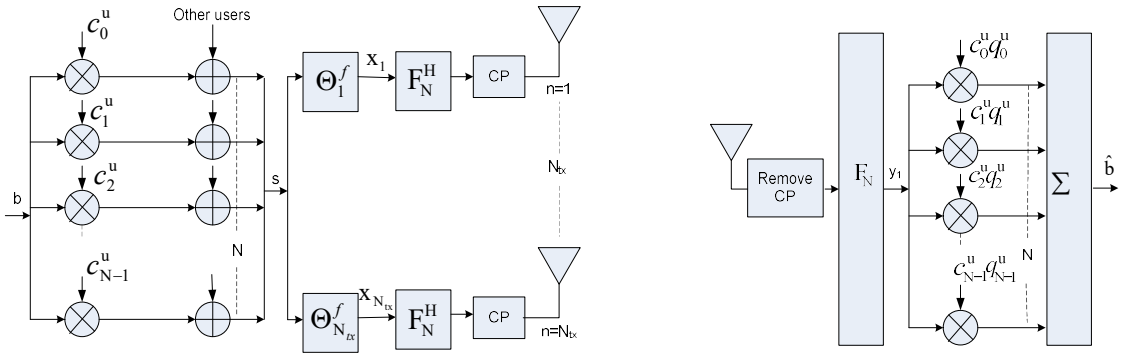


Figure 4.1 CDD MC-CDMA synchronous system model (downlink).

### 4.2 CDD and STBC MC-CDMA System Modelling

In this section, CDD and STBC schemes are introduced for MC-CDMA system and their SER analysis is presented.

#### 4.2.1 CDD MC-CDMA

A block diagram of CDD MC-CDMA system is shown in Figure. 4.1 The equiprobable data stream of the *u*th user containing *Fa* information bits is simply modulated and mapped as symbols, $b_1^u, b_2^u, \ldots, b_F^u$, selected from the *M*-ary signal constellation *A*, where $a = \log_2 M$. $a = \log_2 M$. Then, $\{b_i^u\}_{i=1}^F$ are converted into *P* parallel streams and spread by any suitable spreading sequence. In the downlink case, the

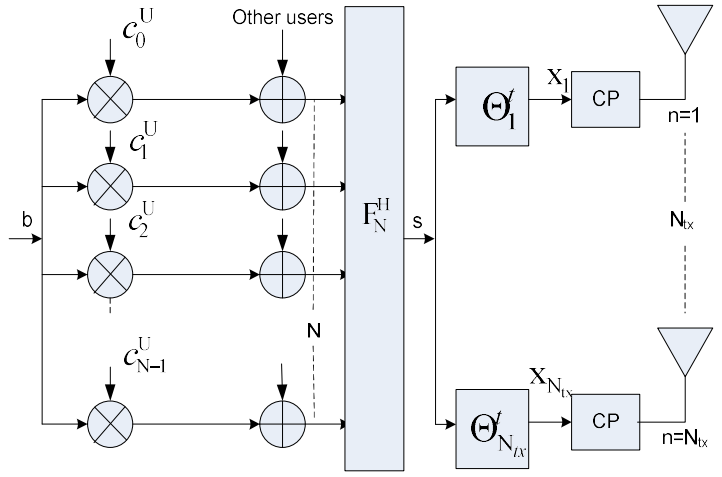


Figure 4.2 Simplified CDD MC-CDMA transmitter model (downlink).

other users are spread by their specific sequences and the resulting spread chips of all *U* users are added synchronously and modulated by an *N* point IFFT given by (2.40) For

analytical convenience, consider $P = 1$, i.e. only a single data symbol $b^u$ for each user $u$, which makes $G = N$ and the simplified downlink transmitter model is shown in Figure 4.2. In the uplink case, the same model holds for the $u$th user in the absence of other users' signals. Expressing (2.40) in vector form

$$\mathrm{s} = \mathbf{G}\mathbf{b}\boldsymbol{F}_N^H \tag{4.1}$$

where column vector **b** of length $U$ represents the single data symbols of $U$ users with **G** and $\boldsymbol{F}_N^H$ are the $U \times N$ and $N \times N$ Walsh-Hadamard and IFFT matrices, respectively. Thespread and IFFT modulated column vector of length $N$ is given by **s**.

The vector **s** is then replicated on $N_{tx}$ branches, where each branch is cyclically shifted by CDD matrices $\Theta_n^t, n = 1, \ldots, N_{tx}$. Finally, after the insertion of CP (which is at least the length of the last $L$ samples of each vector $\mathrm{s}\Theta_n^t$ ), the signals are simultaneously transmitted from the $N_{tx}$ antennas. The transmitted signal (ignoring CP) from the $n$th antenna is given by

$$x_n = \frac{1}{\sqrt{N_{tx}}} s\Theta_n^t = \frac{1}{\sqrt{N_{tx}}} \mathbf{b}\mathbf{G}\boldsymbol{F}_N^H\Theta_n^t \tag{4.2}$$

where $1/\sqrt{N_{tx}}$ is the power normalization factor and

$$\Theta_n^t = \begin{bmatrix} 0 & I_{(n-1)L} \\ I_{N-(n-1)L} & 0 \end{bmatrix} \qquad \forall n \in [1, N_{tx}] \tag{4.3}$$

where $\boldsymbol{I}_N$ is $N \times N$ Identity matrix. For $n = 1$, $\boldsymbol{I}_0$ represents 0.

At the receiver, after the removal of CP, the received signals are processed by the $N \times N$ FFT matrices $\boldsymbol{F}_N$. Ignoring the user index $u$ for the time being, the ISI free signal at the $r$th receive antenna can be written as

$$y_r = \sum_{n=1}^{N_{tx}} \mathrm{H}_{r,n}\, x_n + z_r, \qquad \forall r \in [1, N_{rx}] \tag{4.4}$$

which are length $N$ column vectors corresponding to one MC-CDMA symbol. Here, $\mathbf{z}_r$ is the i.i.d. AWGN vector for the $r$th receive antenna and $\mathbf{H}_{r,n} = \mathrm{diag}\big[H_{r,n}(0), .., H_{r,n}(N-1)\big]$ with $H_{r,n}(k)$ given in (2.26)

For simple OFDM system, CDD converts the spatial diversity into frequency and the receiver effectively sees the signal coming from a single antenna. This was verified analytically where the CDD matrices $\Theta_n^t$ were replaced by their frequency-domain equivalent PD matrices $\Theta_n^f$and placed before the IFFT blocks. It was shown that by appropriately selecting matrices $\Theta_n^f$, the $L$ taps of all $N_{tx}$ channels can be shifted such that they become consecutive in their delay lags. By doing so, the overall system can be represented by a single frequency selective channel with longer $N_{tx}L$ taps (at each receive antenna).

The CDD and PD matrices were shown to be linked as $\Theta_n^t F_N^H = F_N^H \Theta_n^f$ which makes CDD matrices $\Theta_n^t$, even for MC-CDMA system, simply the $N\times N$ permutation matrices with the structure given in (4.3). Based on these analysis, the CDD MC-CDMA also collapses to a single transmit antenna system with a highly selective channel and the received signal of (4.4) can be written as6

$$y_r = \frac{1}{\sqrt{N_{tx}}}\mathbf{H}_r\mathbf{s} + \mathbf{z}_r, \qquad \forall r \in [1, N_{rx}]$$

(4.5)

where $\mathbf{H}_r$ is now the diagonal channel matrix of (3.38) Also, with the inclusion of user index $u$, the frequency responses of (2.26) can be expressed as

$$H_r^u(k) = \frac{1}{\sqrt{N}} \sum_{l=0}^{N_{tx}L-1} h_r^u(l) e^{-j2\pi k\ /}$$

(4.6)

with the frequency domain fading parameters $m_f^{cdd}$and $\Omega_f^{cdd}$given in (3.43)and (3.44) respectively with the MAI and noise variances given by

$$\sigma^2_{MAI_{cdd}} = \frac{E_c}{N_{tx}}(U-1)\Omega_f^{cdd} \sum_{k=0}^{N-1} \left(\beta_r^{u'}(k)\right)$$

(4.7)

And

$$\sigma^2_{\eta_{cdd}} = N_0 \sum_{k=0}^{N-1} \left(\beta_r^{u'}(k)\right)^2$$

(4.8)

Finally, in (2.46) with $E_c = E_s/N$ and after some simplification, the instantaneous SNR of an CDD MC-CDMA system becomes

$$\gamma_{r_{cdd}} = \frac{\frac{2}{N}\sum_{k=0}^{N-1}\left(\beta_r^{u'}(k)\right)^2}{(U-1)\frac{\Omega_f^{cdd}}{N} + \frac{N_0}{E_s/N_{tx}}} \tag{4.9}$$

### 4.2.2 STBC MC-CDMA

In this section, the STBC of [73] is presented with frequency correlated subcarriers. The extension to more specific

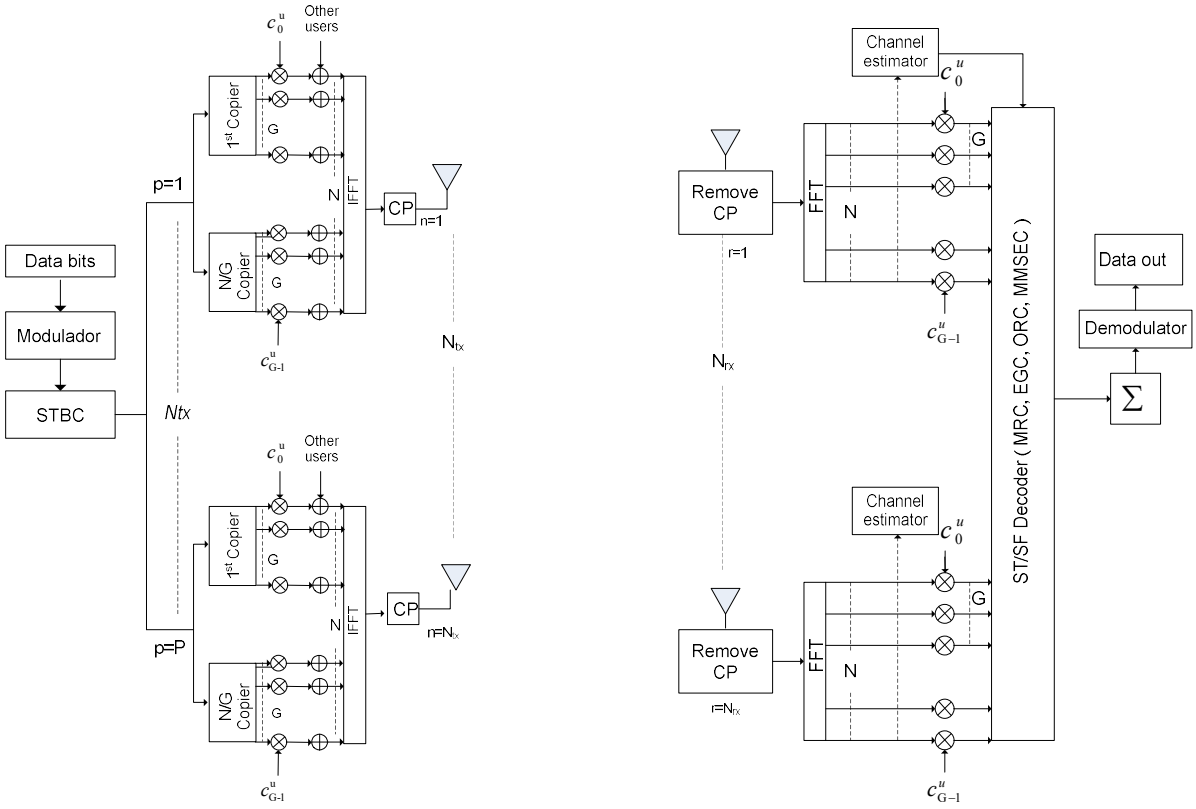


Figure 4.3 STBC MC-CDMA system model.

In Figure 4.3, the complete system model of a STBC MC-CDMA is shown. The data symbols $b_1^u, b_2^u, \ldots, b_F^u$ of the $u$th user are encoded by a ST block encoder defined by a $\hat{T}_b \times N_{tx}$column orthogonal matrix $\mathcal{G}$ explained in detail in chapter 3. These ST encoded symbols are then passed to the spreading section, where each symbol is copied $\mathcal{G}$ times and multiplied with the spreading code of the $u$th user. The resultant coded and spread symbols are modulated by the $N$-point IFFT. After the insertion of CP, the signals are normalized and transmitted. For analytical convenience, consider $P = 1$, i.e. all $U$ users employ the full $N$ MCCDMA subcarriers in Figure. 4.4.

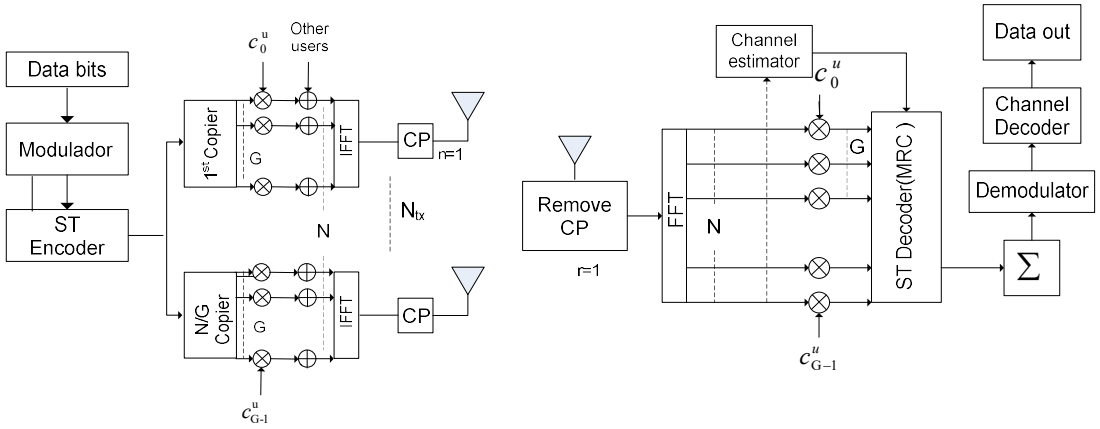


Figure 4.4 Simplified STBC MC-CDMA system model (downlink)

$$\begin{bmatrix} y_r^1 \\ \vdots \\ y_r^{\hat{T}_b} \end{bmatrix} = \sqrt{\frac{E_c}{N_{tx}R}} \sum_{u=0}^{U-1} \sum_{k=1}^{N} c^u(k) G \begin{bmatrix} H_{r,1}^u(k) \\ \vdots \\ H_{r,N_{tx}}^u(k) \end{bmatrix} + \begin{bmatrix} z_r^1(k) \\ \vdots \\ z_r^{\hat{T}_b}(k) \end{bmatrix} \tag{4.10}$$

Assuming the channel responses remains constant for $\hat{T}_b$time slot and perfect CSI is available at the receiver, then using the decoding method of [73] the recovered MC-CDMA symbols at the $r$th receive antenna can be written as

$$\begin{bmatrix} V_r^1 \\ \vdots \\ V_r^F \end{bmatrix} = \sqrt{\frac{\kappa E_c}{N_{tx}R}} \sum_{u=0}^{U-1} \sum_{k=1}^{N} c^u(k) \hat{\mathrm{H}}(k) \begin{bmatrix} b_1^u \\ \vdots \\ b_F^u \end{bmatrix} + \begin{bmatrix} \hat{z}_r^1(k) \\ \vdots \\ \hat{z}_r^F(k) \end{bmatrix} \tag{4.11}$$

Where

$$\hat{\mathrm{H}}(k) = \begin{bmatrix} \sum_{n=1}^{N_{tx}} \left|H_{r,n}^{u}(k)\right|^2 & \cdots & 0 \\ \vdots & \ddots & \vdots \\ 0 & \cdots & \sum_{n=1}^{N_{tx}} \left|H_{r,n}^{u}(k)\right|^2 \end{bmatrix} = \sum_{n=1}^{N_{tx}} \left|H_{r,n}^{u}(k)\right|^2 \cdot \mathrm{diag}[I]$$

$$\hat{\mathrm{H}}(k) = \begin{bmatrix} \sum_{n=1}^{Ntx} \left|H_{r,n}^{u}(k)\right|^2 & \cdots & 0 \\ \vdots & \ddots & \\ 0 & & \sum_{n=1}^{Ntx} \left|H_{r,n}^{u}(k)\right|^2 \end{bmatrix} = \sum_{n=1}^{Ntx} \left|H_{r,n}^{u}(k)\right|^2 \cdot \mathrm{diag}[1] \tag{4.12}$$

and $\kappa$ is a constant, which for $G_2; H_3$ and $H_4$, $\kappa = 1$, while for $G_3$ and $G_4$, $\kappa = 2$[71].

The exact expressions of modified noise terms $[\hat{z}_r^1(k), \ldots, \hat{z}_r^F(k)]^T$ varies from symbol to symbol and depends as well on the number of transmit and receive antennas and can be taken from [75]

From (4.11) and (4.12) it can be observed that the STBCs transform the MIMO channel into an equivalent SISO channel with the MAI and noise variances represented by

$$\sigma_{MAI_{stbc}}^2 = \sqrt{\frac{\kappa E_c}{N_{tx} R}} (U-1)\Omega_f \sum_{n=1}^{N_{tx}} \sum_{k=0}^{N-1} \left(\beta_{r,n}^{u'}(k)\right)^2 \tag{4.13}$$

and

$$\sigma_{\eta_{stbc}}^2 = N_0 \sum_{k=0}^{N-1} \sum_{n=1}^{N_{tx}} \left(\beta_{r,n}^{u'}(k)\right)^2 \tag{4.14}$$

Finally, with $E_c = E_s/N$ and after some simplification, the instantaneous SNR of STBC MC-CDMA system can be expressed as

$$\gamma_{r_{stbc}} = \frac{\frac{2}{N} \sum_{k=0}^{N-1} \sum_{n=1}^{N_{tx}} \left(\beta_{r,n}^{u'}(k)\right)^2}{(U-1)\frac{\Omega_f}{N} + \frac{N_0}{\kappa\, E_s/N_{tx} R}} \tag{4.15}$$

### 4.3 Performance Analysis- STBC & CDD MC-CDMA

Based on the analysis of section 4.2.1 and 4.2.2, it is concluded that the MIMO MC-CDMA system employing CDD is equivalent to a SISO/SIMO system with an enhanced delay spread, whereas the STBC MC-CDMA system also collapses to an equivalent SISO/SIMO model. In this section, the SER of the subject systems are presented based on MGF approach introduced previously in chapter 3.

The square of a Nakagami RV, i.e. $\gamma_r = \beta_{r,n}^2$ follows the Gamma distribution with *pdf* defined in (3.16) and the MGF of CDD and STBC MC-CDMA systems expressed as

$$\Phi_{\gamma_r}(\mu) = \int_0^{\infty} e^{-\mu\gamma_r} p_{\gamma_r}(\gamma_r) d_{\gamma_r} = \left(1 + \frac{\mu\bar{\gamma}_r}{\hat{m}}\right)^{-\hat{m}} \tag{4.16}$$

Where, $\Phi_{\gamma_r}(\mu) = \Phi_{\gamma_{cdd}}(\mu) = \Phi_{\gamma_{stbc}}(\mu)$ with the instantaneous SNR $\gamma_r = \gamma_{r\,cdd} = \gamma_{r\,stbc}$. Also, the parameter $\hat{m} = \hat{m}_{cdd} = \hat{m}_{stbc}$ and $\bar{\gamma}_r$ represents the average SNR. Next the parameters $\hat{m}$ is derived for CDD and STBC MC-CDMA.

For the case of CDD MC-CDMA system, it can be shown that the unitary DFT matrices link the frequency $\beta_r^{u'}(k)$ and impulse $\alpha_r^{u'}(l)$ responses by [52]

$$\sum_{k=0}^{N-1} \left(\beta_r^{u'}(k)\right)^2 = \sum_{l=0}^{N_{tx}(L-1)} \left(\alpha_r^{u'}(l)\right)^2 \tag{4.17}$$

Let $\Psi_{cdd} = \frac{1}{N}\sum_{k=0}^{N-1}\left(\beta_r^{u'}(k)\right)^2$ in the instantaneous SNR expression of (5.9), since the taps $\left\{\left(\alpha_r^{u'}(l)\right)^2\right\}_{l=0}^{N_{tx}(L-1)}$ are mutually uncorrelated, the fading parameter $\hat{m}_{cdd}$ and mean power $\hat{\Omega}_{cdd}$ for the correlated MC-CDMA subcarriers becomes

$$\hat{m}_{cdd} = \frac{E^2[\Psi_{cdd}]}{\mathrm{var}[\Psi_{cdd}]} = \frac{\sum_{l=0}^{N_{tx}L-1} e^{-\delta}}{\sum_{l=0}^{N_{tx}L-1} \frac{e^{-2\delta l}}{m}} \tag{4.18}$$

or simply

$$\widehat{m}_{cdd} = \left(\frac{1-e^{-2\delta}}{1-e^{-2N_{tx}L\delta}}\right)\left(\frac{1-e^{-N_{tx}L\delta}}{1-e^{-\delta}}\right)^2 m$$

(4.19)

with $\widehat{\Omega}_{cdd} = \Omega_f^{cdd}$ as given in (2.31)

Using (4.19), the average uplink SNR $\bar{\gamma}_{r_{cdd}}^{U_l}$ for the CDD MC-CDMA system can finally be expressed as

$$\bar{\gamma}_{r_{cdd}}^{U_l} = \left(\underbrace{\frac{U-1}{N}}_{A} + \underbrace{\frac{1}{\frac{E_s}{N_0}\widehat{\Omega}_{cdd}/N_{tx}}}_{B}\right)^{-1}$$

$$\bar{\gamma}_{r(cdd)}^{U_l} = \left(\underbrace{\frac{U-1}{N}}_{A} + \underbrace{\frac{1}{\frac{E_s}{N_0}\hat{\Omega}_{cdd}\Big/N_{tx}}}_{B}\right)^{-1} \tag{4.20}$$

and the downlink average SNR by $\bar{\gamma}_{r_{cdd}}^{D_l} = (2\mathrm{A} + \mathrm{B})^{-1}$

Similarly, for the case of STBC MC-CDMA

$$\sum_{n=1}^{N_{tx}}\sum_{k=0}^{N-1}\left(\beta_{r,n}^{u'}(k)\right)^2 = \sum_{n=1}^{N_{tx}}\sum_{l=0}^{L-1}\left(\alpha_{r,n}^{u'}(l)\right)^2$$

(4.21)

with the fading parameter $\widehat{m}_{stbc}$ and mean $\widehat{\Omega}_{stbc}$ for the correlated MC-CDMA subcarriers given by

$$\widehat{m}_{stbc} = \frac{\sum_{n=1}^{N_{tx}}\sum_{l=0}^{L-1} e^{-\delta l/n}}{\sum_{n=1}^{N_{tx}}\sum_{l=0}^{L-1} e^{-2\delta l/m}}$$

(4.22)

or simply

$$\widehat{m}_{stbc} = \left(\frac{1-e^{-2\delta}}{1-e^{-2L\delta}}\right)\left(\frac{1-e^{L\delta}}{1-e^{-\delta}}\right) m N_{tx}$$

(4.23)

with $\widehat{\Omega}_{stbc} = \Omega_f$ as given in (2.31)

The average uplink SNR $\bar{\gamma}_{r_{stbc}}^{U_l}$ for the STBC MC-CDMA system becomes

$$\bar{\gamma}_{r_{stbc}}^{U_l} = \left( \underbrace{\frac{U-1}{N}}_{A} + \underbrace{\frac{1}{\frac{E_s}{N_0}\kappa\,\widehat{\Omega}_{stbc}/RN_{tx}}}_{C} \right)^{-1} \tag{4.24}$$

and the downlink SNR is given by $\bar{\gamma}_{r_{stbc}}^{U_l} = (2\mathrm{A} + \mathrm{C})^{-1}$.

Now it is straightforward to calculate the closed-form error rates expressions for CDD and STBC MC-CDMA systems for coherent *M*-ary signals following the framework of section 3.4. The error performances of subject systems are evaluated by averaging the conditional SER $P_s(E\lceil\gamma_r)$ over the *pdf* of the instantaneous SNR $\gamma_r$ given in (3.19).

### 4.3.1 *M*-PSK

For *M*-PSK modulation, using the average SNR values of CDD (4.20), and STBC (4.24) with $\widehat{m} = \widehat{m}_{cdd} = \widehat{m}_{stbc}$ of (4.19), (4.23), the expression for the average SER of the CDD and STBC MC-CDMA with frequency correlated subcarriers can be expressed in closed form as (3.22) by [11]

$$P_s(E) = \Phi_{\gamma_r}(g_{MPSK}) \left\{ \frac{1}{2\sqrt{\pi}} \frac{\Gamma(\widehat{m}+1/2)}{\Gamma(\widehat{m}+1)} \quad {}_2F_1\left( \widehat{m}, \frac{1}{2}; \widehat{m}+1; \frac{1}{\frac{1+g_{MPSK}\bar{\gamma}_r}{\widehat{m}}} \right) \right.$$
$$\left. + \frac{\sqrt{1-g_{MPSK}}}{\pi} F_1\left( \frac{1}{2}, \widehat{m}, \frac{1}{2}-\widehat{m}, \frac{3}{2}; \frac{1-g_{MPSK}}{1+\frac{g_{MPSK}\bar{\gamma}_r}{\widehat{m}}} 1-g_{MPSK} \right) \right) \tag{4.25}$$

For complete derivation, please refer to chapter 3 and Appendix C.

### 4.3.2 *M*-QAM

For *M*-QAM modulation, using the average SNR values of CDD (4.20) and STBC (4.24) with $\widehat{m} = \widehat{m}_{cdd} = \widehat{m}_{stbc}$ of (4.19), (4.23) the closed-form expression for the average SER of the CDD and STBC MC-CDMA with frequency correlated subcarriers can be given as (3.25) by [11]

$$P_s(E) = \frac{2q}{\sqrt{\pi}} \frac{\Gamma\left(\hat{m}+\frac{1}{2}\right)}{(\hat{m}+1)} \Phi_{\gamma_r}\left(g_{MQAM}\right) \quad {}_2F_1\left(\hat{m}, \frac{1}{2}; \hat{m}+1; \frac{1}{\frac{1+g_{MQAM}\bar{\gamma}_r}{\hat{m}}}\right)$$

$$-\frac{2q^2 \Phi_{\gamma_r}\left(2_{g_{MQAM}}\right)}{\pi(2\hat{m}+1)} F_1\left(1, \hat{m}, 1; \hat{m}+\frac{3}{2}; \frac{1+\frac{g_{MQAM}\bar{\gamma}_r}{\hat{m}}}{1+\frac{2g_{MQAM}\bar{\gamma}_r}{\hat{m}}}, \frac{1}{2}\right) \tag{4.26}$$

For complete derivation, please refer to chapter 3 and Appendix C.

### 4.3.3 Performance Results

In this section, numerical results based on the derivations made in the section 4.3.2 are verified with Monte-Carlo based MCCDMA system simulator employing CDD and STBC diversity techniques. These results provide an insight and the tradeoff between the number of paths *L*, Nakagami parameter *m* and transmit antennas $N_{tx}$. All results are produced for SER versus SNR ($E_s/N_o$). For simplicity $N = G$.

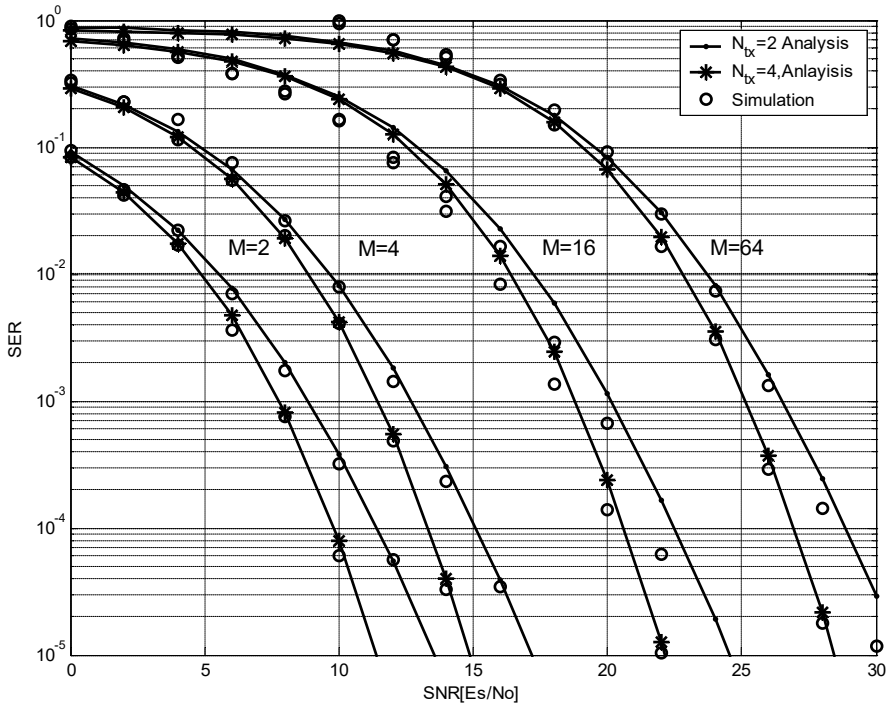


Figure 4.5 Performance of an CDD MC-CDMA system with N=16, L=3,m=1 and δ=0

**CDD MC-CDMA**

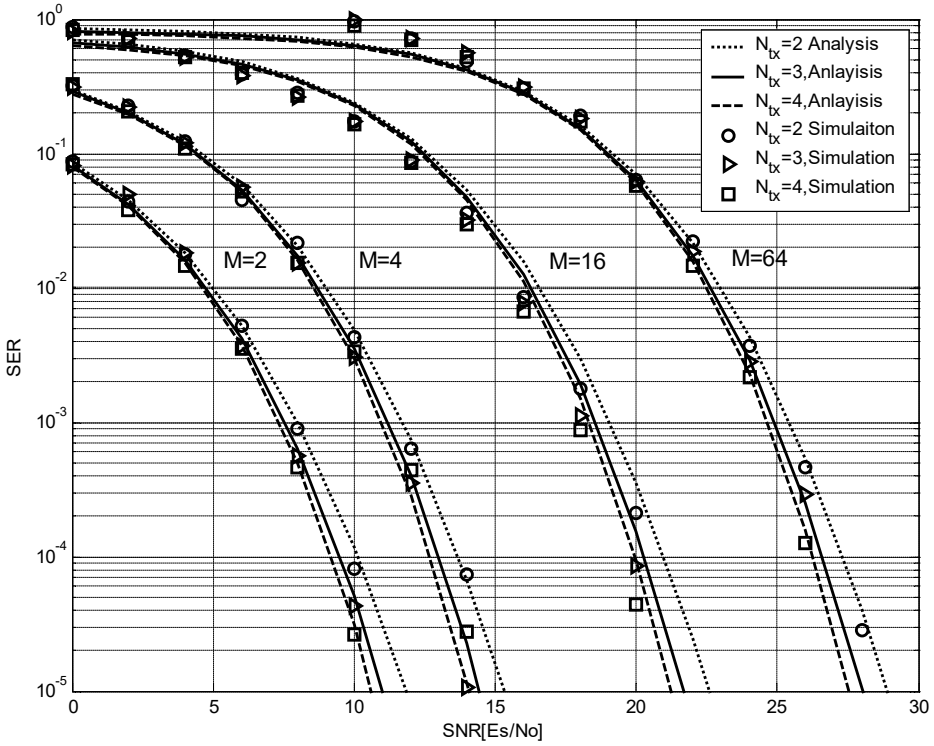


Figure 4.6 Performance of a CDD MC-CDMA system with Ntx = 2; 3; 4, N = 16, L = 1, m=5.

From Figures 4.5 and 4.6, it is evident that a CDD MC-CDMA system performs well in both low and high delay spread environments and depending on the channel conditions the desired SER performance can be achieved by trading the CDD branches and most importantly without any change to the receiver structure. Analytical results are generated by using (4.25) and (4.26) with $\widehat{\Omega}_{cdd}/N_{tx}$.

**STBC MC-CDMA**

For the performance evaluation of STBC MC-CDMA system, a full rate transmission matrix $G_2$ is used for $N_{tx}$ = 2, while for $N_{tx}$ = 3,4 transmit antennas, half rate matrices $G_3$ and $G_4$ of [73] have been chosen. The SER evaluation has been done by normalizing the sub-channels to unity. Considering the Rayleigh fading case ($m$ = 1), in Figure. 4.7, the numerical SERs are plotted for $N_{tx} = 2,3,4$ with a channel order of $L$ = 2.

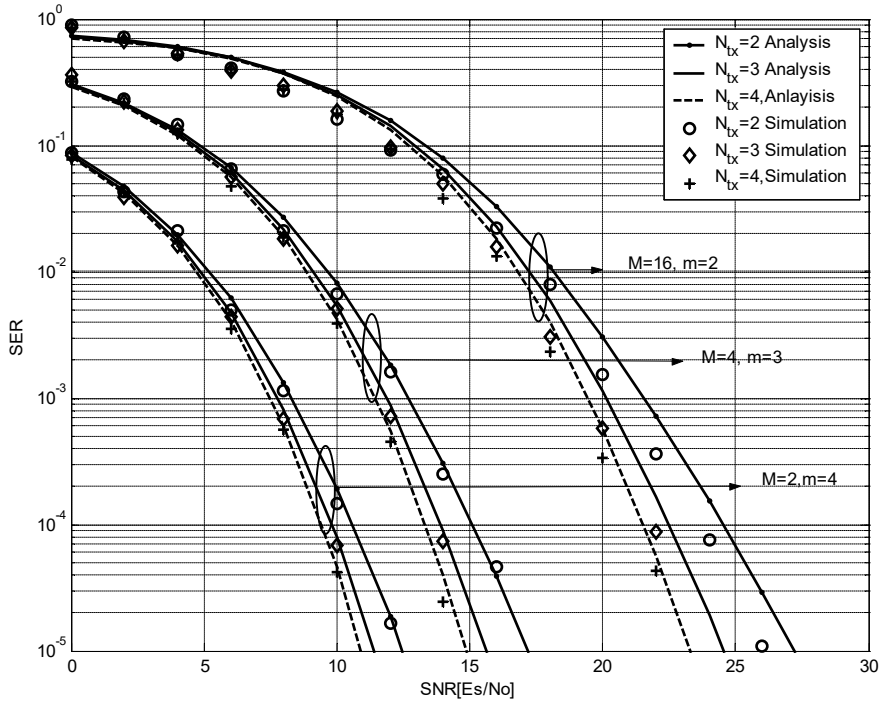


Figure 4.7 Performance comparison of STBC MC-CDMA system with Ntx=2,3,4 N=16, L=1, m=2,3,4 and δ=0

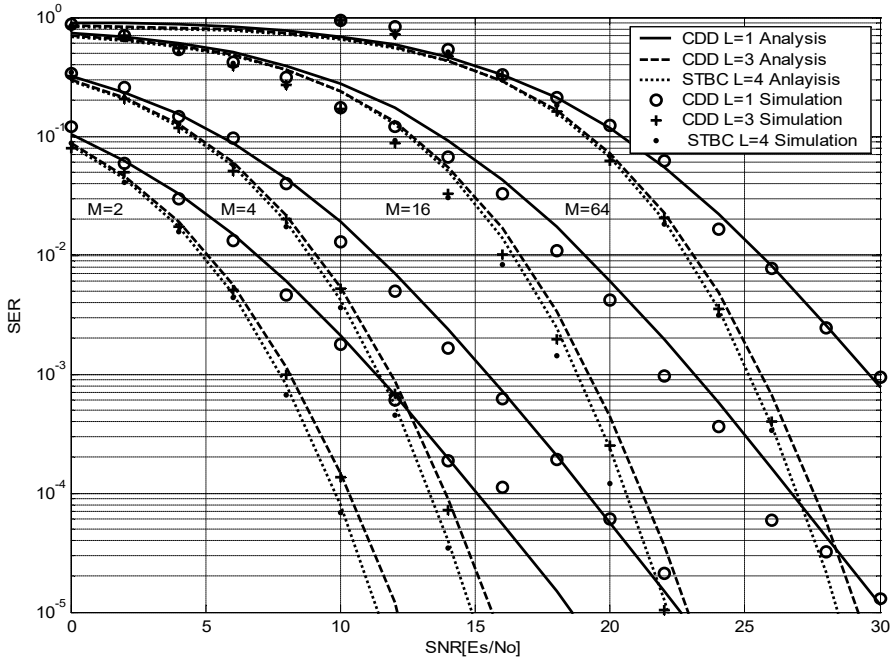


Figure 4.8 Performance comparison of STBC and CDD MC-CDMA systems with Ntx=3, Nrx=1, N=16, L=1,3,4, m=1 and δ=0

For the non-Rayleigh fading case, Figure 4.8 uses varying Nakagami-*m* values with different modulation indices *M*. It is important to highlight that for both CDD and STBC, the combination of higher channel orders ($L$ >2), transmit antenna ($N_{tx}$ > 3) and Nakagami parameter ($m$ > 4), results in saturated improvement in performances; unless additional receiver chains are employed.

In Figure 4.8, both, CDD and STBC diversity techniques are plotted with $N_{tx}$ = 3 and $m$ = 1. As expected, STBC performs better than CDD because of higher channel order and consequently, the diversity gain.

## 4.4 Performance Comparison- STBC&CDD MC-CDMA

### 4.4.1 Simulation Results

#### Uncoded Performance Comparison

In Figure 4.9. single user case, STBC for three and four transmit antennas only outperform the full rate STBC at high SNRs for the same spectral efficiency. In contrast to this, both CDD and STBC with $N_{tx}$ = 2 achieve the same diversity level. The curves for CDD with $N_{tx}$ = 3,4 show further improvement in the system performance. Hence, in a single user case CDD outperforms STBC even in an uncoded system.

The BER curves for an uncoded fully loaded system are shown in Figure 4.10. For an uncoded fully loaded system STBCoutperform CDD in all cases.

#### Coded Performance Comparison

In Figure 4.11, the full rate STBC and CDD are compared with half rate convolutional codes. It can be seen that CDD performs extremely well with channel coding, without any additional complexity or idealistic assumptions.

The effect of interleaving on diversity schemes is shown in Figure 4.12 The curves for a single transmit antenna with and without interleaving is also plotted for comparison. It is noticed that for a fully loaded system, the gain is less because of MAI.

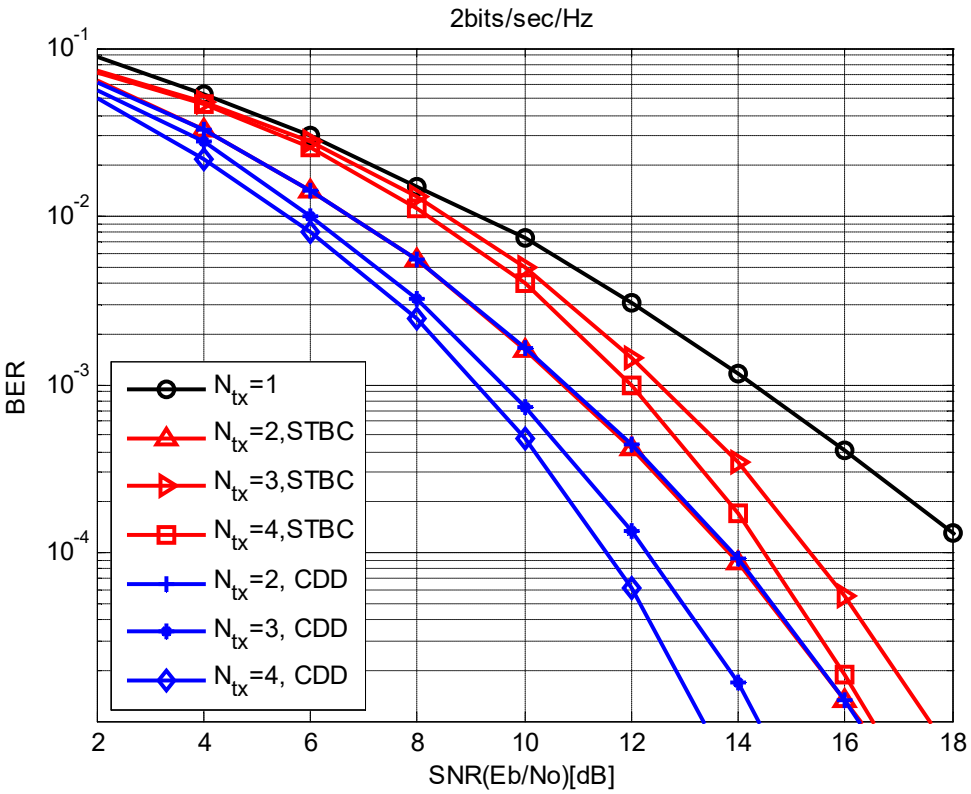


Figure 4.9 Bit error performance for a single user uncoded MC-CDMA system.

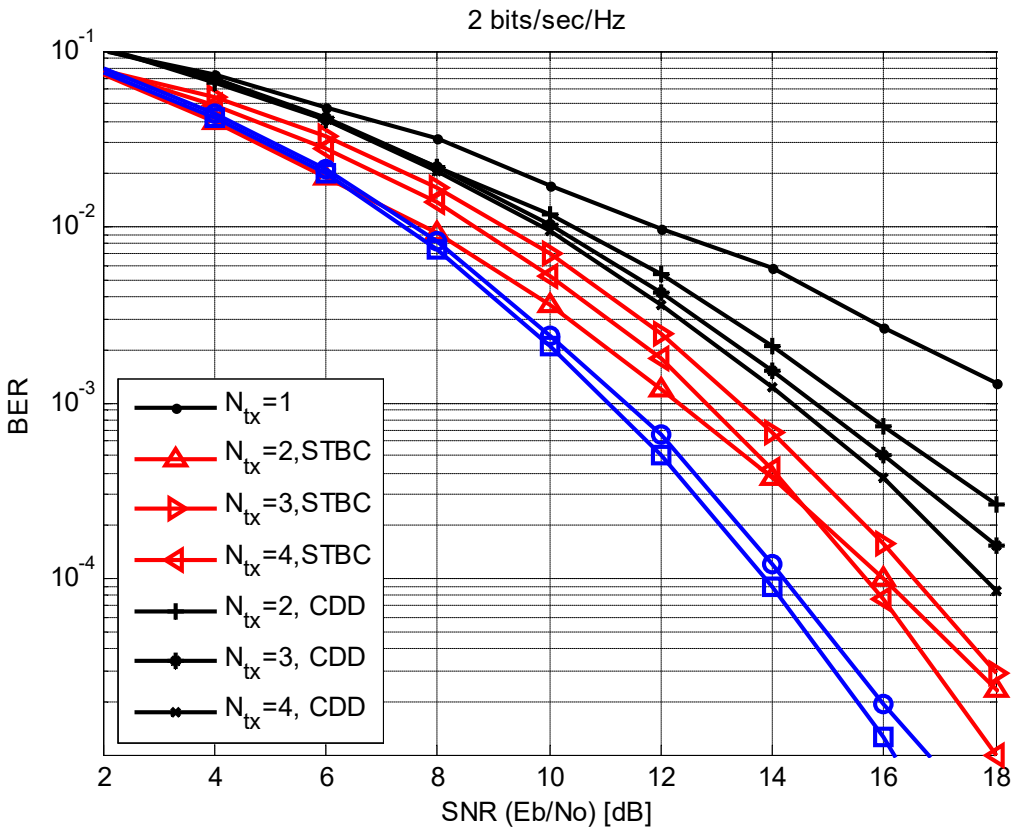


Figure 4.10 Bit error performance for a fully loaded uncoded MC-CDMA system.

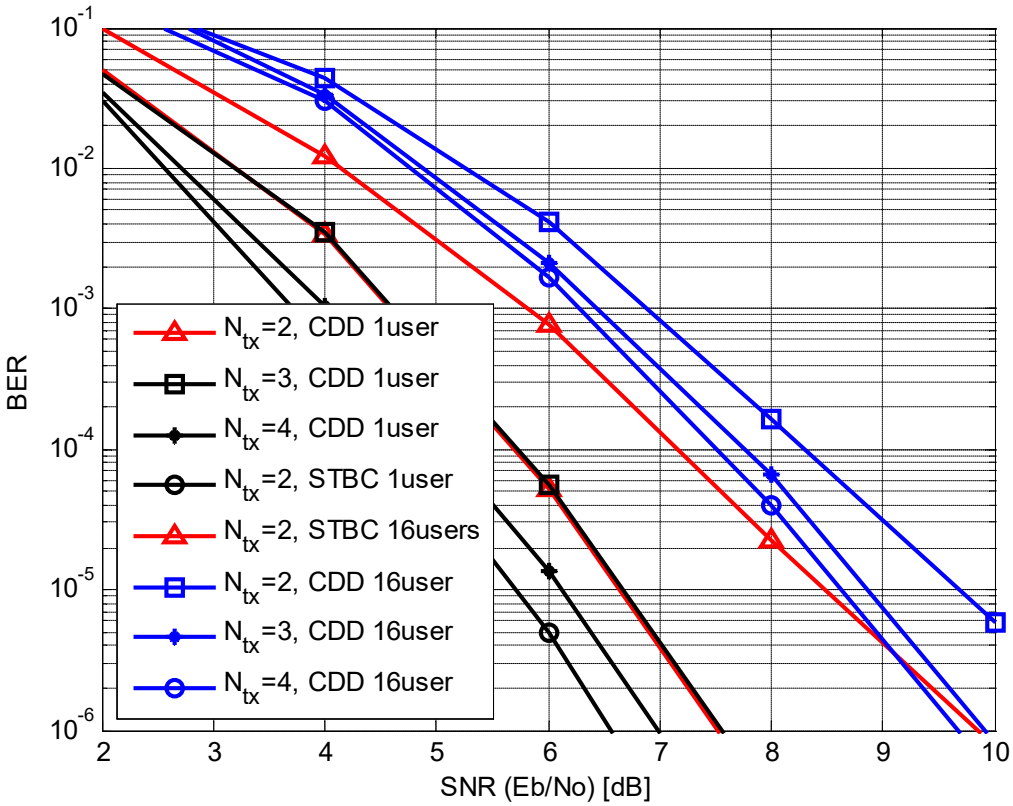


Figure 4.11 Bit error performance for coded MC-CDMA system.

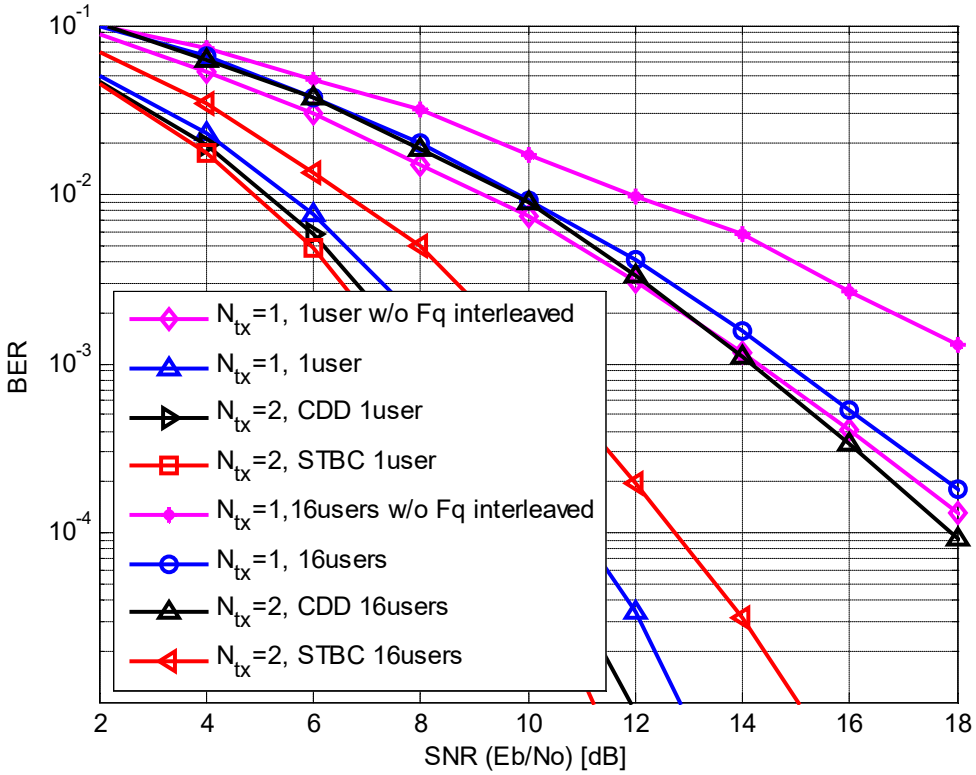


Figure 4.12 Effect of frequency interleaving on STBC and CDD schemes.

## 4.5 MIMO-OFDM performance Comparison

### 4.5.1 Simulation Overview OFDM-256 IEEE 802.16-2004

The OFDM-256 IEEE 802.16-2004[3] standard specifies the physical layer (PHY) for Channel Coding. According to the transmission structure the Channel Coding is based on three steps: randomizer, FEC, and interleaving. Regarding to the reverse link the corresponding operations are applied at the reception.

A randomizer is implemented which adds a pseudo-random binary sequence to the DL and UL bit stream in order to avoid long rows of zeros or ones for better coding performance. Following by a tail byte needed to bring the convolutional coder in zero state after each burst.

The forward error correction (FEC) scheme consists of the concatenation of a Reed-Solomon (RS) outer code and a convolutional inner code (CC).The encoding is performed

[3] The WiMAx platfrom simulation was implemented according to the **IEEE 802.16-2004 standard by the author.**

by first passing the data block format through a systematic RS(N=255,K=239,T=8) encoder using GF($2^8$) and then passing it through a zero-terminating convolutional encoder with constraint length 7. The CC rate varies between ½ and ¾, this paper is focus on ½ for comparative reasons.

Where

*N is the number of overall bytes after encoding*

*K is the number of data bytes after encoding*

*T is the number of data bytes which can be corrected.*

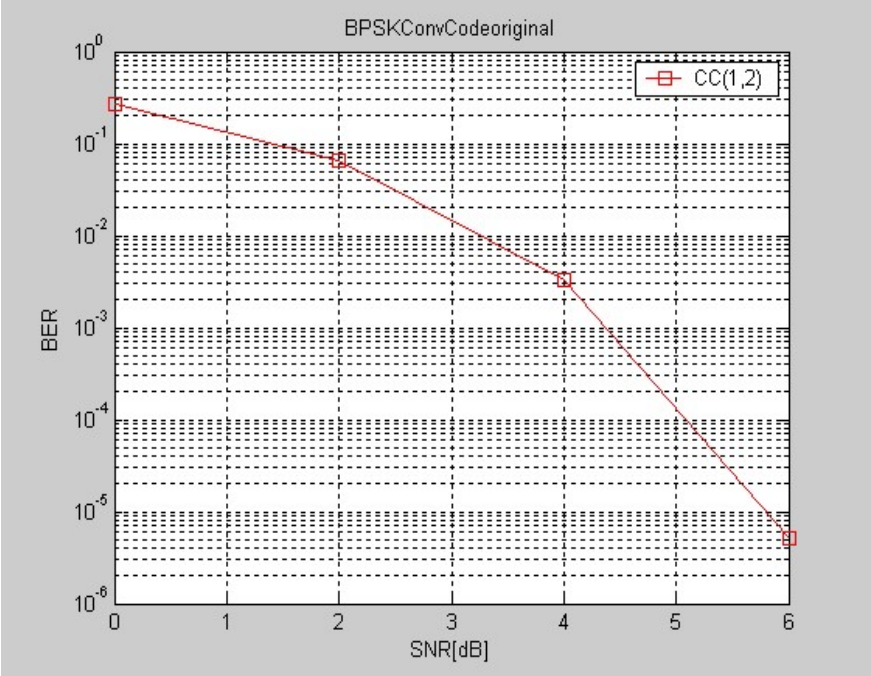


Figure 4.13 BPSK ½ Convolutional Code.

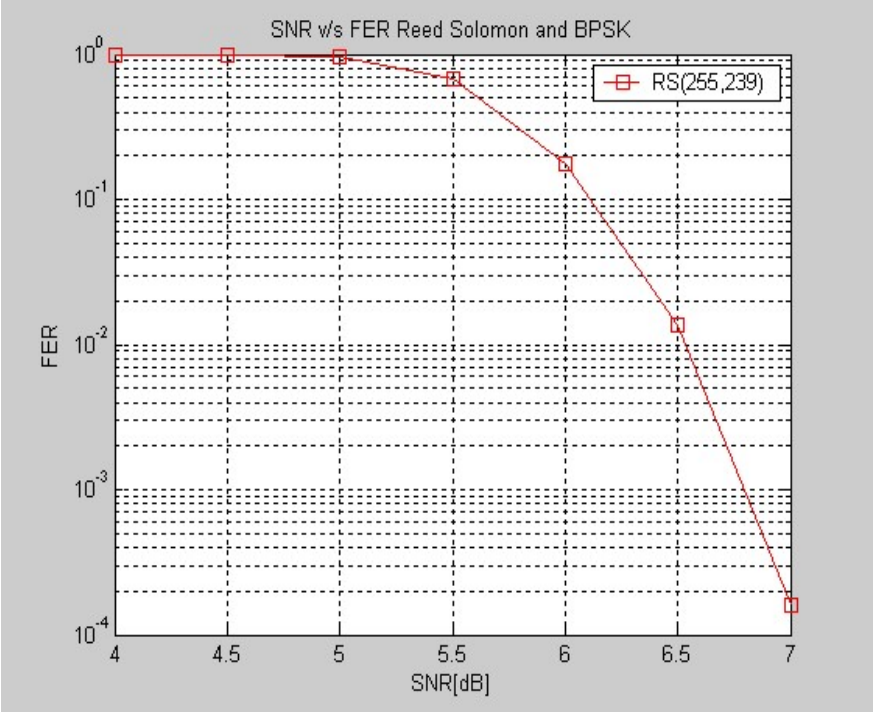


Figure 4.14 SNR vs FER Reed Solomon Code and BPSK

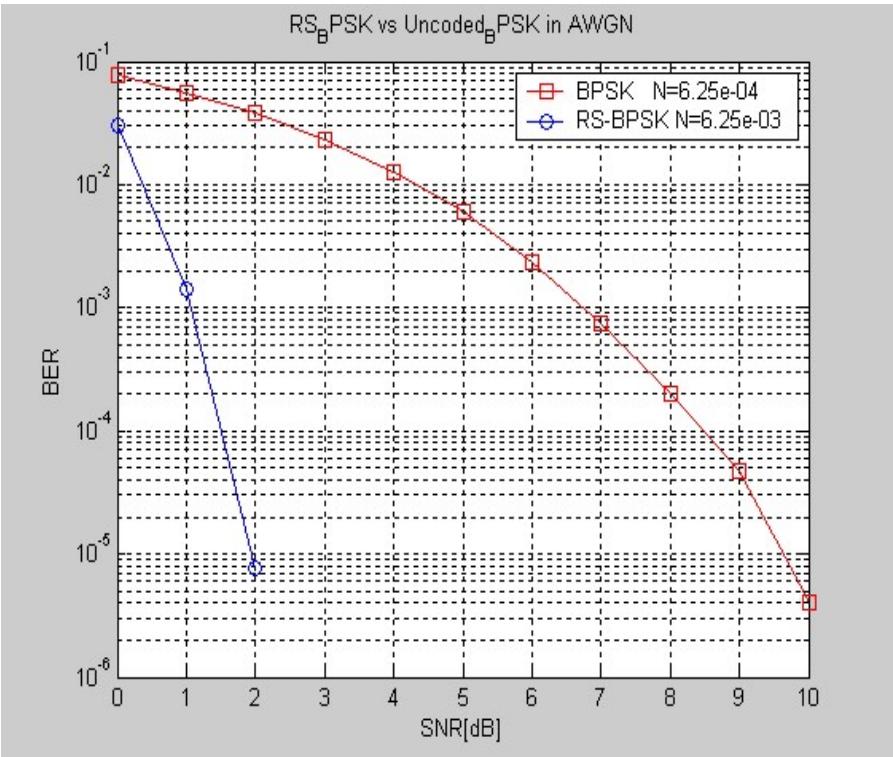


Figure 4.15 BER coded vs uncoded BPSK by RS

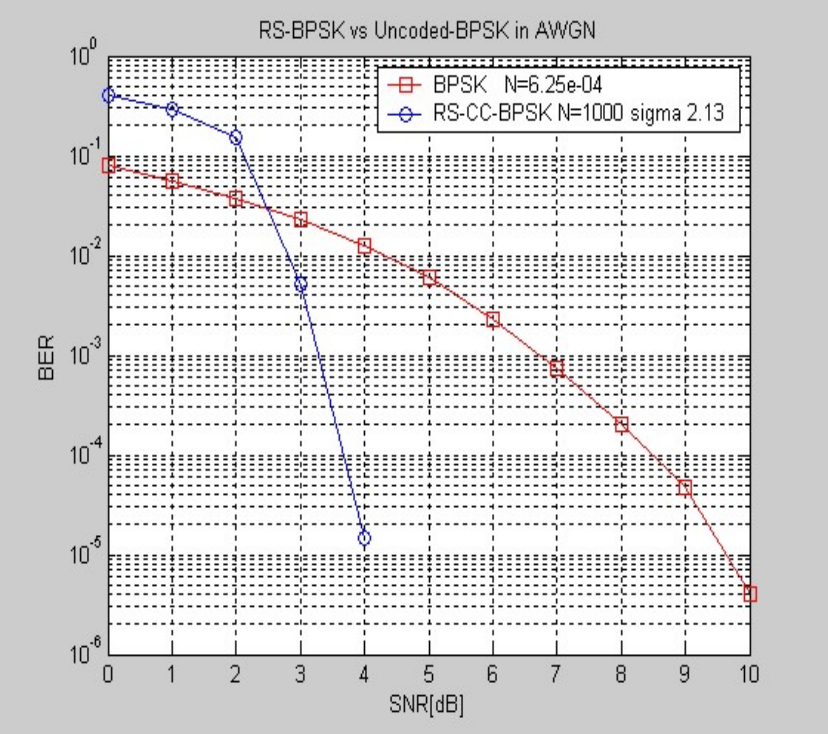


Figure 4.16 BER coded vs uncoded BPSK concatenated CC-RS

The Reed-Solomon encoding shall be derived from the following polynomials

Code Generator Polynomial based on $\lambda$ as a RS factor.

$g(x) = (x + \lambda^0)(x + \lambda^1)(x + \lambda^2) \dots (x + \lambda^{2T-1}),\ \ \lambda = 02_{HEX}$

Fiel Generator Polynomial

$p(x) = x^8 + x^4 + x^3 + x^2 + 1$

This code is shortened and punctured to enable variable block sizes and variable error-correction capability. The concatenation of both codes is made rate-compatible by a puncturing and shortening patterns bits, to enable variable block sizes and variable error-correction capability. It is known that the RS coder corrects burst errors at the byte level. It is particularly useful for OFDM links in the presence of multipath propagation. Besides the correctively over independent bit errors provided by the CC.

In order to reduce the effect of burst errors an Interleaving composed of a block and bit interleaver is also implemented. The block interleaver maps adjacent coded bits onto non-adjacent subcarriers to overcome burst errors. The bit interleaver maps adjacent coded bits alternately onto less and more significant bits of the constellation to avoid long runs of unreliable bits. After puncturing, the binary coded bits are sent to a Space Time Block

Code (STBCs)-OFDM, which maps bits to antennas and tones so as to exploit full diversity in both space and frequency.

The interleaved bits are then mapped to Gray coded data symbols. binary phase shift keying (BPSK) quaternary PSK (QPSK), 16-quadrature amplitude modulation (QAM), and 64-QAM are the modulation schemes to modulate bits to the complex constellation points. The FEC options are paired with the modulation schemes to form burst profiles, i.e., PHY modes of varying robustness and efficiency. For comparison proposes only BPSK is considered in this paper. Space Time Block Code (STBCs) is an optional feature that can be implemented in the DL to provide increase diversity.

*Table 4.1 Simulation Layout Comparison CDD*

Table 0.1 Parameters of the simulation system

| | | |
|---|---|---|
| FFT-length | $N_{FFT}$ | 256 |
| No. of subcarriers | $Nc$ | 256 |
| Bandwidth | B | 6 MHz |
| Subcarrier spacing | $f_{sc}$ | B/ $Nc$= 23.437 kHz |
| OFDM symbol duration | $T_{OFDM}$ | $1/\Delta f_{sc}$ = 42.7 $\mu sec$ |
| Sampling time | $T_s$ | $T_{OFDM}$ / $N_{FFT}$ = 0.166 $\mu sec$ |
| Guard interval length | | 64 samples |
| Modulation | M = 2 | BPSK, |
| Detection | | ML,MRC |
| Channel coding | FEC | RS(255,239,8) outer coded concatenated with $(133,171)_8$ convolutional code, rate ½, Viterbi decoding |
| Delay profile | | 3-tap, SUI-3,power decay |
| Max. delay profile | $\tau_{max}$ | 0.9 $\mu sec$ |
| Doppler frequency | $f_D$ | 6.6 Hz (3km/hr@ 2.4GHz) |
| Channel estimation | | Perfect |

*Simulation results*

*Uncoded performance comparison*

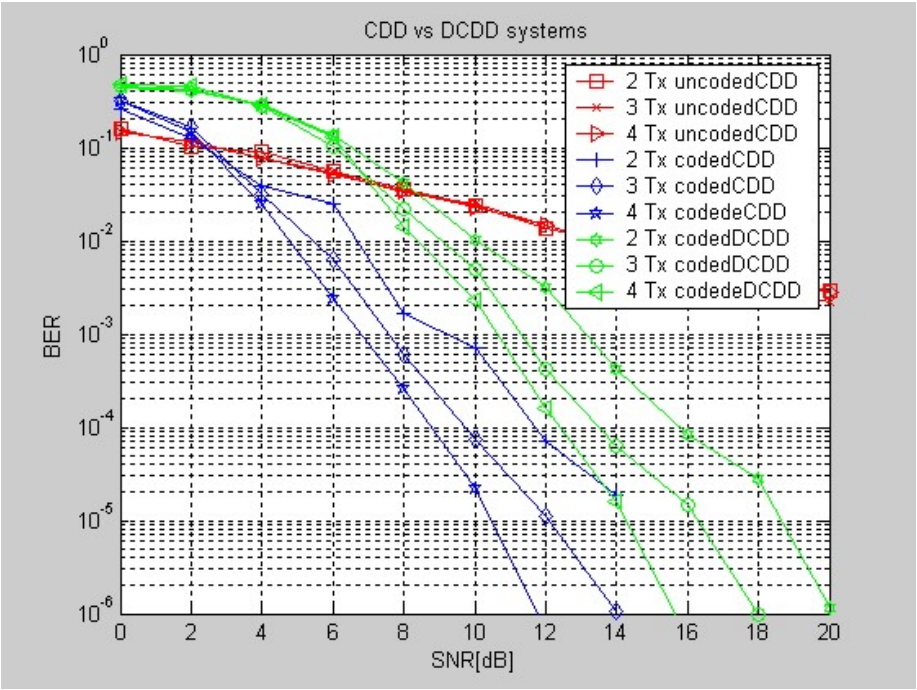


Figure 4.17 Uncoded performances for a single user CDD vs DCDD systems

The link level performance assesses the behavior of realistic communications systems in terms of error-rates versus the receiver signal –to-noise ratio (SNR). For comparison proposal a simple communication system modulator/demodulator utilizing binary phase shift keying (BPSK) is considered, which operates over a wireless channel with spectral efficiency of 1 bit/s/Hz. The main reason of any link simulator is to find an equivalent SNR at which ideally is error-free for transceivers of finite complexity, as the error of such system only decreases asymptotically with an increasing SNR. Therefore, to guarantee an error-free link, the SNR has to approach infinity (for the given additive Gaussian noise model).

That has obviously little meaning for a system designer, which is the reason why finite complexity transceivers are said to yield a virtually error-free communication when the achieved error-rate falls bellow a certain threshold. To visualize the trade-off for complexity-performance, a CDD system for coherence detection shows a better practical performance approach against a DCDD performance in case of non-coherence detection. On the other hand the curves show respectively, the advantage provided by introducing Frame Error Correction (FEC). For this simulations only a half rate convolutional encoder(R=1/2, $(133,171)_8$) and soft Viterbi decoder are used for channel coding and decoding. It can be seen the benefits getting better performance without increasing the

complexity at the receiver as said before. A simulation platform based on the HIPERLAND/2 standard mode1 [95] has been used to compare the Bit Error Rate (BER) performance between the CDD vs DCDD transmit diversity schemes with an outer channel code. A total bandwidth of 20 MHz with a sampling rate of 0.05 $\mu sec$ or 16 samples has been employed. A 64 subcarrier point IFFT/FFT is employed for a 64 data subcarriers. This gives a subcarrier spacing of 312.5 kHz.
For CDD and DCDD with *NTx*= 2,3,4 schemes there is no compensation for the rate loss in order to evaluate them with the same symbol mapping.

### 4.5.1 Throughput

There are numerous MIMO-OFDM systems. To adequately analyse the advantages and drawbacks of the systems presented here, each system was simulated. Two performance metric were used: PER and throughput ratio. A packet was assumed to be in error if any one bit was not received adequately.
Once the PER was obtained via simulation, the throughput ratio was calculated using the formula: Number of information bits Total number of transmitted bits SNR

$$Throughput \quad Ratio = \frac{\text{Number of information bits}}{\text{Total number of transmitted bits}}\left(1-\wp(\text{SNR})\right) \tag{4.27}$$

where $\wp(\text{SNR})$ is the PER for a particular SNR value obtained via simulation.

*Simulation Parameters*

As mentioned earlier, MIMO systems where *Nrx=Ntx* are considered in this work. Specifically, the $2\times 2$ and $4\times 4$ cases were considered in this performance study. Each MIMO system was simulated with the 3 various equalising techniques discussed: ML, MMSE, and ZF. Furthermore, each system was simulated both with and without a channel code. The code used was the ½ rate convolution code as used earlier and specified in WiMAX With the exception of ML equalisation, both hard and soft decisions were used to de-map the symbols when the bit-stream was coded. With Ml, only hard-decisions were used as ML inherently makes hard decisions on the symbols. Each system had *N=64* subcarriers, with CP length of *C*=16 symbols. The packet length was 1024 bits which included 6 zero bits at the end of each packet if the bit-stream was coded. The zero state at the end of each packet.

It was assumed that the channel was perfectly known at the receiver and that the channel remained static throughout the transmission of each packet. To simulate the channel, each channel path was assumed i.i.d. and was drawn from complex Gaussian distribution with zero mean and variance (2$L$)-1 per dimension, where the channel length, $L$ was set to 10 and was assumed sampled at the symbol period. The channel length of 10 was adequate frequency selectivity without being greater than the length of the CP.

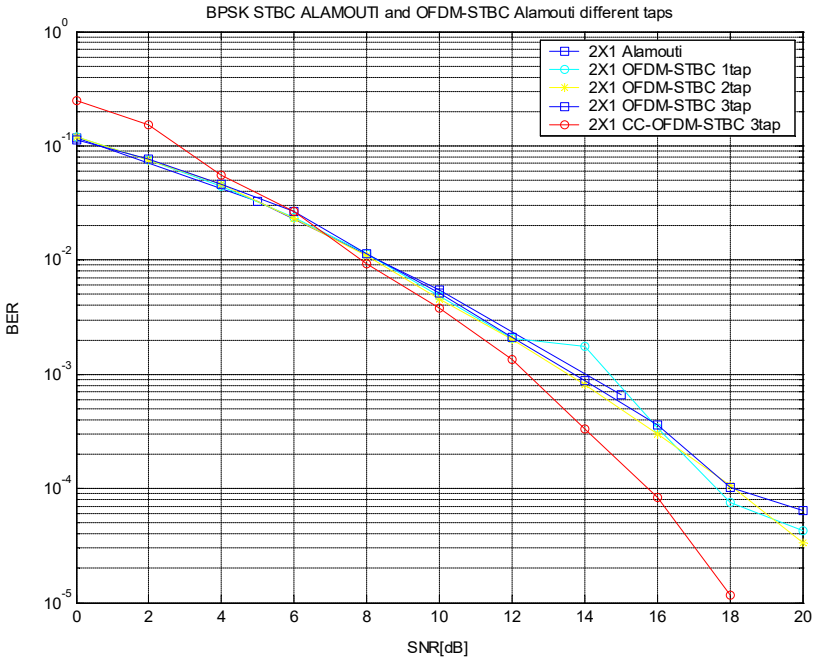


Figure 4.18 2Tx-1Rx CC-OFDM-STBC system

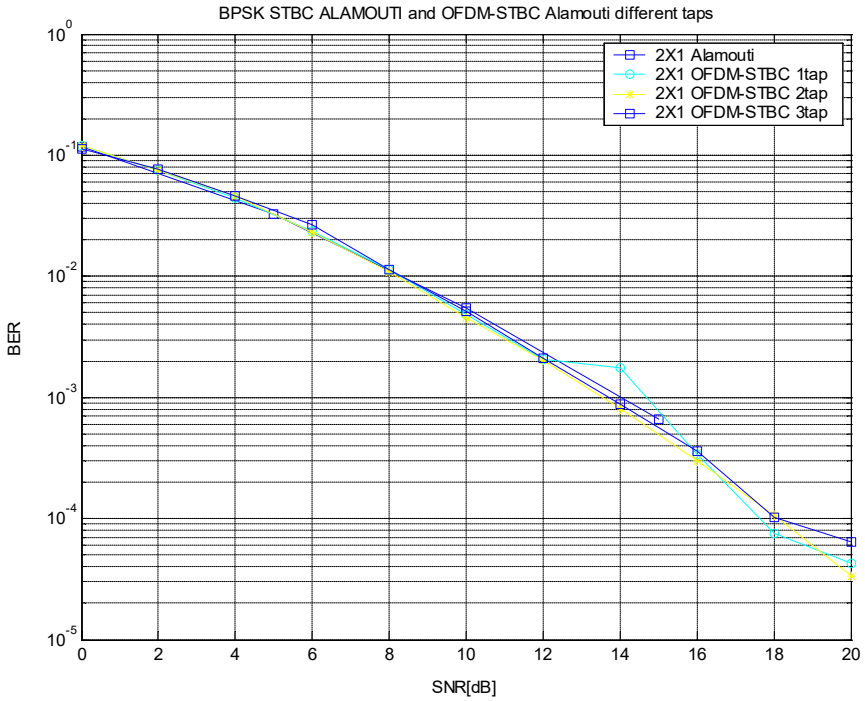


Figure 4.19 2Tx-1Rx OFDM-STBC for several taps

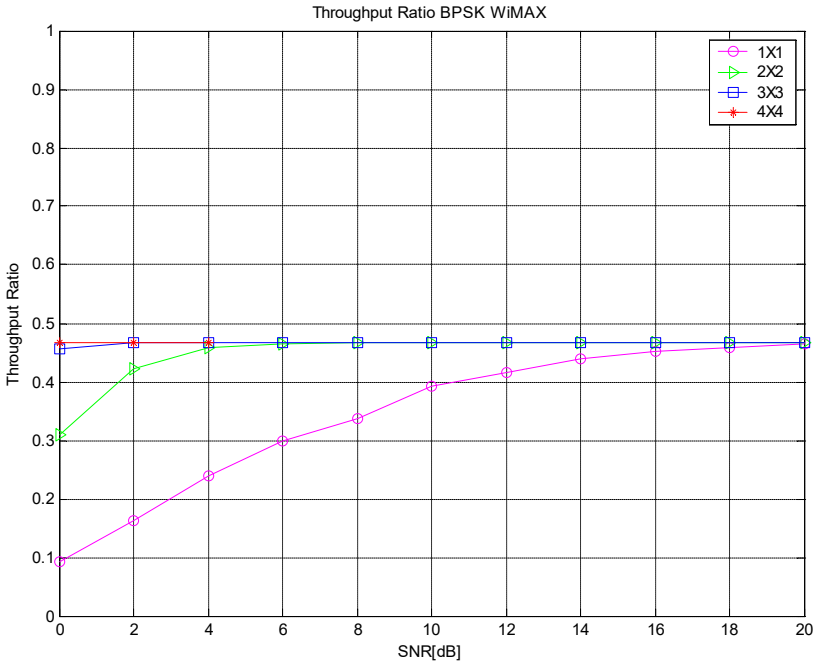
Throughput Ratio BPSK WiMAX
Throughput Ratio
SNR[dB]
1X1
2X2
3X3
4X4

(a)

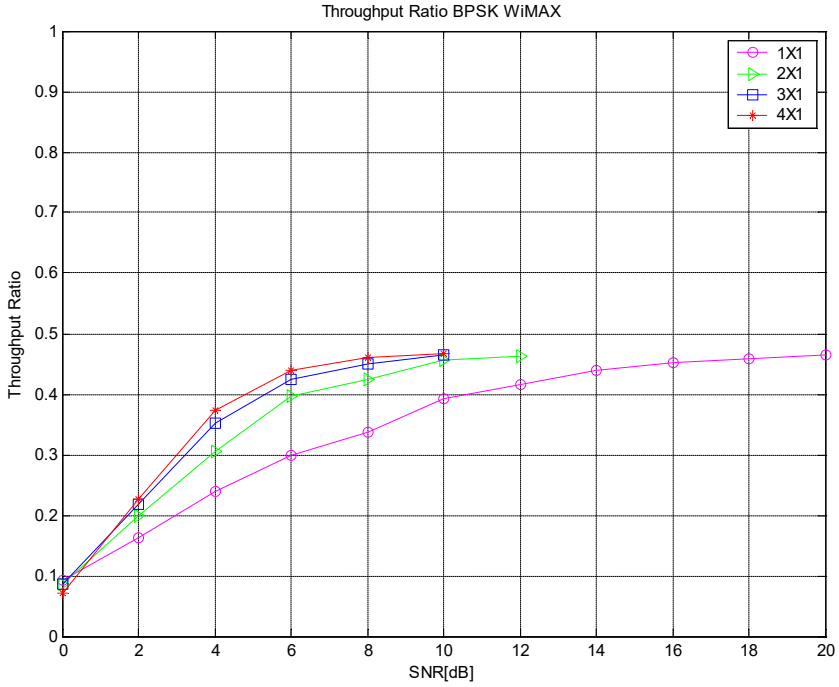
Throughput Ratio BPSK WiMAX
Throughput Ratio
SNR[dB]
1X1
2X1
3X1
4X1

(b)

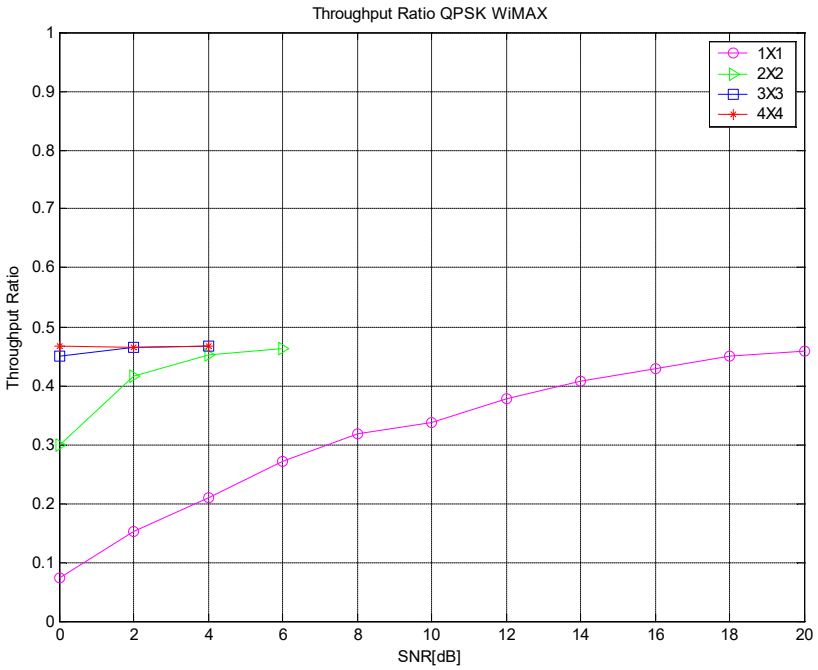


(c)

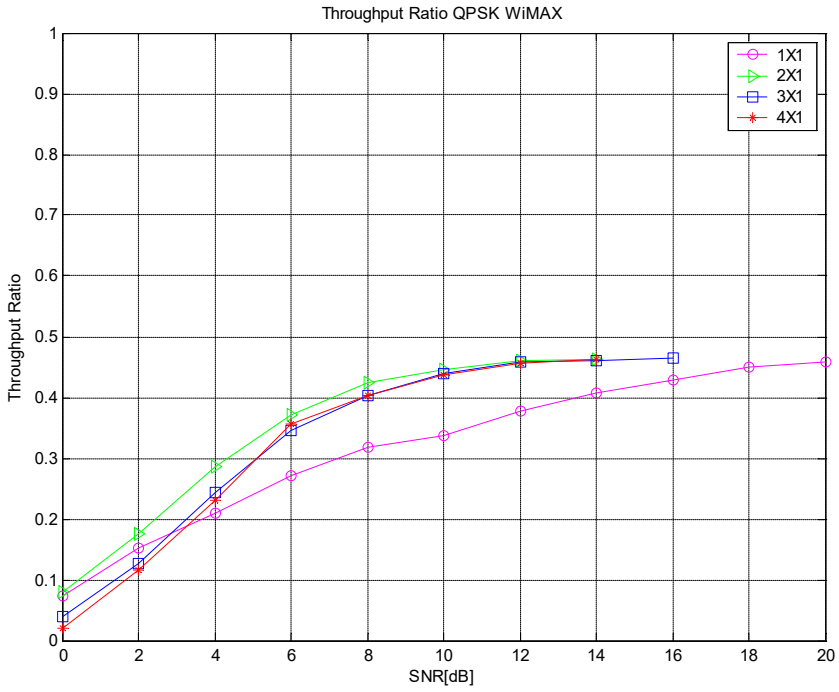


(d)

Figure 4.20 Throughput generated for BPSK and QPSK in WiMAX system

Having evaluated the proposed systems based on complexity, error rate performance and throughput, it is clear that no one system will provide low complexity with low error rate and high throughput. The $4\times4$ STBC systems provide excellent error rate performance but provide less throughput even the $2\times2$ STBC systems.

Annex I

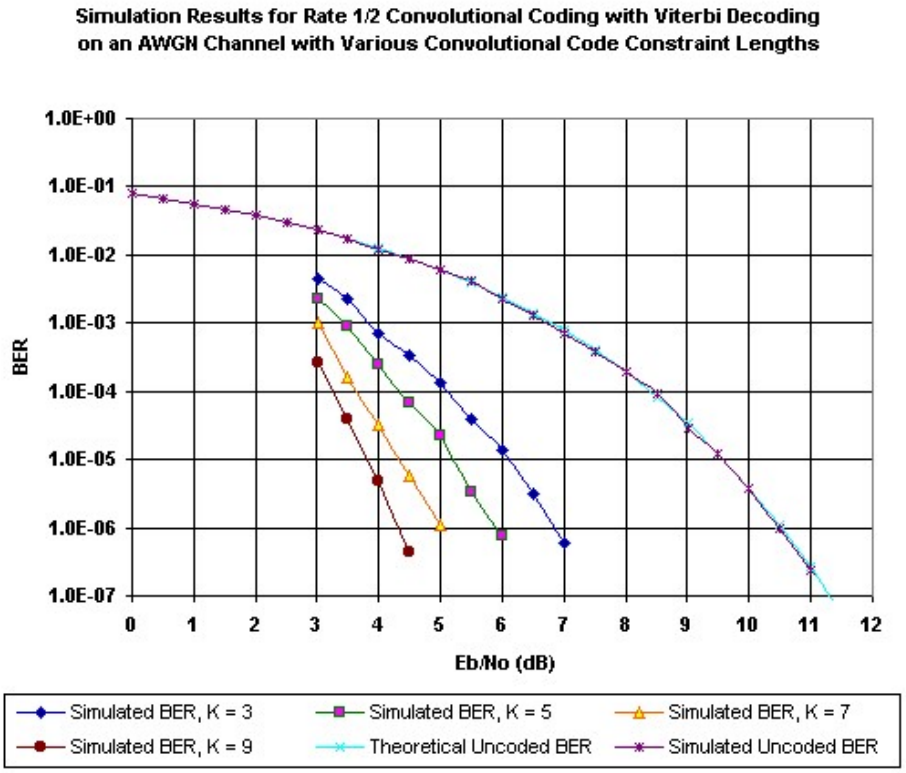


Figure 4.21 Simulation Results for Rate ½ Convolutional Coding with Viterbi Decoding

In order to provide reliable simulation results every component of the protocol was benchmarked independently with the theoretical performance. Figure 4.21 shows the performance for ½ rate Convolutional Coding with Viterbi Decoding on an AWGN Channel with Various Convolutional Code Constraint Lengths.

## 4.5 Summary

In this chapter the system modelling along with performance analysis of CDD and STBC MC-CDMA systems were presented.

The comparison is done with variable number of transmit antennas and different system loading conditions. Interleaving (time and frequency) methods are well known for randomizing the error distribution which helps in improving the performance of any given

system with the help of FEC or channel coding. For this reason, frequency interleaving is also included in the comparative study of CDD and STBC MC-CDMA system.

This chapter has shown how narrowband MIMO systems can be used in wideband channels with OFDM thus achieving higher data rates. Achieving large data rates however, is not the only objective of a wireless system. Factors such as reliability and complexity must also be considered. To this end, MIMO-OFDM systems were analysed, first with a mathematical framework, then via simulation. Complexity, error rate performance, and throughput were the metrics used for analysis.

# Chapter 5

# Distributed Cooperative Multi-hop Relaying Systems

## 5.1 Introduction

We advocate the introduction of cooperative methods into omnipresent wireless communication systems. Even for highly centralized systems such as the cellular wireless communication networks, cooperation demonstrates its strength in offering increased quality in service with less complex terminals.

The concept of Cooperative communications has been proposed recently as an effective way to mitigate channel impairments. In an effort to improve the performance of wireless networks, there has been increased interest to answer: how the signals should be distributed to and collected from wireless terminals in the most efficient manner. The developments in this direction will yield to enhanced coverage, throughput, and QoS, as well as cost-efficient and compact wireless terminals. Although the use of advanced signal processing techniques and smart antennas as in [80], have evolved dramatically, for practical reasons, these techniques alone do not seem to be sufficient to enable ubiquitous high data rate coverage.

For instance, it may be infeasible to deploy complex antenna systems at wireless portable terminals; and alternatively a drastic increase in the number of access points is not economically justifiable. Therefore, more fundamental enhancements are necessary for the very ambitious capacity, throughput, and coverage requirements of wireless communications. Towards that end some major modifications in the wireless network structure itself are needed. The authors present an algorithm to enable integration of multi-hop capability in conventional wireless networks, Cooperative spatial cyclic delay diversity (CDD) is proposed applied to systems such as Multi Carrier Code Division Multiple Access (MC-CDMA), as Figure 5.2. The intermediate relayers /routers in such

multi-hop augmented networks may need low-complexity; the analysis shows that the presence of CDD as in [71] helps in achieving the maximum frequency diversity from the broadband channel into a highly selective one. The data is no decoded except for CDD by the relaying terminals until it reaches the final target sink.

The contribution presents the implementation of fractional allocation strategies rather than advantages of cooperation at the physical layer. To accomplish a logical thread in deriving the fractional allocation strategies, this research was mainly organized by presenting the theoretical foundations which are laid on the frequency domain Nakagami-*m* fading channel model with regards to specifically CDD-MC-CDMA system. The analysis of how CDD MC-CDMA collapses to a single transmit antenna system with highly selective channe presented was previously presented and used to derive closed form expressions.

In this chapter throughput-maximizing resource allocation strategies are derived showing the numerical and simulation results to support the derivation of resource allocation strategies for distributed cooperative STBC and CDD multi-carrier systems.

It is aim of this chapter to analyse the behavior of distributed-MIMO multi-stage communication networks with the aid of the theory developed in the previous chapter. An example realization of the system Figure 5.4 and the named communication network depicted in Figure 5.2. Of major interest here is to maximize the end-to-end throughtput by optimally assigning resources in terms of frame duration, frequency band and tramsission power for each of the terminals. These resources are usually constrained, thus calling for effective allocation strategies. Since resources have to be shared among all terminals involved, the allocation strategies to be developed are referred as fractional resource allocation strategies.

The two major approaches to accomplish a relaying network are transparent or regenerative relaying. For the transparent case, a relaying terminal receives a signal stream, process it and re-transmits it. From a capacity perspective it is clear that regenereative relaying outperforms transparent relaying for the particular communication scenario of SISO relaying over falat Rayleigh fading channels. Additionally, regenerative relaying allows the deployment of MIMO capacity enhancement technologies at each relaying stage. These are the reasons why regenerative relaying is considered in this thesis. It is therefore the aim to allocate fractional resources to each relaying terminalsuch as to maximize the end-to-end throughtput in dependency of prevailing channel

conditions.

The problem formulation to similar resource allocation problems with partial solutions to achieve maximum throughtput has been analysed in [39] [40]. A generic operational mode of wireless network is defined in [93], that covers both routing, scheduling and power control. Joint routing problem. In [[91], a joint scheduling-power control solution to the multiple access problem in wireless ad-hoc networks is introduced.

In [86], a jointly optmal scheduling, routing and power control algorithm achieving max-min fair rate allocation in one-dimensional network is presented. The capacity regions for wireless ad-hoc networks with an arbritary numbero of nodes and topology are studied in previously. Here, the transmission rate to match the SNR at the receiver. In recent research, the capacity region and optimal power allocation scheme for a multi-user fading broadcast channel is derived in which minimum rates must be maintained for each user in all fading states.

Three types of capacity (ergodic, zero-outage and outage with nonzero outage) regions for fading broadcast channels and their correspondingoptimal resource allocation that achieves the boundary of the ergodic capacity region is derived by solving an optimization problem over a set of time-invarient Gaussian broadcast channels with a onstrained total average transmit powe. Finally, the capacity region of the downlink broadcast channel in fading and additive white Gaussian noise dor the time-division, frequency-division, and code-division is studied in [31].

All solutions to the respective optimization problems, however, requieres somo form of numerical optimization. It is the ain of this chapter to introduce for the first explicit resource allocation strategies for regenerative distributed-MIMO multi-satage communication scenerarios contrained by a total utilized power $S$, bandwidth W and frame duration $T$.

This chapter is organized as follows. In 5.1, the system assumptions are introduced, as well as the notation to be used thorught the remainder of the chapter. It is also demonstrated how to relate the obtained fractional bandwidth and power of a TDMA-based system. Subsequent analysis therefore focused onto FDMA-based system only.

Analysis then split intro egorgodic and non-ergodic flat fading channels, the optimum fractional resource allocation strategies for each are then introduced in 3.2 and 3.3, respectively. In each of the sections, the following communication scenarios have been analysed in sufficient depth; (1) distributed-MIMO muti0stage relaying without resource reuse, (2) distributed-MIMO multi-stage relaying with resource reuse, and (3) distributed

O-MIMO multi-stage relaying with and without resource reuse. A network with resources reuse allows allocating e.g, the same fractional bandwidth to tminals which have sufficient spatial separation. That is shown to influence the fractional resource allocation strategy.

In 3.4, it is then shown that the very same algorithms are also applicable to frequency selective fading channels, which makes them applicable to currently deployed CDMA and OFDMA based communication systems.

Finally a summary of the results of this chapter, the research contribution, and future research.

Notation: Upper and lower bold face letters represent matrices and column vectors, respectively. Superscript $(\cdot)^H$ and $(\cdot)^T$ denote Hermitian, and transpose, respectively. E[·] is for expectation. $I_x$ and $F_x$ are used for the X×X identity and normalized unitary fast Fourier transform (FFT) matrices; diag[x] stands for a diagonal matrix with x on its main diagonal.

## 5.2 System Model

### 5.2.1 General Deployment

With reference to Shannon's definition of channel capacity, regenerative relaying allows the utilisation of two access methodologies: frequency division multiple access (FDMA) and time division multiple access (TDMA). FDMA-based regenerative relaying implies that the totally available bandwidth *W* is orthogonally or non-orthongonally partitioned among the relaying CSD tiers, as depicted in Figure 5.2; communication may occur continuously over the entire frame duration *T*. On the other hand, TDMA-based regenerative relaying implies that total frame duration *T* is orthogonally or non-orthogonally partitioned into slots among the relaying CSD tiers, as depicted in Figure 5.3; communication occurs over the entire bandwidth *W*.

For orthogonal relaying, available resources are divided such that no interference between the relaying stages occurs. Thus, bandwidth/frame has to be fractioned into non overlapping frequency-bands slots such that at any time they are used by only one relaying link. On the other hand, non orthogonal relaying allows resources to be re-used among stages, which leads to interference between the relaying CSD tiers.

The encoding, distributed relaying and decoding process is described for an FDMA based relaying system as follows.

**Source ST**- In an FDMA-based relaying system, the s-ST continuously broadcast the data to the remaining r-STs in the first relaying CSD tier, utilising negligible power and bandwidth, and possibly not deploying all of its available sensor elements.

**First relaying CSD Tier**. The first CSD relaying tier is formed by $q_1$ spatially adjacent STs (including the s-ST). Each of the involved STs possess $n_{1.i}$ sensor elements for inter CSD relaying purposes, where the first subscript relates to the first CSD relaying tier and $1 \leq i \leq q_i$ .

After cooperation between the s-ST and the remaining r-STs of the first relaying CSD tier, the data is space-time encoded according to a given code book with $t_1 = \sum_{i=1}^{q_1} n_{1,i}$ spatial dimensions. Each ST then transmits only $n_{1,i\in(1,q_1)}$ spatial dimensions such that no transmitted codeword is duplicated. Transmission from the first relaying CSD tier is accomplished at frequency band $W_1$ with total transmission power $S_1$.

**Second Relaying CSD Tier**. The second CSD relaying tier is formed by $q_2$ spatially adjacent MTs such that their inclusion into the CSD yields capacity benefits to the communication system.

Each of the $q_2$ STs possesses $n_{2,i\in(1,q_2)}$ sensor elements. Some STs may cooperate among each other, thereby forming $Q_2$ clusters, where $1 \leq Q_2 \leq q_2$. The case of $Q_2 = 1$ represents the scenario where all STs cooperate, whereas $Q_2 = q_2$ means that none of the STs cooperate. The former case clearly yields the best performance however, at the expenses of additional transceiver complexity to realise the cooperative; also additional bandwidth and power are required to accomplish the relaying process. The later case yields less gain; however, it will be shown that the performance of such system still outperforms a traditional SISO relaying system.

The $j^{th}$ cluster assumed to contain $r_{2,j}$ receive sensor, where $1 \leq j \leq Q_2$ and $\sum_{i=1}^{q_2} n_{2,i} = \sum_{j=1}^{Q_2} r_{2,j}$. Therefore, $Q_2$ MIMO channels are created, each with $t_1$transmit sensors and $r_{2,j\in(1,Q_2)}$ receive sensors.

After cooperation, the data is space-time decoded and re-encoded according to a given code book with $t_2 = \sum_{i=1}^{q_2} n_{2,i}$, spatial dimensions. Again, each ST then re-transmits only $n_{2,i\in(1,q_2)}$ spatial dimensions such that no re-transmitted code word is duplicated. Re-transmission from the second relaying CSD tier is accomplished at frequency band $W_2$ with total transmission power $S_2$.

$v^{th}$ Relaying CSD tier. The reception, cooperation, de-coding, re-encoding and retransmission process is congruent to the proceeding described above. Again, $Q_v$ MIMO channels created. All of these MIMO channels will have $t_{v-1}$ transmit atennas and $r_{v,j\in(1,Q_v)}$ receive sensors. After coopertation, the data is space-time decoded ad re encoded according to a given code book with $t_v = \sum_{i=1}^{q_v} n_{v,i}$ spatial dimensions. Re transmission from the $v^{th}$ relaying CSD tier is accomplished at frequency band $W_v$ with total power $S_v$.

$V^{th}$ Relaying CSD Tier. The final relaying tier contains the t-ST. Similar to the $1^{st}$ tier, only cooperative STs are considered here (no cooperation between the r-STs and the t-ST would terminate the data flow in the respective r-STs). Therefore, there will be one MIMO channel with $t_{v-1}$ transmit antenna and $\sum_{i=1}^{q_V} n_{V,i}$ receive sensors.

**Target ST**. After cooperation between the r-STs and the t-ST, the data is space-time decoded and passed on to the information sink in the t-ST.

A TDMA-based sysem operates exactly like the above-described FDMA-based relaying system, with the only difference that all fractional bandwidths $W_{v\in(1,K)}$ need to be replaced by fractional frame durations $T_{v\in(1,K)}$ . Here, *K* denotes the number of relaying stages and is related to the number of CSD relaying tiers via *K*=*V*-1.

For any scenario, the total communication duration is normalised to *T* and the total bandwidth to *W*. For orthogonal TDMA and FDMA-based relaying systems, $T = \sum_{v=1}^{K} T_v$ and $W = \sum_{v=1}^{K} W_v$, respectively. For non-orthogonal (interfering) relaying systems, the sum of all utilised fractional resourcces need to add-up to *T* and *W* respectively.

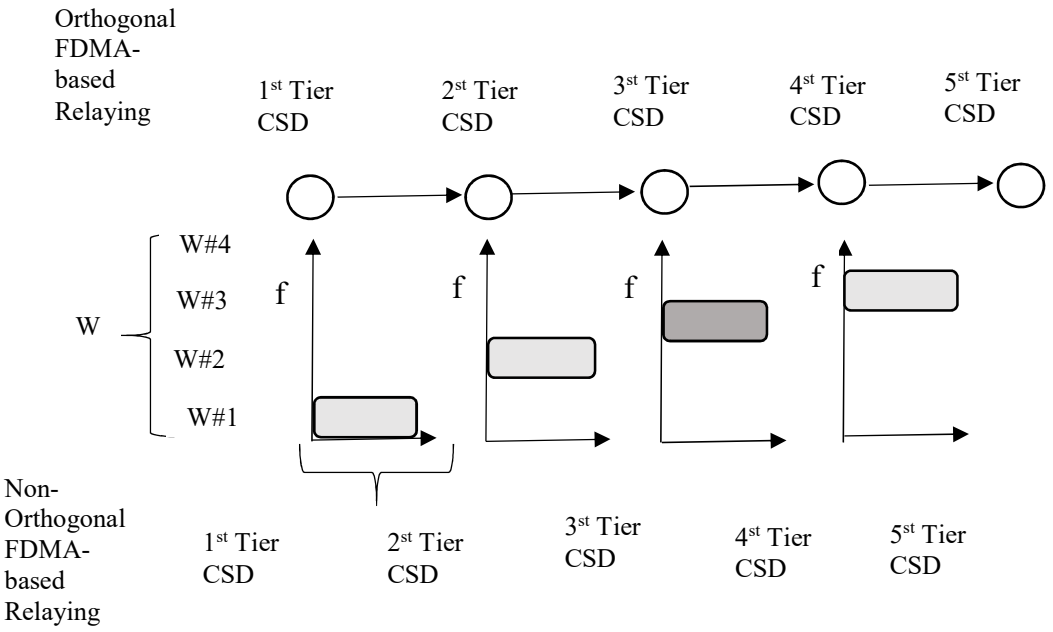

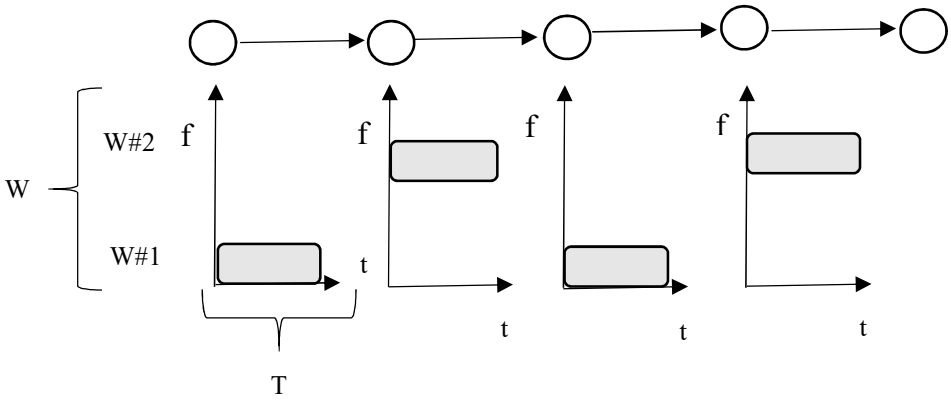
W
W#2
W#1
f
t
T

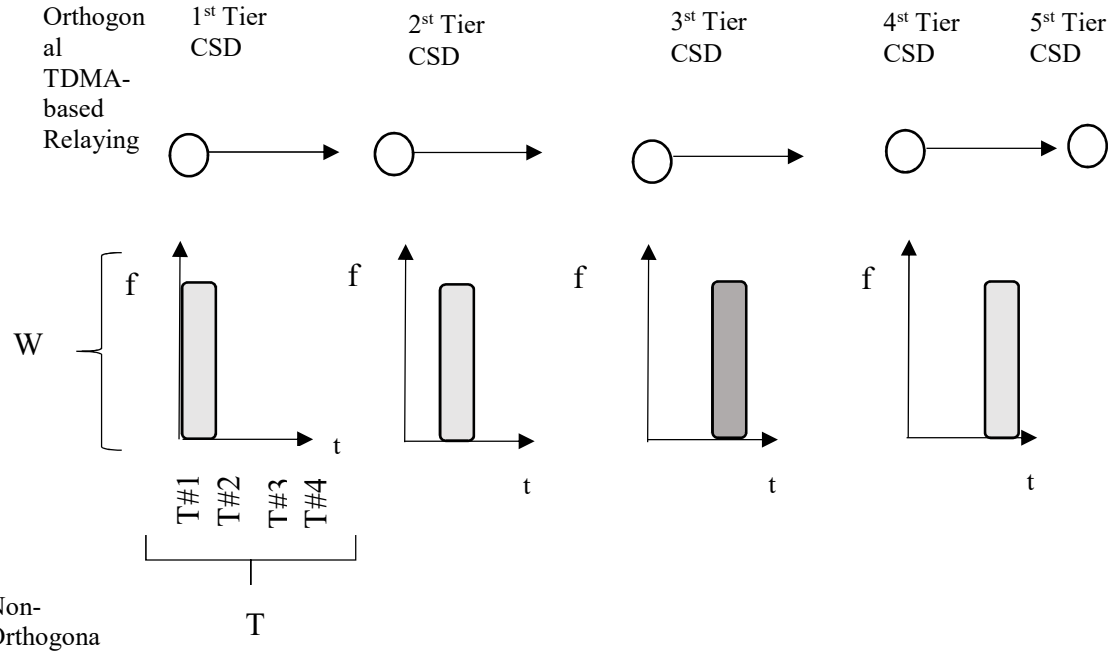
Orthogonal TDMA-based Relaying
1st Tier CSD
2st Tier CSD
3st Tier CSD
4st Tier CSD
5st Tier CSD
W
f
t
T#1
T#2
T#3
T#4
T

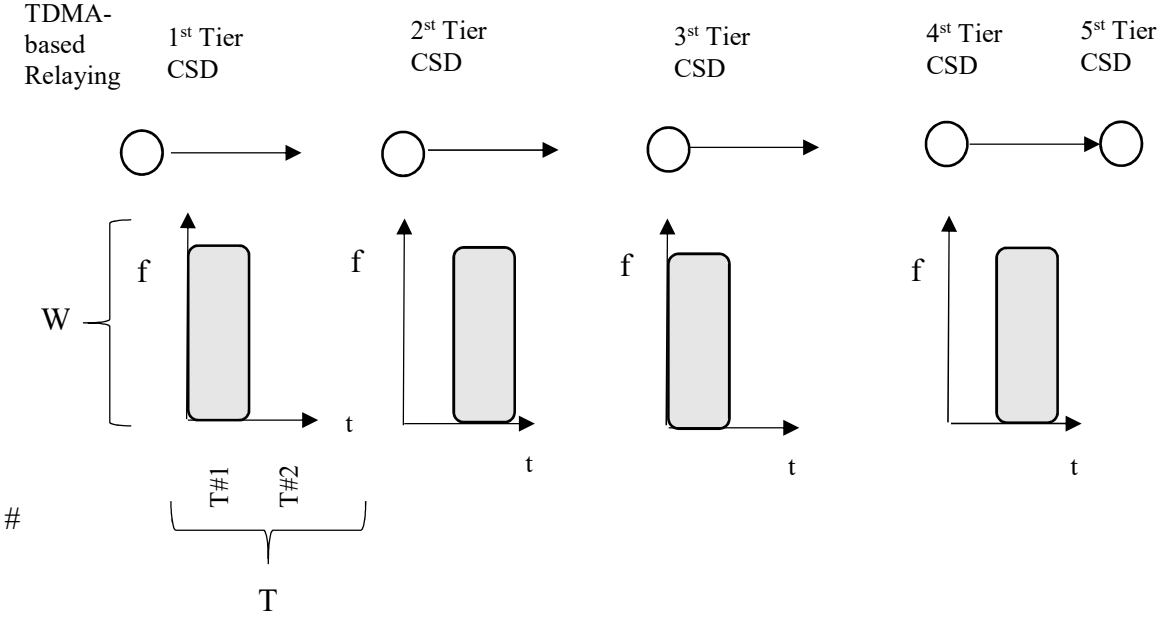
Non-Orthogona TDMA-based Relaying
1st Tier CSD
2st Tier CSD
3st Tier CSD
4st Tier CSD
5st Tier CSD
W
f
t
T#1
T#2
T

#

Figure 5.1 Principle of FDMA and TDMA based relaying.

### 5.2.2 Extension to Resource Reuse Networks

The introduced communication scenario is easily extended to the case where resources in terms of fractional frame duration or bandwidth are reused after a given number of relaying CSD tiers, without yielding any interference to the other stages utilising the same resources. The concept is similar to the frequency re-use concept in cellular systems, which relies on the radio propagation inherent pathloss. The suggested system ddeployment is depicted in Figure 5.5.

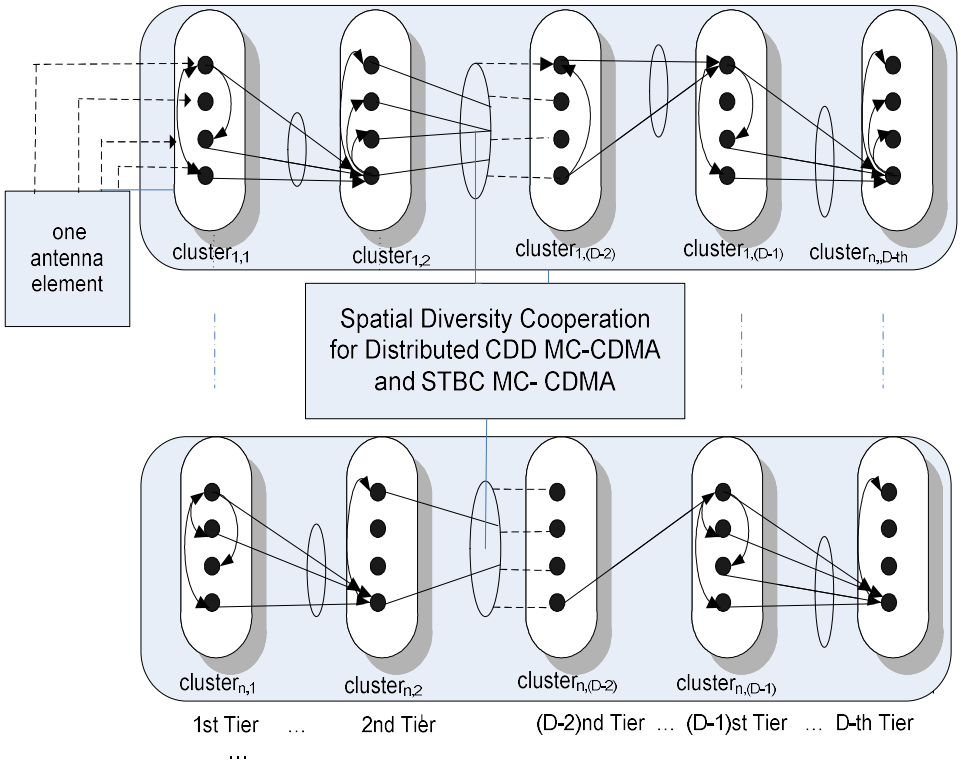


Figure 5.2 Multistage Sensor CDD-MC-CDMA Cooperative Spatial Diversity.

The distributed multi-hop network architecture makes full use of MC-CDMA frequency domain spreading properties and provides excellent spatial and frequency diversity Figure 5.6. The system performance evaluation is provided in terms of symbol error rate (SER)

and end-to-end bit error rate (BER). Additionally fractional frame duration and transmitted power control are implemented to achieve maximum data throughput. Multi-stage CDD with low complexity implementation yields significant performance improvement as a relaying network where the synchronization among the terminals involved in the relaying process is assumed to be predetermined. Furthermore, Monte-Carlo simulation results are presented when compared to traditional non-distributed networks to support the analytical framework.

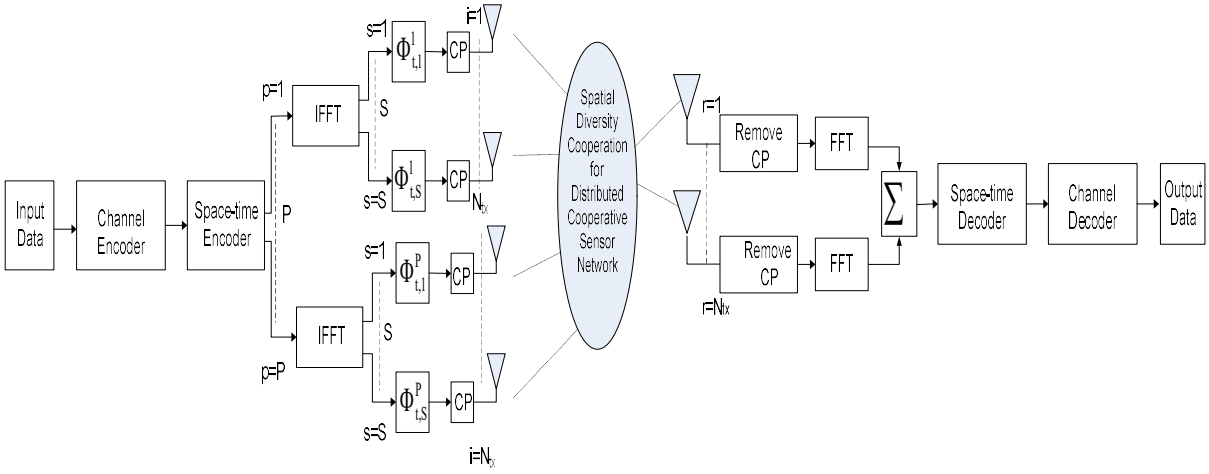


Figure 5.3 Spatial Diversity Cooperation for Distributed Cooperative Sensor Networks

The general sysem model obeys the same topology as depiced in Figure 1.1, i.e. a source ST (s-MT) communicates with a target ST (t-ST) via a given number of relaying STs(r-STs). Spatially adjacent r-STs are grouped into relaying Virtual Antenna Arrays (r-VAAs), the exact configuration of which has been thoroughlty explained in Chapter 3. The therein described system configurations are sufficiently precise for dealing with the capacity os such networks.

However, the deployment of realistic transceivers requires further explanations of how such system would work in reality. It is hence the aim of this section to provide this missing information. Of interest here are the transmitter and receiver used, as well as the prevailing communication channel.

**Transceiver Model**

The functional blocks of the transceivers forming the distributed-MIMO multi-stage relaying network are depicted in Figure 5.7. The top of Figure relates to the source CSD containing the s-ST; the middle relates to an arbitrary relaying CSD tier; and the bottom relates to the target CSD containing the s-ST. In the figure, each CSD tier is shown to consist of three terminals; it is, however, understood that any reasonable number of terminals can be accommodated.

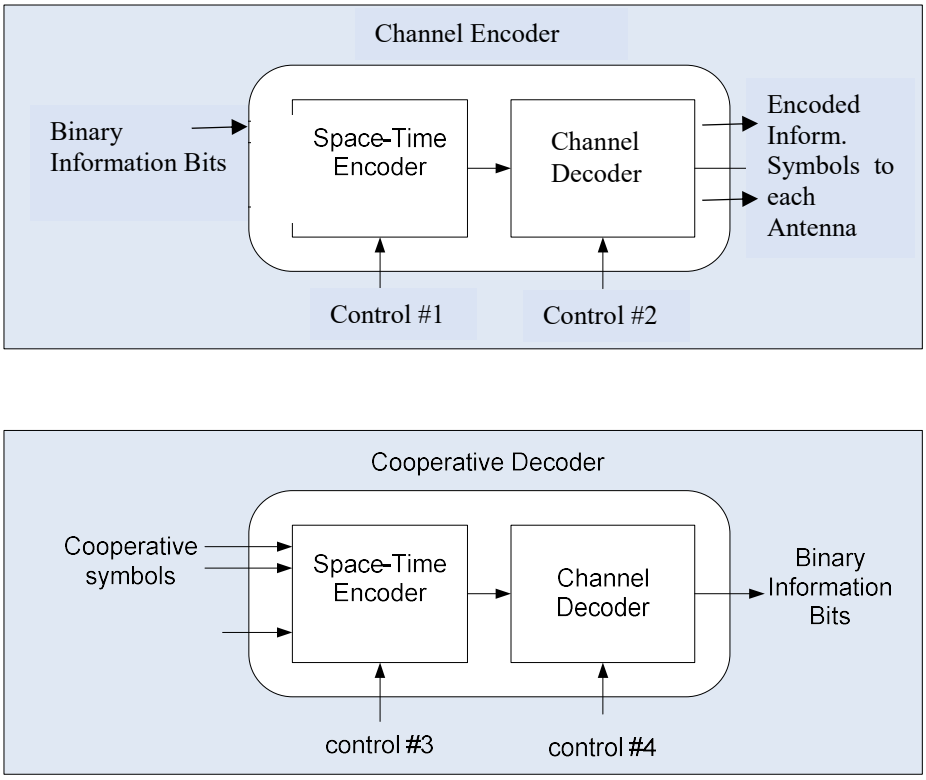


Figure 5.4 Distributed Encoder and Decoder

Specifically, the information source passes the information to a cooperative transceiver, which relays the dta to spatially adjacent r-STs belonging to the same CSD. Again, thisis assumed to happen over an air interface distinctic to the interface used for inter-stage communication or an air interface not requiring any optimisaition, and is not further dealt with.

It is also assumed that these cooperative links are error-free due to the short communication distance. Each of the terminals in the CSD perform distributed encoding of the information according to ome prior specific rules. That information is the

transmitted from the spatially distributed terminals after having been synchronized. Note that the problem related to synchronization is beyond the scope of this thesis.

Any of the relaying CSD tiers functions as follows. First, each r-MT within that VAA receives the data which is optionally decoded before being passed onto the cooperative transceiver. Ideally, every terminal cooperate with every other terminal; however, any amount of cooperation is feasible. If not decoding is performed, then an unprocessed or a sampled version of the receiver signal is exchanged with the other r-STs. Note that unprocessed relaying is equivalent to transparent relaying. After cooperation, appropriate decoding is performed. The optained information is the re-encoded in a distributed manner, synchronized and re-transmitted to the following relaying CSD tier.

As for the target CSD, the functional blocks are exactly the opposite to the source CSD. All terminals receive the information, possibly decode it, then pass it onto the cooperative transceivers which relay the data to the target terminal. The data is processed and finally delivered to the information sink.

The functional blocks of the dristributed transcoder, i.e. encoder and decoder, are now elaborated on in more detail. To this end, the encoder and decoder are shown in Figure 5.1.

Generally, the role of a channel encoder is to insert sufficient redundancy into the signal to mitigate the detrimental effects of noise and the fading channel. The insertion of redundancy decrese the data rate, where (with a good channel code) a decrease in rate comes along with an increase in coding gain. Together with the additional complesity, thee need to be trade-off to yield optimum performance in terms of the BER versus $E_b/N_0$, where $E_b$ is the information bit energy and $N_0$ is the noise power spectral density.

The channel code is traditionally accomplished by means of a convolutional code, which ‘convolutes’ the redundancy into the original signal stream. Nowadays, it is considered to be a low complexity code and is often found to be available within communication chipsets.

The channel encoder may also consist of two or more concatenated codes, which are preferably connected by interleavers which breaks long error sequences.

A channel encoder within a distributed encoder does not normally differ from a non-distributed encoder; however, it is generally possible to design channel codes which reflect the distributed nature of the encoding process.

The role of space time encoder is to utilize the additional spatial dimension created by sufficiently spaced antenna elements to increase the system performance. If each antenna

element is used to tranmsit independent data streams, then such spatial multiplexing technique is referred to as BLAST. Clearly, the data rate of such a system increases linearly with the number of transmit antennas; however, the lack of spatial redundancy makes it more susceptible to noise and interference when compared to coding techniques described previously chapter 3.

The functionality of distributed space-time codes (STCs) differs from a traditional deployment because only a fraction of the entire space-time codeword is transmitted from any of the spatially distributed terminals. The transmission across all terminals then yields the complete space-time codeword. Therefore, a control signal to each distributed space-time eencoder is essential, as it tells each of them which fraction of the entire space-time codeword to pass onto the transmitting antenna(s). This is indicated as Control #2 in Figure 5.1?. This control information is assumed to be available to the space-time encoder, and is thus not discussed further in this thesis.

The cooperative decoder can be realized as the inversion of all processes at the cooperative transmitter. Here, the space-time decoder is fed with the signals directly received from available antenna(s), as well as the information received via the cooperative links from adjacent terminals. Again, a control signal I needed in which specifies he type of information fed into the space-time decoder, to allow for optimum decoding. For example the control signal could inform the decoder that the relayed signals are a one bit representation of the sampled soft information available at the respective cooperative relaying terminals.

After the space-time decoding process, the information is passed on to the channel decoder wich performs the inverse process to the channel encoder. In a cooperative transcoder, the produced binary information output may then be fed into the cooperative ancoder, to get relayed to the next CSD tier.

In subsequence analysis, a more realistic relaying access shcme based on TDMA is assumed. Therefore, the entire bandwidth $W$ is utilized by all relaying links, whereas only a fraction of the total frame duration $T$ is used by each stage to relay the information to the consectutive stage.

A brief overview of the potential application for CSDs with realistic encoding schemes has been presented. It is clear that neither an in-depth analysis to these codes can be exposed her nor can all possible code combinations be assessed. Further analysis and assessments therefore concentrate on a few samples, i.e. only the cases of no encoding and space-time block encoding.

### 5.3.1 Transmitter

In an MC-CDMA system, each user transmit $P$ symbols during a signaling interval leading to the processing gain $G$ of $N/P$. The equiprobable data stream of the $u$th user containing $Fa$ information bits is modulated and mapped as symbols $b_1^u, b_2^u, \ldots, b_F^u$ selected from $M$-ary phase shift keying ($M$-PSK) or $M$-ary quadrature amplitude modulation ($M$-QAM) signal constellation A, where $a=\log_2 M$. Then $\left\{b_f^u\right\}_{f=1}^{F}$ are converted into $P$ parallel streams and spread by any suitable spreading sequence. In the downlink case, the other users are spread by their specific sequences and the resulting spread chips of all $U$ users are added synchronously and modulated by an $N$ point inverse fast Fourier transform (IFFT) given by

$$s(t)=\sqrt{E_c}\sum_{u=0}^{U-1}\sum_{p=0}^{P-1}\sum_{g=0}^{G-1}b_p^u c_g^u e^{j\frac{2\pi}{T}(gP+p)t} \tag{5.1}$$

where $E_c$ is the energy per subcarrier, or chip, and $E_c=E_s/N$ , where $E_s$ is the energy per symbol before spreading. $T$ is the signaling interval during which $P$ symbols per user are generated $b_p^u$ and $c_g^u$ are the $p$th symbol and $g$th chip of the $u$th user, respectively. For analytical convenience, we consider $P=1$, which makes $G=N$ . Expressing (5) in vector form

$$\mathrm{s}=F_N^H\,\mathrm{Gb} \tag{5.2}$$

where column vector **b** of length $U$ represents the single data symbols of $U$ users with **G** and $\boldsymbol{F}_N^H$ are the $U\times N$ and $N\times N$ Walsh-Hadamard and IFFT matrices, respectively. The spread and IFFT modulated column vector of length $N$ is given by **s**.

The vector **s** is then replicated on $N_{tx}$ branches, where each branch is cyclically shifted by CDD matrices $\Theta_n^t$, $n=1,\ldots,N_{tx}$. Finally, after the insertion of cyclic prefix (CP) (which is at least the length of the last $L$ samples of each vector $\Theta_n^t\mathbf{s}$), the signals are simultaneously transmitted from the $N_{tx}$ antennas. Ignoring CP, the signal transmitted from the $n$th antenna is given by

$$\mathrm{x}_n=\frac{1}{\sqrt{N_{tx}}}\Theta_n^t\mathrm{s}=\frac{1}{\sqrt{N_{tx}}}\Theta_n^t\boldsymbol{F}_N^H\mathbf{Gb} \tag{5.3}$$

where $1/\sqrt{N_{tx}}$ is the power normalization factor.

### 5.3.2 Receiver

CDD converts the spatial diversity into frequency and the receiver sees the signal coming from only a single antenna as in [71]. To verify it analytically, an equivalent frequency-domain transmitter model is considered, where the CDD matrices $\Theta_n^t$ are replaced by their frequency-domain equivalent PD matrices $\Theta_n^f$ and placed before the IFFT blocks.

At the receiver, after the removal of CP, the received signals are processed by $N\times N$ FFT matrices $\boldsymbol{F}_N$. The input-output relationship from $\mathbf{x}_n$ to $\mathbf{y}_r$ , can be written as

$$\mathbf{y}_r = \sum_{n}^{N_{tx}} \mathbf{H}_{r,n}\mathbf{x}_n + z_r \qquad \forall r \in [1, N_{rx}] \tag{5.4}$$

which are length $N$ column vectors corresponding to one MC-CDMA symbol. Here, $\mathbf{z}_r$ is the independent identically distributed (i.i.d.) AWGN vector for the $r$th receive antenna and $\mathbf{H}_{r,n}$=diag[$H_{r,n}(0)$,…, $H_{r,n}(N\text{-}1)$] with $H_{r,n}(k)$ given in (3). We can simplify $\mathbf{H}_{r,n}$, as

$$\mathbf{H}_{r,n} = \sum_{l=0}^{L-1} h_{r,n}(l)\mathbf{W}_l \qquad \forall r \in [1, N_{rx}] \tag{5.5}$$

where $\mathbf{W}_l$=diag[1,$e^{-j2\pi l/N}$,…, $e^{-j2\pi l/(N-1)/N}$].

Selecting the matrices $\Theta_n^f = \text{diag}\left[1, e^{j\Theta_n^f}, \ldots, e^{j\Theta_n^f(N-1)}\right] \forall n \in [1, N_{tx}]$, with entries $\Theta_n^f = -2\pi(n-1)L/N$, which makes

$$W_l\Theta_n^f = W_{l+(n-1)L}, \quad \forall \in [0, L-1], n \in [1, N_{tx}] \tag{5.6}$$

Hence, for each receive antenna the equivalent channel vector becomes $\mathbf{h}_r$=[$(\mathbf{h}_{r,1})^T$, $(\mathbf{h}_{r,2})^T$ ,…, $(\mathbf{h}_{r,N_{tx}})^T$]$^T$, with the $l$th entry of $\mathbf{h}_r$ being $h_r(l)$=$h_r$⌞$l/L$⌟+1($l$ mod $L$). Now, since $\mathbf{h}_r$ has length $N_{tx}L$, it can be viewed as coming from a single frequency selective channel. Based on (10), the diagonal matrix $\mathbf{H}_{r,n}$, can be expressed in terms of longer equivalent channels as

$$\mathbf{H}_r = \sum_{n=1}^{N_{tx}} \mathbf{H}_{r,n}\Theta_n^f = \sum_{l=0}^{N_{tx}L-1} h_r(l)\mathbf{W}_l, \quad \forall r \in [1, N_{rx}] \tag{5.7}$$

Thus, the PD matrices $\Theta_n^f$ shift the delay lags of the $n$th

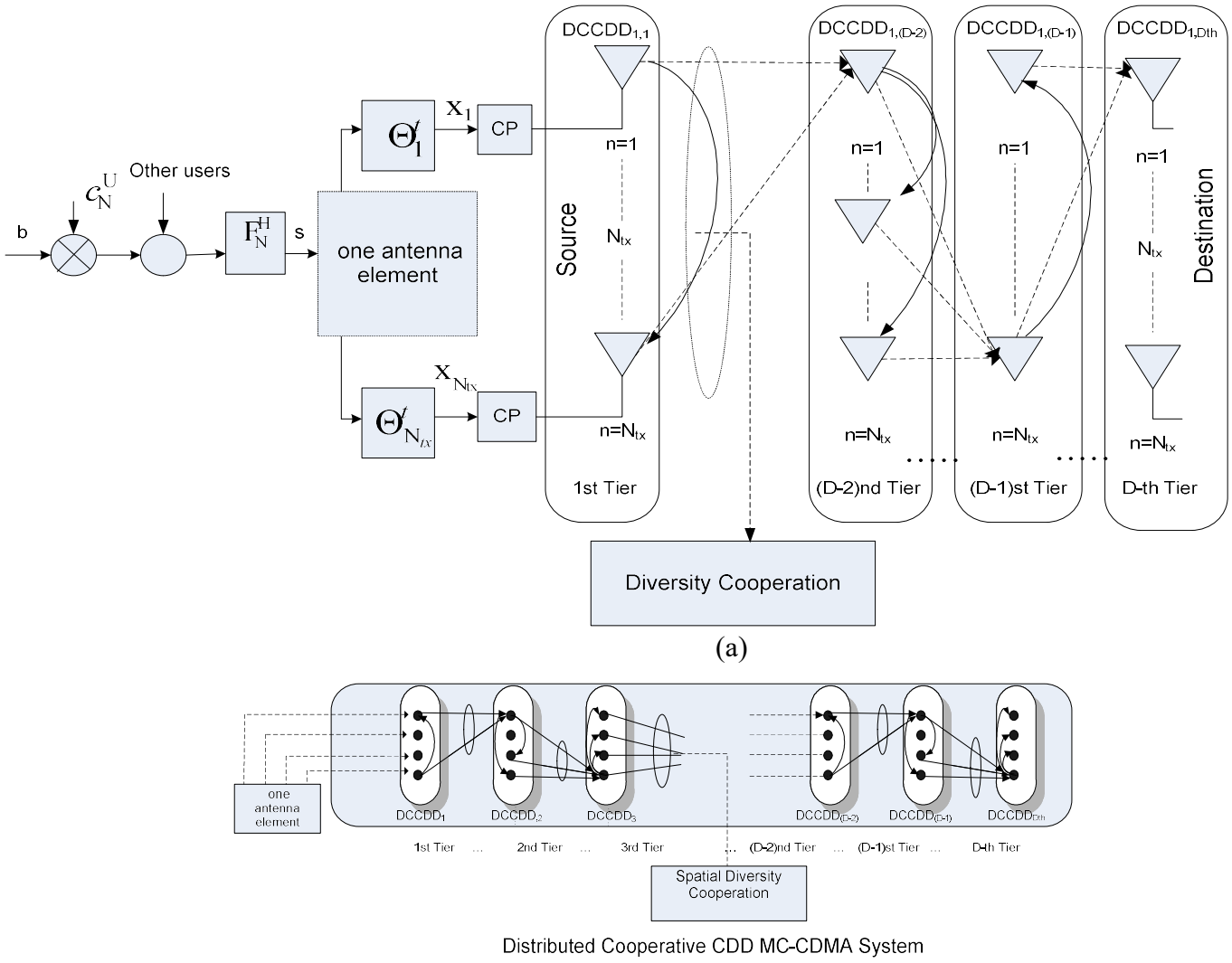


Figure 5.5 (a) Diversity Cooperation (b) Distributed Cooperative CDD MC-CDMA.

channel from [0,$L$-1] to [($n$-1)$L$, $n$($L$-1)]. The actual implementation of CDD is achieved in the time-domain. The CDD and PD matrices are linked via the DFT transformation, we can write

$$\Theta_n^t F_N^H = F_N^H \Theta_n^f \tag{5.8}$$

Rewriting the frequency responses of (3) at the $k$th subcarrier as

$$H_r(k) = \frac{1}{\sqrt{N}} \sum_{l=0}^{NtxL-1} h_r(l) e^{-j2\pi kl/N} \tag{5.9}$$

where the channel transfer function $|H_r(k)| = \beta_r(k)$.

## 5.4 Performance Analysis

Based on the previous analysis, we have shown that the MIMO MC-CDMA system employing CDD is equivalent to a SIMO system with an enhanced delay spread, whereas the STBC MC-CDMA system also collapses to an equivalent SISO model. Next, considering the square of Nakagami RV, ie $\gamma_r = \beta^2_{n,r}$ follows the Gamma distribution with *pdf* [59]

$$p_{\gamma_r}(\gamma_r) = \frac{\left(\frac{\hat{m}}{\bar{\gamma}_r}\right)^{\hat{m}}}{\Gamma(\hat{m})}\gamma_r^{\hat{m}-1} exp\left(-\frac{\hat{m}}{\bar{\gamma}_r}\gamma_r\right), \qquad \gamma_r \geq 0 \tag{5.10}$$

and the moment generating function (MGF)

$$\Phi_{\gamma_r(s)} \int_0^\infty e^{-s\gamma_r}\, p_{\gamma_r(\gamma_r)} d\gamma_r = \left(1 + \frac{s\bar{\gamma}_r}{\hat{m}}\right)^{-\hat{m}} \tag{5.11}$$

where $\bar{\gamma}_r$ is the average SNR.

Adopting the analysis of [83], it can be shown that for the case of CDD MC-CDMA system, the unitary DFT matrices link the frequency $\beta_r(k)$ and impulse $\alpha_r(l)$ responses by $\sum_{k=0}^{N-1}\left(\beta_r(k)\right)^2 = \sum_{k=0}^{N_{tx}(L-1)}\left(\alpha_r(l)\right)^2$. Let $\Psi_{(CDD)} = 1/N \sum_{k=0}^{N-1}\left(\beta_r(k)\right)^2$, since the taps $\left\{\left(\alpha_r(l)\right)^2\right\}_{l=0}^{N_{tx(L-1)}}$ are mutually uncorrelated, the fading parameter $\hat{m}_{CDD}$ and mean power $\hat{\Omega}_{CDD}$ for the correlated CDD MC-CDMA subcarriers become

$$\hat{m}_{CDD} = \frac{E^2[\Psi_{CDD}]}{\text{var}[\Psi_{CDD}]} = \frac{\left(\sum_{l=0}^{N_{tx}L-1} e^{-\delta l}\right)^2}{\sum_{l=0}^{N_{tx}L-1} \frac{e^{-2\delta l}}{m}} = \left(\frac{1-e^{-2\delta}}{1-e^{-2N_{tx}L\delta}}\right)\left(\frac{1-e^{N_{tx}L\delta}}{1-e^{-\delta}}\right)^2 m \tag{5.12}$$

with

$$\hat{\Omega}_{CDD} = \frac{1-e^{-NtxL\delta}}{1-e^{-\delta}}\left(\frac{\Omega_0}{N}\right) \tag{5.13}$$

and the average SNR is given by

$$\bar{\gamma}_{r_{(CDD)}} = \left(2\frac{U-1}{N} + \frac{1}{((E_s/N_0)\hat{\Omega}_{CDD})/N_{tx}}\right)^{-1} \tag{5.14}$$

Similarly, for the case of STBC MC-CDMA. $\sum_{n=1}^{N_{tx}}\sum_{k=0}^{N-1}\left(\beta_{r,n}(k)\right)^2 = \sum_{n=1}^{N_{tx}}\sum_{l=0}^{L-1}\left(\alpha_{r,n}(l)\right)^2$, with the fading parameter $\hat{m}_{STBC}$ and mean power $\hat{\Omega}_{STBC}$ for the correlated MC-CDMA subcarriers given by

$$\hat{m}_{(STBC)} = \frac{\left(\sum_{n=1}^{Nt_x}\sum_{l=0}^{L-1} e_n^{-\delta l}\right)^2}{\sum_{n=1}^{Nt_x}\sum_{l=0}^{L-1} e_n^{-2\delta l}/m} = \left(\frac{1-e^{-2\delta}}{1-e^{-2L\delta}}\right)\left(\frac{1-e^{L\delta}}{1-e^{-\delta}}\right)^2 mN_{tx} \tag{5.15}$$

with $\hat{\Omega}_{STBC} = \Omega_f$ as given (4). The average SNR is given by

$$\bar{\gamma}_{r(STBC)} = \left(2\frac{U-1}{N} + \frac{1}{((E_s/N_0)k\hat{\Omega}_{STBC})/RN_{tx}}\right)^{-1} \tag{5.16}$$

The error performance for the systems are evaluated by averaging the conditional SER $P_s(E|\gamma_r)$ over the *pdf* of the instantaneous SNR $\gamma_r$. Employing the MGF for transforming the single integrals into hypergeometric functions following the same approach used in [27] [84]

$$P_s(E) = \int_0^{\infty} P_s(E|\gamma_r) p_{\gamma_r}(\gamma_r) d\gamma_r \tag{5.17}$$

*A. M-QAM*

For brevity, only the conditional SER for coherent detection *M*-QAM signals is considered as given by [27] [84]

$$P_s(E|\gamma_r) = \frac{4q}{\pi}\int_0^{\frac{\pi}{2}} exp\left\{-\frac{\gamma_r g_{MQAM}}{sin^2\theta}\right\} d\theta - \frac{4q^2}{\pi}\int_0^{\frac{\pi}{4}} \left\{-\frac{\gamma_r g_{MQAM}}{sin^2\,\theta}\right\} d\theta \tag{5.18}$$

where $q$=(1-(1/√$M$)) and $g_{MQAM} = 3/2(M-1)$. Using (5.11), (5.17) and (5.18), the average SER with *M*-QAM modulation is given in by (5.19) as [59][26].

$$P_s(E) = \frac{2q}{\sqrt{\pi}}\frac{\Gamma\left(\hat{m}+\frac{1}{2}\right)}{\Gamma(\hat{m}+1)}\Phi_{\gamma_r}(g_{MQAM}) \quad {}_2F_1\left[\hat{m}, \frac{1}{2}; \hat{m}+1; \frac{1}{1+\frac{g_{MQAM}\bar{\gamma}_r}{\hat{m}}}\right]$$
$$-\frac{2q^2\Phi_{\gamma_r}(2g_{MQAM})}{\pi(2\hat{m}+1)} F_1\left[1, \hat{m}, 1; \hat{m}+\frac{3}{2}; \frac{1+\frac{g_{MQAM}\bar{\gamma}_r}{\hat{m}}}{1+\frac{2g_{MQAM}\bar{\gamma}_r}{\hat{m}}}, \frac{1}{2}\right] \tag{5.19}$$

Γ(x) is the complete gamma function, ${}_2F_1$(a,b;c;x) is the Gauss hypergeometric function and $F_1$(a,b,b',c;x,y) is referred as Appell hypergeometric function, both of them defined in [27][84].

### 5.5 Maximum end to end Throughput

Based on the analysis of Section III, the BER $P_b(E)$ is related to the SER via [91]

$$P_b(E) \approx \frac{P_s(E)}{\log_2(M)} \tag{5.20}$$

The fractional resource allocation rules are considered so that the errors in consecutive stages become independent. The normalized end-to-end throughput can be expressed for a CDD MC-CDMA system as [85].

$$\Phi = \min_{\upsilon\in(1,K)}\{\alpha'_\upsilon \log_2(M_\upsilon)\} \cdot \left(1 - P_{f,e2e}(E)\right) \tag{5.21}$$

where $\alpha'_\upsilon$ and $M_\upsilon$ are the fractional frame duration and modulation index of the $\upsilon^{\text{th}}$ stage respectively, and $P_{f,e2e}(E)$ is the end-to-end FER. For a lossless direct communication link, the normalized throughput is given by $\alpha'_\upsilon \log_2(M)$ [bits/s/Hz]. According to a relaying system with $K$ stages, the weakest link determines the throughput, consequently $\min_{\upsilon\in(1,K)}\{\alpha'_\upsilon \log_2(M_\upsilon)\}$. Under the knowledge that $P_{f,e2e}(E)$ is a function of $M_{\upsilon\in(1,K)}$ and the fractional transmission power allocated to each stage, the following optimization process is proposed for such as diversity scheme. First, the modulation indices $M_{\upsilon\in(1,K)}$ are fixed, this condition reduces (25) to limiting case where $SNR\rightarrow\infty$ is considered

$$\Phi = \min_{\upsilon\in(1,K)}\{\alpha'_\upsilon \log_2(M_\upsilon)\} \tag{5.22}$$

where the fractional frame duration $\alpha'_\upsilon$ need to be chosen such as to maximize $\Phi$ under constraint $\sum_{\upsilon=1}^{K} \alpha'_\upsilon = 1$ To this end all $\alpha'_\upsilon \log_2(M_\upsilon)$are considered which results in

$$\alpha'_\upsilon = \frac{\prod_{\omega=1,\omega\neq\upsilon}^{K} \log_2(M_\omega)}{\sum_{k=1}^{K}\prod_{\omega=1,\omega\neq k}^{K} \log_2 M_\omega} \tag{5.23}$$

In order to maximize the throughput, the end-to-end BER needs to be minimizing for a $B$ frame length in bits

$$\Phi = \min_{\upsilon\in(1,K)}\{\alpha'_\upsilon \log_2(M_\upsilon)\} \cdot \left(1 - P_{b,e2e}(E)\right)^B \tag{5.24}$$

Defining a non-decreasing (in $\Phi$) metric

$$\Phi' \cong \exp\left[\frac{\log\left(\frac{\Phi}{\min_{\upsilon\in(1,K)}\{\alpha'_\upsilon \log_2(M_\upsilon)\}}\right)}{B}\right] - 1 \tag{5.25}$$

It can easily be shown that

$$\Phi' \approx -P_{b,e2e}(E) \tag{5.26}$$

Then, the optimum modulation order $M_{\upsilon\in(1,K)}$ has to be determined in dependency of the previously derived fractional resource allocations, by permuting all possible modulation order at each stage. The end-to-end BER expression for independent BERs $P_{b,\upsilon\in(1,K)}(E)$ caused by independent SERs $P_{s,\upsilon\in(1,K)}(E)$ is shown as

$$P_{b,2e2}(E) = 1 - \prod_{\upsilon=1}^{K}\left(1 - P_{b,\upsilon}(E)\right) \tag{5.27}$$

which, at low BERs at every stage, can be approximated as

$$P_{b,e2e}(E) \approx \sum_{\upsilon=1}^{K} P_{b,\upsilon}\,(E) \approx \sum_{\upsilon=1}^{K} \frac{P_{s,\upsilon}(E)}{\log_2(M_\upsilon)} \tag{5.28}$$

Further analysis is done for the case of equal channel gains. Assuming that each stage is allocated a fractional power $\beta'_\upsilon$, the above given dependency can be expressed in conjunction ith the SERs $P_{s,\upsilon}(\cdot)$=$P_{QAM}(\cdot)$ $P_{s,\upsilon}(\cdot) = P_{QAM}(\cdot)$. The SERs for M-QAM in the $\upsilon^{th}$ relaying stage is hence upper-bounded by [85]

$$P_{b,e2e}(E) \le \sum_{\upsilon=1}^{K} A_{,\upsilon}\,(1 + B_\upsilon \beta'_\upsilon)^{-\hat{m}_\upsilon} \tag{5.29}$$

where $$A_\upsilon = 2_{q_\upsilon}/\log_2(M_\upsilon) \tag{5.30}$$

and $$B_\upsilon = \begin{cases} \left(\left(g_{MQAM,\upsilon}\right)\frac{\overline{\gamma}_{r,\upsilon}}{\hat{m}_\upsilon}\right)_{CDD} \\ \left(\frac{\left(g_{MQAM,\upsilon}\right)}{R_\upsilon}\frac{\overline{\gamma}_{r,\upsilon}}{\hat{m}_\upsilon}\right)_{STBC} \end{cases} \tag{5.31}$$

where $R_\upsilon$ is the STBC rate of the $\upsilon^{th}$ stage. Adopting the analysis by [85], in order to derive the fractional power allocations $\beta'_{\upsilon\in(1,K)}$, for a distributed systems, (36) obeys

$$\beta'_\upsilon \approx \left[\sum_{\upsilon=1}^{K} \alpha'_\omega \left(\frac{\hat{m}_\upsilon^{-1} A_\upsilon^{-1} B_\upsilon^{\hat{m}_\upsilon}}{\hat{m}_\omega^{-1} A_\omega^{-1} B_\omega^{\hat{m}_\omega}}\right)^{\frac{1}{\hat{m}_{max}+1}}\right]^{-1} \tag{5.32}$$

where $\hat{m}_{\max} = \operatorname{argmax}(\hat{m}_1, \ldots, \hat{m}_K)$.

### 5.6 Performance Results

In this section, numerical results based on the derivations made in previous section are presented and verified with a Monte-Carlo system simulator based on distributed

CDD and STBC MC-CDMA. The results are produced for SER versus SNR, defined as the transmitted symbol energy over the noise power spectral density ($E_s/N_o$) and for the end-to-end Throughput BER versus SNR [dB].

In Figure. 4.8, a comparison between CDD and STBC diversity techniques is shown. For simplicity, $N$=$G$ and the worst case fading profile $m$=1 (Rayleigh fading) has been chosen. As the diversity order is always similar if equal number of multipaths are realized, therefore, for the clarity of error curves, CDD has been simulated with channel orders of $L$=1,3,while STBC employs $L$=4. As expected, STBC performs better than CDD because of higher channel order and consequently, the diversity gain. However, the complexity of the cooperative distributed CDD system is significant less according to the following approach in terms of end to end throughput.

The performance of the developed algorithm is assessed by means of Figure. 4, 5 and 6. In Figure 4, if reference is made to the non-optimized scenario, then only the fractional transmission power is meant not to be optimized since the frame duration is easily related to the modulation order, It can be observed that the optimum yield performance for any of the depicted configurations. Furthermore, the gain of an optimized system is highest for very asymmetric cases. At a target end-to-end BER of $10^{-5}$, a performance improvement about 3dB is obtained.

The throughput of a distributed CDD MC-CDMA and STBC MC- CDMA system are illustrated by means of Figure 5.8 and Figure 5.9 respectively. In Figure 5.8 it can be observed that in the region of low SNR, the developed allocation strategy performs worse than the optimum one. This is obvious, as the fractional durations have been derived assuming the SNR→∞. For most of the transitional region from zero-throughput to maximum-throughput, however, the derived allocations yield near-optimum throughput. In contrast, no optimization exhibits drastic losses in the transitional region.

The fractional allocation algorithm allows a final numerical optimization to be performed in each relaying stage over all possible modulation indexes. In Figure 5.9 such numerical optimization was performed for a 2-stage network with $p$=[0,10]dB and $t_{1,2}$=$r_{1,2}$=2.Each stage could choose a modulation index belonging to the set $M_{1,2}$=(2,4,16,64,256).The performance gains in terms of increased throughput are clear from both Figure 5.8 and

Figure 5.9, where the near-optimum adaptive modulation per stage is compared against various fixed combinations. At any SNR, the developed algorithm clearly outperforms any of the fixed configurations. If the system was to operate at 20dB, it can only reach 2bits/s/Hz; The optimum selection is 64-QAM with an optimized fractional power allocation, which yields a performance benefit of 30%.

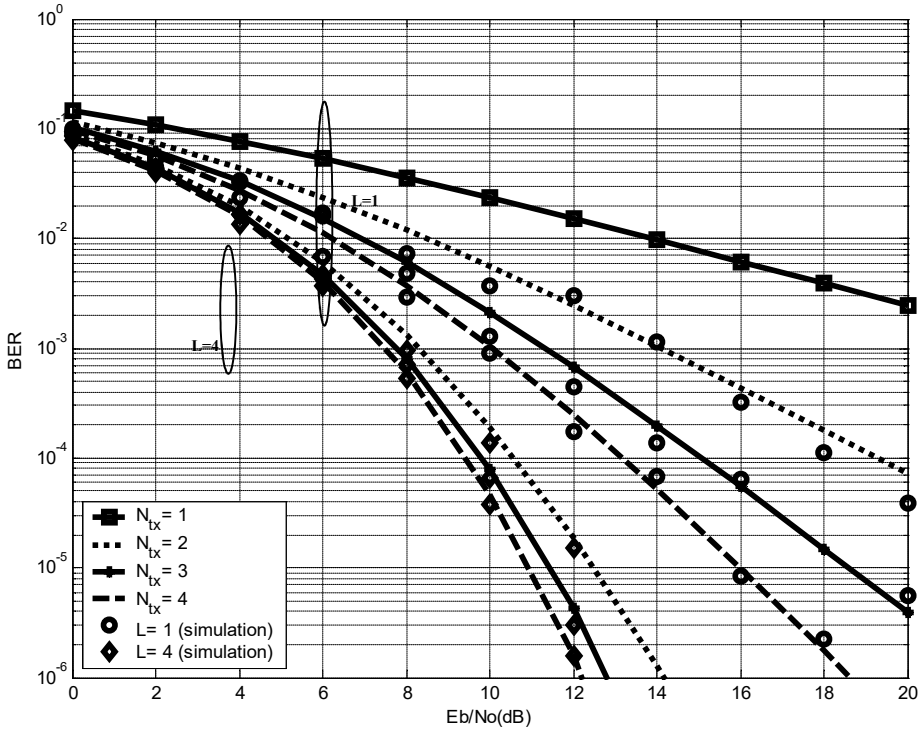


Figure 5.6 Performance of CDD MC-CDMA system with $N$=64, $L$=1,4 and δ=0

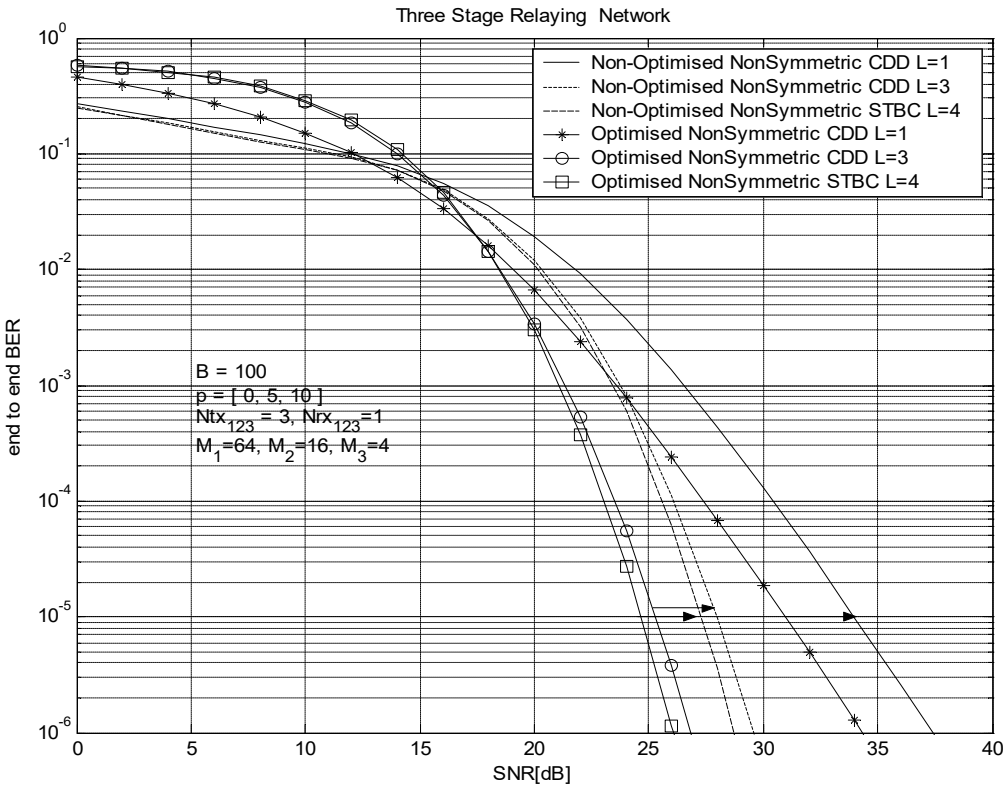


Figure 5.7 Comparison between non-optimized and optimized end-to-end BER for various configuration of a three-stage CDD and STBC relaying network.

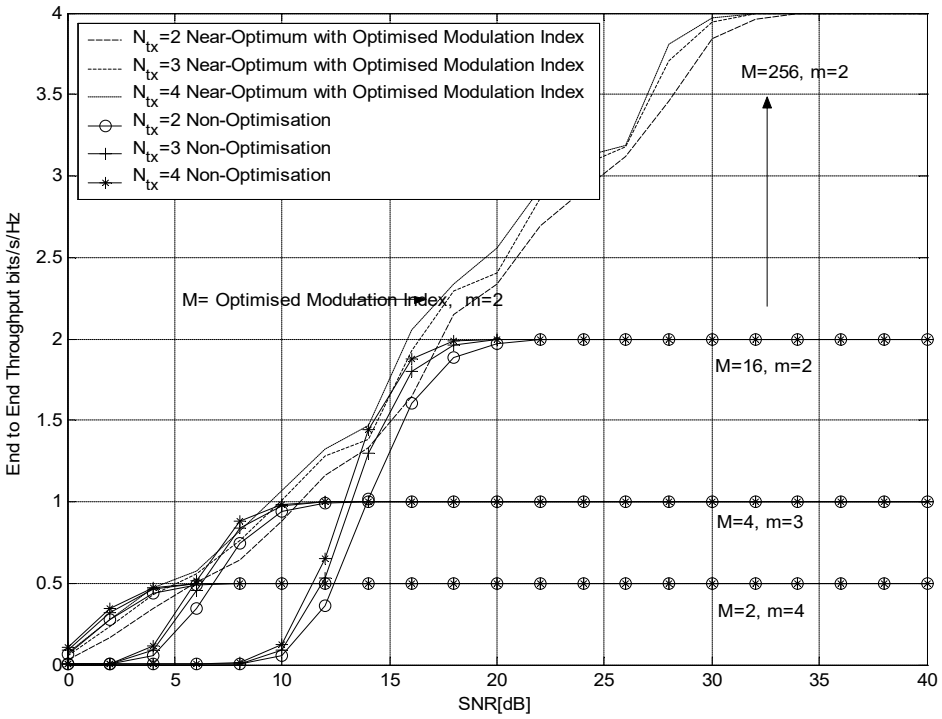


Figure 5.8 Throughput for various configurations of D-CDD MC-CDMA relaying network.

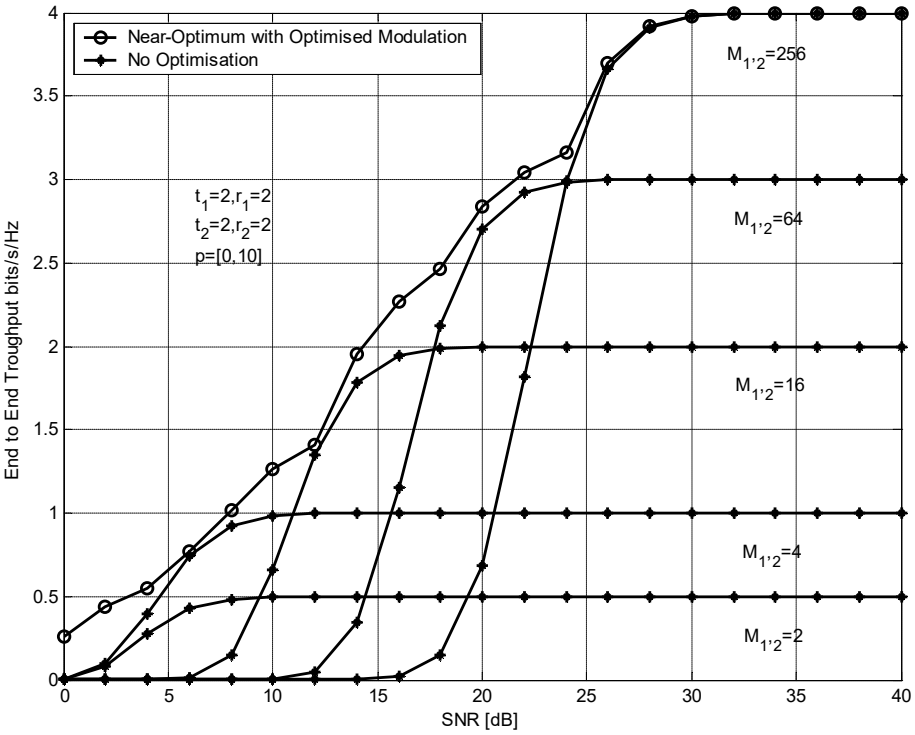


Figure 5.9 Numerically optimized modulation index for D-STBC MC-CDMA network.

## 5.7 Relay assisted and Cooperative CDD MC-CDMA Network with Frequency-Correlated Subcarriers.

### 5.7.1 Maximizing the end-to-end Throughput

Assumed is regenerative relaying, where the terminal selection and routing path is determined prior to transmission. The obtained information is then re-encoded in a distributed CDD MC-CDMA manner, synchronized and re-transmitted to possible decode it , then pass it onto the cooperative transceivers which relay the data to the destination terminal. The data is processed and finally delivered to the information sink. With reference to the previous analysis the BER $P_b(E)$ is related to the SER via (5.24) the end-to-end BER expression for independent BERs $P_{b,\upsilon\in(1,K)}(E)$ caused by independent SERs $P_{s,\upsilon\in(1,K)}(E)$ is shown as (5.27) and (5.28) can be approximated as (5.33)

$$P_{b,e2e}(E) \approx \sum_{\upsilon=1}^{K} P_{b,\upsilon}(E) \tag{5.33}$$

In order to maximize the throughput, the end-to-end BER needs to be minimizing

$$\Phi = \min_{\upsilon\in(1,K)}\{\alpha'_\upsilon \log_2(M_\upsilon)\}\cdot\left(1-P_{b,e2e}(E)\right)^B \tag{5.34}$$

where B is the frame length in bits.

Defining a non-decreasing (in Φ) metric and based on [36] $\Phi' \approx -P_{b,e2e}(E)$. Then a frame-by-frame detection, is realized by adding a cycled redundancy check (CRC) of negligible overhead to each transmitted frame. Based on [?] and the above-said, the normalized throughput at the *υth* stage can be expressed as

$$\Theta_\upsilon = \alpha'_\upsilon \log_2(M_\upsilon)\cdot\left(1-P_{s,\upsilon}(E)\right)^{D_\upsilon} \tag{5.35}$$

$$\approx \alpha'_\upsilon \log_2(M_\upsilon)\cdot\left(1-D_\upsilon P_{s,\upsilon}(E)\right) \tag{5.36}$$

where $\alpha'_\upsilon$ is the fractional frame duration, $M_\upsilon$ is the modulation order, $P_{s,\upsilon}(E)$ is the SER, and $D_\upsilon \in N$ is the frame duration in symbols used in the $\upsilon$th stage, $D_\upsilon$ can be related to the fractional frame duration $\alpha'_\upsilon$ as $D_\upsilon = \alpha'_\upsilon D \cdot \alpha'_\upsilon$. The throughput in each stage can be upper-bounded.

$$\Theta_{\upsilon} \leq \alpha'_{\upsilon} \log_2(M_{\upsilon}) \left(1 - \frac{\alpha'_{\upsilon} A_{\upsilon} D}{\left(1+B_{\upsilon}\beta'_{\upsilon}\right)^{\overline{\widehat{m}}_{\upsilon}}}\right) \tag{5.37}$$

$$A_{\upsilon} = \begin{cases} \frac{M_{\upsilon-1}}{M_{\upsilon}} & \text{for M} - \text{PSK} \\ 2q_{\upsilon} & \text{for M} - \text{QAM} \end{cases} \tag{5.38}$$

and

$$B_{\upsilon} = \begin{cases} g_{MPSK,\upsilon} \frac{\overline{\gamma}_{r,\upsilon}}{\widehat{m}_{\upsilon}} & \text{for M} - \text{PSK} \\ g_{MQAM,\upsilon} \frac{\overline{\gamma}_{r,\upsilon}}{\widehat{m}_{\upsilon}} & \text{for M} - \text{QAM} \end{cases} \tag{5.39}$$

Equating all throughputs given in (5.37) at sufficiently high SNR, the fractional frame durations are obtained as

$$\alpha'_{\upsilon} = \frac{\prod_{\omega=1,\omega\neq\upsilon}^{K} \log_2(M_{\omega})}{\sum_{k=1}^{K} \prod_{\omega=1,\omega\neq k}^{K} \log_2(M_{\omega})} \tag{5.40}$$

For a high SNR, the SER at each stage is negligible; the limiting throughput $\Theta_{\infty}$ is evaluated as from (5.11) and (5.37) as

$$\Theta_{\infty} \cong \Theta(\text{SNR} \to \infty) = \frac{\prod_{\omega=1}^{K} \log_2(M_{\omega})}{\sum_{k=1}^{K} \prod_{\omega=1,\omega\neq k}^{K} \log_2(M_{\omega})} \tag{5.41}$$

The fractional power allocations are then easily derived as

$$\beta'_{\upsilon} \approx \left[\sum_{\omega=1}^{K} \alpha'_{\upsilon} \left(\frac{\alpha'_{\upsilon} A_{\upsilon}^{-1} B_{\upsilon}^{u_{\upsilon}}}{\alpha'_{\omega} A_{\omega}^{-1} B_{\omega}^{u_{\omega}}}\right)^{\frac{1}{\overline{\widehat{m}}_{\upsilon\max}}}\right]^{-1} \tag{5.42}$$

where $\widehat{m}_{\upsilon_{max}} = \text{argmax}(\widehat{m}_1, \ldots, \widehat{m}_K)$.

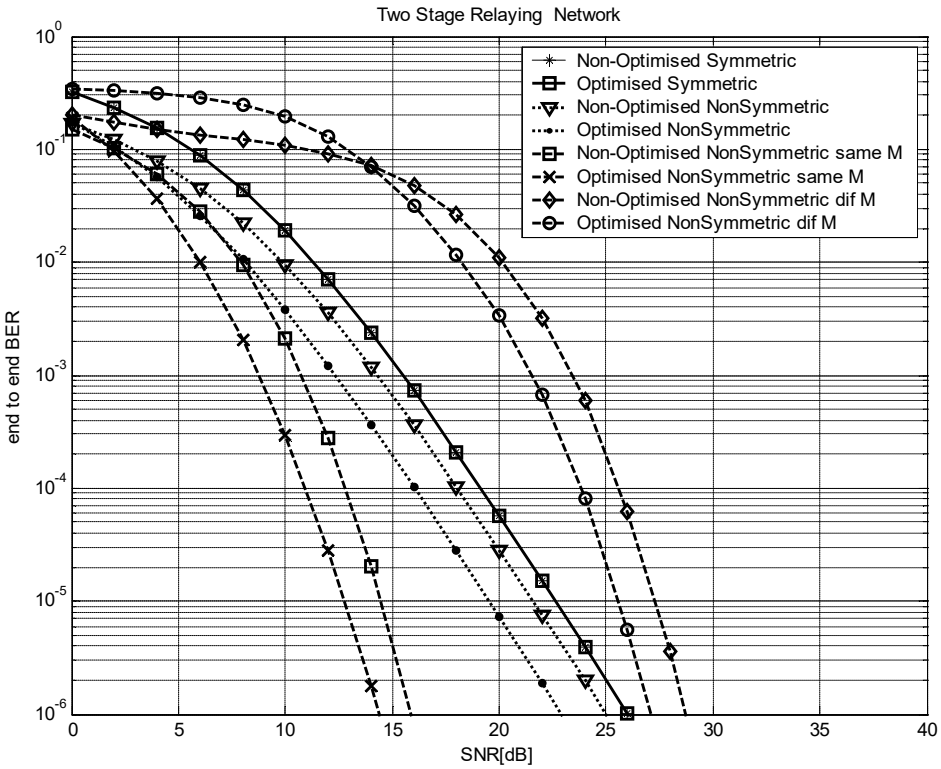


Figure 5.10 Comparison between optimum and non-optimised end-to-end BER for various configurations of a two-stage relaying DCCDD MCCDMA networks with Frequency- Correlated Subcarriers

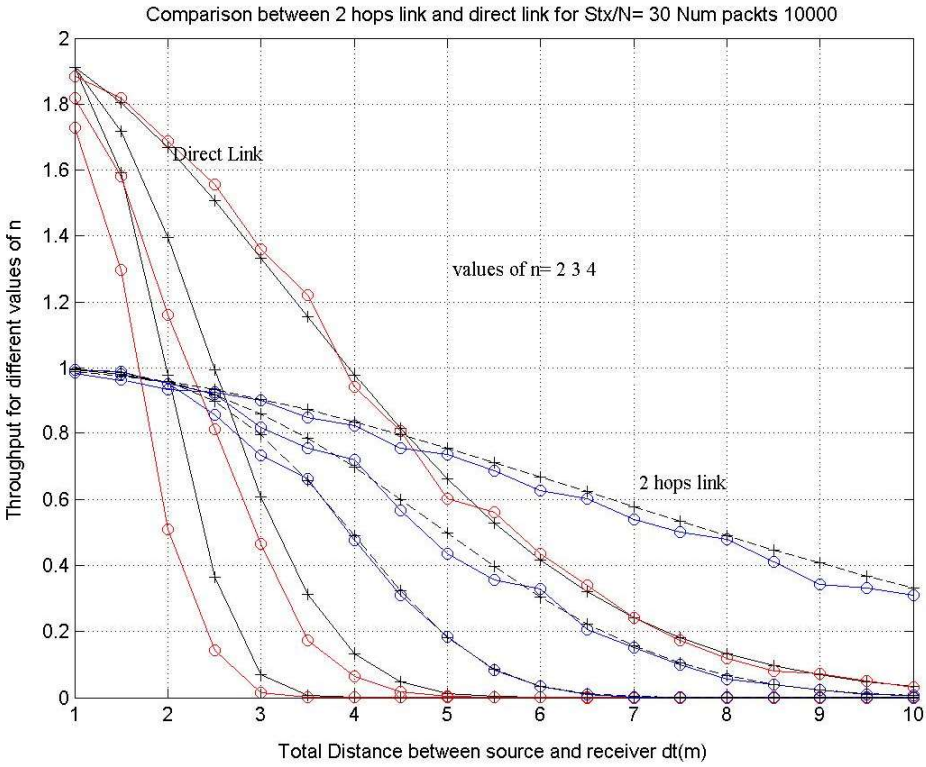


Figure 5.11 Comparison between 2 hops links and direct link.

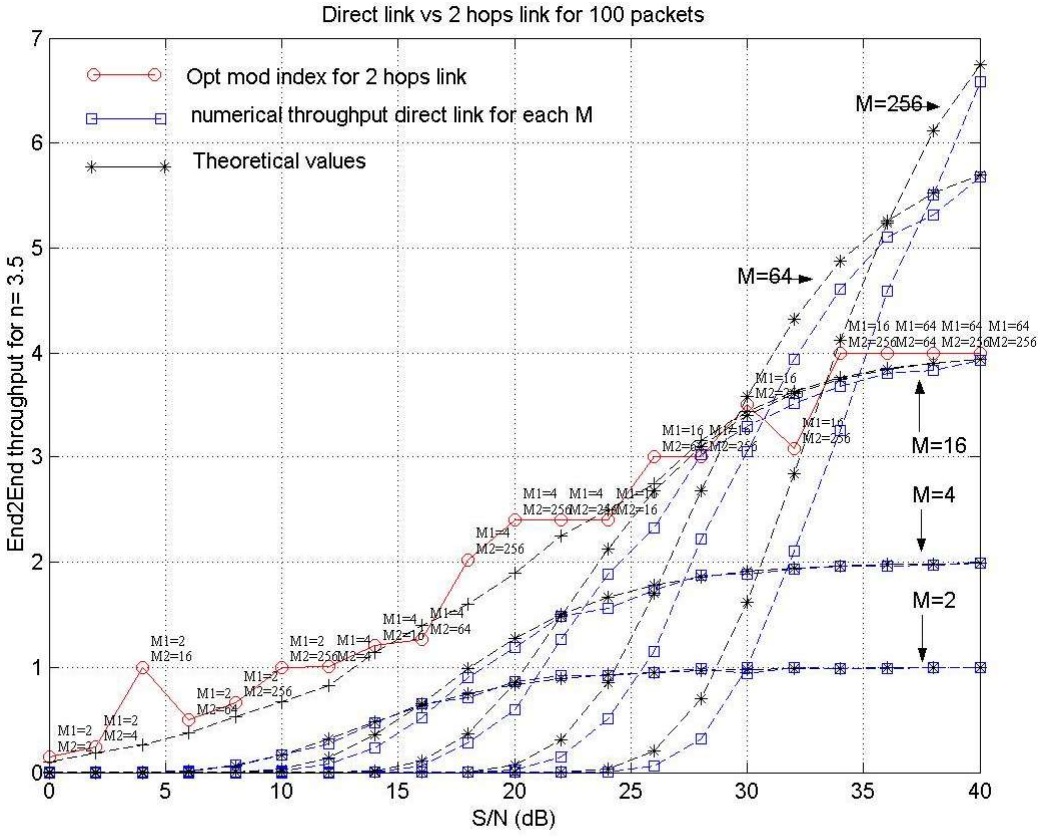


Figure 5.12 End to end throughput for two stage relayings

The comparison between 2 hop links and direct link is presented in Figure 5.11 for different distances and pathloss values

In order to implement the modulation scheme for two stages relaying, the proposed modulation algorithm is implemented by figure 5.11.

## 5.6 Interference Effect on Throughput

In order to evaluate the interference effects, the next simulation environment is presented. Two links, one of them is case of study and the other one is the interference source. We define the same transmitted power for both sources. The path loss model used is the simplest one $(d_0/d)^n$, where n is the path loss index (n=3.5 for urban environments). Also, we will consider the same distance between source to relay node and relay node to receiver for the link under study. Something important to consider is that each single hop (if hop by hop link is decided instead of Direct link) is $2^n$ stronger that the direct link.

To generate interferences, we defined a routine in which it is possible to select the starting time of transmission for the disturber link. The strength of the interference signal depends on the distance between the disturber source and our receiver, and also depends on the total among of time the source and the disturber source transmit together. The scheduling used is something like TDMA, for that, when both sources transmit at the same time they interfere themselves.

### 5.6.1 Throughput values without interferences

*Parameters two hops link:*
Stx from -70 to -10 dB
N=-100 dB
Total Distance =10 metres.
Distance each hop=5 metres

n =3.5
$t_1 = t_2 = 1$
$r_1 = r_2 = 1$
$R_1 = R_2 = 1$
$M_1 = M_2 = 4$

Attenuation hop 1 = 10 log $((1/5)^{3.5})$ = -24.46 dB
Attenuation hop 2 = 10 log $((1/5)^{3.5})$ = -24.46 dB
Interferences =0

*Parameters Direct link:*
Stx from -70 to -10 dB

N = -100 dB
Total Distance =10 metres.
n =3.5
$t_o = r_0 = 1$
$R_0 = 1$
$M_0 = 4$

Attenuation hop 1 = 10 log $((1/10)^{3.5})$ = -35 dB?
Interferences =0

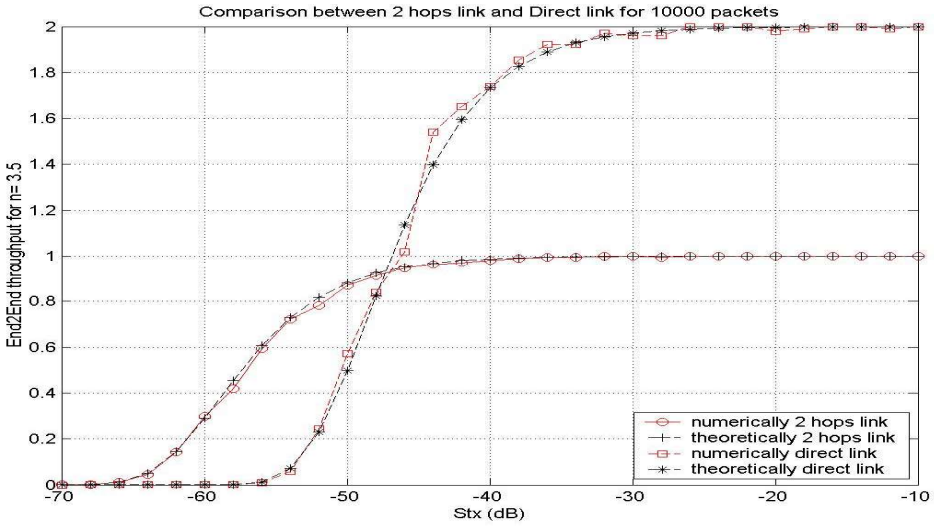


Figure 5.13 Throughput values without interferences

### 5.6.2 Throughput values with interferences

*Parameters two hops link:*
Stx from -70 to -10 dB
N -100 dB
Total Distance=10 metres.
Distance each hop=5 metres
n =3.5
$t_1 = t_2 = 1$
$r_1 = r_2 = 1$
$R_1 = R_2 = 1$
$M_1 = M_2 = 4$

Attenuation hop 1 = 10 log $((1/5)^{3.5})$ = -24.46 dB
Attenuation hop 2 = 10 log $((1/5)^{3.5})$ = -24.46 dB

*Parameters Direct link:*
Stx from -70 to -10 dB
N -100 dB
Distance Total=10 metres.
n (path loss index) =3.5
t0=r0=1
R0=1
M0=4

Attenuation hop 1 = 10 log $((1/10)^{3.5})$ = -35 dB

The effect that interferences cause on throughput in Figure 5.11 and Figure 5.12 are related which the disturber source is transmitting and the strength of the interfering signal (distance from disturber source and receiver). The Signal Noise Interference Ratio was calculated through;

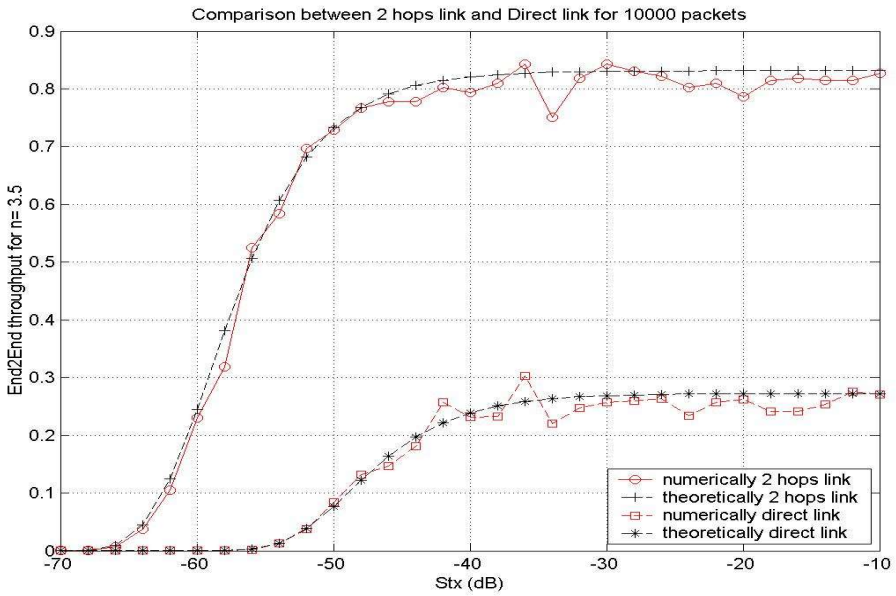


Figure 5.14Throughput values without interferences

The strength of the attenuation is S interference = Stx – 45.53 dB, really low, but the interference takes 50% of the time for Direct link and 100 % of the time for the 2nd hop of the two hops link. We can see that the signal which comes form direct link is strongly perturbed by interferences

$$SNI = \frac{Stx \cdot att1}{N + S\,\text{int} \cdot att2 \cdot \gamma} \tag{5.43}$$

We have supposed that *Stx*=*Sint*. Further more, att1is given by the distance between source and desiderated receiver and att2 is given by the distance between disturber source and the desiderate receiver. γ is the factor which says how many time the disturber source interferes. Generally, Direct link is much more truncated than the two hops link.

## 5.7 Summary

The contribution of the chapter is the performance improvement on cooperative networks result of the proposed D-CDD topology and allocation strategies when compare to D-STBC architecture. The analysis was deducted from closed-form expressions of SER of coherent CDD and STBC MC-CDMA systems, over Nakagami-*m* fading channels. Spatially adjacent antennas have been grouped into CDD MC-CDMA and STBC relaying system. It has been shown that both systems can achieve $N_{tx}\times L$ diversity order; however, compared to CDD, the STBC system suffers from rate loss for more than two transmit antennas and also the receiver complexity increases for all configurations.

Anexo

## 5.3 Nakagami-*m* Channel Model

Let **H**(*k*) be a $N_{rx}\times N_{tx}$ channel matrix which contains the complex channel frequency responses at the *k*th subcarrier. Considering a frequency selective fading channel with *L* independent taps, the time-domain channel impulse response from the *r*th receive to the *n*th transmit antenna can be modeled as a tapped delay line and expressed as (2.1) to be show by (5.1?)(6.1?)

$$h_{r,n}(t) = \sum_{l=0}^{L-1} h_{r,n}(l)\delta(\tau - \tau_l)$$

(A.5.1)

where $\delta(\cdot)$ is the Kronecker delta function and the taps $h_{r,n}(l) = \alpha_{r,n}(l)e^{j\theta_l}$ are uncorrelated with phase $\theta_l$ uniformly distributed over $[0,2\pi]$ for all receive-transmit antenna pairs (*r*,*n*). Each tap amplitude $\alpha_{r,n}(l) = \left|h_{r,n}(l)\right|$ is modeled as Nakagmai-*m* random variable, where, omitting the subscripts, the probability density function (*pdf*) is given by (2.20) and (2.21)

$$p(\alpha) = \frac{2}{\Gamma(m)}\left(\frac{m}{\Omega}\right)^m \alpha^{2m-1}\exp\left(-\frac{m}{\Omega}\alpha^2\right), \qquad \alpha \geq 0$$

(A.5.2)

Here, $\Gamma(\cdot)$ is the Euler Gamma function and $\Omega = E[\alpha^2]$, $m = E^2[\alpha^2]/E\left[\left(\alpha^2 - E(\alpha^2)\right)^2\right]$. For each tap and all (*r*,*n*) antenna pairs, $\Omega_{r,n}(l) = E\left[\left|h_{r,n}(l)\right|^2\right]$ with $m_{r,n}^l \geq 1/2$ being the fading parameter, $m_{r,n}^l = 1$ represents a frequency selective MIMO Rayleigh fading channel. For notational convenience and simplicity, we further assume equal fading parameters for all *l* and (*r*, *n*) pairs, thereby reducing $\Omega_{r,n}(l)$ and $m_{r,n}^l$ to only $\Omega_l$ and *m*, respectively. The power delay profile (PDP) can be represented by $\Omega_l = \Omega_0 e^{-l\delta}$, where $\delta \geq 0$ is the rate of average power decay and $\Omega_0$ is the average power of the first tap.

In an OFDM based system, the channel frequency response between a pair of antennas (*r*,*n*) can be expressed as

$$H_{r,n}(k) = \frac{1}{\sqrt{N}} \sum_{l=0}^{L-1} h_{r,n}(l) e^{-j2\pi k /}$$

(A.5.3)

where $H_{r,n}(k)$ is the frequency response of the channel for the *k*th subcarrier, which is exactly the (*r*,*n*) th element of the channel matrix **H**(*k*) of (3.2). This confirms that for a specific pair (*r,n*), the channel frequency responses are the discrete Fourier transforms (DFT) of the same impulse responses and hence, correlated in frequency, albeit the MIMO channel being spatially uncorrelated, i.e. the channels taps are independent for different antenna indices (*r,n*).

Based on the derivation of [81], the frequency domain modeling of Nakagami-*m* fading channels revels that $\beta_{r,n}(k) = \left|H_{r,n}(k)\right|$ also approximately follows the Nakagami-*m* distribution with the fading parameter $m_f$ and mean power $\Omega_f$ given by [82]

$$m_f = \frac{1}{\left(\frac{1}{m} - 1\right)\left(\frac{1 - e^{-2L\delta}}{1 - e^{-2\delta}}\right)\left(\frac{1 - e^{-\delta}}{1 - e^{-L\delta}}\right)^2 + 1}, \qquad \Omega_f = \frac{1 - e^{-L\delta}}{1 - e^{-\delta}}\left(\frac{\Omega_0}{N}\right)$$

(A.5.4)

# Chapter 6

# Relay Assisted and Cooperative CDD MC-CDMA Network with Frequency-Correlated Subcarriers

.

## 6.1 Introduction

A relaying network based on cooperative spatial diversity cyclic delay diversity (CDD) and space-time (ST) block coded is investigated. The distributed multi-hop network architecture makes full use of MC-CDMA frequency domain spreading properties and provides excellent spatial and frequency diversity. This scheme benefits from full diversity of orthogonal ST-block and employs CDD to increase the channel selectivity. Multi-stage CDD as proposed with low complexity implementation yields significant performance improvement as relaying network. Our relaying scheme has the best rate when used with optimum transmit antenna configurations.

Equipped with CDD, fraction of the total number of transmit antennas is used to extract the frequency (multipath) diversity, while the source and target nodes employing ST block codes provide maximum spatial diversity. The benefits provided by achieving full diversity (spatial and multipath) and increasing frequency selectivity are evaluated in terms of symbol error rate (SER) and end-to-end bit error rate (BER). Additionally fractional frame duration and transmitted power control are implemented to achieve higher data transmission rates. Furthermore, Monte-Carlo simulation results are presented when compared to traditional non-distributed networks to support the analytical framework.

Traditionally, relays have been used to extend the range of wireless communication systems. However, in recent years, many exciting applications of relay communications

have emerged [86]. One such emerging application is to assist in the communication between the source and destination terminals via some cooperative protocol, by controlling medium access coupled with the appropriate modulation or coding [83]. In such cooperative schemes, it has been found that the diversity of the communication system can be improved.

With interest from both the research and industrial communities gaining momentum, there is an urgent need to better understand as well as keep track of cutting edge research in cooperative and relay communications. In this context we propose a Distributed Cooperative Serial Spatial Relaying Network (DC-SSRN) based on the Diversity of MIMO-CDD. The vision for this includes Multi Carrier Code Division Multiple Access (MC-CDMA) system [87] [88], which is a promising candidate to support multimedia services and applications. By combining the benefits of the constituents, these multicarrier (MC) based systems deployed with multiple-input multiple-output (MIMO) techniques are well known for boosting the system's capacity and spectral efficiency as shown in [89] [80] and [90] .

Although MIMO antenna systems can improve the capacity and reliability of wireless communications by utilizing multiplexing gain and diversity gain, respectively, packing multiple antennas on a small mobile terminal poses implementation difficulty. The cooperative communication approach proposed in this work provides a design alternative, where neighbor nodes share their information and transmit cooperatively as a virtual multiple-input single-output (VMISO) virtual antenna array, thus providing diversity without the requirement of additional antennas at each node. The main advantages of the proposed cooperative communication scheme include: increasing the communications reliability over a time-varying channel, increasing the transmission rate and decreasing communication delay across the network, reducing transmit power, decreasing interference, and improving spatial frequency reuse, enlarging transmission range and extending network coverage.

Comparing with most existing work on cooperative communications focuses on various issues at the physical layer, and the advantages are often demonstrated by analyzing signaling strategies based on information theory. In this article the main point focus on how physical-layer cooperation can influence and be integrated with a low complexity

structure for higher throughput and more reliable communication, rather than advantages of cooperation at the physical layer. The throughput of these systems can be drastically increased by exploiting the knowledge of one's own transmitted signal, throughout the exchange of information between multiple users through relay(s).
To this end Distributed Space-Time Cooperative (DSTC) systems were introduced in [85] .In the space-time systems of [85] antennas are no longer collocated at the transmitter or the receiver; the antennas are distributed to relays, which cooperate in order to construct the space-time coded transmissions.

Among other transmit diversity scheme is Cyclic delay diversity (CDD) which creates replicas/echoes of the originally transmitted sequences at the receiver thus increases the frequency selectivity of the channel. These replicas change the characteristics of the channel in such a way that it seems to be highly frequency selective; resulting in randomization of the error distribution of the transmission. For MC-CDMA systems, CDD may be the simplest solution in low-delay-spread environments and also provides excellent frequency diversity even with relatively small spreading factors. The combination of induced frequency selectivity from CDD branches and inherent frequency domain spreading helps in improving the system's performance independent of forward error correction (FEC) or channel codes, which is otherwise compulsory in a simple OFDM system (i.e., without time or frequency domain spreading) [96].

It can be considered as STCs with no additional complexity at the receiver. CDD can be used for any number of transmit antennas and can be applied to existing systems without changing the receiver. Different approaches have been used in [70] [91] [92][71][93]**Error! Reference source not found.**[95] that theoretical diversity limits can be achieved by trading complexity, additional processing and incorporating additional pre-coding arrangements.
To date, few studies have considered transmit diversity to improve the performance of MC-CDMA system [67] [96]. Mostly, these works have focused only on the application of ST block codes. In this thesis, we present DC-SSD scheme which provides a simple solution to realize an excellent performance, low complexity and highly spectrally efficient MIMO MC-CDMA system. The simulation results show that the DC-SSD scheme outperforms its constituents by a significant margin.

While fairly extensive research has been carried out for the physical layer cooperative communication networks, to the best of our knowledge[86]. Cooperative communications require unique features in terms of fractional frame duration and transmission power control, which should be considered for a distributed and cooperative multipoint-to-multipoint environment. The contribution of this thesis is the derivation of throughput-maximizing resource allocation strategies for such as distributed cooperative relaying networks (DCRN) where the indoor fading distribution was often found to obey a Nakagami-*m* distribution, which is thus particularly important for cooperative serial spatial diversity networks.

Clusters of CDD nodes near each transmitter form virtual multiple-input single-output (VMISO) link to a receiver on the routing table and as far as possible to the transmitter. Space-time codes are utilized to support transmission over a long distance, thus reducing the number of transmission hops and spatially adjacent n are allowed antennas to communicate/cooperate with each other by CDD scheme improving communications reliability. Adaptive modulation and coding (AMC) and multimode transmission are schedule together according to the channel condition to improve the network throughput.

This chapter is organized as follows: First, we present the frequency domain Nakagami-*m* fading channel model and the serial ST-CDD system model in 6.2. The conversion of a MIMO CDD MC-CDMA into a SIMO serial relaying system is analyzed in 6.3. The performance analysis for the subject diversity techniques and the average SERs of *M*-ary signals with correlated MC-CDMA subcarriers is presented in 6.4 as well as the allocation strategies and the end-to-end throughput derivations. Numerical and simulation results are compared in 6.5 to support the derived allocation strategies.

**Link Level Perfomance**

The previous chapter dealt with the maximum achievable throughput over distributed MIMO multi-stage communication networks in dependency of certain communication condition, e.g. weather the channel is ergodic or non-ergodic which implied that transceivers of infinite complexity are available to thee system designer.

The link level performance, on the other hand, assess the behaviour of realistc transceivers

## 6.2 Serial Spatial Diversity Scheme for OFMA Systems

Let $N_{tx}$, $N_{rx}$, $N$, $G$ and $L$ represent the total number of transmit antennas, receive antennas, subcarriers, spreading factor and channel order, respectively. The system's user capacity is restricted to $U \leq G$, where $U$ is the number of active users.

### 6.2.2 Analytical Seral Spatial Diversity System Model

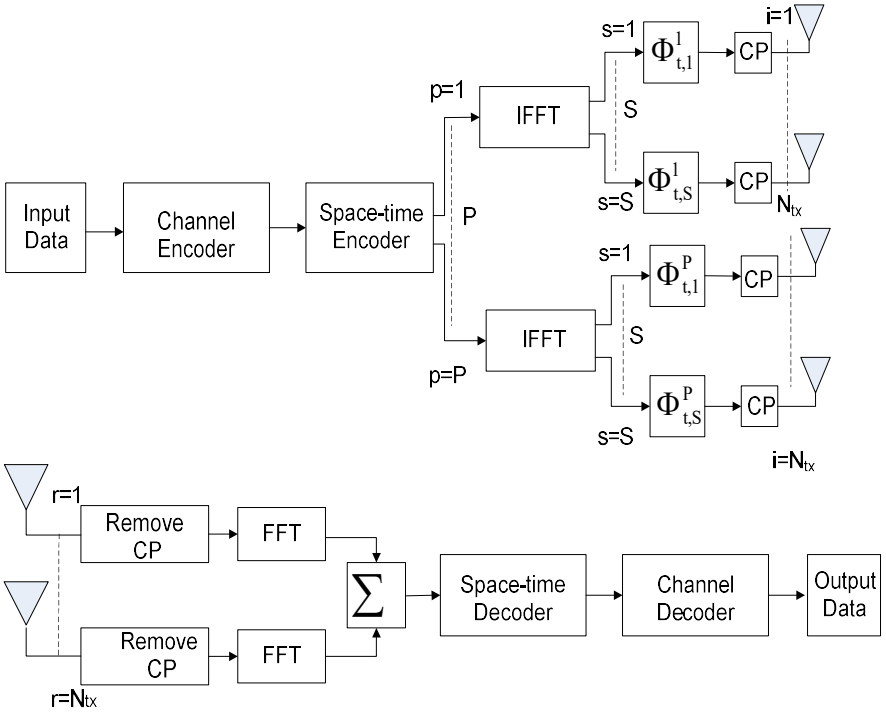


Figure 6.1 Serial Spatial Diversity scheme system model.

The implementation of SSD scheme is shown in 0 The ST-encoder splits the data stream into $p$=1, 2,…, $P$ branches, where $P$ is the number of primary streams of size $N \times 1$. Each output stream of the encoder is processed by the $N$ point inverse fast Fourier transform (IFFT) matrix $F_N^H$ and then a set of CDD matrices $\Phi_{t,s}^p$ are applied on each of the primary streams. Here $s$=1,2,…,$S$ represent the number of secondary streams generated by cyclically delaying each primary stream by CDD matrices $\Phi_{t,s}^p$ . The subscript $t$ in the CDD matrices $\Phi_{t,s}^p$ represents that the secondary streams are generated after the IFFT operation and therefore in the time domain. After inserting the cyclic prefix (CP) (which is the last $L$ samples of the $N$ symbols i.e. one OFDM symbol), the data is transmitted from a total of $N_{tx}$ antennas simultaneously after up conversion and power normalization.

CDD, which is implemented in time domain, has its frequency domain equivalent, known as Phase Diversity (PD) [71]. The equivalence between PD and CDD is the property of the DFT which represents that a cyclically delayed CDD signal in the time domain corresponds to a phase factor in the frequency domain. In other words a cyclic delay of $\Phi_{t,s}^{p}$in the time domain is a multiplication of phase factor $e^{j2\pi/N\Theta_{t,s}^{p}}$ in the frequency domain, where the phase is linearly increasing with the subcarrier index; it is very helpful in theoretical analysis.Following the same approach, we draw an equivalent frequency domain system model for our SSD schem. It can been see that in the equivalent system model the CDD matrices $\Phi_{t,s}^{p}$ are replaced by their frequency domain equivalent matrices $\Phi_{s}^{p}$, placed before the IFFT blocks. At the receiver the CP is removed, the received signals are processed by the FFT matrices $\boldsymbol{F}^{N}$ and sent to the ST- decoder.

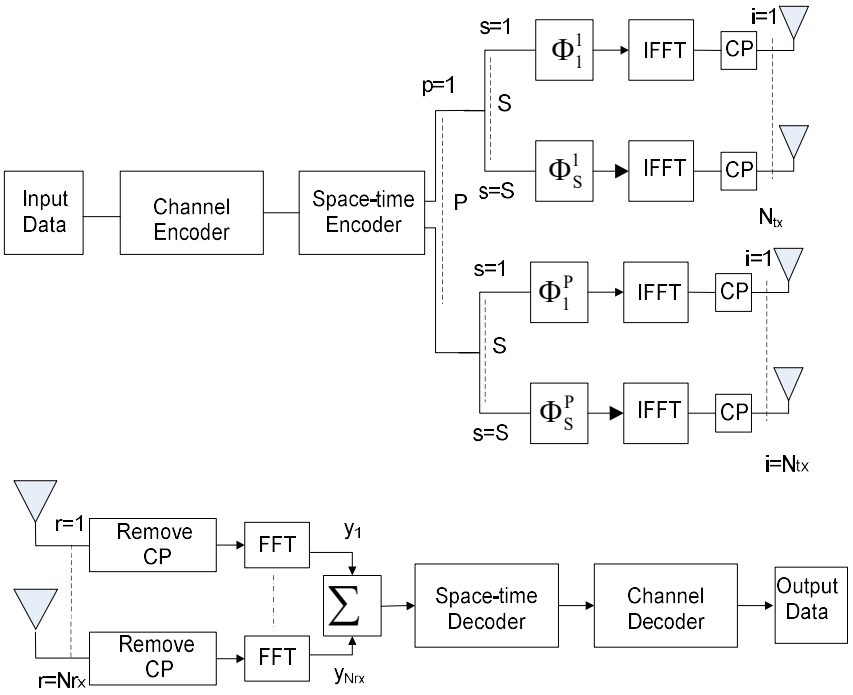


Figure 6.2 Frequency domain system model for Serial Spatial Diversity scheme.

The input-output relationship form the $x_s^p$ to $y_r^p$which are $N\times1$ vectors corresponding to one OFDM symbol, can be written as

$$y_r^p = \sum_{s=1}^{S} H_{r,s}^{p}\, x_s^p \qquad \forall r \in [1, N_{rx}] \quad \forall p \in [1, P]$$

(6.1)

where $H_{r,s}^{p}$ is the diagonal channel matrix, $P$ is the number of the primary streams from the ST encoder, $S$ represent the number of secondary streams for each primary stream $p$. The total number of transmit antennas are given by

$$N_{tx} = \sum_{p=1}^{P} N_s^p \qquad \forall s \in [1, S] \tag{6.2}$$

$x_s^p$ is output of PD matrix $\Phi_s^p$, which generate $S$ secondary stream for each of primary stream $p$. It must be noted here that number of secondary streams for each primary stream can be different which allow a very flexible transmitter structure $y_r^p$ is the total noise-less received signal at the output of the FFT in the receiver. The overall received signal plus noise can be expressed as

$$y_r = \left( \sum_{p=1}^{P} y_r^p \right) + n_r \qquad \forall r \in [1, N_{rx}] \tag{6.3}$$

where $\mathbf{n}_r$ represents the independent and identically distributed AWGN noise vector of size $N \times 1$.

The PD matrices $\Phi_s^p$ converts the total $N_{tx}$ frequency selective channels, each having ($L$+1) taps, to $P$ frequency selective channels each with $S$ ($L$+1) taps. In order words, the receiver will see the signal coming from only $P$ antennas, each with longer channel responses of length $S(L+1)$, regardless off the fact that a total of $N_{tx}$ antennas have been used for transmission. To verify it analytically, we start with the channel matrix in (8) that can be fully explained by

$$\mathrm{H}_{r,s}^{p} = \left[ \mathrm{H}_{r,s}^{1}, \ldots, \mathrm{H}_{r,s}^{p} \right]^{T} \tag{6.4}$$

where

$$H_{r,s}^{p} = \mathrm{diag}\left[ H_{r,s}^{p}(0), \ldots, H_{r,s}^{p}(N-1) \right] \tag{6.5}$$

With

$$H_{r,s}^{p}(k) = \sum_{l=0}^{L} h_{l,r}^{p}(l)\, e^{-j2\pi k n_1 / N} \tag{6.6}$$

For convenience, we rewrite the channel matrix $H_{r,s}^{p}$ as

$$\widehat{\mathrm{H}}_{r,s}^{p} = \sum_{l=0} h_{r,s}^{p} W_{l}^{p} \qquad \forall r \in [1, N_{rx}] \quad \forall p \in [1, P] \tag{6.7}$$

where $W_l^p = \mathrm{diag}\left[1, e^{-j2\pi l/N}, e^{-j4\pi l/N}, \ldots, e^{-j2\pi\,(N-1)/N}\right]$.

This channel representation shows that for each primary stream $p$, the channel taps $\sum_{l=0}^{L} h_{r,s}^{p}(l)$ can be different but they possess the same delay lags l in the FFT domain, as evident by the diagonal matrices $W_l^p$. Our aim is to shift the ($L$+1) taps of all channels in such a way that for each primary stream $p$. the channel taps $\sum_{l=0}^{L} h_{r,s}^{p}(l)$ become consecutive in their delay lags. By doing so, we can represent the overall system as $P$ frequency selective channels with longer $S$ ($L$+1) taps, at each receive antenna. To achieve this we have to design the PD matrices $\Phi_s^p$ . We follow the approach of [71] and select the matrices as

$$\Phi_{s}^{p} = \mathrm{diag}\left[1, e^{j\Phi_s^p}, \ldots, e^{j\Phi_s^p (N-1)}\right] \qquad \forall p \in [1, P] \quad \forall s \in [1, S] \tag{6.8}$$

If we choose $\Phi_s^p = -2\pi(s-1)(L+1)/N$, it is straightforward to show

$$W_{l}^{p}\Phi_{s}^{p} = W_{l+(s-1)(L+1)}^{p} \qquad \forall l \in [0, L] \quad \forall p \in [1, P] \quad \forall s \in [1, S] \tag{6.9}$$

Now, defining the equivalent longer channel vectors $h_r^p$ corresponding to the $r$th receive antenna for each stream $p$

$$h_{r}^{p} = \left[\left(h_{r,1}^{p}\right)^{T}, \left(h_{r,2}^{p}\right)^{T}, \ldots, \left(h_{r,S}^{p}\right)^{T}\right]^{T} \tag{6.10}$$

with the $l$th entry of $h_r^p$ by $h_r^p(l) = h_{r,\lfloor l/(L+1)\rfloor}^{p}(L+1)$. Now since $h_r^p$ has length $S$ ($L$+1) for each $p$, it can be viewed as coming from $P$ frequency selective channels. Based on (6.12), finally we can write the diagonal matrix in terms of longer equivalent channel as

$$\mathrm{H}_{r}^{p} = \sum_{s=1}^{S} \mathrm{H}_{r,s}^{p}\,\Phi_{s}^{p} = \sum_{l=0}^{S(L+1)-1} h_{r}^{p}(l) W_{l} \quad \forall r \in [1, N_{rx}] \quad \forall p \in [1, P] \tag{6.11}$$

Hence, we can conclude that the PD matrices $\Phi_s^p$ shifts the delays lags of the $s$th channel from [0, $L$] to [($s$-1) ($L$+1), s ($L$+1) -1], for each primary stream. In order to clearly, lets take an example with $P$=2 and $S$=1, which means that for both the primary stream $p$=1, 2 $\Phi_s^p$ become $\Phi_1^1 = \Phi_2^1 = I_N$, which correspond to no phase delayed signals and from the total $N_{tx}$=2 transmit antennas the original ST-encoded symbols are transmitted. Therefore for $S$=1 our scheme collapses to ST-coded system with the total of transmit antennas $N_{tx}$=$P$ .Lets take $P$=2 and $S$=2. In this case for both the primary stream $p$=1, 2 and $s$=1,

$\Phi_s^p$ are again $\Phi_1^1 = \Phi_2^1 = I_N$ which leads to (6.18)

$$\widehat{\mathrm{H}}_{r,1}^1 \Phi_1^1 = \mathrm{diag}\left(\sqrt{N} F_{0:L} \mathrm{h}_{r,1}^1\right)$$
$$\widehat{\mathrm{H}}_{r,1}^2 \Phi_1^2 = \mathrm{diag}\left(\sqrt{N} F_{0:L} \mathrm{h}_{r,1}^2\right) \quad (6.12)$$

and for $s$=2 the matrices $\Phi_2^1 = \Phi_2^2$ becomes

$$\widehat{\mathrm{H}}_{r,2}^1 \Phi_2^1 = \mathrm{diag}\left(\sqrt{N} F_{(L+1):(2L+1)} \mathrm{h}_{r,2}^1\right)$$
$$\widehat{\mathrm{H}}_{r,2}^2 \Phi_2^2 = \mathrm{diag}\left(\sqrt{N} F_{(L+1):(2L+1)} \mathrm{h}_{r,2}^2\right) \quad (6.13)$$

where $\boldsymbol{I}_N$ and $\boldsymbol{F}_N$ are the $N \times N$ identity and FFT matrices respectively $\boldsymbol{F}_{0:L}$ and $\boldsymbol{F}_{(L+1)(2L+1)}$ represent the first ($L$+1) and ($L$+1)-(2$L$+1)columns of the FFT matrix $\boldsymbol{F}_N$, given by

$$F_N = \begin{bmatrix} f^0 & f^0 & f^0 & \cdots & f^0 \\ f^0 & f^1 & f^2 & \cdots & f^N \\ f^0 & f^2 & f^4 & \cdots & f^{2N} \\ \vdots & \vdots & \vdots & \ddots & \vdots \\ f^0 & f^N & f^{2N} & \cdots & f^{NN} \end{bmatrix} \quad (6.14)$$

where $f^k = e^{-j2\pi k/}$ .

So far, the analysis is done by considering the frequency domain matrices $\Phi_s^p$. However, in actual the time domain CDD matrices $\Phi_{t,s}^p$ are used for implementation with the representation of PD matrices $\Phi_s^p$ so we can write

$$F_N^H \Phi_s^p = \begin{bmatrix} f_0^T \\ \\ f_{N-1}^T \end{bmatrix} \Phi_s^p = \begin{bmatrix} f_{(s-1)(L+1)}^T \\ \vdots \\ f_{(s-1)(L+1)-1}^T \end{bmatrix} \quad \forall p \in [1, P] \quad (6.15)$$

where $f_k^T$ is the $k$th row of IFFT matrix $F_N^H$. Following (6.11) as [71], shows that left multiplying the matrices $\Phi_s^p$ by the IFFT matrix $F_N^H$ is equivalent to permuting the rows of $F_N^H$ circularly. Hence, the CDD matrices $\Phi_s^p$ are the $N \times N$ permutation matrices such that

$$\Phi_{t,s}^p F_N^H = F_N^H \Phi_s^p \quad (6.16)$$

Where

$$\Phi_{t,s}^p = \begin{bmatrix} 0 & I_{(s-1)(L+1)} \\ I_{N-(s-1)(L+1)} & 0 \end{bmatrix} \qquad \forall s \in [1, S] \quad \forall p \in [1, P] \quad (6.17)$$

The rate of our SSD scheme is given by

$$R_{SSD} = r_{cc} r_{stc} \quad (6.18)$$

where $r_{cc}$ is the rate of the outer channel code (necessary only for ST-block codes) and $r_{stc}$ is the rate of employed ST-encoder.

### 6.3 System Model Based on MC-CDMA

In this section, we present the proposed Cooperative Serial Spatial Diversity (CSSD) scheme based on the previous analysis. Spatial diversity is extracted by using the well known space time block code STCs and additional transmit relaying antennas are used to exploit the multipath diversity with the help of CDD.

#### 6.3.1 Transmitter

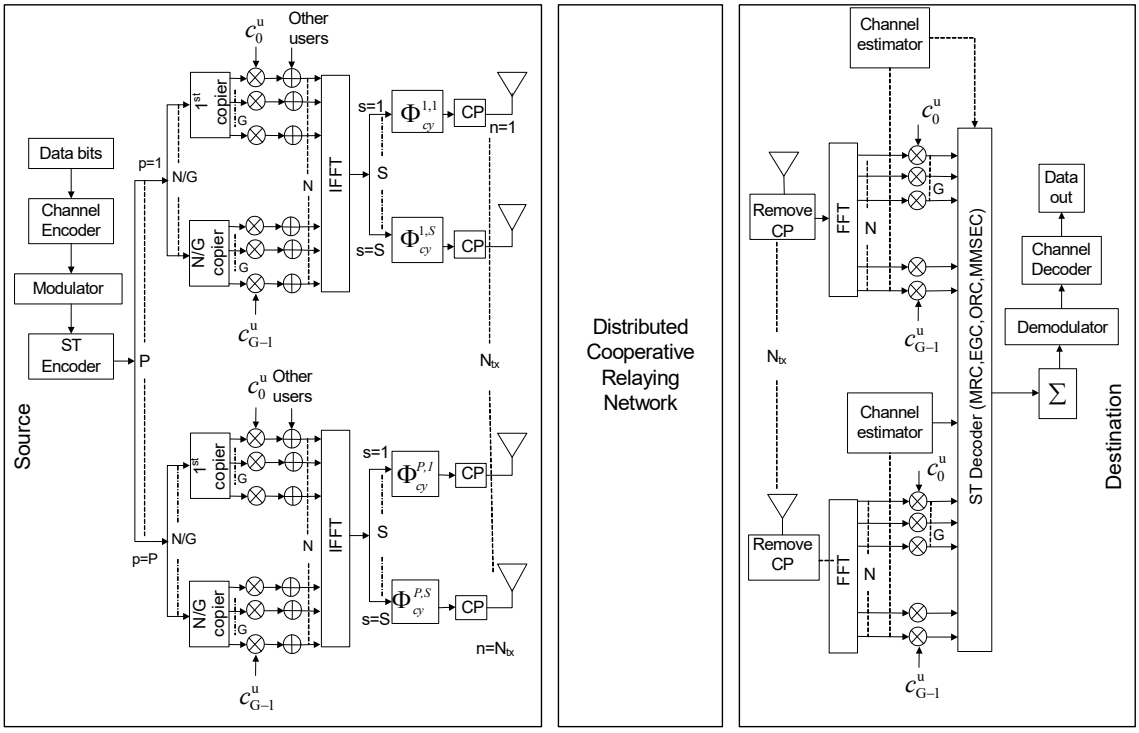


MC-CDMA system model employing the SSD scheme

Figure 6.3 MC-CDMA system model

A synchronous downlink MC-CDMA system equipped with SSD scheme is shown in 0 Each user may transmit $Q$ symbols during a signaling interval leading to the processing gain $G$ of $N/Q$. The equiprobable data stream of the *uth* user is first channel encoded then modulated and mapped as symbols, These modulated symbols are then passed to a diversity encoder based on ST-block coding mechanism [45][98]. These coded symbols are placed on $P$ branches and passed to their respective spreading section, where each symbol is copied $G$ times and multiplied with the spreading sequence (Walsh-Hadamard)

of the *u*th user. The remaining users' data streams are similarly spread by their specific sequences. Then, the resulting coded chips of all users are added synchronously and modulated by an *N*-point inverse fast fourier transform (IFFT). After IFFT, the output signal of the *p*th ST-encoded branch can be expressed as

$$x_p(t) = 1/\sqrt{N} \sum_{u=0}^{U-1} \sum_{q=0}^{Q-1} \sum_{g=0}^{G-1} b_q^{u,p} c_g^u \, e^{j2\pi/N(gQ+q)t} \tag{6.19}$$

where *t* is the time index $b_q^{u,p}$ and $c_g^u$ are the $qth$ ST coded symbol and $g$th chip of the *u*th user, respectively.

Next, each signal $x_p(t)$ is replicated on *S* CDD relays and each one is cyclically shifted or delayed by a specific delay, $\Theta_{cy}^{p,s}$ $s$=1,2,…,*S*. Due to the insertion of these cyclic delays $x_p(t)$, becomes

$$\underbrace{x_p\left(t - \Theta_{cy}^{p,s}\right)_{\mathrm{mod}} N}_{Cyclically\ delayed\ signal} = \frac{1}{\sqrt{N}} \sum_{u=0}^{U-1} \sum_{q=0}^{Q-1} \sum_{g=0}^{G-1} \underbrace{e^{j2\pi/N\Theta_{cy}^{p,s}} b_q^{u,p} c_g^u e^{j2\pi/N(gQ+q)t}}_{Phase\ delayed\ signal} \tag{6.20}$$

Finally, to avoid ISI caused by the multipath channel, a CP of length $L_{cp}$ is added for each cyclically delayed ST-encoded branch (*p,s*), there after, the signals are transmitted from a total of $N_{tx}$ antennas simultaneously after radio frequency up-conversion and normalization.

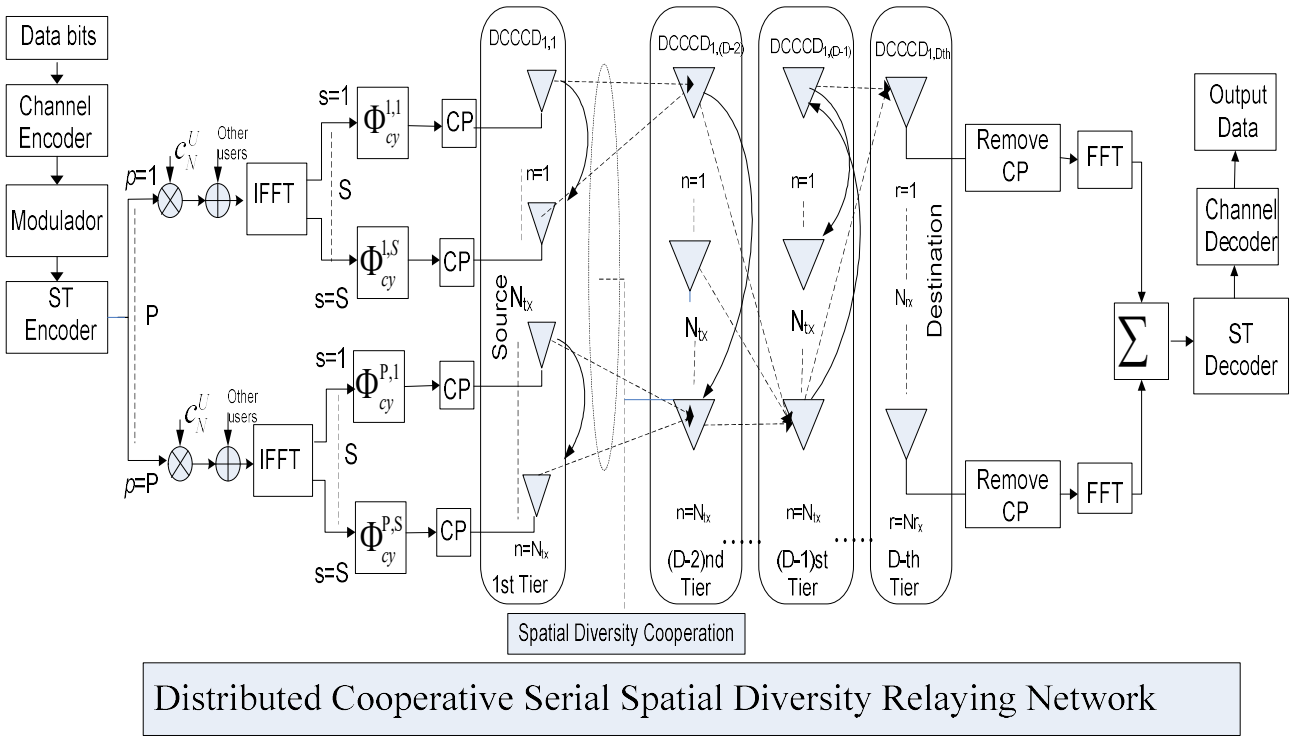


Figure 6.4 Distributed Cooperative

The Distributed Cooperative Relaying Network shown in Figure 6.4 provides a flexible transmit antenna configuration by allowing any number of CDD relaying for each ST-encoded branch. The ST-encoded branch and CDD relay indices (*p, s*) can be mapped to the transmit antenna index by $n = (p-1)S + s$, for $1 \le n \le N_{tx}$. The delays should be such that the $L$ channel taps of all $S$ channels belonging to each branch $p$ should become consecutive in their delay lags. By doing so, the overall system can be represented by $P$ frequency selective channels; each with $SL$ channel taps [91]. To achieve this, we select the cyclic delays as $\Theta_{cy}^{p,s} = (s-1)L$ for $p \in [1, P], s \in [1, S]$. This ensures that for each ST-encoded branch $p$, the delays lags of the $s$th channel are shifted from [0, $L$-1] to [($s$-1)$L$, $s$($L$-1)].Since, $L$ is not always known at the transmitter, the cyclic delay could be chosen simply by replacing $L_{cp}$ with $L$.

### 6.3.2 Receiver

The receiver section remains the same a ST block coded one, as the additional CDD relays do not impose any change. In other words, the receiver sees the signal coming from only $P$ antennas, each with longer impulse responses of length $SL$, regardless of the fact that a total of $N_{tx}$ antennas have been used for transmission. This enhanced impulse response

changes the channel transfer function of (6.4) $H_{r,n}(k) = 1/\sqrt{N}\sum_{l=0}^{S(L-1)} h_{r,n}(l)\, e^{-j2\pi kl/N}$, which confirms the conversion of spatial diversity of $S$ CDD relaying, for each $p$, into frequency.

At the receiver, after the removal of CP and subsequent processing by $N$-point FFT, the channel is estimated for each subcarrier. The received symbols are then multiplied with the spreading code previously assigned to the desired user and fed to a ST decode/combiner. Lastly, the symbols are de-modulated and decoded.

### 6.4 Performance Analysis

The square of Nakagami RV, ie $\gamma_r = \beta_{n,r}^2$, follows the Gamma distribution with *pdf* [59]

$$p_{\gamma_r}(\gamma_r) = \frac{\left(\frac{\hat{m}}{\bar{\gamma}_r}\right)^{\hat{m}}}{\Gamma(\hat{m})}\gamma_r^{\hat{m}-1}\exp\left(-\frac{\hat{m}}{\bar{\gamma}_r}\gamma_r\right), \quad \gamma_r \geq 0 \tag{6.21}$$

and the moment generating function (MGF)

$$\Phi_{\gamma_r}(s) = \int_0^\infty e^{-s\gamma_r}\, p_{\gamma_r}(\gamma_r)d\gamma_r = \left(1 + \frac{s\bar{\gamma}_r}{\hat{m}}\right)^{-\hat{m}} \tag{6.22}$$

where $\bar{\gamma}_r$ is the average SNR. Following [35], it can be shown that for the case of CDD MC-CDMA system

$$\hat{m}_{(CDD)} = \left(\frac{1 - e^{-2\delta}}{1 - e^{-2N_{tx}L\delta}}\right)\left(\frac{1 - e^{-N_{tx}L\delta}}{1 - e^{\delta}}\right)^2 m \tag{6.23}$$

with $\hat{\Omega}_{CDD} = \Omega_f^{CDD}$ as given previously

Using the average uplink SNR $\bar{\gamma}_{r(CDD)}^{U_l}$ for the CDD MC-CDMA system can finally be expressed as

$$\bar{\gamma}_{r_{CDD}}^{U_l} = \left(\underbrace{\frac{U-1}{N}}_{A} + \underbrace{\frac{1}{E_s/N_0\hat{\Omega}_{CDD}/N_{tx}}}_{B}\right)^{-1} \tag{6.24}$$

and the downlink average SNR by $\bar{\gamma}_{r_{CDD}}^{D_l} = (2A + B)^{-1}$

Similarly for the case of STBC MC-CDMA, based on [35]

$$\widehat{m}_{STBC} = \left(\frac{1 - e^{2\delta}}{1 - e^{-2L}}\right)\left(\frac{1 - e^{L\delta}}{1 - e^{-\delta}}\right) mN_{tx} \tag{6.25}$$

with $\widehat{\Omega}_{STBC} = \Omega_f$. The average uplink SNR $\bar{\gamma}_{r_{STBC}}^{U_l}$ for the STBC MC-CDMA system becomes

$$\bar{\gamma}_{r_{STBC}}^{U_l} = \left(\underbrace{\frac{U-1}{N}}_{A} + \underbrace{\frac{1}{\frac{E_s}{N_0} k\widehat{\Omega}_{STBC}/RN_{tx}}}_{C}\right)^{-1} \tag{6.26}$$

and the downlink SNR is given by $\bar{\gamma}_{r_{STBC}}^{D_l} = (2A + C)^{-1}$.

The closed-form error rate expression for CDD and STBC MC-CDMA system with coherent *M*-QAM modulation in Nakagami-*m* fading employing the MGF based approach and transforming the single integrals into hypergeometric functions is presented. The same approach has been used in [26] for the error rate evaluation of single carrier system in flat fading environments. The error performance for the subject system are evaluated by averaging the conditional SER $P_s(E|\gamma_r)$over the *pdf* of the instantaneous SNR $\gamma_r$, i.e.,

$$P_s(E) = \int_0^{\infty} P_s\,(E|\gamma_r) p_{\gamma_r}(\gamma_r) d\gamma_r \tag{6.27}$$

### 6.4.1 M-QAM

The conditional SER for coherent detection *M*-QAM signals is given by [59] and [26]

$$P_s(E|\gamma_r) = \frac{4q}{\pi}\int_0^{\frac{\pi}{2}} \exp\left\{-\frac{\gamma_r g_{MQAM}}{\sin^2\theta}\right\} d\theta - \frac{4q^2}{\pi}\int_0^{\frac{\pi}{4}} \left\{-\frac{\gamma_r g_{MQAM}}{\sin^2\theta}\right\} d\theta \tag{6.28}$$

where $q = \left(1 - 1/\sqrt{M}\right)$ and $g_{MQAM} = 3/2\,(M-1)$. Using (19), (24) and (23), the average SER with *M*-QAM modulation is given in (6.25) .

Γ(x) is the complete gamma function ${}_2F_1(a,b;c;x)$is generalized hypergeometric function with 2 parameters of type 1 and 1 parameter of type 2, it is sometimes referred to as the Gauss hypergeometric function. The function $F_1(a,b,b',c;x,y)$ is a hypergeometric function of two variables, which is sometimes referred to as Appell hypergeometric function, both of them defined in [27] and [84] note again that the infinite summations can be truncated after sufficient terms.

$$P_s(E) = \frac{2q}{\sqrt{\pi}} \frac{\Gamma\left(\hat{m}+\frac{1}{2}\right)}{\Gamma(\hat{m}+1)} \Phi_{\gamma_r}\left(g_{MQAM}\right) \quad {}_2F_1\left(\hat{m}, \frac{1}{2}; \hat{m}+1; \frac{1}{1+\frac{g_{MQAM}\bar{\gamma}_r}{\hat{m}}}\right)$$
$$- \frac{2q^2 \Phi_{\gamma_r}\left(2g_{MQAM}\right)}{\pi(2\hat{m}+1)} F_1\left(1, \hat{m}, 1; \hat{m}+\frac{3}{2}; \frac{1+\frac{g_{MQAM}\bar{\gamma}_r}{\hat{m}}}{1+\frac{2g_{MQAM}\bar{\gamma}_r}{\hat{m}}}, \frac{1}{2}\right) \tag{6.29}$$

In order to simplify the analysis the error rates obtained in the previous section are utilized here where the bits are Gray-mapped onto the symbol. The BER $P_b(E)$ is related to the SER via [97]

$$P_b(E) \approx \frac{P_s(E)}{\log_2 M} \tag{6.30}$$

The fractional resource allocation rules are considered for the case of correctness of the received signal is done at the corresponding terminal MT (*t*-MT), so that the errors in consecutive stages become independent for the cyclic delay system.

Our analysis is focus on the Maximum Throughput for end-to-end transmission via *K* relaying transmissions. With reference to [85], the normalized end-to-end throughput can be expressed for a CDD MC-CDMA Cooperative relaying system according to [85] as (6.37)

$$\Phi = \min_{\upsilon \in (1,K)} \{\alpha'_\upsilon \log_2 M_\upsilon\} \cdot \left(1 - P_{f,e2e}(E)\right) \tag{6.31}$$

where $\alpha'_\upsilon$and $M_\upsilon$ are the fractional frame duration and modulation index of the $\upsilon th$ stage respectively, and $P_{f,e2e}(E)$ is the end-to-end FER.

For a lossless direct communication link, the normalized throughput is given by $\alpha'_\upsilon \log_2(M)$ [bits/s/Hz] with index $M$ during a fractional frame duration $\alpha'_\upsilon$, which is affected by end-to-end FER $P_{f,e2e}(E)$.

According to a relaying system with $K$ stages, the weakest link determines the throughput, consequently $\min_{\upsilon\in(1,K)}\{\alpha'_\upsilon \log_2(M_\upsilon)\}$. It is thus the aim to derive optimum resources allocation strategies so that the end-to-end link achieves its maximum throughput.

Under the knowledge that $P_{f,e2e}(E)$ is a function of $M_{\upsilon\in(1,K)}$ and the fractional transmission power allocated to each CDD stage, the following optimization process is proposed for such as diversity scheme. To this end, the optimization process is performed according to the following three stages.

First, the modulation indices $M_{\upsilon\in(1,K)}$ are fixed and the limiting case where $SNR\rightarrow\infty$ is considered. This condition reduces (6.31) to

$$\Phi = \min_{\upsilon\in(1,K)}\left\{\alpha'_\upsilon \log_2(M_\upsilon)\right\} \tag{6.32}$$

where the fractional frame duration $\alpha'_\upsilon$ need to be chosen such as to maximize $\Phi$ under constraint $\sum_{\upsilon=1}^{K}\alpha'_\upsilon = 1$. To this end all $\alpha'_\upsilon \log_2(M_\upsilon)$ are considered which results in

$$\alpha'_\upsilon = \frac{\prod_{\omega=1,\omega\neq\upsilon}^{K}\log_2 M_\omega}{\sum_{k=1}^{K}\prod_{\omega=1,\omega\neq k}^{K}\log_2 M_\omega} \tag{6.33}$$

Second, in order to maximize the throughput, the end-to-end BER needs to be minimizing

$$\Phi = \min_{\upsilon\in(1,K)}\{\alpha'_\upsilon \log_2 M_\upsilon\}\cdot\left(1-P_{b,e2e}(E)\right)^B \tag{6.34}$$

where $B$ is the frame length in bits.

Defining a non-decreasing $\Phi$ metric

$$\Phi' \cong \exp\left[\frac{\log\left(\Phi/\min_{\upsilon\in(1,K)}\{\alpha'_\upsilon \log_2 M_\upsilon\}\right)}{B}\right] - 1 \tag{6.35}$$

It can easily be shown that

$$\Phi' \approx -P_{b,e2e}(E) \tag{6.36}$$

Third, the optimum modulation order $M_{\upsilon\in(1,K)}$ has to be determined in dependency of the previously derived fractional resource allocations, by permuting all possible modulation order at each stage.

The end-to-end BER expression for independent BERs $P_{b,\upsilon\in(1,K)}$caused by independent SERs $P_{s,\upsilon\in(1,K)}$is shown as

$$P_{b,e2e}(E) = 1 - \prod_{\upsilon=1}^{K}\Big(1 - P_{b,\upsilon}(E)\Big) \tag{6.37}$$

which, at low BERs at every stage, can be approximated as

$$P_{b,e2e}(E) \approx \sum_{\upsilon=1}^{K} P_{b,\upsilon}\,(E) \approx \sum_{\upsilon=1}^{K} \frac{P_{s,\upsilon}(E)}{\log_2 M_\upsilon} \tag{6.38}$$

Further analysis concentrates on the case of Nakagami fading with equal channel gains per relaying stage. Assuming that each stage is allocated a fractional power $\beta'_\upsilon$, the above given dependency can be expressed in conjunction with the SERs $P_{s,\upsilon}(\cdot) = P_{QAM}$. The SERs for M-QAM in the $\upsilon^{th}$ relaying stage is hence upper-bounded by [85].

$$P_{b,e2e}(E) \le \sum_{\upsilon=1}^{K} A_\upsilon\,(1 + B_\upsilon \beta'_\upsilon)^{-\widehat{m}_\upsilon} \tag{6.39}$$

$$A_\upsilon = \frac{2_{q_\upsilon}}{\log_2 M_\upsilon} \tag{6.40}$$

where

$$B_\upsilon = \begin{cases} \left(g_{MQAM,\upsilon}\dfrac{\bar{\gamma}_{r,\upsilon}}{\widehat{m}_\upsilon}\right)_{CDD} \\ \left(\dfrac{g_{MQAM,\upsilon}}{R_\upsilon}\dfrac{\bar{\gamma}_{r,\upsilon}}{\widehat{m}_\upsilon}\right)_{STBC} \end{cases} \tag{6.41}$$

and

where $R_\upsilon = R_{SSD}$ is the STBC rate of the 1st stage.

In [97], it is shown that the fractional power allocations $\beta'_{\upsilon\in(1,K)}$ have to obey

$$\beta'_\upsilon \approx \left[\sum_{\upsilon=1}^{K} \alpha'_\omega \left(\frac{\hat{m}_\upsilon^{-1} A_\upsilon^{-1} B_\upsilon^{\hat{m}}}{\hat{m}_\omega^{-1} A_\omega^{-1} B_\omega^{\hat{m}}}\right)^{\frac{1}{\hat{m}_{\max}+1}}\right]^{-1} \tag{6.42}$$

where $\hat{m}_{\max} = \operatorname{argmax}(\hat{m}_1, \ldots, \hat{m}_K)$.

### 6.5 Performance Results

In this section, numerical results based on the derivations made in the previously are presented and verified with the simulation results obtained from a Monte-Carlo based MC- CDMA system simulator employing CDD diversity technique. All results are produced for SER versus SNR, defined as the transmitted symbol energy over the noise power spectral density ($E_s/N_o$). For simplicity, equal number of spreading factors and subcarriers has been chosen, i.e. $N$=$G$. Coherence detection with a single receive antenna $N_{rx}$=1 has been employed for all error rate curves. To obtain the numerical SER curves, the sums involving the series representation of both the Gauss and Appell hypergeometric functions are truncated after 11 terms.

In order to provide reliable results it was considered varies Nakagami-*m* values with different modulation indices *M*. By fixing the channel order and increasing *m,* the performance improvement can be observed for different combinations. Analytical results are obtained by (6.33) and (6.42), where they closely match with the simulation results. It is important to highlight that for both CDD and STBC, the combination of higher channel orders ($L$>2), transmit antenna ($N_{tx}$>3) and Nakagami parameter *(*$m$>4), results in saturated improvement in performances; unless additional receiver chains are employed.

In [97] a comparison between CDD and STBC diversity techniques is shown The performance of the developed algorithm is assessed by means of (6.33) and (6.42)

respectively. Note that if reference is made to the non-optimized scenario, then only the fractional transmission power is meant not to be optimized since the frame duration is easily related to the modulation

The first scenario Figure 6.5 is entirely symmetric which leads to the same performance for all three allocation strategies. The second scenario Figure 6.5 is the same as the first, with the only difference that the channel in the second stage is now 10 times stronger than in the first stage such that, this created non-symmetric scenario. It can be observed that the optimum and developed allocation strategy yield the same performance for any of the depicted configurations. Furthermore, the gain of an optimized system over a non-optimized system is highest for very asymmetric cases. At a target end-to-end BER of $10^{-5}$, about 1 dB in power can be saved. The performance for optimum and non-optimized algorithms is implemented according different environments. Figure 6.5 shows the comparison between optimum and non-optimised end-to-end BER for various configuration of a three-stage relaying network with Frequency-Correlated Subcarriers over Nakagami-*m* Fading Channels, where the proposed algorithm provides notable performance improvement.

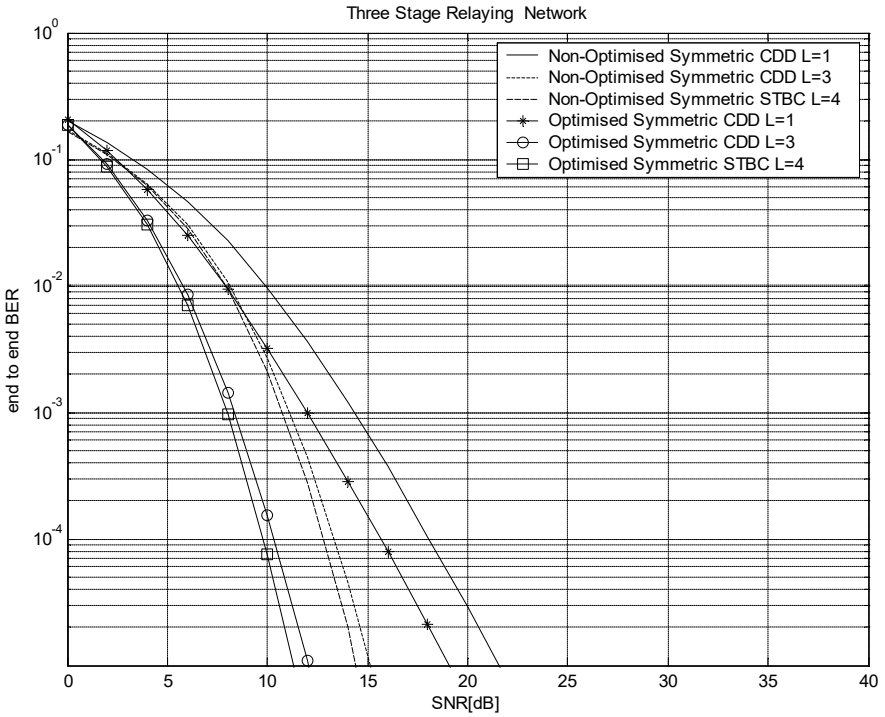


Figure 6.5 Comparison between non-optimised and optimised end-to-end BER for

various configurations of a three-stage relaying network.

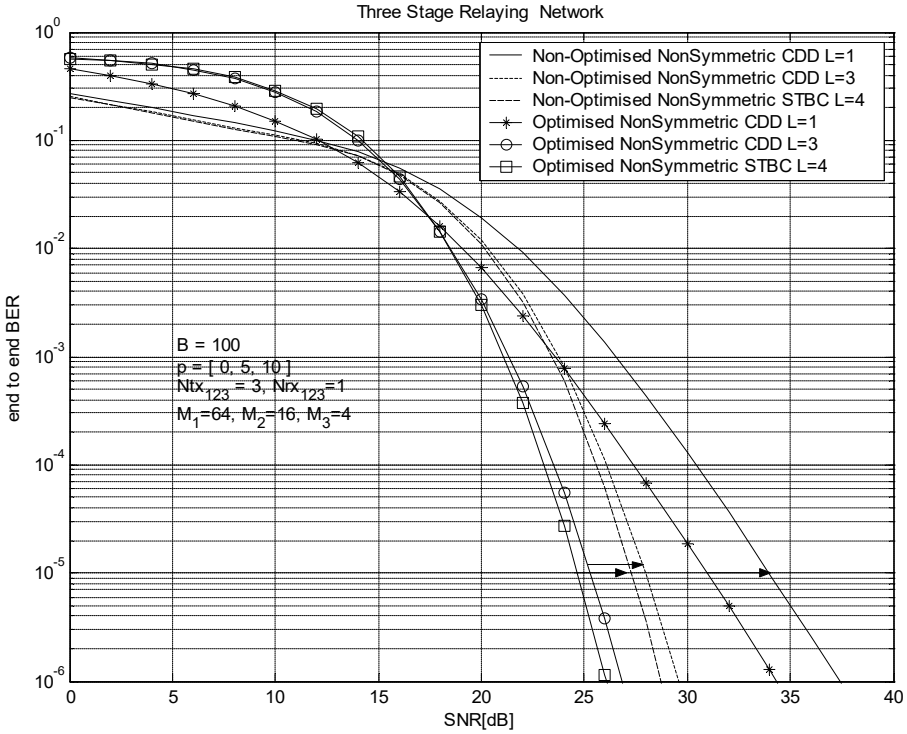


Figure 6.6 Comparison between non-optimised and optimized end-to-end BER for various configuration of a three-stage relaying network.

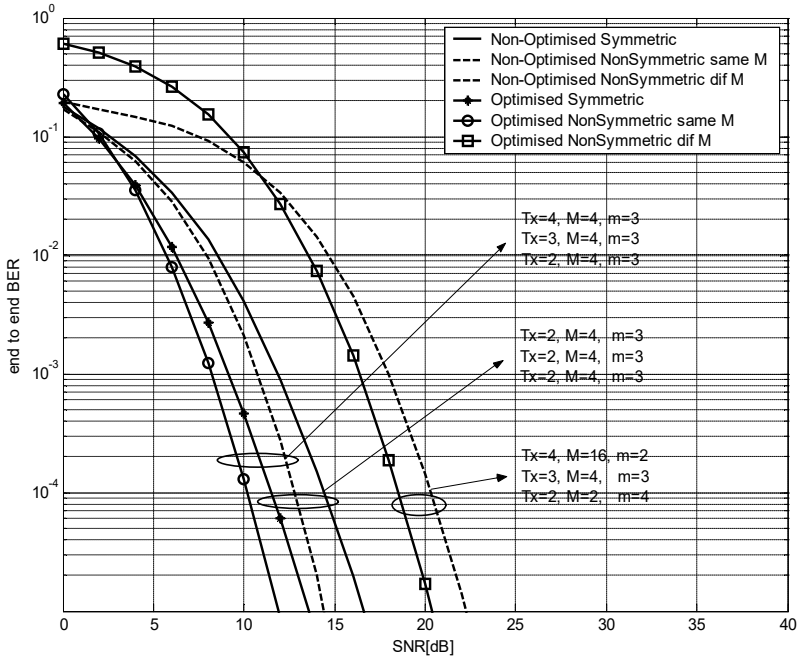

Figure 6.7 Comparison between optimum and non-optimised end-to-end BER for various configuration of a three-stage relaying network with Frequency-Correlated Subcarriers over Nakagami-m Fading Channels.

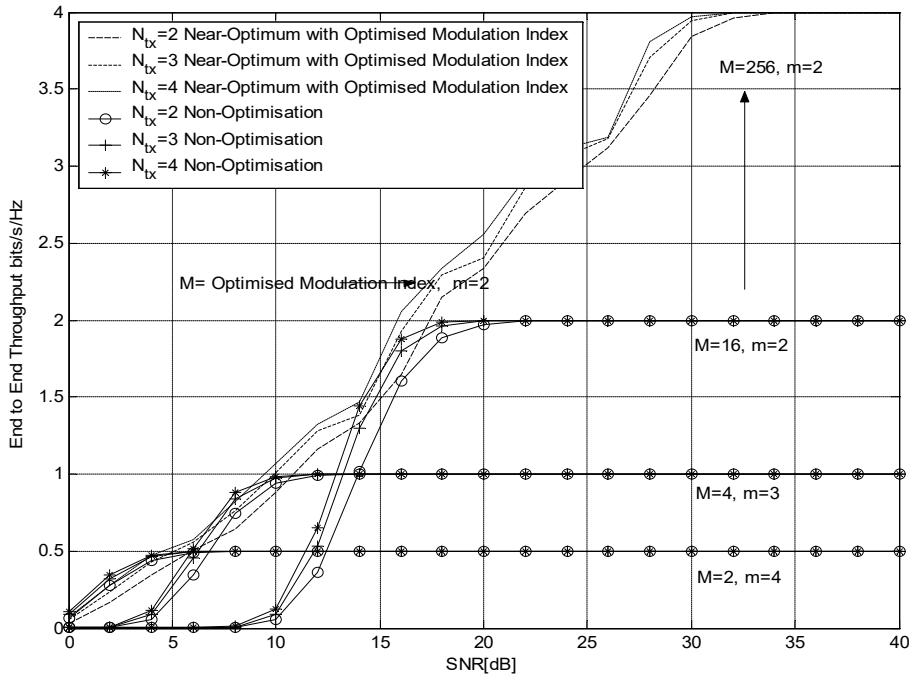


Figure 6.8 Numerically optimized modulation index to yield near-optimum end-to-end throughput, compared to non-optimized MC-CDMA network with Frequency Correlated Subcarriers over Nakagami-m fading Channels.

The throughput of a three-stage system is illustrated by means of Figure 6.8 which utilizes the fractional resource allocation strategies (6.33) and (6.41). The precision of the fractional allocation algorithm for fixed modulation indexes allows performing a final numerical optimization in each relaying stage over all possible modulation indexes. The low complexity of (6.33) and (6.41) guarantees that such optimization comes at little additional computational power.

Such numerical optimization was performed for a 3-stage network with $p$=[0,5,10]dB and $t_{1,2,3} = 2,3,4$ and $r_{1,2,3} = 1$. Each stage could choose a modulation index belonging to the set $M_{1,2,}$=(2,4,16,64,256); where the near-optimum adaptive modulation per stage is compared against various fixed combinations. At any SNR, the developed algorithm clearly outperforms any of the fixed configurations. For example, if the system was to operate at an SNR in the first link of 20 dB, then the best but fixed modulation index can

only reach 2 bits/s/Hz; in this case either 16-QAM or 64-QAM in any of the three stages. The optimum selection is 64-QAM with an optimized fractional power allocation and 2.5 bits/s/Hz, which yields a performance benefit of 25%..

## 6.6 Throughput Analysis of DSC ST-CDD Relaying Networks

### 6.6.1 Maximum Throughput for end-to-end Transmission

*Problem Simplification*
With reference to [85] the normalized end-to-end throughput can be expressed as (6.31) by (6.42)

$$\Theta = \min_{\upsilon\in(1,K)}\{\alpha'_{\upsilon}R_{\upsilon}\log_2(M_{\upsilon})\}\cdot\left(1-P_{f,e2e}(E)\right) \tag{6.43}$$

where $\alpha'_{\upsilon}$and $M_{\upsilon}$ are the fractional frame duration and modulation index of the $\upsilon^{th}$stage respectively. The rate $R_{\upsilon}=r_{cc,\upsilon},r_{stc,\upsilon}$where $r_{cc}$ is the rate of the outer channel code (necessary only for ST-block codes) and $r_{stc}$ is the rate of employed ST-encoder for the evaluation of the end-to-end FER $P_{f,e2e}\,(E)$

For a communication system with $K_{cdd}$ relaying stages, the weakest relay in the chain determines the throughput, hence $\min_{\upsilon\in(1,K)}\{\alpha'_{\upsilon}R_{\upsilon}\log_2 M_{\upsilon}\}$. To this end, the modulation indices $M_{\upsilon\in(1,K)}$ are fixed and the limiting case where SNR→∞ is considered. This reduces (6.43) to (6.44)

$$\Theta = \min_{\upsilon\in(1,K)}\{\alpha'_{\upsilon}R_{\upsilon}\log_2 M_{\upsilon}\} \tag{6.44}$$

where the fractional frame durations $\alpha'_{\upsilon}$ need to be chosen such as to maximize Θ under constraint. $\sum_{\upsilon=1}^{K}\alpha'_{\upsilon}=1$. This is clearly achieved by equating all $\alpha'_{\upsilon}R_{\upsilon}\log_2 M_{\upsilon}$, which results in (6.39) as (6.50)

$$\alpha'_{\upsilon}=\frac{\prod_{\omega=1,\omega\neq\upsilon}^{K}R_{\omega}\cdot\log_2 M_{\upsilon}}{\sum_{k=1}^{K}\prod_{\omega=1,\omega\neq\upsilon}^{K}R_{\omega}\log_2 M_{\omega}} \tag{6.45}$$

then, the normalized throughput is expressed in terms of the end-to-end BER $P_{b,e2e}(E)$ for the total number of sent bits *B as* (6.34) as (6.46)

$$\Theta = \min_{\upsilon\in(1,K)}\{\alpha'_{\upsilon}R_{\upsilon}\log_2 M_{\upsilon}\}\cdot\left(1-P_{b,e2e}(E)\right)^{B}$$

(6.46)

Defining a non-decreasing (in Θ) metric (6.35) is shown (6.47)

$$\Theta' \cong \exp\left[\frac{log\left(\Theta/\min\limits_{\upsilon\in(1,K)}\{\alpha'_\upsilon R\log_2 M_\upsilon\}\right)}{B}\right]-1$$

(6.47)

it can be shown that (6.41) is similar to (6.48)

$$\Phi' \approx -P_{b,e2e}(E)$$

(6.48)

By optimally assigning fractional transmission power to each relaying stage, the optimum modulation order $M_{\upsilon\epsilon(1,K)}$ has to be determined in dependency of the previously derived fractional resource allocations. This is done by permuting all possible modulation orders at each stage such as to maximize the end-to-end throughput.

*Full Cooperation at each Stage*

Under the assumption of full cooperation, each of the $K_{cdd}$ relaying stages experiences independent BERs $P_{b,\upsilon\in(1,K)}(E)$ caused by independent SERs $P_{s,\upsilon\in(1,K)}(E)$. A bit from the source is received correctly at the destination only when at all stages $K_{cdd}$the bit has been transmitted correctly. The end-to-end BER can therefore be expressed as (6.37) which, at low BERs [97] at every stage can be approximated as (6.38).

Assuming that each stage is allocated a fractional power $\beta'_\upsilon$, the above-given dependency can be expressed as (6.49)

$$P_{b,e2e}(E) \approx \sum_{\upsilon=1}^{K}\frac{P_{s,\upsilon}(\hat{m}_\upsilon(N_{tx}\cdot N_{rx})_\upsilon, \hat{m}_\upsilon t_\upsilon, R_\upsilon, R_{cdd}, \gamma_\upsilon, \beta'_\upsilon\cdot S/N, M_\upsilon)}{\log_2 M_\upsilon}$$

(6.49)

where the SERs $P_{s,\upsilon}(\cdot)=P_{PSK/QAM}(\cdot)$ are given thought (6.49), respectively. Furthermore, $\hat{m}_\upsilon(N_{tx}\cdot N_{rx})$, $N_{tx}$ and $N_{rx}$ are the number of transmit and receive antennas in the $\upsilon^{th}$ stage, $R_\upsilon$is the rate of the STBC, $R_{cdd}$the rate of the CDD, $\gamma_\upsilon$ is the average attenuation experienced, *S* is the total power given to deliver the information from source to sink, and *N* is the noise power. The optimization process has only to be performed *w.r.t.* the fractional power allocation $\beta_{\upsilon\in(1,K)}$. Even so, the optimization process is very intricate. To simplify analysis further, an upper bound to the derived SERs for M-PSK

and M-QAM is invoked. To this end, the integrant is upper-bounded by its largest argument, which occurs at $\theta=\pi/2$. The SER for M-PSK in the $\upsilon^{th}$relaying stage is hence upper-bounded as (6.50)

$$P_{s,\upsilon}(E) \leq \frac{\frac{M_\upsilon - 1}{M_\upsilon}}{\left(1 + \beta'_\upsilon \frac{g_{PSK,\upsilon}, \bar{\gamma}_{r,\upsilon}}{\widehat{m}_\upsilon}\right)^{\widehat{m}_\upsilon}}$$

(6.50)

where $g_{PSK,\upsilon} = \sin^2(\pi/M_\upsilon)$. The end-to-end BER for an M-PSK modulation scheme can finally be upper-bounded as (6.51)

$$P_{b,e2e}(E) \leq \sum_{\upsilon=1}^{K} \frac{M_\upsilon - 1}{M_\upsilon \log_2 M_\upsilon}\left(1 + \beta'_\upsilon \frac{g_{\mathrm{PSK},\upsilon}, \bar{\gamma}_\upsilon}{\widehat{m}_\upsilon}\right)^{-\widehat{m}_\upsilon}$$

(6.51)

Following a similar approach, the upper bound for the end-to-end BER of an M-QAM modulation can be derived as (6.52) and (6.53)

$$P_{b,e2e}(E) \leq \sum_{\upsilon=1}^{K} \frac{2q_\upsilon}{log_2 M_\upsilon}\left[\left(1 + \beta'_\upsilon \frac{g_{\mathrm{QAM},\upsilon}\bar{\gamma}_\upsilon}{\widehat{m}_\upsilon}\right)^{-\widehat{m}_\upsilon} + \frac{q_\upsilon}{2}\left(1 + 2\beta'_\upsilon \frac{g_{\mathrm{QAM},\upsilon},\bar{\gamma}_\upsilon}{\widehat{m}_\upsilon}\right)^{-\widehat{m}_\upsilon}\right]$$

(6.52)

$$\approx \sum_{\upsilon=1}^{K} \frac{2_{q_\upsilon}}{\log_2 M_\upsilon}\left(1 + \beta'_\upsilon \frac{g_{\mathrm{QAM},\upsilon}\bar{\gamma}_\upsilon}{\widehat{m}_\upsilon}\right)^{-\widehat{m}_\upsilon}$$

(6.53)

where $g_{QAM,\upsilon} = 3/2(M_\upsilon - 1)$ and $q_\upsilon = 1 - 1/\sqrt{M_\upsilon}$. Note that in (41) the second summand appearing in (40) was neglected due to $q_\upsilon/2 < 1$ and $(1 + 2x)^{-\widehat{m}_\upsilon}$ being much less than $(1 + x)^{-\widehat{m}_\upsilon}$ for $x$ sufficiently large and $\widehat{m}_\upsilon \geq 1$. Either modulation scheme results in an upper bound unified below as (6.59)

$$P_{b,e2e}(E) \leq \sum_{\upsilon=1}^{K} A_\upsilon (1 + B_\upsilon \beta_\upsilon)^{-\widehat{m}_\upsilon}$$

(6.54)

The constants $A_\upsilon$ and $B_\upsilon$ are obtained by comparing (6.54) with (6.51) or (6.53) to arrive at (6.55)

$$A_\upsilon = \begin{cases} \dfrac{M_\upsilon - 1}{M_\upsilon \log_2 M_\upsilon} & for\ \mathrm{M-PSK} \\ \dfrac{2q_\upsilon}{\log_2 M_\upsilon} & for\ \mathrm{M-QAM} \end{cases}$$

(6.55)

and

$$B_\upsilon = \begin{cases} g_{\mathrm{PSK},\upsilon} \dfrac{\bar{\gamma}_{r,\upsilon}}{\hat{m}_\upsilon} & for\ \mathrm{M-PSK} \\ g_{\mathrm{QAM},\upsilon} \dfrac{\bar{\gamma}_{r,\upsilon}}{\hat{m}_\upsilon} & for\ \mathrm{M-QAM} \end{cases}$$

(6.56)

In Appendix

((Derivation I)), it is shown that the fractional power allocations $\beta'_{\upsilon\in(1,K)}$ have to obey (6.57)

$$\beta'_\upsilon \approx \left[ \sum_{\upsilon=1}^{K} \alpha'_\omega \left( \frac{\hat{m}_\upsilon^{-1} A_\upsilon^{-1} B_\upsilon^{\hat{m}_\upsilon}}{\hat{m}_\omega^{-1} A_\omega^{-1} B_\omega^{\hat{m}_\omega}} \right)^{\frac{1}{\hat{m}_{\max}+1}} \right]^{-1}$$

(6.57)

where $\hat{m}_{\max} = \mathrm{argmax}(\hat{m}_1, \ldots, \hat{m}_K)$

### 6.6.2 Performance Results

In this section, analytical and simulations results are presented. The simulation results are obtained from a MC-CDMA Monte-Carlo system for BER and SER versus SNR, which defined as the transmitted bit energy over the noise power spectral density ($E_b/N_o$) and the transmitted symbol energy over the noise power spectral density ($E_s/N_o$) respectively. For simplicity $N$=$G$ has been chosen. Coherence detection has been employed for all error rate curves.

In Figure 5.6 the BER of a direct link CDD MC-CDMA system has been shown that by increasing the number of CDD branches, the improvement in performance is significant for both channel orders, again confirming that CDD is beneficial regardless of the channel conditions. The system performs well and depending on the channel conditions the

desired SER performance can be achieved by trading the CDD branches and most importantly without any change to the receiver structure.

The implementation of the algorithm is based on the results provided by Figure 5.6 the SER of a CDD MC CDMA system. The SERs are shown for a Nakagami fading case and *m* has been set to 5. From Figure 5.6 and , it is evident that a CDD MC-CDMA system performs well in both, low and high delay spread environments and depending on the channel conditions the desired SER performance can be achieved by trading the CDD branches and most importantly without any change to the receiver structure.

In Figure 5.6 a comparison between CDD and STBC diversity techniques is shown. CDD has been simulated with channel orders of $L$=1,3 while STBC employs $L$=4. As expected, STBC performs better than CDD because of higher channel order and consequently, the diversity gain. However, the complexity of the cooperative distributed CDD system is significant less according to the following approach in terms of end to end throughput. t is important to highlight that for both CDD and STBC, the combination of higher channel orders ($L$>2), transmit antenna ($N_{tx}$>3) and Nakagami parameter ($m$>4), results in saturated improvement in performances; unless additional receiver chains are employed. This results will be used for the implementations of the proposed algorithm. described as the main aim contributions by this thesis.

The performance of the developed algorithm is assessed by means of Figure 6.9, Figure 6.10 and Figure 6.11 according to the generalized deployment of distributed and cooperative CDD MC-CDMA network, as depicted in Figure 6.4
Explicitly 6.9 depicts the end-to-end BER versus the SNR in the first link in [dB] for various 2-stage communication scenarios deploying the developed fractional power allocation strategy (45), which is also compared against a numerically obtained optimum and a non-optimum allocation.

The first scenario, where $t_{1,2}$= $r_{1,2}$=1, $M_{1,2}$=4 and p=[0,0]dB, is entirely symmetric which leads to the same performance for all three allocation strategies. The second scenario is the same as the first, with the only difference that the channel in the second stage is now 10 times stronger than in the first stage, i.e. p=[0,10]dB. The resulting non-symmetric scenario reveals a performance difference between the optimized (solid lines) and non-

optimized system is highest for very asymmetric cases; here, for $t_1$=2, $r_1$=2, $t_2$=2, $r_2$=1, $M_1$=256, $M_2$=64 and p=[0,10]dB. . Note that if reference is made to the non-optimized scenario, then only the fractional transmission power is meant not to be optimized since the frame duration is easily related to the modulation order. At a target end-to-end BER of $10^{-5}$, about 1 dB in power can be saved.

Figure 6.10 and Figure 6.11 are similar scenarios as Figure 6.9, but for a three-stage network, where the channel in the second stage is now 10 times stronger than in the first one. It can be observed that the optimum and developed allocation strategy yield the same performance for any of the depicted configurations. Furthermore, the gain of an optimized system over a non-optimized system is highest for very asymmetric cases. This corroborates the importance of the derived allocation strategy.
The error rates obtained in the previous section are utilized here to obtain the end-to-end throughput based on the proposed algorithm. In order to illustrated the maximum achievable throughput by means of a couple of examples.

The throughput of a two-stage system is illustrated by means of Figure 6.12 and Figure 6.13, which utilize the fractional resource allocation strategies (6.50) and **(**6.62). It can be observed that in the region of low SNR, the developed allocation strategy performs as the optimum one.
For most of the transitional region, from zero-throughput to maximum-throughput, the derived allocations yield near-optimum throughput. In contrast, no optimization exhibits drastic losses in the transitional region. For example in Figure 6.9, given the scenario with $t_{1,2}$=2 $r_{1,2}$=1 operating at a SNR in the first link of 15dB, around 0.7 bits/s/Hz are lost which mounts to approximately 50%.

Furthermore, it should be observed that in the region of low SNR, the developed allocation strategy performs equal as the non-optimized one. This is due to the fact that the fractional frame durations have been derived assuming the SNR→∞. Clearly, the strength of the link determines the rate with which the system approaches the limiting throughput for the SNR→∞. This limit will be calculated in the consecutive section.
The precision of the fractional allocation algorithm for fixed modulation indexes allows performing a final numerical optimization in each relaying stage over all possible modulation indexes due to the low complexity of (41) and (45). Such numerical

optimization was performed for a 2-stage network with p=[0,10]dB and $t_{1,2}$=2 and $r_{1,2}$=1. Each stage could choose a modulation index $M_{1,2,}$=(2,4,16,64,256). The performance gains in terms of increased throughput are clear from Figure 6.14 At any SNR, the developed algorithm clearly outperforms any of the fixed configurations.For example, if the system was to operate at an SNR in the first link of 20 dB, then the best but fixed modulation index can only reach 2 bits/s/Hz; in this case either 16-QAM or 64-QAM in both stages. The optimum selection is 64-QAM with an optimised fractional power allocation, which yields a performance benefit of 25%.

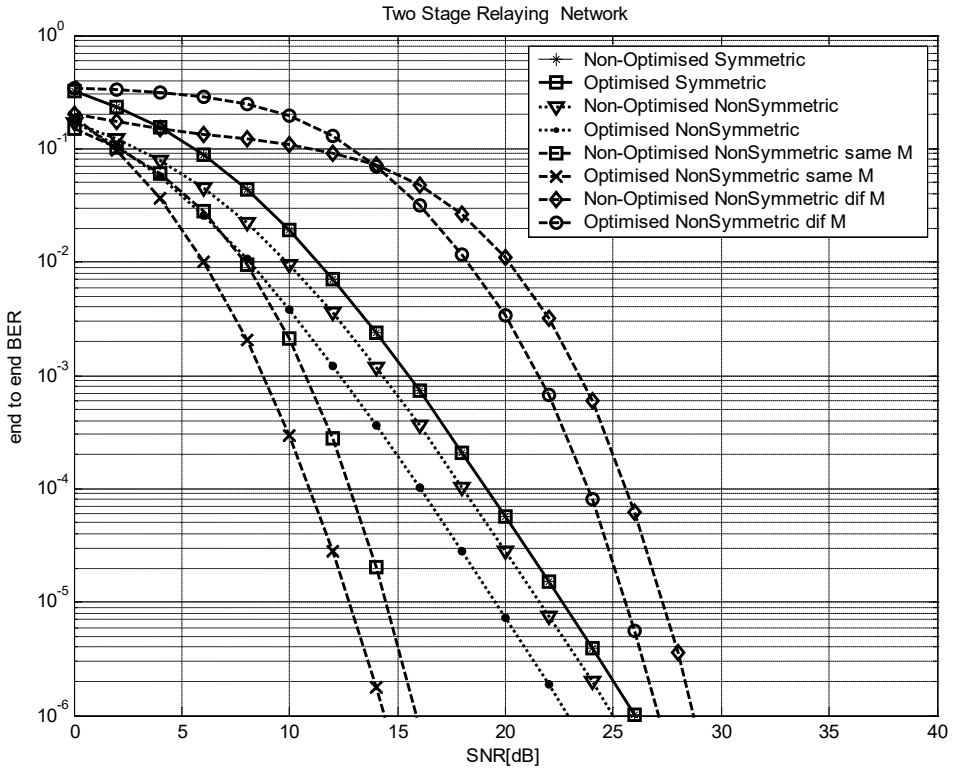


Figure 6.9 Comparison between optimum and non-optimised end-to-end BER for various configurations of a two-stage relaying DCCDD MCCDMA networks with Frequency- Correlated Subcarriers

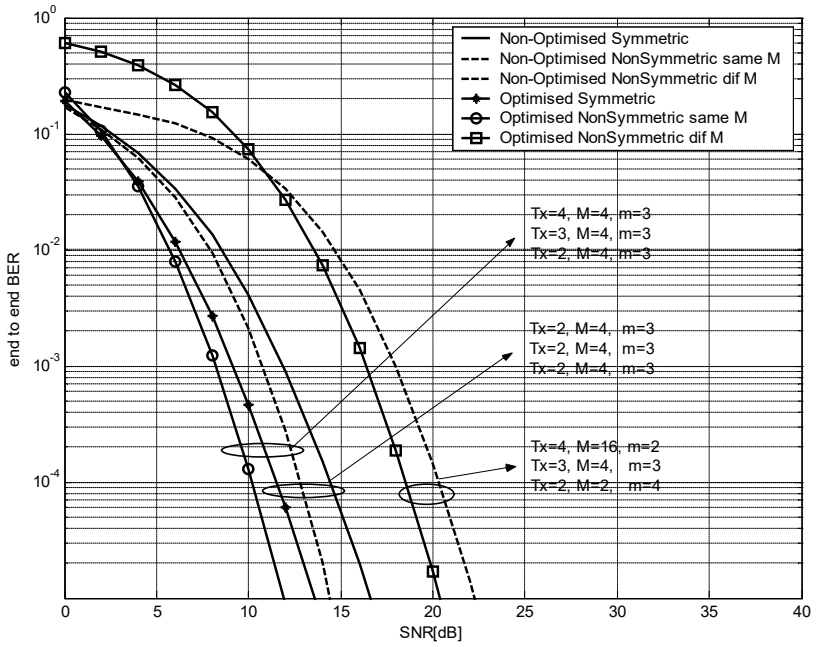


Figure 6.10 Comparison between optimum and non-optimised end-to-end BER for various configuration of a three-stage relaying network with Frequency-Correlated Subcarriers over Nakagami-*m* Fading Channels.

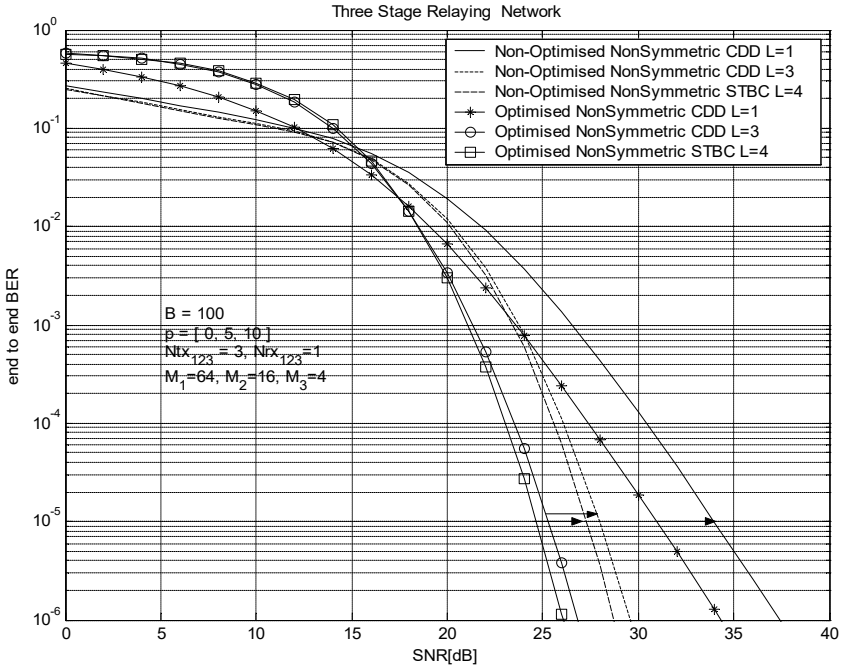


Figure 6.11 Comparison between non-optimised and optimized end-to-end BER for various configuration of a three-stage relaying network.

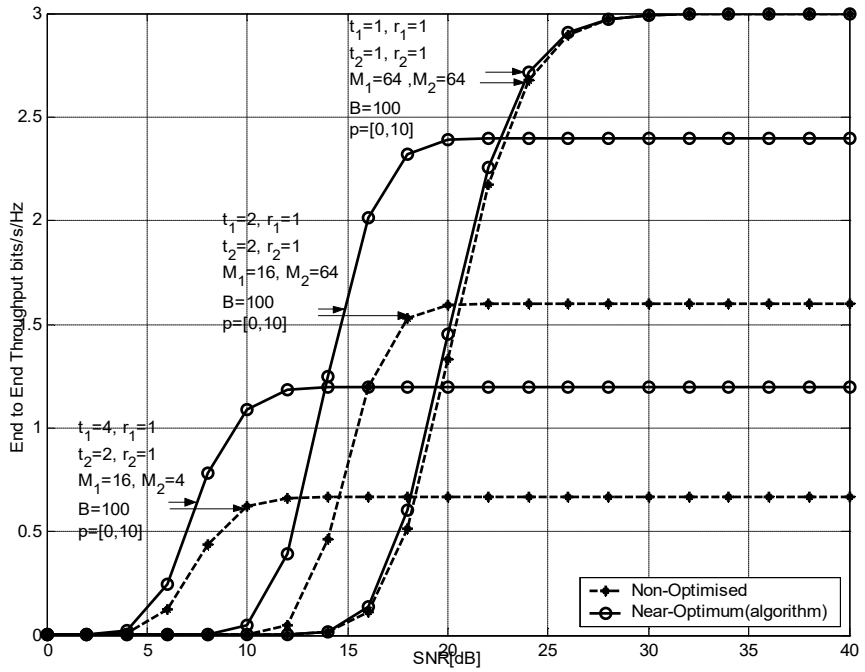


Figure 6.12 Comparison between near-optimum and non-optimised end-to-end throughput for various configurations of a two-stage relaying networks with Frequency- Correlated Subcarriers over Nakagami-*m* Fading Channels

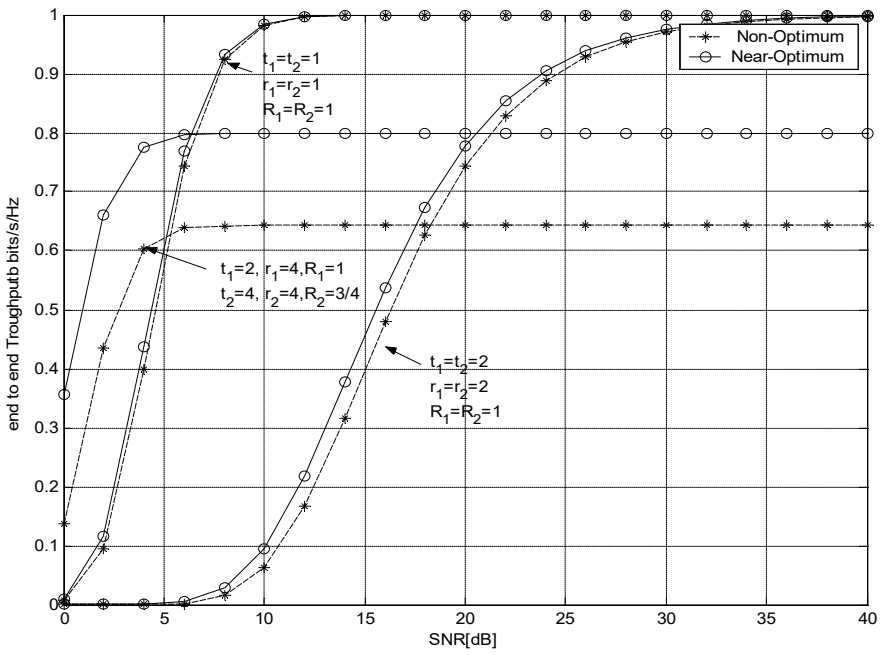


Figure 6.13 Comparison between optimum and near-optimum, as well as non-optimised end-to-end BER for various configurations of a two-stage relaying network.

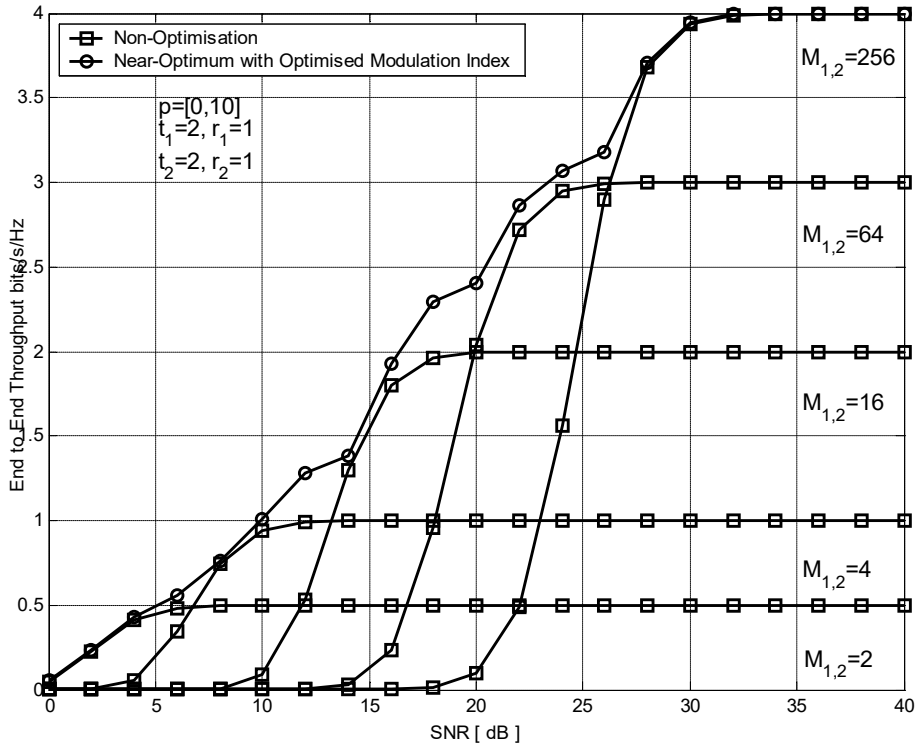


Figure 6.14 Numerically optimised modulation index where $M_{1,2}$=(2,4,16,64,256) to yield near –optimum end-to-end throughput, compared to non-optimised CDD MC-CDMA networks with Frequency-Correlated Subcarriers over Nakagami-m Fading Channels

## 6.7 Summary

The contributions of the chapter have been the explicit allocation strategies for the distributed cyclic delay diversity and STBC multi-hop coded OFDM. The SSD scheme provides a simple solution for the optimum diversity and coding gains. Spatially adjacent antennas have been grouped into CDD MC-CDMA relaying system using the MRC detection technique. The thereby accomplished distributed SIMO relaying channels allow low-complexity cyclic delay diversity coded OFDM to be deployed at each relaying stage. Our approach is to use additional antenna branches with existing STCs which are used to transmit the cyclically delayed replicas.

This approach ensures no additional rate loss and unlike other schemes, rate is only dependent on the employed ST-encoder. The performance of distributed multi-stage CDD MC-CDMA relaying network has been analyzed in terms of error rates, achievable throughput and attainable power savings when compared to traditional non-distributed networks. Channel coding is already an integral part of several system standards and we

rely on this, to extract the multipath diversity with the additional CDD branches. To our knowledge, the proposed Distributed Cooperative Serial Spatial Diversity Relaying Network has the least complexity and best rate of all the other schemes that are guaranteed to achieve full diversity.

The error-rates of distributed-MIMO multi-stage communication transceivers utilizing STBC have been derived, which were then shown to be vital in determining fractional resource allocation rules such as to maximize the normalized end-to-end throughput in dependency of the communication scenario. These strategies have then been tested by means of a few selected communication scenarios. The differences have been highlighted, with the main difference being that transceiver complexity can be traded against performance.

Closed form expressions of SERs fo M-PSK and M-QAM over Nakagami-*m* fading channels with equal channel gains have been derived, by means of the moment generating functions.
Simulation results for selected communication scenarios have confirmed the applicability and precision of the developed algorithms where in dependency of the communication scenario, significant gains can be achieved compared to the case of no optimization.

# Chapter 7

# Concluding Remarks

It was the aim of this thesis to pose and answer many unsolved questions relating to the understanding of relaying communication systems. However, the contributions of the thesis are glued together to give a better picture of the choice of the research conducted.
In this thesis, the concept of Cooperative Distributed Multistage Spatial Diversity has been introduced which was then applied to relaying networks, thereby introducing distributed-MIMO multi-stage communication networks. It has been demonstrated that such a deployment yields significant gains in data throughput independent of the complexity of the available transceivers. A prerequisite for achieving a higher data throughput is the deployment of suitable communication protocols. These have been derived in form of fractional resource allocation strategies for a wide variety of communication scenarios.

An understanding each relaying stage played a central role in deriving the allocation strategies which was the sole purpose of Chapter 5, Consecutive analysis throughout the thesis therefore distinguished between direct and multi-stages relaying networks .Although the topic of MIMO capacity has been the research focus for nearly a decade, novel results on the general CDD/STBC Relaying Throughput have been obtained in Chapter 6.

This is attributed to the solution of the integral which allowed expressing the MIMO performance in closed form.
The same integral was then utilised to derive closed form expressions for the performance of space-time block encoded MIMO channels obeying Rayleigh or Nakagami fading with arbitrary channel gains. The later case was referred to as orthogonalised MIMO (O-MIMO) relaying channel, because space-time clock codes are known to orthogonalise the MIMO detection problem into parallel SISO detection problems. In a similar manner, the performance for O-MIMO channels obeying Rayleigh and Nakagami fading with arbitrary channel gains have been obtained. Finally, at the end of Chapter 3 and Chapter4

suitable approximations to the CDD/STBC and O-CDD and O-STBC performance probabilities have been introduced.
These proved vital in a later stage to derive the fractional allocation rules, because the approximations allowed to decouple the intricate expressions attributed to the MIMO gain from the fractional power, bandwidth and frame duration.

The analysis has then been extended to the multi-stage communication scenario in Chapter 6. The aim was to develop communication protocols which maximised the end-to-end data throughput for a given network topology. As for the *ergodic* channel realisations, it has been shown that maximising the end-to-end throughput is equivalent to maximising the end-to-end *capacity* for the weakest links in the network. The previously exposed exact and approximate expressions of the MIMO allowed to derive fractional power, bandwidth and frame duration allocation strategies which guaranteed near-optimum end-to-end throughput. Not only were the cases of MIMO and O-MIMO relaying considered, but also the possibility to reuse resources in form of bandwidth or frame duration after a given number of relaying stages.

The merits of the derived allocation strategies are their simplicity and precision, thereby rendering a numerical optimisation within each relaying mobile terminal superfluous. The strategies were assessed by means of numerous communication scenarios, all of which confirmed that significant gains in terms of throughput are achieved when comparing to nonoptimised relaying systems.

Chapter 5 was dedicated to relaying systems consisting of finite complexity transceivers. In the introduction to the chapter, it has been shown that such systems are usually quantified by means of error rates versus the signal-to-noise ratio at the detection instant. The different performance measure was the reason why different allocation strategies were expected to achieve optimum end-to-end throughput with such systems. It was also expected that for an increasing complexity of channel and spacetime codes, the allocation strategies derived for infinite and finite-complexity transceivers converge.

Instead, this thesis has dealt with distributed-MIMO multi-stage space-time block encoded communication systems only. The derived fractional resource allocation rules

relied on upper bounds of the occurring error rates, which allows one to extend the analysis to any form of coding as long as the respective upper bounds are given.
The upper bounds required to derive the allocation rules were obtained from closed form expressions of the symbol error rate for space-time block encoded systems operating over Rayleigh and Nakagami fading channels with arbitrary channel gains. These have been derived using analysis exposed in the open literature, as well as in Chapter 2
Consecutively, resource allocation rules in terms of modulation order, fractional power and fractional frame duration were derived assuming a packet based transmission from source to sink. Distinction was then made between relaying systems, where erroneous packets are discarded at the target terminal only or on a stage-by-stage basis. To simplify the derivation of the allocation strategies, only ergodic channels have been assumed which can observed for large block lengths and fast fading channels

The derived algorithms were then assessed by means of a few selected communication scenarios. For these scenarios, it could be shown that considerably higher throughputs are achieved when compared to non-optimised systems. Finally,
From this summary it is clear that research on distributed-MIMO multi-stage communication systems is far from complete. This is mainly due to the fact that the here investigated PHY layer performs only a fraction of the functionalities needed to accomplishes a modern relaying communication system. The analysed single-link scenarios therefore need to be extended to the multi-link case, where more than one source terminal communicates with more than one target terminal over common relaying terminals. Control mechanisms above the PHY layer hence need to be invoked, which are traditionally accomplished by means of two fairly decoupled entities, i.e. the radio resource management (RRM) and the medium access control (MAC).

A final word on the potential applications of the derived communication protocols. In a cellular deployment, one can think of deploying multi-stage  In conclusion, the ultimate purpose of this thesis was to positively contribute to scientific knowledge, clarify several aspects relating to distributed-MIMO multi-stage relaying networks, and hopefully, to pose many questions that may catch the imagination of future researchers.

**Appendix A.1**
**Review of DFT Properties**

The $N$ point IFFT of a frequency-domain complex sequence $X(k)$ is defined as

$$x(n) = \frac{1}{\sqrt{N}} \sum_{k=0}^{N-1} X(k) e^{j\frac{2\pi}{N}nk}, \quad k = 0,1,\cdots,N-1. \tag{A.0.1}$$

Assuming $N$ an integer power of 2, the summation in (A.0.1) can be decomposed into the sum of two separate even and odd terms [25]

$$x(n) = \frac{1}{\sqrt{N}} \left( \sum_{m=0}^{\left(\frac{N}{2}\right)} X(2m) e^{j\frac{2\pi}{N/2}nm} + e^{j\frac{2\pi}{N}n} \sum_{m=0}^{\left(\frac{N}{2}\right)-1} X(2m+1) e^{j\frac{2\pi}{N/2}nm} \right), \tag{A.0.2}$$

where $X(2m)$ and $X(2m + 1)$ representing the even and odd parts, respectively. Also, the Twiddle factor $e^{j\frac{2\pi}{N}n}$ for $n$=0,1,2,…,$N$-1 can be arranged as

$$\begin{aligned} e^{j\frac{2\pi}{N}n} &= e^{j\frac{2\pi}{N}\left((n)_{N/2} + \frac{N}{2} r\left(\frac{n}{N}\right)\right)}, \\ &= (-1)^{r\left(\frac{n}{N}\right)} e^{j\frac{2\pi}{N}(n)_{N/2}}. \end{aligned} \tag{A.0.3}$$

Finally, we can write Eq. (A.0.2) as

$$x(n) = \frac{2}{\sqrt{N}} \left( x_e(n) + (-1)^{r\left(\frac{n}{N}\right)} e^{j\frac{2\pi}{N}(n)_{N/2}} x_o(n) \right), \tag{A.0.4}$$

where $(n)_N$ is the residue of $n$ modulo $N$, $x_e(n)$, $x_o(n)$ the even and odd parts, and $r(\,n/N)$ is for rounding $(n/N)$ to the nearest integer. Also, the conjugate symmetric properties for a complex sequence can be summarized as [25]

$$\begin{aligned} &x(n)_N \overset{FFT}{\leftrightarrow} X(k)_N, \\ &x^*(n)_N \leftrightarrow X^*(-k)_N, \\ &x^*(-n)_N \leftrightarrow X^*(k)_N. \end{aligned} \tag{A.0.5}$$

**Appendix A2**

The conditional PEP of transmitting **s** and deciding in favor of another codeword $\hat{\mathbf{s}}$ for a given realization of the fading channel $\mathcal{H}$, is upper bounded by [45]

$$P(s \to \hat{s} | \mathcal{H}) \le \exp\left( - d^2(s, \hat{s}) \frac{E_s}{4N_0} \right), \tag{A2.0.1}$$

where $E_s$ is the symbol energy, $N_0/2$ is the noise variance per dimension and $\mathcal{H} = \{h_{r,n}(k)\}_{r,n,k}$ which gives the explicit realization of channel over *r,n,k*. The Euclidean distance $d^2(\mathrm{s},\hat{\mathrm{s}})$ is given by

$$d^2(\mathrm{s},\hat{\mathrm{s}}) = \sum_{r=1}^{Nrx}\sum_{k=0}^{N-1}\left|\sum_{n=1}^{Ntx} H_{r,n}(k)e_n(k)\right|^2 \quad , \tag{A2.0.2}$$

where $e_n(k) = S_n(k) - \hat{S}_n(k)$.

Further, rearranging (A2.0.2) as

$$d^2(\mathrm{s},\hat{\mathrm{s}}) = \sum_{r=1}^{Nrx}\sum_{k=0}^{N-1}\left|\mathrm{h}_r \mathrm{W}_f(k)\,\mathrm{e}(k)\right|^2 \tag{A2.0.3}$$

where

$\mathbf{h}_r = \left[\mathbf{h}_{r,1}^H, \mathbf{h}_{r,2}^H, \ldots, \mathbf{h}_{r,Ntx}^H\right]_{1\times LNtx}^H$,

$$\mathrm{W}_f(k) = \mathrm{diag}\left[\mathrm{w}_f(k),\ldots,\mathrm{w}_f(k)\right]_{LNtx\times Ntx} \quad , \tag{A2.0.4}$$

Finally, (A2.0.3)can be written as

$$\begin{aligned} d^2(\mathrm{s},\hat{\mathrm{s}}) &= \sum_{r=1}^{Nrx}\sum_{k=0}^{N-1}\mathrm{h}_r \mathrm{W}_f(k)\,\mathrm{e}(k)\,\mathrm{e}^H(k)\,\mathrm{W}_f^H(k)\,\mathrm{h}_r^H, \\ &= \sum_{r=1}^{Nrx}\left[\sum_{k=0}^{N-1}\mathrm{h}_r \mathrm{W}_f(k)\,\mathrm{e}(k)\,\mathrm{e}^H(k)\,\mathrm{W}_f^H(k)\right]\mathrm{h}_r^H, \\ &= \sum_{r=1}^{Nrx}\mathrm{h}_r \mathrm{D}_{\mathcal{H}}\,\mathrm{h}_r^H . \end{aligned} \tag{A2.0.5}$$

The matrix $\mathbf{D}_{\mathcal{H}}$ of ,(A2.0.5), $\mathbf{D}_{\mathcal{H}} = \sum_{k=0}^{N-1}\mathbf{W}_f(k)\mathbf{e}(k)\mathbf{e}^H(k)\mathbf{W}_f^H(k)$ is an $LN_{tx}\times LN_{tx}$ matrix and depends on the codeword differences and the channel delay profile. Let $r_h$ denote the rank of matrix $\mathbf{D}_{\mathcal{H}}$. Since, it is a non-negative definite Hermitian, the eigenvalues of the matrix can be ordered as

$$\lambda_1 \geq \lambda_2 \geq ,\ldots, \lambda_{r_h} > 0. \tag{A2.0.6}$$

If the codeword symbols **s** and $\hat{\mathbf{s}}$ for the *k*th subcarrier and $N_{tx}$ transmit antennas are the same, i.e. $S_1(k),S_2(k),\ldots,S_{Ntx}(k) = \hat{S}_1(k),\hat{S}_2(k),\ldots,\hat{S}_{Ntx}(k)$, then the codeword difference matrix $\mathbf{e}(k)$ $\mathbf{e}^H(k)$ of (A2.0.5) is an all zero matrix. Conversely, if the codewords, $S_1(k),S_2(k),\ldots,S_{Ntx}(k) \neq \hat{S}_1(k),\hat{S}_2(k),\ldots,\hat{S}_{Ntx}(k)$ then the matrix $\mathbf{e}(k)\mathbf{e}^H(k)$ is a rank one matrix.

Let $\delta_H$ denote the number of instances $k$, $k$ = 0,1,…, $N$-1, so that $S_1(k),S_2(k),\ldots,S_{Ntx}(k) \neq \hat{S}_1(k),\hat{S}_2(k),\ldots,\hat{S}_{Ntx}(k)$, then the rank of matrix $\mathbf{D}_{\mathcal{H}f}$ is determined by $r_h \leq \min(\delta_H, LN_{tx})$ (A2.0.5) where $\delta_H$ is called the symbol-wise Hamming distance.

The rank of matrix $\mathbf{D}_{\mathcal{H}f}$ in (A2.0.5)shows that the maximum possible diversity gain for a STC is $LN_{tx}N_{rx}$, which is the product of resolvable multipaths, transmit and receive antennas. For achieving $LN_{tx}N_{rx}$th order diversity, the code symbol-wise Hamming distance has to be $\delta_H \geq LN_{tx}$, which makes it possible for a given STC to exploit both the transmit and the multipath diversity. When $\delta_H < LN_{tx}$, the achieved diversity gain is $\delta_H N_{rx}$, which means that the multipath channel delay spread effectively enables a slow fading channel to approach a fast fading channel.

Thus, the diversity gain is equal to the one for fast fading channels.

**Appendix A3**

In order to understand the operation of the time domain encoder, consider the basic frequency domain transmission matrix of a two transmit antennas block code [7], given by

$$\mathcal{G}_{2f} = \begin{bmatrix} s_1^f(k)_N & s_2^f(k)_N \\ -s_2^{f*}(k)_N & s_2^{f*}(k)_N \end{bmatrix} \tag{A3.0.1}$$

By using the conjugate symmetric properties of DFT as given by (A.0.5) in Appendix A, the time domain equivalent of the transmission matrix of can be written as

$$\mathcal{G}_{2t} = \begin{bmatrix} s_1(t)_N & s_2(t)_N \\ -s_2^*(-t)_N & s_1^*(-t)_N \end{bmatrix} \tag{A3.0.2}$$

where vectors $\mathbf{s}_i(t)$ represent the time domain equivalent of vector $s_i^f(k)$.

From (A3.0.2), it is clear that the original OFDM symbols remain unaffected and only for the complex conjugate outputs of the transmission matrix, reordering is required for the time domain implementation. In fact, if in frequency domain the $i$th complex conjugate OFDM symbol is given by

$$s_i^{f*}(k) = \left[S_i^*(0), S_i^*(1), S_i^*(2), \ldots, S_i^*(N-1)\right]^T \quad , \tag{A3.0.3}$$

then its time domain equivalent is

$$s_i^*(t) = \left[s_i^*(0), s_i^*(N-1), s_i^*(N-2), \ldots, s_i^*(1)\right]^T \quad \text{(A3.0.4)}$$

Therefore, a simple reordering within the OFDM symbol for the complex conjugate outputs of the encoder can produce the desired frequency domain equivalent. It is now straightforward to generate the time domain transmission matrices for an arbitrary number of transmit antennas. For example, half rate transmission matrices for three and four transmit antennas ST codes are given by (A3.0.1) and (A3.0.2) in Appendix B, respectively.

Finally, the CP is added for each antenna branch and the symbols are transmitted after radio frequency up-conversion and normalization. At the receiver the standard frequency domain decoder can be employed to recover the transmitted signals. The receiver and decoding algorithm of block codes is treated separately in section 3.4.

## Appendix B

### Time-Domain Transmission Matrices

**($\mathcal{G}$) for** $N_{tx} = 3,4$

For $N_{tx} = 3,4$, the time-domain transmission matrices for STBC OFDM are given by (B.0.1) and (B.0.2), respectively.

$$\mathcal{G}_{3t} = \begin{bmatrix} s_1(n)_N & s_2(n)_N & s_3(n)_N \\ -s_2(n)_N & s_1(n)_N & -s_4(n)_N \\ -s_3(n)_N & s_4(n)_N & s_1(n)_N \\ -s_4(n)_N & -s_3(n)_N & s_2(n)_N \\ s_1^*(-n)_N & s_2^*(-n)_N & s_3^*(-n)_N \\ -s_2^*(-n)_N & s_1^*(-n)_N & -s_4^*(-n)_N \\ -s_3^*(-n)_N & s_4^*(-n)_N & s_1^*(-n)_N \\ -s_4^*(-n)_N & -s_3^*(-n)_N & s_2^*(-n)_N \end{bmatrix} \quad \text{(B.0.1)}$$

and

$$G_{4t} = \begin{bmatrix} s_1(n)_N & s_2(n)_N & s_3(n)_N & s_4(n)_N \\ -s_2(n)_N & s_1(n)_N & -s_4(n)_N & s_3(n)_N \\ -s_3(n)_N & s_4(n)_N & s_1(n)_N & -s_2(n)_N \\ -s_4(n)_N & -s_3(n)_N & s_2(n)_N & s_1(n)_N \\ s_1^*(-n)_N & s_2^*(-n)_N & -s_4^*(-n)_N & s_4^*(-n)_N \\ -s_2^*(-n)_N & s_1^*(-n)_N & -s_4^*(-n)_N & s_3^*(-n)_N \\ -s_3^*(-n)_N & s_4^*(-n)_N & s_1^*(-n)_N & -s_2^*(-n)_N \\ -s_4^*(-n)_N & -s_3^*(n)_N & s_2^*(-n)_N & s_1^*(-n)_N \end{bmatrix} \quad \text{(B.0.2)}$$

Time-Domain Transmission Matrices ($G$) for $N_{tx}$ = 3, 4

For $N_{tx}$ = 3, 4, the time-domain transmission matrices for SFBC OFDM are given by (B.0.3) and (B.0.4), respectively.

$$G_{3t} = \begin{bmatrix} s_{1,e}(n)_{N/2} & s_{2,o}(n)_{N/2} & s_{2,e}(n)_{N/2} \\ -s_{1,o}(n)_{N/2} & s_{1,e}(n)_{N/2} & -s_{2,o}(n)_{N/2} \\ -s_{2,e}(n)_{N/2} & s_{2,o}(n)_{N/2} & s_{1,e}(n)_{N/2} \\ -s_{2,o}(n)_{N/2} & -s_{2,e}(n)_{N/2} & s_{1,o}(n)_{N/2} \\ s_{1,e}^*(-n)_{N/2} & s_{1,,o}^*(-n)_{N/2} & s_{2,e}^*(-n)_{N/2} \\ -s_{1,e}^*(-n)_{N/2} & s_{1,e}^*(-n)_{N/2} & -s_{2,o}^*(-n)_{N/2} \\ -s_{2,e}^*(-n)_{N/2} & s_{2,o}^*(-n)_{N/2} & s_{1,e}^*(-n)_{N/2} \\ -s_{2,o}^*(-n)_{N/2} & -s_{2,e}^*(-n)_{N/2} & s_{1,o}^*(-n)_{N/2} \end{bmatrix} \quad \text{(B.0.3)}$$

and

$$G_{4t} = \begin{bmatrix} s_{1,e}(n)_{N/2} & s_{1,o}(n)_{N/2} & s_{2,e}(n)_{N/2} & s_{2,o}(n)_{N/2} \\ -s_{1,o}(n)_{N/2} & s_{1,e}(n)_{N/2} & -s_{2,o}(n)_{N/2} & s_{2,e}(n)_{N/2} \\ -s_{2,e}(n)_{N/2} & s_{2,o}(n)_{N/2} & s_{1,e}(n)_{N/2} & -s_{1,o}(n)_{N/2} \\ -s_{2,o}(n)_{N/2} & -s_{2,e}(n)_{N/2} & s_{1,o}(n)_{N/2} & s_{1,e}(n)_{N/2} \\ s_{1,e}^*(-n)_{N/2} & s_{1,o}^*(-n)_{N/2} & -s_{2,e}^*(-n)_{N/2} & s_{2,o}^*(-n)_{N/2} \\ -s_{1,o}^*(-n)_{N/2} & s_{1,e}^*(-n)_{N/2} & -s_{2,o}^*(-n)_{N/2} & s_{2,e}^*(-n)_{N/2} \\ -s_{2,e}^*(-n)_{N/2} & s_{2,o}^*(-n)_{N/2} & s_{1,e}^*(-n)_{N/2} & -s_{1,o}^*(-n)_{N/2} \\ -s_{2,o}^*(-n)_{N/2} & -s_{2,e}^*(-n)_{N/2} & s_{1,o}^*(-n)_{N/2} & s_{1,e}^*(-n)_{N/2} \end{bmatrix} \quad \text{(B.0.4)}$$

## Appendix C

**Derivation-$I_{1,MPSK}$, $I_{2,MPSK}$ & $I_{2,MQAM}$**

$I_{1,MPSK}$

From (3.4.10), rewriting the term $I_{1,MPSK}$

$$I_{1,MPSK} = \frac{1}{\pi}\int_0^{\frac{\pi}{2}} \Phi_{\gamma_r}\left(\frac{g_{MPSK}}{\sin^2\theta}\right)d\theta\,, \tag{C.0.1}$$

where $g_{MPSK} = \sin^2(\pi/M)$ and (C.0.1) can be rewritten as [39]

$$I_{1,MPSK} = \frac{\Phi_{\gamma_r}(g_{MPSK})}{\pi}\int_0^{\frac{\pi}{2}} \left(\frac{\sin^2\theta}{1-\frac{\hat{m}\cos^2\theta}{\hat{m}+g_{MPSK}\bar{\gamma}_r}}\right)^{\hat{m}} d\theta \tag{C.0.2}$$

By change of variable $v$ $\upsilon = \cos 2\theta$, (C.0.2) can be expressed in simplified form as

$$I_{1,MPSK} = \frac{\Phi_{\gamma_r}(g_{MPSK})}{2\pi}\int_0^1 \upsilon^{-\frac{1}{2}}(1-\upsilon)^{\hat{m}-\frac{1}{2}}\left(1-\frac{\upsilon}{1+\frac{g_{MPSK}\bar{\gamma}_r}{\hat{m}}}\right)^{-\hat{m}} d\upsilon, \tag{C.0.3}$$

The Gauss hypergeometric function is expressed in terms of Gamma function as [27]

$$\begin{aligned} &{}_2F_1(\hat{a},\hat{b}:\hat{c};\hat{d}) = \frac{\Gamma(\hat{c})}{\Gamma(\hat{b})\Gamma(\hat{c}-\hat{b})}\int_0^1 \upsilon^{\hat{b}-1}(1-\upsilon)^{\hat{c}-\hat{b}-1}(1-\hat{d}\upsilon)^{-\hat{a}}\,d\upsilon, \\ &\mathrm{Re}\{\hat{c}\} > \mathrm{Re}\{\hat{b}\} > 0, \left|\hat{d}\right| < 1\,, \end{aligned} \tag{C.0.4}$$

with its simplified form given as

$${}_2F_1(\hat{a},\hat{b};\hat{c};\hat{d}) \cong \sum_{\hat{u}=0}^{\infty}\frac{(\hat{a})_{\hat{u}}(\hat{b})_{\hat{u}}}{(\hat{c})_{\hat{u}}\hat{u}!}\hat{d}^{\hat{u}} \tag{C.0.5}$$

Derivation-$I_{1,MPSK}$, $I_{2,MPSK}$ & $I_{2,MQAM}$

and the Pochhammer's symbol (^$a$)^$u$ given by

$$(\hat{a})_{\hat{u}} = \frac{\Gamma(\hat{a}+\hat{u})}{\Gamma(\hat{a})} \tag{C.0.6}$$

By employing (C.0.4) and (C.0.5), $I_{1;MPSK}$ of (C.0.3) can finally be expressed as

$$I_{1,MPSK} = \frac{\Phi_{\gamma_r}(g_{MPSK})\Gamma\left(\hat{m}+\frac{1}{2}\right)}{2\sqrt{\pi}\Gamma(\hat{m}+1)}\,{}_2F_1\left(\hat{m},\frac{1}{2};\hat{m}+1;\frac{1}{1+\frac{g_{MPSK}\bar{\gamma}_r}{\hat{m}}}\right)\,. \tag{C.0.7}$$

$I_{2;MPSK}$

From chapter 6, rewriting the term $I_{2,MPSK}$

$$I_{2,MPSK} = \frac{1}{\pi}\int_{\frac{\pi}{2}}^{\frac{(M-1)\pi}{M}} \Phi_{\gamma_r}\left(\frac{g_{MPSK}}{\sin^2\theta}\right)d\theta\,,$$

$$= \frac{1}{\pi}\int_{\frac{\pi}{M}}^{\frac{\pi}{2}} \Phi_{\gamma_r}\left(\frac{g_{MPSK}}{\sin^2\theta}\right)d\theta\,, \tag{C.0.8}$$

$$= \frac{\Phi_{\gamma_r}(g_{MPSK})}{\pi}\int_{\pi}^{\frac{\pi}{2}}\left(\frac{\sin^2\theta}{1-\frac{\hat{m}\cos^2\theta}{\hat{m}+g_{MPSK}\bar{\gamma}_r}}\right)^{\hat{m}} d\theta\,.$$

Now, by changing variable $\upsilon = \dfrac{\mathbf{cos}^2\,\theta}{\mathbf{cos}^2\,\dfrac{\pi}{M}}$ and following [73] , (C.0.8) can be expressed in simplified form as

$$I_{2,MPSK} = \frac{\Phi_{\gamma_r}(g_{MPSK})\sqrt{1-g_{MPSK}}}{2\pi}\int_0^1 \upsilon^{-\frac{1}{2}}\left(1-(1-g_{MPSK})\upsilon\right)^{\hat{m}-\frac{1}{2}}$$
$$\left(1-\frac{1-g_{MPSK}}{1+\frac{g_{MPSK}\bar{\gamma}_r}{\hat{m}}}\upsilon\right)^{-\hat{m}} d\upsilon\,, \tag{C.0.9}$$

The Appell hypergeometric function is expressed in terms of Gamma function as

$$F_1\left(\hat{a},\hat{b},\hat{b}';\hat{c},\hat{d};\hat{e}\right) = \frac{\Gamma(\hat{c})}{\Gamma(\hat{a})\Gamma(\hat{c}-\hat{a})}\int_0^1 \upsilon^{\hat{a}-1}(1-\upsilon)^{\hat{c}-\hat{a}-1}\left(1-\hat{d}\upsilon\right)^{-\hat{b}}\left(1-\hat{e}\upsilon\right)^{-\hat{b}'} d\upsilon\,,$$
$$\mathrm{Re}\{\hat{c}\} > \mathrm{Re}\{\hat{a}\} > 0, \left|\hat{d}\right| < 1, \textit{and } \left|\hat{e}\right| < 1\,, \tag{C.0.10}$$

with its simplified form given as [9] [[55]

$$F_1\left(\hat{a},\hat{b},\hat{b}';\hat{c};\hat{d};\hat{e}\right) \cong \sum_{\hat{u}=0}^{\infty}\sum_{\hat{n}=0}^{\infty}\frac{(\hat{a})_{\hat{u}+\hat{n}}\left(\hat{b}\right)_{\hat{u}}}{(\hat{c})_{\hat{u}+\hat{n}}\hat{u}!\hat{n}!}\hat{d}^{\hat{u}}\hat{e}^{\hat{n}}\,. \tag{C.0.11}$$

$$I_{2,MPSK} = \frac{\Phi_{\gamma_r}(g_{MPSK})\sqrt{1-g_{MPSK}}}{F_1\left(\frac{1}{2},\hat{m},\frac{1}{2}-\hat{m};\frac{3}{2};\frac{1-g_{MPSK}}{1+\frac{g_{MPSK}\bar{\gamma}_r}{\hat{m}}},1-g_{MPSK}\right)}. \tag{C.0.12}$$

$I_{2,MQAM}$

From chapter6, rewriting the term $I_{2,MPSK}$

$$I_{2,MQAM} = \frac{4q^2}{\pi}\int_0^{\frac{\pi}{4}} \Phi_{\lambda_r}\left(\frac{g_{MQAM}}{\sin^2\theta}\right)d\theta\,,$$

$$= \frac{4q^2\Phi_{\gamma_r}(2g_{MQAM})}{\pi}\int_0^{\frac{\pi}{4}} \left(\tan^2\theta\right)^{\hat{m}}\left(1-\frac{1+\frac{g_{MQAM}\bar{\gamma}_r}{\hat{m}}}{1+\frac{g_{MQAM}\bar{\gamma}_r}{\hat{m}}}\left(1-\tan^2\theta\right)\right)^{-\hat{m}} d\theta$$

(C.0.13)

By change of variable $\upsilon = 1\text{-}\tan^2\theta$ and using the Appell hypergeometric function, (C.0.13) can be written as

$$I_{2,MQAM} = \frac{q^2\Phi_{\gamma_r}(2g_{MQAM})}{\pi}\int_0^1 \left(1-\frac{1}{2}\upsilon\right)^{-1}(1-\upsilon)^{\hat{m}-\frac{1}{2}}\left(1-\frac{1+\frac{g_{MQAM}\bar{\gamma}_r}{\hat{m}}}{1+\frac{2g_{MQAM}\bar{\gamma}_r}{\hat{m}}}\right)^{-\hat{m}} d\upsilon$$

(C.0.14)

Finally,

$$I_{2,MQAM} = \frac{2q^2\Phi_{\gamma_r}(2g_{MQAM})}{\pi(2\hat{m}+1)}F_1\left(1,\hat{m},1;\hat{m}+\frac{3}{2};\frac{1+\frac{g_{MQAM}\bar{\gamma}_r}{\hat{m}}}{1+\frac{2g_{MQAM}\bar{\gamma}_r}{\hat{m}}},\frac{1}{2}\right)\quad.$$

(C.0.15)

**Appendix D**

Derivation I. To prove ( 6.62 ), eq ( 6.59) is rearranged as follows

$$P_{b,e2e}(e) \le \frac{A_1}{(1+B_1\beta_1')^{u_1}} + \sum_{\upsilon=2}^{K}\frac{A_\upsilon}{(1+B_\upsilon\beta_\upsilon')^{u_\upsilon}}$$

(D01)

$$= \frac{A_1}{(1+B_1\beta_1)^{u_1}} + \sum_{\upsilon=2}^{K}\frac{A_\upsilon}{(1+B_\upsilon\beta_\upsilon')^{u_\upsilon}} \qquad \text{(D02)}$$

$$= \frac{A_1}{\left(1+\alpha_1'^{-1}B_1\left(1-\sum_{\upsilon=2}^{K}\alpha_\upsilon'\beta_\upsilon'\right)\right)^{u_1}} + \sum_{\upsilon=2}^{K}\frac{A_\upsilon}{(1+B_\upsilon\beta_\upsilon')^{u_\upsilon}}$$

(D03)

where the constraints $\sum_{\upsilon=1}^{K}\alpha_\upsilon'\beta_\upsilon' = 1$ for a TDM-based relaying system have been used, in

chapter 6. Without loss of generality, the fractional power allocation $\beta_K'$ for the last relaying stage will be derived. To obtain the optimum fractional power allocations which yield a minimum end-to-end BER, eq. (D03) is differentiated $K$-1 times along $\beta_{\upsilon\in(2,K)}$. The obtained $K$-1 equations are equated to zero to arrive at

$$\frac{u_1 A_1 \alpha_1'^{-1} B_1}{\left(1+\alpha_1'^{-1} B_1\left(1-\sum_{\upsilon=2}^{K}\alpha_\upsilon'\beta_\upsilon'\right)\right)^{u_1+1}} = \frac{u_2 A_2 B_2}{\left(1+B_2\beta_2'\right)^{u_2+1}} \tag{D04}$$

$$\vdots$$

$$= \frac{u_K A_K B_K}{\left(1+B_K\beta_K'\right)^{u_K+1}} \tag{D05}$$

For low target SERs, $B_\upsilon\beta_\upsilon' \gg 1$ for any $\upsilon\in(1,K)$, which allows rearranging the above equations to

$$\frac{\alpha_1'^{-u_1} B_1^{u_1}}{u_1 A_1}\left(1-\sum_{\upsilon=2}^{K}\alpha_\upsilon'\beta_\upsilon'\right)^{u_1+1} = \frac{B_K^{u_K}}{u_K A_K}\left(\beta_K'\right)^{u_K+1} \tag{D06}$$

$$\frac{B_2^{u_2}}{u_2 A_2}\left(\beta_2'\right)^{u_2+1} = \frac{B_K^{u_K}}{u_K A_K}\left(\beta_K'\right)^{u_K+1} \tag{D07}$$

$$\vdots$$

$$\frac{B_{K-1}^{u_{K-1}}}{u_{K-1} A_{K-1}}\left(\beta_{K-1}'\right)^{u_{K-1}+1} = \frac{B_K^{u_K}}{u_K A_K}\left(\beta_K'\right)^{u_K+1} \tag{D08}$$

The above set of equations is difficult to resolve in closed form in favor of any $\beta_{\upsilon\in(1,K)}$. To this end, the ($u_{\max}$+1)-st square root is taken of eqs (D05)-(D06), where $u_{\max}$=argmax($u_1$,…,$u_K$). The choice of $u_{\max}$ is motivated by the fact that the error in approximating $(\beta_\upsilon')^y$ by $\beta_\upsilon'$ for $0<\beta_\upsilon'<1$ and y≤1 is smaller compared to the case when y>1. Since such approximation is vital in further steps, it has to be made sure that the approximation error for the above equations is minimized. This justifies the choice of $u_{\max}$, as it guarantees that $y=(u_\upsilon+1)/(u_{\max}+1)\le 1$ for any $\upsilon\in(1,K)$. Eqs. (D05)-( D06) can hence be recast into

$$\alpha_1'^{-1}\left(\frac{B_1^{u_1}}{u_1 A_1}\right)^{\frac{1}{u_{\max}+1}}\left(1-\sum_{\upsilon=2}^{K}\alpha_\upsilon'\beta_\upsilon'\right) \approx \left(\frac{B_K^{u_K}}{u_K A_K}\right)^{\frac{1}{u_{\max}+1}}\left(\beta_K'\right) \tag{D09}$$

$$\left(\frac{B_2^{u_2}}{u_2 A_2}\right)^{\frac{1}{u_{\max}+1}}(\beta_2') \approx \left(\frac{B_K^{u_K}}{u_K A_K}\right)^{\frac{1}{u_{\max}+1}}(\beta_K') \tag{D10}$$

$$\vdots$$

$$\left(\frac{B_{K-1}^{u_{K-1}}}{u_{K-1} A_{K-1}}\right)^{\frac{1}{u_{\max}+1}}(\beta_{K-1}') \approx \left(\frac{B_K^{u_K}}{u_K A_K}\right)^{\frac{1}{u_{\max}+1}}(\beta_K') \tag{D11}$$

Eqs. (D09)-(D11) are now easily resolved in favor of $\beta_2'$,…, $\beta_K'$,

$$\beta_2' \approx \beta_K'\left(\frac{u_K^{-1} A_K^{-1} B_K^{u_K}}{u_K^{-1} A_K^{-1} B_K^{u_2}}\right)^{\frac{1}{u_{\max}+1}} \tag{D12}$$

$$\vdots$$

$$\beta_{K-1}' \approx \beta_{K-1}'\left(\frac{u_K^{-1} A_K^{-1} B_K^{u_K}}{u_{K-1}^{-1} A_{K-1}^{-1} B_{K-1}^{u_{K-1}}}\right)^{\frac{1}{u_{\max}+1}} \tag{D13}$$

which, when inserted into (D09), yield

$$\beta_K' \cdot \sum_{\upsilon=1}^{K} \alpha_\upsilon'\left(\frac{u_K^{-1} A_K^{-1} B_K^{u_K}}{u_\upsilon^{-1} A_\upsilon^{-1} B_\upsilon^{u_\upsilon}}\right)^{\frac{1}{u_{\max}+1}} = 1 \tag{D14}$$

where $\beta_K'$ is now obtained and shown to be equivalent to (6.62) for $\upsilon=K$. Other coefficients are similarly obtained. This concludes the proof.

# List of Publications

1- L. Guerrero, F. Said and A.H. Aghvami, Member, IEEE, “Performance Comparison of Distributed Cooperative STBC and CDD MC-CDMA multi-hop Relaying Systems”, VTC 2010-Fall, IEEE72nd , Ottawa, ON, 04-October 2010 Page(s): 1-5
Vehicular Technology Conference Fall (VTC 2010-Fall), 2010 IEEE 72nd,

2- L.Guerrero, F. Said, A. Lodhi, A. H. Aghvami, “Relay assisted and Cooperative CDD MC-CDMA Network with Frequency-Correlated Subcarriers” Personal, Indoor and Mobile Radio Communications, 2009 IEEE 20th International Symposium on PIMRC.2009 13-16 Sept. 2009 Page(s): 1858 - 1862

3- L.Guerrero, F. Said, A. Lodhi, A. H. Aghvami, “Performance Analysis of Distributed CDD MC-CDMA Sensor Networks with Frequency-Correlated Subcarriers over Nakagami-m Fading Channels” VTC Spring 2008: 81-85

4- Laura Guerrero, Fatin Said, Afzal Lodhi, A. Hamid Aghvami: “Throughput of Distributed Cyclic Delay Diversity MC-CDMA Relaying over Nakagami-m Fading Channels” IEEE Wireless Communications and Networking Conference, 2008. WCNC 2008, Las Vegas, NV proceedings page(s): 76 – 81

5- W. Hashim, F. Said, A.H.Aghvami and L.Guerrero, “Non-coherent Sequence Detection for OFDM System with Cyclic Delay Diversity”, IET Smart Antennas and Cooperative and Communications Workshop, London, UK, October 2007.

6- L. Guerrero, A. Lodhi, F. Said, A.H. Aghvami,” Performance Analysis of Distributed Cyclic Delay Diversity MC-CDMA for Relaying Networks “,IET Smart Antennas and Cooperative and Communications Workshop, London, UK, October 200

# References


[1] J. Winters, “On the capacity of radio communication systems with diversity in Rayleigh fading environment,” IEEE Journal on Selected Areas in Communications,vol. 5, pp. 871–878, June 1987.

[2] V. Tarokh, N. Seshadri, and A. R. Calderbank, “Space-time codes for high data rate wireless communicatio: Performance criterion and code construction,” IEEE Transactions on Information Theory, vol. 44, no. 2, pp. 744–765, March 1998.

[3] R. V. Nee, G. Awater, M. Morikura, H. Takanashi, M. Webster, and K. W. Halford, “New highrate wireless LAN standards,” *IEEE Communications Magazine*, pp. 82–88, December 1999

[4] “IEEE Standard 802.16-2004,” *Part 16: Air interface for broadband wireless access systems*, October 2004

[5] C. E. Shannon, “A mathematical theory of communication,” *Bell Systems Technology Journal*, vol. 27, pp. 379–423 and 623–656, July–October 1948

[6] G. J. Foschini and M. J. Gans, “On limits of wireless communications in a fading environment when using multiple antennas,” Wireless Personal Communications, vol. 6, pp. 311–335, March 1998.

[7] E. Telatar, “Capacity of multi-antenna Gaussian channels,” European Transactions on Telecommunications, vol. 10, pp. 585–596, November 1999.

[8] S. Alamouti, “A simple transmit diversity technique for wireless communications,” IEEE Journal on Selected Areas in Communications, vol. 16, no. 8, pp. 1451–1458, October 1998.

[9] G. J. Foschini, “Layered space-time architecture for wireless communication in a fading environment when using multi-element antennas,” Bell Labs Technical Journal, vol. 1, pp. 41–59, Autumn 1996

[10] L. Zheng and D. Tse, “Diversity and multiplexing: A fundamental tradeoff in multiple antenna channels,” IEEE Transactions on Information Theory, vol. 49, no. 5, pp. 1073–1095, May 2003.

[11] H. Shin and J. Lee, “Exact symbol error probability of orthogonal space-time block codes,” in Proc. IEEE Global Telecommunications Conference, November 2002, pp. 1197–1201.

[12] B. Lu and X.Wang, “Space-time code design in OFDM systems,” in Proc. IEEE Global Telecommunications Conference, SanFrancisco, CA, November 2000, pp. 1000– 1004.

[13] ——, “Space-time-frequency transmit diversity in broadband wireless OFDM systems,” in Proc. 8th International OFDM Workshop, Hamburg, Germany, September 2003.

[14] A. Wittneben, “A new bandwidth efficient transmit antenna modulation diversity scheme for linear digital modulation,” in Proc. IEEE International Conference on Communications, Geneva, May 1993, pp. 1630–1634.

[15] X. Ma and G. Giannakis, “Space-time-multipath coding using digital phase sweeping or circular delay diversity,” IEEE Transactions +on Signal Processing, vol. 53, pp. 1121–1131, March 2005.

[16] A. Lodhi, F. Said, M. Dohler, and A. H. Aghvami, “Closed-form symbol error probabilities of STBC and CDD MC-CDMA with frequency-correlated subcarriers over nakagami-m fading channels,” IEEE Transactions on Vehicular Technology, accepted.

[17] A. Lodhi, F. Said, M. Dohler, and A. H. Aghvami, “Performance comparison of space-time block coded and cyclic delay diversity MC-CDMA systems,” IEEE Wireless Communications, vol. 12, pp. 38–45, April 2005.

[18] E. Stauffer, D. Tujkovic, and A. Paulraj, “Code rate-diversity-multiplexing tradeoff,” IEEE Transactions on Information Theory, submitted.

[19] A. J. Paulraj, D. A. Gore, R. U. Nabar, and H. B¨olcskei, “An overview of MIMO communications - a key to Gigabit wireless,” Proceedings of the IEEE, vol. 92, pp. 198–218, February 2004.

[20] H. B¨olcskei and A. Paulraj, “Space-frequency coded broadband OFDM systems,” in Proc.Wireless Communications and Networking Conference, Chicago, IL, September 2000, pp. 1–6.

[21] Z. Liu, Y. Xin, and G. Giannakis, “Linear constellation precoding for OFDM with maximum multipath diversity and coding gains,” IEEE Transactions on Communications, vol. 51, pp. 416–427, March 2003.

[22] Y. Xin, Z. Wang, and G. Giannakis, “Space-time diversity systems based on linear constellation precoding,” IEEE Transactions on Wireless Communications, vol. 2, pp. 294–309, March 2003.

[23] Z. Liu, Y. Xin, and G. Giannakis, “Space-time-frequency coded OFDM over frequency selective fading channels,” IEEE Transactions on Signal Processing, vol. 50, pp. 2465–2476, October 2002.

[24] W. Su, Z. Safar, M. Olfat, and K. J. R. Liu, “Obtaining full-diversity space-frequency codes from space-time codes via mapping,” IEEE Transactions on Signal Processing, vol. 51, pp. 2905–2915, November 2003.

[25] S. B. Weinstein and P. M. Ebert, “Data transmission by frequency division multiplexing using the discrete Fourier transform,” IEEE Transactions on Communications Technology, vol. 19, pp. 628–634, October 1971.

[26] H. Shin and J.H. Lee ”Exact symbol error probability of orthogonal space-time block codes,” Proc. Of the IEEE Globecom, Taipei, Taiwan, Nov. 17-21, pp. 1547-1552, 2002

[27] M. Abramowitz and I.A. Stegan Handbook of Mathematical Functions. Dover Publications, Inc., 9th ed., 1970

[28] A. Dammann and S. Kaiser, “Standard conformable antenna diversity techniques for OFDM and its application to DVB-T system,” in Proc. IEEE Global Telecommunications Conference, November 2001, pp. 3100–3105.

[29] M. Dohler, F. Said, A. Ghorashi, H. Aghvami, “Improvements in or Relating to Electronic Data Communication Systems”, Publication No. WO 03/003672, priority date 28 June 2001.

[30] M.Dohler, *Virtual Antenna Arrays*, PhD Thesis, King’s College London, 2003

[31] T. Cover, A. el Gamal, “Capacity Theorems for the Relay Channel,” *IEEE Trans. on Inform. Theory*, vol. IT-25, no. 5, pp.572-584, September 1979.

[32] Sendonaris, E. Erkip, B. Aazhang, “User Cooperation Diversity - Part I: System Description,” IEEE Transactions on Communications, vol. 51, no. 11, November 2003,pp. 1927-1938.

[33] A. Sendonaris, E. Erkip, B. Aazhang, “User Cooperation Diversity - Part II: Implementation Aspects and Performance Analysis,” IEEE Transactions on Communications,vol. 51, no. 11, November 2003, pp. 1939-1948.

[34] H. B¨olcskei, M. Borgmann, and A. Paulraj, “Space-frequency coded MIMO-OFDM with variable multiplexing-diversity tradeoff,” in Proc. IEEE International Conference on Communications, May 2003, pp. 2837–2841.

[35] A.Lodhi, F.Said, M.Dohler and A.H.Aghvami, “Closed-Form Symbol Error Probabilities of STBC and CDD MC-CDMA with Frequency-Correlated Subcarriers over Nakagami-m Fading Channels”IEEE Transactions on Vehicular Technology,November2006.

[36] M. Dohler, M. Arndt, D. Barthel, A. Lodhi, and A. H. Aghvami, “Closed-form symbol error probabilities of distributed orthogonal space-time block codes,” in Proc. IEEE Vehicular Technology Conference, Melbourne, Australia, May 2006, pp. 1908–1912.

[37] A. Lodhi, F. Said, M. Dohler, and A. H. Aghvami “Time domain implementation of space-time/frequency block codes for OFDM systems,” IEE Proceedings on Communications, vol. 153, pp. 633–638, October 2006.

[38] L. Guerrero, F. Said and A.H. Aghvami, Member, IEEE, “Performance Comparison of Distributed Cooperative STBC and CDD MC-CDMA multi-hop Relaying Systems”, VTC 2010-Fall, IEEE72nd , Ottawa, ON, 04-October 2010 Page(s): 1-5

[39] L.Guerrero, F. Said, A. Lodhi, A. H. Aghvami, “Relay assisted and Cooperative CDD MC-CDMA Network with Frequency-Correlated Subcarriers” Personal, Indoor and Mobile Radio Communications, 2009 IEEE 20th International Symposium on PIMRC.2009 13-16 Sept. 2009 Page(s): 1858 – 1862

[40] L.Guerrero, F. Said, A. Lodhi, A. H. Aghvami, “Performance Analysis of Distributed CDD MC-CDMA Sensor Networks with Frequency-Correlated Subcarriers over Nakagami-m Fading Channels” VTC Spring 2008: 81-85

[41] Laura Guerrero, Fatin Said, Afzal Lodhi, A. Hamid Aghvami: “Throughput of Distributed Cyclic Delay Diversity MC-CDMA Relaying over Nakagami-m Fading Channels” IEEE Wireless Communications and Networking Conference, 2008. WCNC 2008, Las Vegas, NV proceedings page(s): 76 – 81

[42] W. Hashim, F. Said, A.H.Aghvami and L.Guerrero, “Non-coherent Sequence Detection for OFDM System with Cyclic Delay Diversity”, IET Smart Antennas and Cooperative and Communications Workshop, London, UK, October 2007.

[43] L. Guerrero, A. Lodhi, F. Said, A.H. Aghvami," Performance Analysis of Distributed Cyclic Delay Diversity MC-CDMA for Relaying Networks ",IET Smart Antennas and Cooperative and Communications Workshop, London, UK, October 2007

[44] A. Dammann and S. Kaiser, "Standard conformable antenna diversity techniques for OFDM and its application to DVB-T system," IEEE Global Telecommunictions Conference (GLOBECOM 2001), pp. 3100-3105, November 2001.

[45] B. Lu and X.Wang, "Space-time code design in OFDM systems," in Proc. IEEE Global Telecommunications Conference, SanFrancisco, CA, November 2000, pp. 1000– 1004.

[46] S. R. Saunders, Antenna And Propagation For Wireless Communication Systems. New York: John Wiley & Sons, 2000.

[47] J. G. Proakis, Digital Communications, 4th ed. New York: McGraw-Hill, 2001.

[48] P. A. Bello, "Characterization of randomly time-variant linear channels," IEEE Transactions on Communications, vol. 11, pp. 360–393, December 1963.

[49] K. Fazel and S. Kaiser, Multi-Carrier and Spread Spectrum Systems. New York: John Wiley, 2003.

[50] W. C. Jakes, Microwave Mobile Communications. Wiley, 1974.

[51] M. K. Simon and M. S. Alouini, Digital Communication over Fading Channels, 2nd ed. John Wiley & Sons, 2004.

[52] Z. Kang, K. Yao, and F. Lorenzelli, "Nakagami-m fading modeling in the frequency domain for OFDM system-performance analysis," IEEE Communications Letters, vol. 7, pp. 484–486, October 2003.

[53] V. DaSilva and E. Sousa, "Prformance of orthogonal CDMA codes for quasisynchronous communication systems," in Proc. IEEE Universal Personal Communications, Ottawa, Canada, October 1993, pp. 995–999.

[54] Z. Yang, B. Lu, and X. Wang, "Bayesian Monte-Carlo multiuser receiver for spacetime coded multicarrier CDMA systems," IEEE Journal on Selected Areas in Communications, vol. 19, pp. 1625–1637, August 2001.

[55] Z. Kang and K. Yao, "On the performance of MC-CDMA over frequency selective nakagami-m fading channels with correlated and independent subcarriers,"

in Proc. IEEE Global Telecommunications Conference, Los Angeles, CA, USA, November 2004, pp. 2859–2863.

[56] J. Park, J. Kim, and S. Choi, “Performance of MC-CDMA systems in nonindependent rayleigh fading,” in Proc. IEEE International Conference on Communications, 1999, pp. 506–510.

[57] M. Nakagami, The m distribution-A general formula of intensity distribution of rapid fading; Statistical Methods in RadioWave Propagation. W. G. Hoffman, Ed. Oxford, U. K.: Pergamon, 1960.

[58] S. Zummo andW. E. Stark, “Error probability of coded STBC systems in block fading environments,” IEEE Transactions on Wireless Communications, vol. 5, pp. 972–977, May 2006.

[59] M.K. Simon and M. S. Alouini, Digital Communication over Fading Channels, John Wiley and Sons, 2nd edition, 2004

[60] L. Hanzo, M. M¨unster, B. J. Choi, and T. Keller, OFDM and MC-CDMA for broadband multi-user communications, WLANs and broadcasting. John Wiley & Sons, 2003.

[61] D. Huang and K. B. Letaief, “Symbol-based space diversity for coded OFDM systems,”IEEE Transactions on Wireless Communications, vol. 3, pp. 117–127, January 2004.

[62] B. Wang and T. Adali, “Joint impulse response shortening for discrete multitone systems,” in Proc. IEEE Global Telecommunications Conference, 1999, pp. 2508–2512.

[63] N. Yee, J.-P. Linnartz, and G. Fettweis, “Multicarriers CDMA in indoor wireless radio networks,” in Proc. IEEE International Symposium on Personal, Indoor and Mobile Radio Communications, Yokohama, Japan, September 1993, pp. 109–113

[64] A. Chouly, A. Brajal, and S. Jourdan, “Orthogonal multicarrier techniques applied to direct sequence spread spectrum CDMA systems,” in Proc. IEEE Global Telecommunications Conference, Houston, TX, USA, 1993, pp. 1723–1728.

[65] K. Fazal and L. Papke, “On the performance of convolutionally-coded CDMA/OFDM for mobile communication system,” in Proc. IEEE International Symposium on Personal, Indoor and Mobile Radio Communications, Yokohama, Japan, September 1993, pp. 468–472.

[66] L. Vandendorpe, “Multitone direct sequence CDMA system in an indoor wireless environment,” in Proc. 1st IEEE Symposiam on Communication and Vehicular Technology, 1993.

[67] Z.Li and M. Latva-aho, “Performance of space-time block coded MC-CDMA in Nakagami fading channels,” IEE Electronics Letters, vol. 39, no. 2, pp. 222-224, Jan 2003.

[68] S. Hara and R. Prassad, “Overview of multicarrier CDMA,” IEEE Communications Magazine, vol. 35, pp. 126–133, December 1997.

[69] L. Yang and L. Hanzo, “Multicarrier DS-CDMA: A multiple access scheme forubiquitous broadband wireless communications,” IEEE Communications Magazine, vol. 35, pp. 116–124, October 2003.

[70] H. Bölcskei, M. Borgmann and A. Paulraj, “Space-frequency coded MIMO-OFDM with variable multiplexing-diversity trade-off,” International Conference on Commun. (ICC), pp. 2837-2841, May 2003.

[71] X. Ma and G.Ginnakis,”Space-time-multipath coding using digital phase sweeping or circular delay diversity,” to appear in IEEE Trans. Signal Processing, 2004.

[72] A. Lodhi, F. Ostuni, F. Said, M. Dohler, and A. H. Aghvami, “Diversity transmitter and method,” UK Patent Application 0504061.3, filed 28th Feb. 2005.

[73] V. Tarokh, N. Seshadri, and A. R. Calderbank, “Space-time block codes from orthogonal design,” IEEE Transactions on Information Theory, vol. 45, no. 5, pp. 1456–1467, July 1999.

[74] K. F. Lee and D. B.Williams, “A space-time coded transmitter diversity technique for frequency selective fading channels,” in Proc. IEEE Sensor Array and Multichannel Signal Processing Workshop, 2000, pp. 149–152.

[75] B. Vucetic and J. Yuan, Space-Time Coding. John Wiley & Sons, 2003.

[76] H. F. Lu and P. V. Kumar, “Rate-diversity tradeoff of space-time codes with fixed alphabet and optimal constructions for PSK modulation,” IEEE Transactions on Information Theory, vol. 49, no. 10, pp. 2747–2751, October 2003.

[77] Z. Li and M. Latva-aho, “Performance of space-time block coded MC-CDMA inNakagami fading channels,” IEE Electronics Letters, vol. 39, pp. 222–224, January 2003.

[78] M. Abramowitz and I. A. Stegan, Handbook of Mathematical Functions, 9th ed. Dover Publications, Inc., 1970.

[79] A. Erdelyi, Higher Transcendental Functions, 9th ed. Mcgraw-Hill, 1953.

[80] V. Tarokh, H. Jafarkhani and A. R. Calderbank, "Space-time block codes from orthogonal design," IEEE Transactions on Information Theory, Vol. 45, pp.1456-1467, July 1999.

[81] M. Nakagami, "The *m* distribution-A general formula of intensity distribution of rapid fading," in Statistical Methods in Radio Wave analysis," IEEE Communications Propagation, W. G. Hoffman, Ed. Oxford, U.K.: Pergamon, 1960

[82] Z. Kang, K. Yao and F.Lorenzelli, "Nakagami-m fading modelling in the frequency domain for OFDM system-Performance Letters, vol.7, no.10, pp.484-486, 2003

[83] A. Wittneben, "A New Bandwidth Efficient Transmit Antenna Modulation Diversity Scheme for Linear DigitalModulation," IEEE ICC, May 1993, pp. 1630–34

[84] A. Erdelyi, Higher Transcendental Functions. New York, Mcgraw-Hill, vol. 1, 1953

[85] Dohler, M. Arndt, M. Barthel,D.Lodhi,A.Aghvami,A.H."Closed-Form Symbol Error Probabilities of Distributed Orthogonal Space-Time Block Codes" Vehicular Technology Conference, 2006 VTC Spring 2006, Volume 4: 1908-1912

[86] T.J. Harrold, A. R. Nix, "Capacity Enhancement Using Intelligent Relaying for Future Personal Communications Systems", Proceedings of VTC-2000 Fall, pp. 2115-2120.

[87] S. Hara and R. Prassad, "Overview of multicarrier CDMA," IEEE Commun Mag, vol. 35, no.12, pp. 126-133, Dec. 1997.

[88] L. Yang and L. Hanzo, "M ulticarrier DS-CDMA: A multiple access scheme for ubiquitous broadband wireless communications," IEEE Commun. Mag., pp. 116-124, Oct. 2003.

[89] S.M. Alamouti, "A simple transmit diversity technique for Wireless Communications," IEEE Journal on Selected Areas in Communications, Vol. 16, pp. 1451-1458, October 1998.

[90] V. Tarokh, N. Seshandri and A. R. Calderbank, "Space-time codes for high data rate wireless communication: Performance criterion and code construction," IEEE Transactions on Information Theory, Vol. 44, pp. 744-764, March 1998.

[91] Y. Xin, Z. Wang and G. Ginnakis, “Space-time diversity systems based on linear constellation precoding,” IEEE Trans. On Wireless Commun., vol.2, pp.294-309, Mar. 2003.

[92] Z. Liu, Y. Xin and G. Ginnakis, “Linear constellation precoding for OFDM with maximum multipath diversity and coding gaisn,” IEEE Trans. On Commun., vol. 51, pp. 416-426, Mar. 2003.

[93] W. Su, Z. Safar and K. J. Ray Liu, “Diversity analysis of space-time-frequency coded broadband OFDM systems”, Fifth European wireless conf., Feb. 2004, Barcelona, Spain.

[94] D. Huang and K. Ben Letaief, “Symbol-based space diversity for coded OFDM systems”, IEEE Trans. On Wireless Commun., vol.3, NO. 1, Jan. 2004, pp. 117-127.

[95] G. Bauch, “Space-time-frequency Transmit Diversity in Broadband Wireless OFDM Systems,” in Proc. Of 8th International OFDM Workshop, Hamburg, Germany, September 24-25, 2003.

[96] A. Lodhi, F. Said, M. Dohler, and A.H. Aghvami, “Performance comparison of space-time block coded and cyclic delay diversity MC-CDMA Systems,” IEEE Wireless Commun., vol. 12, no. 2, pp. 38-45, Apr. 2005.

[97] J.G. Proakis, “Digital Communications”,3rd Edition McGraw Hill International Editions, 1995, pp. 274-278

[98] H. Bölcskei, M. Borgmann, and A. Paulraj, “Space-frequency coded MIMO-OFDM with variable multiplexing-diversity,” in Proc. ICC, pp. 2837-2841, May 2003

[99] A. Lodhi, F. Said, M. Dohler, and A. H. Aghvami, “Cyclic delay diversity based space-time/space-frequency coded MC-CDMA system,” IEEE Vehicular Technology, vol. 1, pp. 22–29, September 2006.

[100] A. Lodhi, F. Said, M. Dohler, and A. H. Aghvami, “Combined spatial and multipath diversity transmitter for OFDM systems,” IEE Proceedings on Communications, submitted.

[101] A. Lodhi, F. Said, M. Dohler, and A. H. Aghvami, “An error probability analysis of STBC MC-CDMA with frequency-correlated subcarriers,” in Proc. IEEE Vehicular Technology Conference, Montreal, Canada, September 2006.

[102] Lodhi, “Exact BER analysis of CDD MC-CDMA system with frequency-correlated subcarriers,” in Proc. IEEE Vehicular Technology Conference, Montreal, Montreal, Canada, September 2006.

"What sets worlds in motion is the interplay of differences, their attractions and repulsions.
Life is plurality, death is uniformity.
By suppressing differences and peculiarities by eliminating different civilizations and cultures, progress weakens life and favours death.
The ideal of a single civilization for everyone, implicit in the cult of progress and technique, impoverishes and mutilates us.
Every view of the world that becomes extinct, every culture that disappears, diminishes a possibility of life"

Octavio Paz